Study of polymer crosslink density by time domain NMR spectroscopy

Murali Krishna Dibbanti

Ph.D. Thesis

European Doctorate in Materials Science
Department of Materials Science
University of Milano-Bicocca

June 2015

Supervisor: *Prof.Dr. Roberto Simonutti*
Co-Supervisor: *Dr. Medaglia Gabriele*
Dean of the Doctorate course: *Prof. Gian Paolo Brivio*

Contents

Abstract

Elastomeric polymers are important materials for many applications due to their exceptional long-range elastic property obtained by crosslinking. Crosslinking is the process of creating three dimensional network structures in the polymer materials and induces elasticity. Hence, the precise characterization of the crosslink density (i.e. molecular weight (M_c) between crosslinks) is essential for tuning the elastic response in polymer networks.

There are several techniques available for polymer network crosslink density measurement, among them equilibrium swelling and nuclear magnetic resonance (NMR) spectroscopy are widely used. Particularly multiple-quantum (MQ) NMR spectroscopy technique is emerging as an excellent tool for network characterization in the molecular level for last three decades. The unique advantage of this technique over the equilibrium swelling is that it gives the crosslink density together with crosslink distribution, besides being a rapid and solvent free technique. MQ NMR can be applied on inexpensive low resolution instrument without compromising on the data quality, where chemical shift resolution is not necessary. Moreover, other NMR pulse sequences are available for characterizing other polymer properties such as bound rubber fraction in filled networks, polymer dynamics, segmental motions etc.

In the present work, MQ proton NMR has been used to obtain the dipolar coupling constant and the crosslink density in different classes of elastomers (commercial formulation for tire industry, shape memory ionic elastomers and advanced application polyacrylates networks).

The robustness of the crosslink density measurements obtained from equilibrium swelling method (both phenomenological and statistical models) was compared with MQ NMR results in formulation for tire application. Thiol probes were applied to quantify ranking of sulfidic bridges as a function of curing time in the network. The Kraus, Lorenz and Parks correction for filler restriction on swelling was validated from the MQ NMR results and is significant finding. Differently from the published papers, focused on the effect of different vulcanization conditions at the optimum curing time, here the kinetics of vulcanization was studied. In this way a detailed and comprehensive picture of the polymer network as a function of curing time was provided. Baum-Pines MQ NMR pulse sequence allows the measurement of dipolar coupling constants and hence crosslink density in sulfur cured natural

rubber, carbon black (N234) filled polyisoprene, polybutadiene and polyisoprene/polybutadiene blend networks. The network degradation was studied by measuring the crosslink density as a function of curing time.

The crosslink density and bound rubber fraction around the ionic domains in a shape memory polymer network - carboxylated nitrile butyl rubber (XNBR) - have been obtained by the combination of Baum-Pines and 5 pulse MQ NMR sequences. The combined approach of Baum-Pines and 5 pulses MQ NMR gives crosslink density, allowing the estimation of bound rubber fraction as well. The measured bound rubber fraction has been further validated by magic sandwich echo NMR experiments, standard approach in this field. Finally the vulcanization curves and temperature dependent mechanical properties have been studied by rubber processing analyzer (RPA), using time-temperature superposition principle.

In principle, the methods presented here can also be applied to other classes of elastomers. For example, polyacrylates are an important class of polymers with a growing number of applications where literature on NMR studies is scarce. Thus, a proof-of-principle study was performed using the five pulse MQ sequences to measure dipolar coupling constants in thermally cured (crosslinked) polybutylacrylate networks, detecting differences associated to different sample preparation and crosslinking.

Therefore this study allows proposing time domain-NMR as an inexpensive, fast and solvent-free (green) technique readily available for quality control and day to day R&D purposes both for tyre applications and for a wide range of other elastomers and it was the primary aim of this work.

Chapter 1
Introduction

1.1 Elastomers

The name elastomer comes from the ability of polymer to regain its original shape after removal of load caused to deform its initial state or shape. Elasticity is the inherent property of networked polymers. The networks are created either physical (entanglement) or chemical crosslinks between polymer chains. Physical crosslinks are in general not permanent since they may completely or partially disappear on swelling or increase in temperature. Chemical crosslinks are permanent chemical bonds between polymer chains and are irreversible. Chemical networks can create either from the origin of synthesis or by randomly joining segments in already formed macromolecule chains. Sulfur cure, peroxide cure and high-energy irradiations are familiar methods of random crosslinking. Creation of crosslinks (chemical bonds) between polymer chains and achieving the polymer network by the addition of crosslink agents and heating under pressure is called the vulcanization or curing. Most of the rubber industries or automotive tyre industries use the vulcanization to achieve the elasticity in rubber products. The main vulcanization agents find extensive uses in the rubber industry are sulfur and peroxides. In sulfur vulcanization systems, cyclic octaatomic sulfur molecules with closed ring structure opens and form bridge between carbon atoms in the neighbouring chains whereas peroxide vulcanization, based on a radical pathway and creates direct bond between carbon-carbon. In sulfur vulcanization, it is common to use accelerators also for dual purpose of increasing rate of sulfur crosslinking in rubber and crosslink density. Formation of networks by end-linking individual chains by certain functional linkages is the most appropriate method of forming well-defined structures. The functionality of a linkage is defined as the number of chains meeting at the network junction. A perfect network should have at least trifunctionality and does not contain any defects such as dangling ends, loops etc and will discuss later.

1.2 Crosslinked Polymer Networks

We can define the polymer network in multiple ways, for the sake of ease, network is defined as the three dimensional polymer structure, in which polymer chains are linked either physically or chemically and transform the polymer system from plastic behavior to elastic is called the network. Physical crosslinks are created by aggregation of polymer chains (entanglements), ionic hoops, lamellar, fibrillar or reticular systems exhibit particular ordered structures and are not permanent. Chemical crosslinks are permanent and are created by covalent bonding between polymer molecules such a sulfur vulcanized polyisoprene structure is as shown in Figure 1.1. A single sulfur or polysulfur could crate links between polymer chains, '*n*' indicates number of sulfur atoms. Peroxides typically react with the elastomer chains by removing hydrogen atoms from the carbon backbone of the polymer, thus creating highly active radicals on the chain, which attach to a similar site on another chain. This creates a carbon to carbon crosslink, which is stronger than sulfur to carbon link and more thermally stable such a structure is shown in Figure 1.2.

Our main interest in this particular study is to analyse the chemical crosslinks of a network by estimating the appropriate network parameters such as a crosslink density, distribution, network defects etc. For an instant we restricted to covalent crosslink density of a different polymer networks under studied. The network analysis or characterization can be done by obtaining network parameter i.e. molecular weight between crosslink junctions. The network parameters can obtain by applying different network models in equilibrium swelling method [1] and on applying polymer dynamics theory and simulations together with NMR experimental data [2]. The network models will discuss briefly in chapter 3.

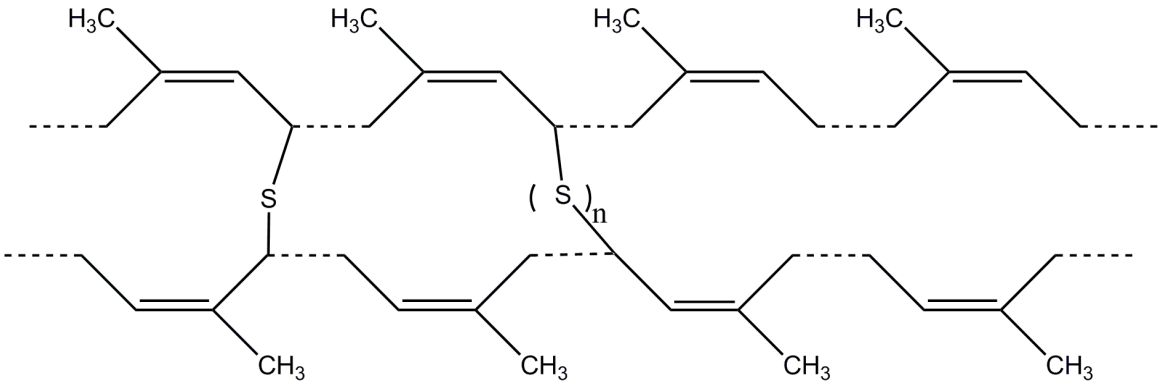

Figure 1.1 *Mono and poly sulfide crosslinking in polyisoprene polymer. 'n' indicates number of sulfur atoms.*

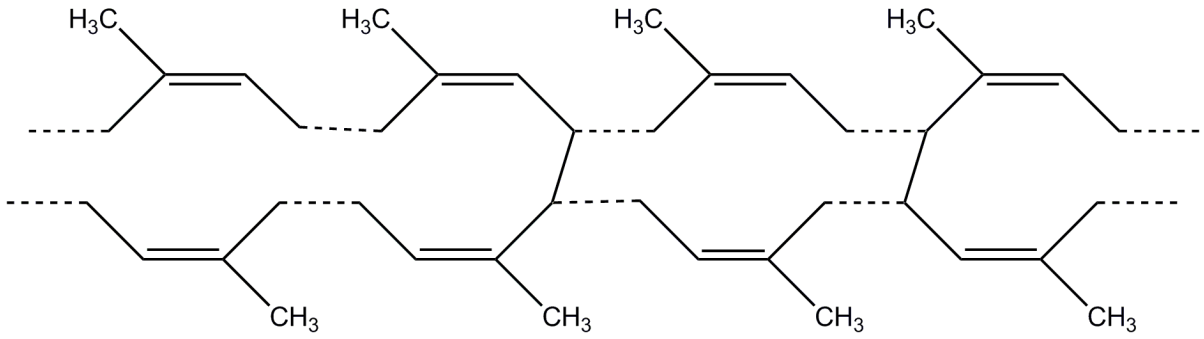

Figure 1.2 *Dicumyl peroxide (DCP) crosslinking in polyisoprene polymer. The direct chemical bond creates between backbone carbons of two polymer chains.*

1.3 Filled Networks

Creating of chemical crosslinks and transforming the polymer from plastic behaviour to elastic behaviour alone is not enough for real time applications. Most of the applications demands good mechanical and load bearing capacity. These requirements can be achieved by reinforcing of elastomer network with particulate fillers. Simply adding of fillers cannot help; need to understand whether added fillers are improving reinforcement to the network or not. The most commonly used fillers in the rubber industry are silica and various grades of carbon black [3-7]. Day to day growing demand for various applications and to improve the desired properties of polymers, various kinds of nano fillers [8-10] are rigorous subject of study.

The study of filler reinforcement is broader subject. The present work is not concern about the systematic study of various filled elastomers and their influence on mechanical properties but we limited to carbon black filler and how it creates topological restrictions to the crosslinked networks measured by MQ NMR and equilibrium swelling methods.

1.4 NMR Spectroscopy

Nuclear magnetic resonance is one of the most complex spectroscopy techniques. However this complexity can be the source of enormous information about the structure and dynamics of the simple to complex polymeric systems. Better knowledge of NMR phenomenon allows to understanding NMR literature and conduct NMR experiments and elucidation of additional information of the system under study. Continues knowledge has to be gained to utilize great variety of NMR experiments most effectively and correctly. Nuclear magnetic resonance phenomenon can be described in a most simple way as follows.

1.4.1 Nuclear Magnetic Resonance

Exchange of energy between two systems at a specific frequency is called resonance. Magnetic resonance corresponds to the energetic interaction between spins and electromagnetic radio frequency (RF).

The energy required to induce flipping and obtain an NMR signal is just the energy difference between the two nuclear orientations (states) and is shown in Figure 1.3. It depends on the strength of the magnetic field B_o in which the nucleus is placed and gyromagnetic ratio of nucleus:

$$\Delta E = \gamma \hbar B_0 \tag{1.1}$$

Where γ gyromagnetic ratio and is constant for particular type of nucleus. $\hbar = h/2\pi$, h planck's constant and B_o is strength of static magnetic field.

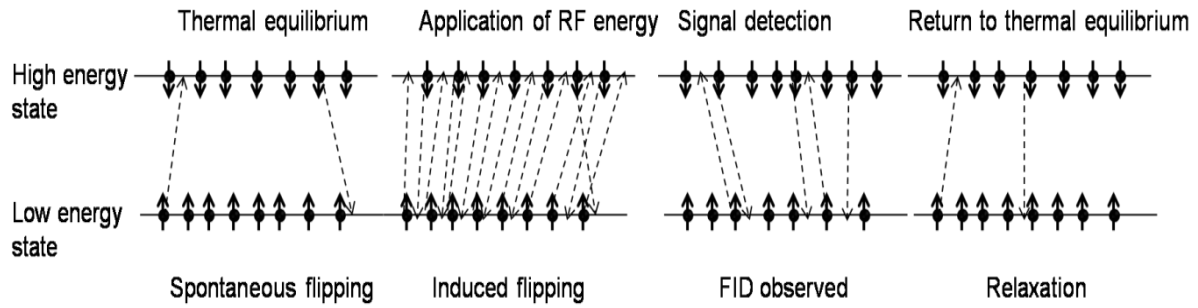

Figure 1.3 *Schematic representation of system of spin-1/2 nuclei in a magnetic field of strength B_o at thermal equilibrium, RF excited, free induction decay and final relaxation.*

Only nuclei those spin with the same frequency as the electromagnetic RF pulse will respond to that RF pulse. There is a modification of spin equilibrium and absorption of electromagnetic energy by atomic nuclei, which is called excitation. The frequency of the radiation necessary for absorption of energy depends on characteristic of the type of nucleus (e.g., ^{1}H, followed by ^{13}C, ^{31}P, ^{19}F, ^{15}N ^{29}Si etc. all of these nuclei are spin ½ nuclei. There are NMR active integral spin nuclei also available such as a ^{2}H, ^{6}Li, and ^{14}N etc.). The frequency also depends on chemical environment of the nucleus and is allows to identify the chemical structure of sample under study, for example, the methyl and hydroxyl protons of methanol absorb at different frequencies, the length of time and the manner in which the nuclei dissipate absorbed energy can also be used to reveal information regarding a variety of dynamic processes. The NMR frequency also depends on spatial location in the magnetic field if that field is not everywhere uniform. This is more important for good resolution of spectra of sample under study. There are techniques also available to better reduce the field inhomogeneities dephasing effect by applying refocusing pulses [11].

When the system returns from this state of imbalance to equilibrium (relaxation), there is an emission of electromagnetic energy which generates current in the spectrometer receiver coil and it contains information about the system. Excitation modifies energy levels and spin phase and is achieved by applying simple pulse or by complex pulse sequences. At the quantum level, a very few spins jump to a higher energy state (from parallel to anti-parallel). The consequence on the macroscopic net magnetization vector is a spiral movement down to the XY-plane as shown in Figure 1.4. In a rotating frame of reference, the net magnetization vector tips down during excitation. The flip angle is in function of the strength and duration of the electromagnetic RF pulse.

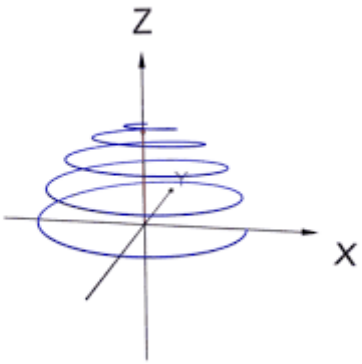

Figure 1.4 *The net magnetization moment down to the xy-plan by the application of pulse.*

1.4.2 Boltzmann Equation

The extent to which one orientation (energy state) is favored over the other depends on the strength of the small nuclear magnet (nuclei gyromagnetic ratio) and the strength of the strong magnetic field *Bo* in which it is placed. In practice, we do not put one nucleus in a magnetic field. Rather a huge number (approaching Avogadro's number) of nuclei are in the sample that is placed in a magnetic field. The distribution of nuclei in the different energy states (i.e., orientations of nuclear magnets) under conditions in which the nuclear spin system is unperturbed by application of any RF energy is given by the Boltzmann equation:

$$\frac{N_2}{N_1} = e^{-\frac{\Delta E}{kT}} = e^{-\frac{h\vartheta}{kT}} \tag{1.2}$$

Where N_2 and N_1 represent the population (i.e., number) of nuclei in upper and lower energy states, respectively, *k* is the Boltzmann constant, and T is the absolute temperature (K). To give some idea of the consequences of increasing magnetic field on the population of spin states, the distribution of a small number (about two million) of hydrogen nuclei, calculated from Equation (1.2) is shown in Figure 1. 5. For protons in an 18.8 T magnetic field (ν_o = 800 MHz) at thermal equilibrium at room temperature, the population ratio will be 0.999872. That means for every 999872 nuclei in the upper energy state there are 1,000,128 nuclei in the lower energy state. Such a small difference between energy states gives NMR phenomenon.

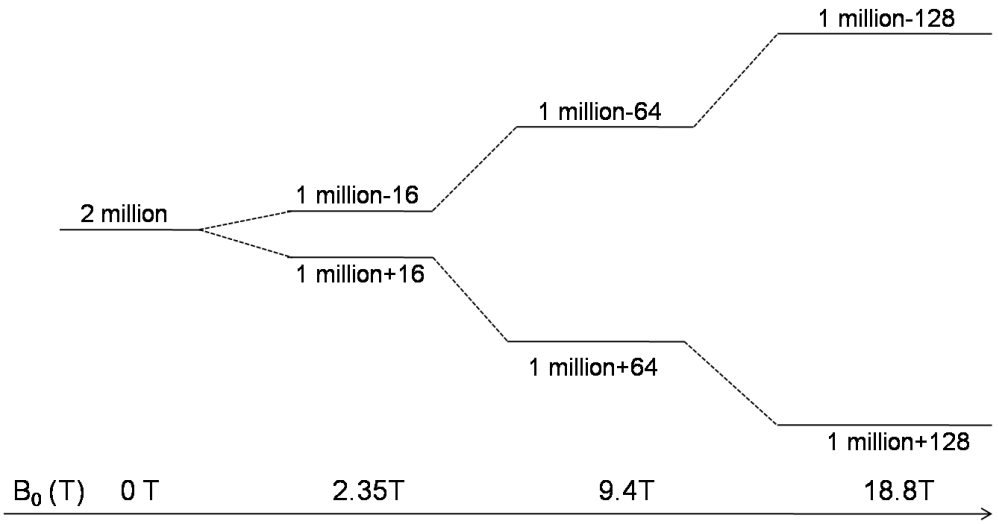

Figure 1. 5 *Dipole spin population difference between energy states depends on static (B_0) field.*

1.4.3 NMR relaxation mechanisms

After destroying equilibrium state of spin system by applying RF pulse, the spin system return to equilibrium of net magnetization is called "relaxation". During relaxation, electromagnetic energy is retransmitted; this RF emission is called the NMR signal. In NMR two types of relaxation mechanisms occur:

1) Longitudinal relaxation (T_1) corresponds to longitudinal magnetization recovery.
2) Transverse relaxation (T_2) corresponds to transverse magnetization decay.

1) Longitudinal relaxation (T_1)

T_1 relaxation is due to energy exchange between the spins and surrounding lattice (spin-lattice relaxation), re-establishing thermal equilibrium. As spins go from a high energy state back to a low energy state, RF energy is released back into the surrounding lattice and the reason called spin-lattice relaxation.

The recovery of longitudinal magnetization follows an exponential curve. The recovery rate is characterized by the material-specific time constant T_1. After time T_1, longitudinal magnetization has returned to 63% of its final value as shown in Figure 1. 6. T_1 values are longer at higher field strengths.

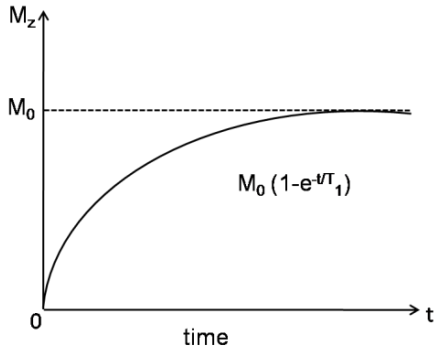

Figure 1. 6 *The recovery of longitudinal relaxation time.*

2) Transverse relaxation (T_2)

T_2 relaxation results from spins getting out of phase. As spins move together, their magnetic fields interact (spin-spin interaction), slightly modifying their precession rate. These

interactions are temporary and random. Thus, spin-spin relaxation causes a cumulative loss in phase resulting in transverse magnetization decay.

Transverse magnetization decay is described by an exponential curve, characterized by the time constant T_2. After time T_2, transverse magnetization has lost 63 % of its original value as shown in Figure 1. 7. Transverse relaxation is faster than longitudinal relaxation (most probably). T_2 values are unrelated to field strength.

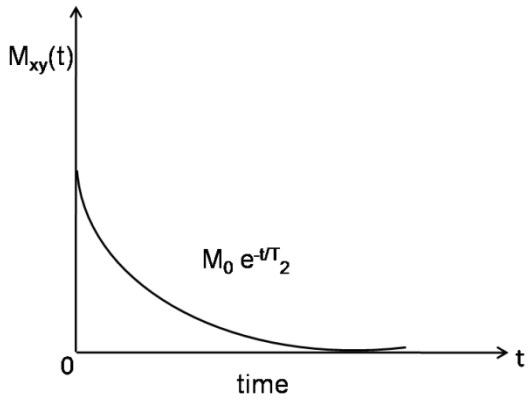

Figure 1. 7 *Decay of transversive relaxation.*

1.4.4 Time domain NMR

NMR usually relies on Fourier transform of the free induction decay (FID) to obtain information on the nuclear neighbourhood in terms of spectral chemical shift. In TD-NMR, FID is analyzed directly. The information on the chemical environment of each nucleus is neglected, but the analysis provides information on molecular mobility. The underlying physical principles are the same: a sample containing spin active nuclei, such as ^{1}H, immersed in a static magnetic field B_0 develops a macroscopic magnetization vector M. In NMR experiments the sample is irradiated with electromagnetic pulses in order to perturb M from thermodynamic equilibrium. In the classical description [12] of NMR, pulses rotate M from its equilibrium position by an angle that depends on their duration. The observable is the current circulating in the receiver coil, proportional to the component of the magnetization M in the xy-plane (perpendicular to the B_0 direction).

The characteristic features of the TD-NMR signal are informative of the morphology, topology and dynamics of a wide array of polymer matrices, among which are elastomeric materials.

The TD-NMR gives enormous information about the polymeric materials by performing the as simple as Bloch Decay [13, 14] experiment to complex multiple-quantum experiment [2]. The information provided by TD-NMR even at low fields is robust and able to give reliable information for as sensitive as a forensic context [13, 14] even by detecting the changes occur in the same commercial products produced in different batches.

1.4.4.1 Bloch Decay experiment

In the Bloch Decay (BD) experiment, a single pulse is applied to rotate the proton magnetization M by 90°, thus maximizing the measured signal immediately after the pulse. By the Boltzmann law of statistics M is proportional to the number of proton spins and inversely proportional to the temperature. Hence a measurement of the current intensity in the coil just after the pulse and at a fixed temperature will give an evaluation of the number of protons in the sample, which is standard method for measurement of hydrogen content in distillate petroleum products.

Hahn echo [11], solid echo [15] and CPMG [16] experiments could provide T_2 relaxation times which intern reflects the dynamics and structure of the system. Choice of pulse sequence may depend on the nature of studying material, means soft or hard or liquid nature of the sample. T_1 measurements performed either saturation recover or inversion recovery pulse is prerequisite for any other NMR measurements in order to find the appropriate recycle delay (must set to $\geq 5T_1$). T_1 measurements are also helpful to study the polymer side chains and segmental motions or internal motions [17].

1.4.4.2 Solid echo sequence (T_2)

Solid echo [15] provides T_2 relaxation time by completely refocusing of strong dipolar interactions (dipolar and quadrupolar couplings) typical of highly constrained polymer chains. This sequence can refocus also the hard phase magnetization, with a significant loss of intensity at longer times. By selecting an initial echo time of about 80 ms also possible to completely exclude the detection of residual magnetization from the rigid phase, and insulate the magnetization of the softer phase. It is generated by a 90° pulse applied at a time τ after the first 90° excitation pulse as shown in Figure 1. 8. The two 90° pulses must be 90° out of phase. The echo maximum is at a time τ after the second pulse. The echo delay τ should be smaller than the inverse coupling strength.

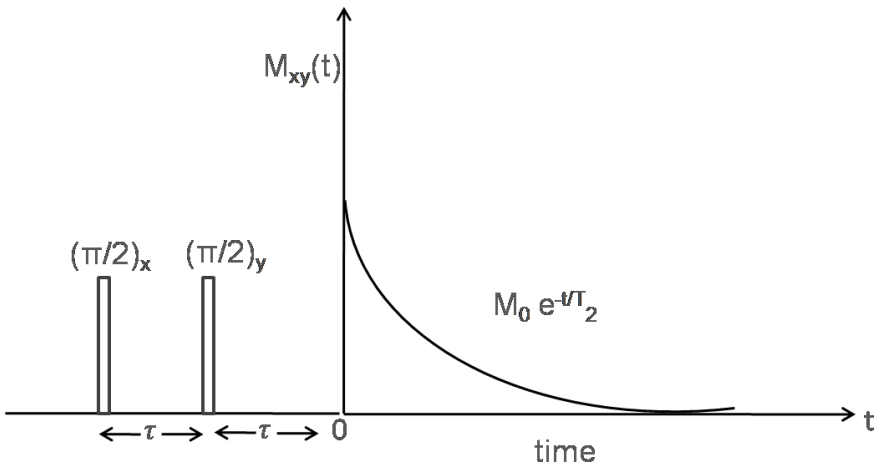

Figure 1. 8 *Solid echo pulse sequence and obtained signal intensity fitted with exponential function to obtain T_2.*

1.4.4.3 CPMG sequence (T_2)

Carr Purcell Meiboom Gill (CPMG) pulse sequence [16] designed to measure the transverse relaxation time T_2. This sequence consists of a first 90° pulse followed by a train of equally spaced 180° pulses shown in Figure 1 9. The signal is measured in the midpoint between each pair of 180° pulses and the obtained decaying curve is fitted against $M_0\exp(-t/T_2)$. This measurement is also based on total FID intensity rather than on the intensity of a single frequency domain peak.

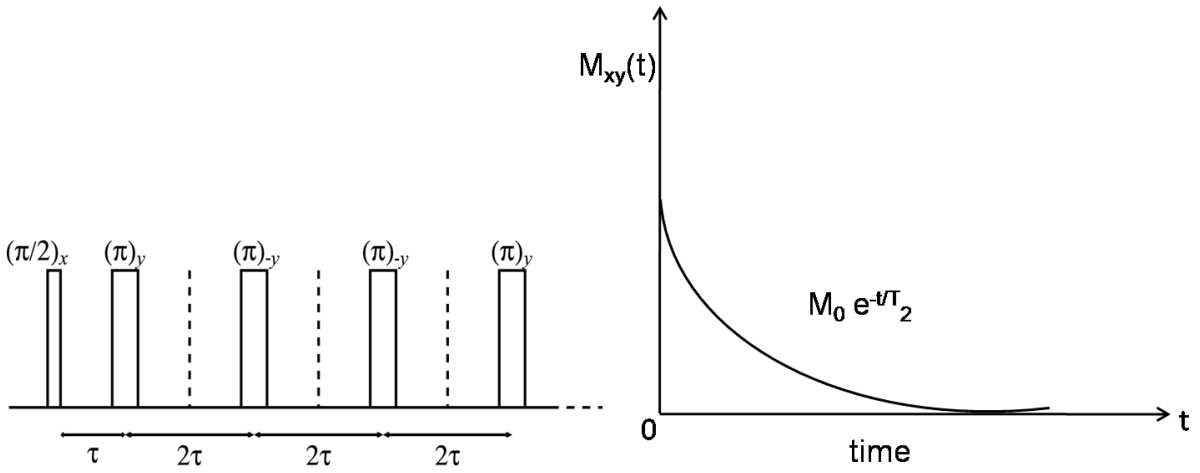

Figure 1 9 *CPMG pulse sequence and obtained signal intensity fitted with exponential function to obtain T_2.*

1.4.4.4 Hahn echo sequence (T_2)

Hahn echo [11] is more efficient pulse sequence to measure T_2. The 180° refocusing pulse suppress the magnetic field inhomogeneities and chemical shift effects.

The Hahn echo pulse sequence is as shown in Figure 1. 10 consist of a 90° pulse and 180° refocusing pulse. By the 90° pulse flips the magnetization in the XY-plane, during the first τ delay, the magnetization evolves according to its chemical shift (and field inhomogeneities) and then a 180° pulse will apply and is inverts the magnetization. (This pulse can be applied along X or Y axis). Following the inversion pulse, another τ delay will apply, during this delay, the magnetization refocus, at the end of the second delay; the echo will be lined up.

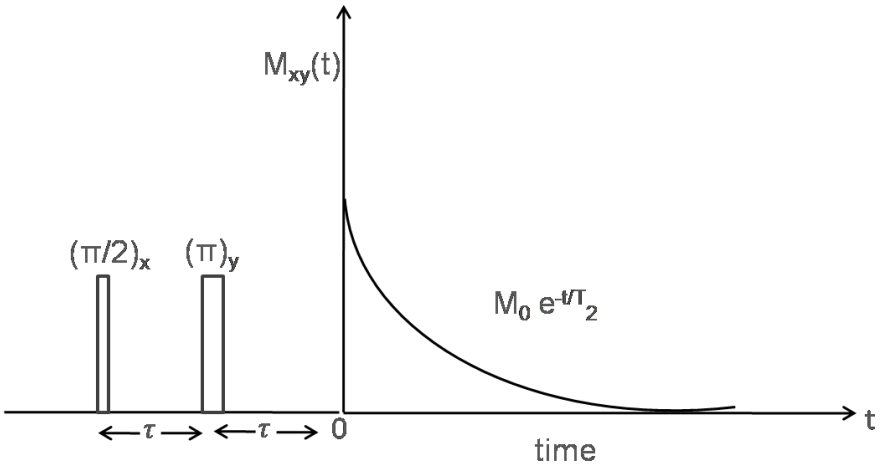

Figure 1. 10 *Hahn echo pulse sequence and obtained signal intensity fitted with exponential function to obtain T_2.*

Multiple-quantum nuclear magnetic resonance (MQ NMR) is one of the most successful and versatile technique for studying networked polymer structures and a dynamics [18]. The basis of MQ NMR is that orientation dependent interaction between dipolar spins and leaves residues of dipolar couplings. The magnitude of dipolar coupling constant is proportional to the network crosslink density. The detail picture of MQ NMR will discuss in chapter 2. The NMR phenomenon is understood by the various interactions in a system of spins in the magnetic field.

1.4.5 Types of NMR Interactions

The basis for NMR phenomenon is to understand the various interactions experienced by the system of N spins in a magnetic field. When an atomic nucleus is placed in a static magnetic field, the ground state will split into different energy levels depends on the strength of the magnetic field and is called the Zeeman interaction and is the most basic interaction in NMR. When the radio frequency energy is applied to the same system in addition to the static magnetic field, various interactions are comes into picture and these interactions are perturbations to the basic Zeeman interaction. The different interaction energies can be described in terms of Hamiltonian [21-24]. In NMR, we can distinguish nuclear spin interactions into internal and external interactions and their interaction Hamiltonian is represented as

$$\hat{H} = \hat{H}_{ext} + \hat{H}_{int} \tag{1.3}$$

Where

$$\hat{H}_{ext} = \hat{H}_z + \hat{H}_{RF} \quad \text{and} \quad \hat{H}_{int} = \hat{H}_{CS} + \hat{H}_D + \hat{H}_J + \hat{H}_Q \tag{1.4}$$

Where $\hat{H}_z$, $\hat{H}_{RF}$, $\hat{H}_{CS}$, $\hat{H}_D$, $\hat{H}_J$ and $\hat{H}_Q$ are Zeeman, radio-frequency, chemical shift, direct spin-spin, indirect spin-spin and quadrupole interactions respectively.

The Zeeman interaction is the largest followed by the quadrupolar interactions which are on the order of MHz. The chemical shift and direct dipolar coupling are on the order of kHz while the indirect spin-spin coupling is only tens of Hz. All these interactions are expressed with Hamiltonian.

The dynamics of the N spins can be explained by classical mechanics by neglecting the interaction between spins but the interaction between the spin is the key basis for nuclear magnetic resonance. It is necessary to treat quantum mechanical formalism to describe the dynamics of N coupled spins. In NMR, spectroscopic information is measured as a statistical ensemble over the individual spins. The quantum mechanics is the best way to describe ensemble of spins with the help of density operator.

Density Operator

Density operator theory is a powerful, elegant and relatively simple formalism for describing the quantum mechanical system. Here we used density operator formalism [19, 20] to derive the equation of motion for different interactions in spin systems.

Properties of Density Operator

Consider a system is in a state $|\psi(t)\rangle$ at a time t, we can expanded the state

$$|\psi(t)\rangle = \sum_n a_n\ (t)|u_n\rangle \tag{1.5}$$

We assume that $|\psi(t)\rangle$ is normalized,

$$\langle\psi(t)|\psi(t)\rangle = 1 = \sum_n \sum_m a_n\ (t)a_m^*(t)\langle u_m|u_n\rangle$$

$$= \sum_n |a_n\ (t)|^2 \tag{1.6}$$

Suppose that we have an observable, represented as operator *A*.

The matrix elements of *A* in this basis are

$$A_{mn} = \langle u_m|A\ u_n\rangle = \langle Au_m|\ u_n\rangle$$

$$A_{mn} = \langle u_m|A|\ u_n\rangle \tag{1.7}$$

The expectation (average) value of *A* at time t, for the system in a state $|\psi(t)\rangle$

$$\langle A\rangle = \langle\psi(t)A\psi(t)\rangle \tag{1.8}$$

$$= \sum_n \sum_m a_n\,(t) a_m^*(t) A_{mn}$$

We see that $\langle A \rangle$ is an expansion quadratic in the $\{a_n\}$ coefficient

Consider the operator $|\psi(t)\rangle\langle\psi(t)|$. It has the matrix elements.

$$\langle u_m|\psi(t)\rangle\langle\psi(t)|u_n\rangle = a_m\,(t) a_n^*(t) \tag{1.9}$$

These matrix elements appear in the calculation of expectation values$\langle A \rangle$.

Hence define,

$$\hat{\rho}(t) = |\psi(t)\rangle\langle\psi(t)| \tag{1.10}$$

Equation (1.10), $\hat{\rho}(t)$ is called the density operator. The density matrix or operator has the following properties:

1) Projector $\hat{\rho}^2 = \hat{\rho}$
2) Hermiticity $\hat{\rho}^\dagger = \hat{\rho}$
3) Normalized $T_r \hat{\rho} = 1$
4) Positivity $\hat{\rho} \geq 0$

One can derive the equation of motion for the density operator from time dependent Schrödinger equation

$$i\,\hbar \frac{d}{dt}|\psi(t)\rangle = H(t)|\psi(t)\rangle \tag{1.11}$$

$H(t)$ is the Hamiltonian.

The time evolution of the density operator may be computed according to

$$\frac{d}{dt}\hat{\rho}(t) = \frac{d}{dt}[\![|\psi(t)\rangle\langle\psi(t)|]\!]$$

$$= \frac{1}{i\hbar} H(t)\ |\psi(t)\rangle\langle\psi(t)| - \frac{1}{i\hbar}\ |\psi(t)\rangle\langle\psi(t)|\ H(t)$$

$$= \frac{1}{i\hbar}[H(t), \hat{\rho}(t)] \tag{1.12}$$

Equation (1.12) is called ***Liouville-Von Neuman*** equation [23].

The time evolution of the density matrix we can also describe by applying a unitary operator, the time shift operator $U(t, t_o)$ also called the projector.

$$U(t, t_o) = e^{-iH(t-t_o)}$$

$$= \hat{\rho}(t) = U(t, t_o).\hat{\rho}(t_o).U^{\dagger}(t, t_o) \tag{1.13}$$

Now we will derive the Hamiltonian for different interactions.

The interaction energy between nuclear spins and magnetic fields in NMR is give by the following equations classically. Let us consider nuclei that have magnetic moments $\overrightarrow{\mu_i}$ in a magnetic field of strength $\overrightarrow{B_o}$ then the interaction energy is

$$E = -\overrightarrow{\mu_i}.\vec{B}_o \tag{1.14}$$

Summing over all dipoles and replacing classical magnetic moment μ_i with quantum mechanical magnetic moment $\gamma_i \hbar \vec{I}$, the general Hamiltonian is written as

$$H = -\hbar \sum_i \gamma_i\, \vec{I}_i.\vec{B}_o \tag{1.15}$$

Where 'i' represents i^{th} spins.

1.4.5.1 The Zeeman Interaction Hamiltonian

The Zeeman interaction Hamiltonian [21] is defined as

$$H_z = -\hbar \sum_i \gamma_i \vec{I}_i . \vec{B}_o \tag{1.16}$$

$\vec{B}_o$ is used to specify the static field of the instrument.

$$H_z = -\hbar \sum_i \gamma_i \left[I_{ix} B_{x+} I_{iy} B_{y+} I_{iz} B_z \right] \tag{1.17}$$

Where B_x, B_y and B_z are corresponding components of normalized vectors $\overrightarrow{B_n}$ Generally we consider $\vec{B}_o$ field is set to z-axis direction so that $B_x = B_y = 0, B_z = 1$

Now Equation (1.17) becomes

$$H_z = -\hbar B_o \sum_i \gamma_i \ I_{iz} \tag{1.18}$$

1.4.5.2 R.F field Interaction Hamiltonian

Let us consider a RF field of angular frequency Ω_{rf} and a phase angle Φ applied along the positive x- axis direction produces an oscillating magnetic field and the representation is as follows

$$\vec{B}_{rf}(t) = 2B_{rf} \cos\left(\Omega_{rf} \, t - \Phi\right)\vec{\imath} \tag{1.19}$$

And the interaction energy $E = -\vec{\mu}.\vec{B}$ and quantum mechanical magnetic momentum is $\gamma_i \hbar \vec{I}$.

Therefore the RF field Hamiltonian [22]

$$H_{rf}(t) = -2B_{rf}\, cos\big(\Omega_{rf}\, t - \Phi\big) \sum_i \gamma_i I_{xi} \tag{1.20}$$

B_{rf} is the strength of the applied RF field. The $H_{rf}(t)$ can be viewed as arising from two components that are of equal magnitude and angular frequency, but rotating in opposite directions in the *xy*-plane. This is reason for multiplication factor 2 in the original Hamiltonian in the Equation (1.20)

1.4.5.3 Chemical shift Interaction Hamiltonian

$$H_{cs} = -\hbar \sum_i \gamma_i\, \vec{I}_i.\, \hat{\sigma}_i\, \vec{B}_o \tag{1.21}$$

Where $\hat{\sigma}_i$ is chemical shift tensor. The magnitude of chemical shift is relatively small but it is important especially in high resolution spectra.

1.4.5.4 Direct spin-spin Interaction Hamiltonian

The classical interaction energy between two dipoles [22], of dipole moment $\overrightarrow{\mu_i}$ and$\overrightarrow{\mu_j}$, which are separated by a vector $\vec{r}$ is

$$E_{Dij} = \frac{\vec{\mu}_i.\vec{\mu}_j}{r^3} - \frac{3(\vec{\mu}_i.\vec{r})\big(\vec{\mu}_j.\vec{r}\big)}{r^5} \tag{1.22}$$

$\vec{r}$ points from dipole *i* to dipole *j*, mean $\vec{r}_{ij} = \vec{r}_i.\vec{r}_j$ and classical magnetic moment is replaced with quantum mechanical equivalent as $\gamma\, \hbar \vec{I}$

$$E_D = \sum_i \sum_{j>i} \frac{\overrightarrow{\mu_i}.\vec{\mu}_j}{r_{ij}^3} - \frac{3(\vec{\mu}_i.\vec{r}_{ij})(\vec{\mu}_j.\overrightarrow{r_{ij}})}{r_{ij}^5} \quad (1.23)$$

And hence dipole-dipole interaction Hamiltonian

$$H_D = \frac{\gamma_i \gamma_j \hbar^2}{r_{ij}^3}\left[\vec{I}_i.\vec{I}_j - \frac{3}{r_{ij}^2}[\vec{I}_i.\vec{r}_{ij}].[\vec{I}_j.\vec{r}_{ij}]\right] \quad (1.24)$$

1.4.5.5 Indirect spin-spin Interaction Hamiltonian

Indirect spin-spin coupling also called scalar coupling or j-coupling [21] and its strength is very less compared other interactions. J-coupling contains the information about bond distance and angel and also connectivity of molecules.

The energy involved in scalar coupling between spins *i* and *j* can be written as

$$E_{J\,ij} = \frac{\overrightarrow{\mu_i}.\overrightarrow{\mu_j'}}{r_{ij}^3} \quad (1.25)$$

Where $\overrightarrow{\mu_j'}$is the effective magnetic moment of spin *j*, which is not necessarily collinear with $\vec{\mu}_j$ as a result of the indirect through bond interaction. The scalar coupling tensor $\hat{J}'$ as a 3x3 matrix,

$$\hat{J}_{ij}'.\overrightarrow{\mu_j} = \frac{1}{r_{ij}^3}\overrightarrow{\mu_j'} \quad (1.26)$$

$$E_{J\,ij} = \overrightarrow{\mu_i}\,\vec{J}_{ij}'\;\overrightarrow{\mu_j} \quad (1.27)$$

The Hamiltonian is obtained by replacing $\overrightarrow{\mu_i}$with quantum mechanical magnetic moment $\gamma_i \hbar \overrightarrow{I_i}$.

$$H_J = h \sum_i \sum_{j>i} \overrightarrow{I}_i . \vec{J}_{ij} \vec{I}_j \tag{1.28}$$

1.4.5.6 Quadrupole Interaction Hamiltonian

Nuclei with spin $I > \frac{1}{2}$ exhibit electric quadrupole moment (Q_i) which interacts with the local field gradient in the molecule. The spin Hamiltonian for quadrupolar interaction is

$$H_Q = \sum_i \frac{eQ_i}{2I_i(2I_i - 1)\hbar} \vec{I}_i \hat{V}_i \vec{I}_i \tag{1.29}$$

Where Q is the nuclear quadrupole moment, I is the nuclear spin quantum number, $\hat{V}_i$ is the electric field gradient tensor at the site of nuclei *i*, *e.* is the elementary charge.

If the quadrupolar interaction is much smaller than the Zeeman interaction, secular approximation may be used to discard higher terms.

In the rest of this thesis, we are concerned about dipolar–dipolar interaction. Since the residual dipolar coupling constant is directly related to the structure of the polymer network and is a consequence of dipole-dipole interaction. We will discuss the pulse sequence needed to detect multiple-quantum coherences and obtained experimental result in the chapter 2.

1.5 Conclusions

NMR is one of the best spectroscopy techniques to diagnoses the polymer materials. It is more complex than the other spectroscopy techniques and gives enormous information about the dynamics, structure, chemical compositions etc. Many of NMR experiments can perform on inexpensive low resolution instruments without chemical shift resolution and without Fourier transform of experimental data.

Chapter 2
Multiple-quantum NMR Spectroscopy for Polymer Network Analysis

2.1 Introduction

In this chapter, we will explicate the meaning of multiple-quantum (MQ) coherence in case of spin-1/2 dipolar coupled systems, and review the experimental approaches to accomplish the detection of such a phenomenon and its application to rubber networks. We will focus our interest on the excitation and detection of MQ and more specifically double-quantum (DQ) coherence on the proton (^{1}H) systems under static conditions with low resolution Nuclear Magnetic Resonance (NMR) spectrometer.

The first experimental evidence of MQ phenomenon was carried out with CW NMR spectroscopy in the end of 1950s. However, until the mid-1970s the time domain MQ spectra of this kind were not investigated, due to insufficient developments in theoretical (average Hamiltonian theory) and experimental methods. The overview of most important methods and applications of this phenomenon through 1980 has been described in the literature [25]. A detailed analysis of the theoretical concepts and experimental techniques up to 1982 is found in the reference [26]. The first solid-state MQ experiments were carried out by the group of A. Pines [18, 27] in the middle of 1980s on high field instruments. They were used the samples (like Benzene partially oriented in nematic liquid crystal) where no other NMR methods are necessary to improve the spectral resolution, because the dipole-dipole coupling between spins is much reduced due to high mobility of the system.

2.2 Multiple-quantum NMR

Solid-state MQ NMR methods are outstanding structural elucidation methods for characterization of the network [2] and liquid crystal polymers [18] where direct dipole-dipole interactions can be used to create coherences of high order. After experimental detection of MQ phenomenon several improvements have been accomplished by various research groups, due to realization of robustness and significance of the technique in structure

elucidation in the molecular scale level. Since early 2000's, K. Saalwachter has been working on the development of MQ NMR techniques especially for the application of vulcanized elastomer networks characterization [2, 57]. The MQ coherences can be described by a time-dependent density operator whose elements are completely at sufficient long times. MQ NMR technique allows obtaining distribution of dipolar coupling constant in addition to its value. The following sections will briefly review the basics of MQ NMR.

2.2.1 Dipolar coupling and molecular structure

The dipolar interaction between two spins is evaluated in terms of Hamiltonian and has been derived in chapter 1. An expression for dipolar coupling constant (D_{ij}) between two spins *i* and *j*, separated by distance r_{ij} with an angle θ_{ij} of the *i*-*j* vector relative to the magnetic field (B_o) direction is given by Equation (2.1). The vector diagram of the magnetic dipoles orientation in an external static field (B_o) is as shown in Figure 2.1.

$$D_{ij} = \frac{\mu_o \hbar}{4\pi} \cdot \frac{\gamma_i \gamma_j}{r_{ij}^3} \cdot \frac{1}{2} \cdot (3cos^2\theta_{ij} - 1) \tag{2.1}$$

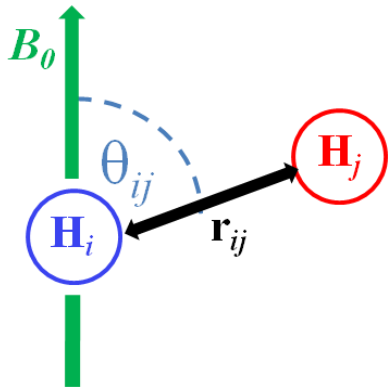

Figure 2.1 *Schematic of dipole-dipole interaction dependency on orientation and separation (r_{ij}) of two dipoles in a static magnetic field (B_0).*

In case of homo nuclear dipolar interaction, the gyromagnetic ratios γ_i and γ_j are equal, and in such a case Equation (2.1) can be reduced to Equation (2.2).

$$D_{ij} = \frac{\mu_o \hbar}{4\pi} \cdot \frac{\gamma^2}{r_{ij}^3} \cdot \frac{1}{2} \cdot (3cos^2\theta_{ij} - 1) \tag{2.2}$$

The local anisotropy motion in the system leaves the residuals of dipolar interaction. Measurement of non-zero time-averaged dipolar couplings from the NMR experimental spectrum therefore can provide enormous information about molecular structure and dynamics [28-30]. The first experimental evidence of such an experiment was carried out by A. Pines group in the early 1980's [31-33] with a benzene molecule oriented in a liquid crystal as well as simulated spectra for different possible structures of symmetric six-carbon systems in the high field NMR.

2.2.2 Realization of multiple-quantum coherences or spectra

MQ coherences are not directly observable with NMR coil like the single-quantum coherences which satisfy the allowed transition between the states with selection rule $\Delta M = \pm 1$. MQ coherence those are satisfy the selection rule $\Delta M \neq \pm 1$ and can be detected indirectly using coherence transfer [28] by two or multi-dimensional spectroscopic methods. These spin-forbidden MQ coherences cannot be created directly but must be excited indirectly with a sequence of RF pulses. The usefulness of observing MQ transitions can be understood by considering the schematic energy level diagram for a system of N coupled spins $I = \frac{1}{2}$ as shown in Figure 2.2.

Now the challenge is to find a way to absorb and emit photons only in groups of '*N*'. Pulse sequences are designed by applying appropriate pulse delays and phases with the advent of quantum mechanical operator formalism [34]. To observe high order, selectivity requires many phase shifts. Due to this reason and also to keep in mind those practicalities of instrumental limitations, the focus is limited to few orders of MQ coherences. W.S.Warren et al. pointed out that 10-quantum transition in a 10-spin system can be enhanced by more than four orders of magnitude and also MQ sequences are much more efficient than normal wideband pumping of selective coherences [33]. J. Baum et al. [31] showed that the dipole-dipole interactions can create coherences of very high order up to 100.

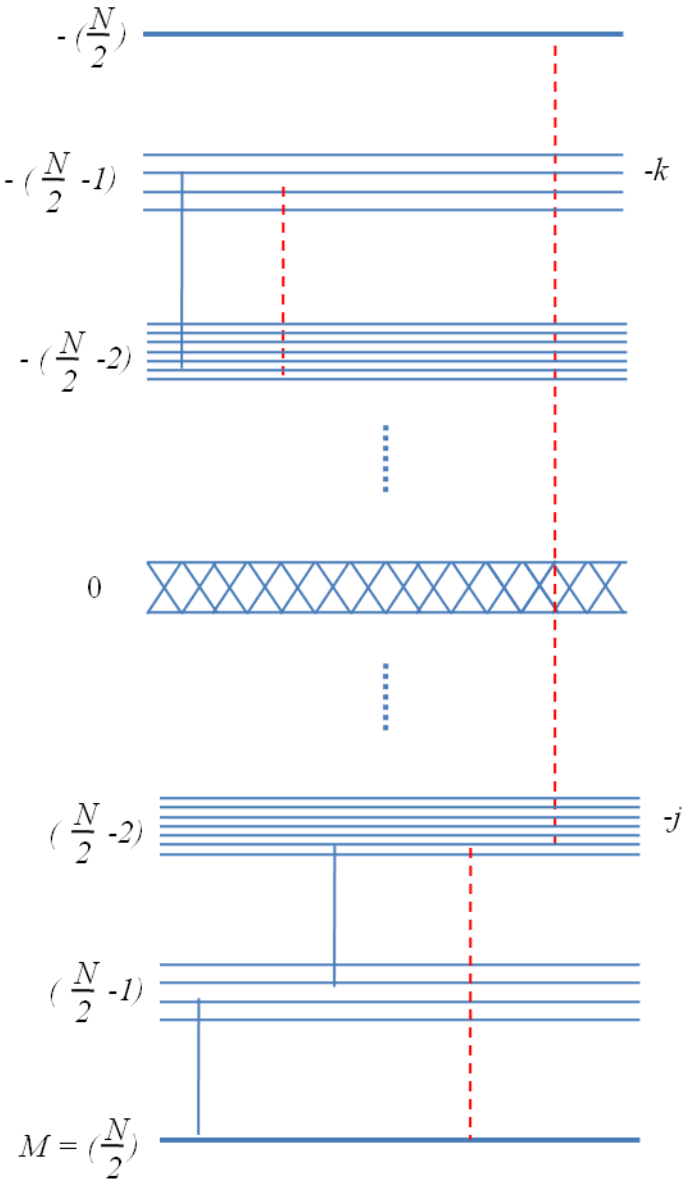

Figure 2.2 *The energy level diagram of N coupled* $\frac{1}{2}$ *spins in the magnetic field. The groups of energy levels are characterized by the magnetic Zeeman quantum number M. The splitting in each groups are due to chemical shifts and couplings between the spins. The solid vertical lines indicate allowed* $(\Delta \boldsymbol{M} = \pm \mathbf{1})$ *one-quantum transitions and the red colored dashed vertical lines indicate forbidden multiple-quantum* $(\Delta \boldsymbol{M} = \pm \boldsymbol{n}, \boldsymbol{n} = \mathbf{0}, \mathbf{1}, \mathbf{2}, \ldots \boldsymbol{N})$ *transitions [33]*

2.3 Average Hamiltonian theory for multiple-quantum NMR

The effect of any sequence of irradiating pulses and delays between the pulses on a general system can be represented by a single unitary transformation *U* called the propagator. Calculating resultant *U* directly by multiplying *U*'s of each part of the sequence is extremely tedious if many eigenstates are involved. By the average Hamiltonian theory, one can avoid these tedious calculations.

The total Hamiltonian, H(t) of a system is given by Equation (2.3).

$$H(t) = H_{int} + H_1(t) \tag{2.3}$$

Where H_{int} is the internal Hamiltonian of the system and it may be due to many effects as discussed in chapter 1. In our present discussion, the interaction is considered as mainly due to direct dipole-dipole interaction. $H_1(t)$is time dependent Hamiltonian arising due to applied radio frequency (RF) and is controlled by experimenter. $H_1(t)$ is termed cyclic with cycle time t_c if $H_1(t)$, propagator $U_1(t)$ are periodic and if t_c is the shortest interval that constitutes a periodic for both $U(t)$ and $H_1(t)$.Propagator $U_1(t)$ is given by Equation (2.4).

$$U_1(t) = Texp[-i\int_0^t H_1(t')dt'] \tag{2.4}$$

Where *T* is the *Dyson time-ordering* operator.

$H_{int}$is considered to be time independent, so *H(t)* is cyclic if $H_1(t)$ is cyclic. If $H_1(t)$ is a pulse sequence made up of an integral number *N* of cycles, the propagator for the entire sequence is the N^{th} power of the propagator corresponding to one cycle, and therefore only a single cycle need to be considered. The propagator for a single cycle can be calculated using Equation (2.5) that constitutes the Magnus expansions.

$$U = \exp(-iHt_c) = \exp[-i(\bar{H}^{(0)}+\bar{H}^{(1)}+\bar{H}^{(2)} \cdots\cdots\cdots + \bar{H}^{(n)} + \cdots\cdots\cdots)t_c] \tag{2.5}$$

Where the terms $\bar{H}^{(0)}$, $\bar{H}^{(1)}$,$\bar{H}^{(2)}$ and $\bar{H}_{int}(t)$ in Equation (2.5) are given by Equations (2.6), (2.7), (2.8) and (2.9) respectively.

$$\bar{H}^{(0)} = \frac{1}{t_c}\int_0^{t_c} \bar{H}_{int}\,(t).\,dt, \tag{2.6}$$

$$\bar{H}^{(1)} = \frac{-i}{2t_c}\int_0^{t_c} dt_2 \int_0^{t_2} dt_1\,[\bar{H}_{int}(t_2), \bar{H}_{int}(t_1)] \tag{2.7}$$

$$\bar{H}^{(2)} = \frac{-1}{6t_c}\int_0^{t_c} dt_3 \int_0^{t_3} dt_2 \int_0^{t_2} dt_1\,\{[\bar{H}_{int}(t_3), [\bar{H}_{int}(t_2), \bar{H}_{int}(t_1] + \left[\bar{H}_{int}(t_1), [\bar{H}_{int}(t_2), \bar{H}_{int}(t_3)]\right]\} \tag{2.8}$$

$$\bar{H}_{int}(t) = U_1^{-1}(t) H_{int} U_1(t) \tag{2.9}$$

This is merely a *Magnus expansion* of the propagator in powers of the cycle time.

The average Hamiltonian expansion is a perturbation expansion in powers of a parameter t_c that has a physical meaning; t_c and $H_{int}(t)$ are simultaneously varied by lengthening the sequence.

For this reason, $\bar{H}^{(i)}$ is termed a correction term of order *i* and is proportional to$(t_c)^i$.

$\bar{H}^{(0)}$ is the zero order or average Hamiltonian, and *H* is the effective Hamiltonian.

The advantage of propagator operator given by Equation (2.5) is that, a complex time dependent process has been expressed by a time independent Hamiltonian.

The pulse sequences are usually designed so that $\bar{H}^{(0)}$ has some particular desired property and then high-order terms are minimized. The general two dimensional MQ experiments consist of the four steps or periods as shown in Figure 2.3

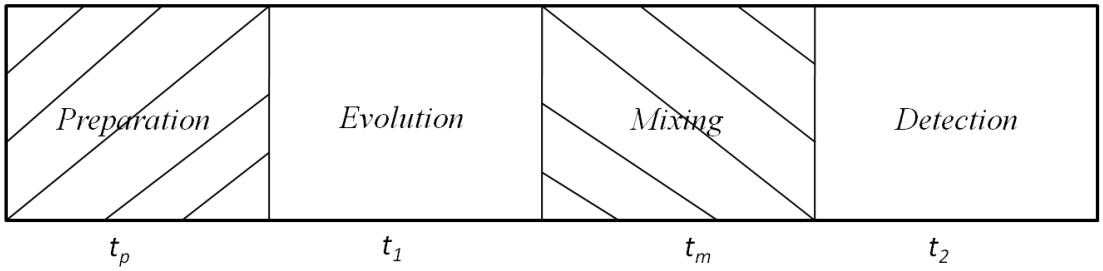

Figure 2.3 *General Schematic of 2-D NMR experiments to detect multiple-quantum coherences.*

1. Preparation period: The even order coherence can realize with the dipolar Hamiltonian and is given by Equations (2.10) and (2.11).

$$\bar{H}(0) = \frac{1}{3}\left(H_{yy} - H_{xx}\right) \tag{2.10}$$

$$\bar{H}(0) = -\frac{1}{2}\sum_{i<j} D_{ij}\left(I_{i+}I_{j+} - I_{i-}I_{j-}\right) \tag{2.11}$$

This desired dipolar coherence Hamiltonian average is obtained by the application of number of pulses and this pulse train is commonly called pulse sequence. The DQ pulse sequence is shown in Figure 2.4. This sequence consists of eight pulses and is subdivided into four subcycles separated by dotted lines in the Figure 2.4. By proper combination of two or more subcycles, the overall pulse sequence could compensate the RF inhomogeneities and resonance offset effects [31]. The delays between π/2 pulses of duration t_p are Δ_1 and $\Delta_2=2\Delta_1+t_p$ and the total cycle time t_c is equal to $12(t_p+\Delta_1)$.

2. Evolution period: During the evolution period, the system responds to the internal Hamiltonian (H) as given by Equation (2.12)

$$H = H_z + H_{zz} \tag{2.12}$$

Where H_z contains order dependent offset term resulting from time proportional phase incrimination. The interferogram is mapped out point-by-point for successive values of t_1. The spectral width of the MQ spectrum is given by $1/\Delta t_1$ and the number of orders detected = ± n_{max} is determined by the phase increment, $\Delta\phi = 2\pi/2\ n_{max}$. Both Δt_1 and $\Delta\phi$ must be chosen so that all signals from different coherence orders fit into the available without aliasing and overlapping.

3. Mixing period: After evolving in the local fields for a time t_1, the MQ coherences are converted to observable single quantum coherences through the action of mixing period propagator. Since the average Hamiltonian of Equation (2.11) is a pure DQ operator, time

reversal is accomplished here by a simple 90^o phase shift of each pulse in the eight-pulse cycle. The mixing period therefore contains pulses with phases y and $\bar{y}$, irrespective of any manipulations of the phases in the preparation period.

4. Detection period: After mixing for time (t_m), a delay is inserted during which spurious transverse magnetization is allowed to decay. The desired signal, stored as population information along the *z*-axis, is detected with a $(\pi/2)_x$ pulse, followed by a 100 μs spin-locking pulse along *y*. Spin temperature inversion, achieved by a 180^o phase alteration of the detection pulse, is used to reduce artifacts arising from receiver ringing. A single point in t_2 is then sampled for each values of t_1 with width of the single-quantum spectrum determining the optimum receiver bandwidth.

In time-domain MQ spectroscopy, MQ transitions are detected indirectly in three-step process, in contrast to CW detection.

1. Excitation of MQ coherences
2. Free evolution, normally in the absence of RF perturbations
3. Conversion into observable single-quantum coherence which is subsequently detected.

This is as same as two dimensional spectroscopy as explained in earlier in this chapter.

All NMR experimental approaches used for analysis of network structures rely on the anisotropy of segmental motions in polymeric systems. From this anisotropy of segmental motions, hydrogen quadruple and dipolar interactions are incompletely averaged, leaving small residual quantities. Measurement of these residual interactions is usually carried out by analysis of line shape or relaxation functions [35-40], or by application of elaborated pulse sequences [41-51]. These pulse sequences are designed to be more sensitive only to the desired interactions and to suppress unwanted contributions from, slow dynamics or susceptibility effects etc. MQ NMR technique is fall into second category.

The original pulse sequence [18] designed to obtain such a desired interaction is shown in Figure 2.4. The total excitation (t_{exe}) and reconversion (t_{rec}) times are expressed as $t_{exe} = t_{rec} = n_c t_c$. t_c and n_c denotes time for one cycle and number of cycles respectively. The corresponding excitation or reconversion block of such a pulse sequence is given by Equation (2.10). When applied for longer times, the stability of this sequence has been proved to be challenged by flip-angle deviation caused by weak B_1 field heterogeneity in combination with considerable shift dispersion caused by shimming problem due to irregular sample shape in high field. Especially with low field instruments, there are strong field inhomogeneities, pulse

imperfections etc. that causes losses in the signal. To avoid such effects, similar to Tycko's [30] work, who has introduced 24 180^o pulses in order to achieve good offset compensation, Saalwachter found that 4 180^o pulses in between every 2 90^o pulses is enough to achieve desire stability and also keep the duty cycle at the minimum and such a pulse sequence is shown in Figure 2.5 with appropriate delays between the pulses $\Delta_1 = t_c/24 - t_p/2$ and $\Delta_2 = t_c/12 - 3t_p/2$, where t_p is 90^o pulse length. The clear differences in reference and DQ intensity obtained by original Baum-Pines [18] (Figure 2.4) and modified or improved Baum-Pines [2] (Figure 2.5) are shown in Figure 2.16.The pulse sequence could be applied using different t_c and n_c. The DQ selection was performed using four-step phase cycle for the carrier phase (Φ_o) of the reconversion period ($\Delta\Phi$= 0^o, 90^o, 180^o, 270^o) while inverting the receiver phase for alternating scans. This yields an overall 16-step phase cycle. Due to this reason, in DQ experiments, minimum 16 scans should be used for data acquisition for completion of phase cycling. The different stages of multiple-quantum experiments scheme is shown in Figure 2.6. τ_d before read out pulse is optional dephasing delay, which is set to zero in our experiments.

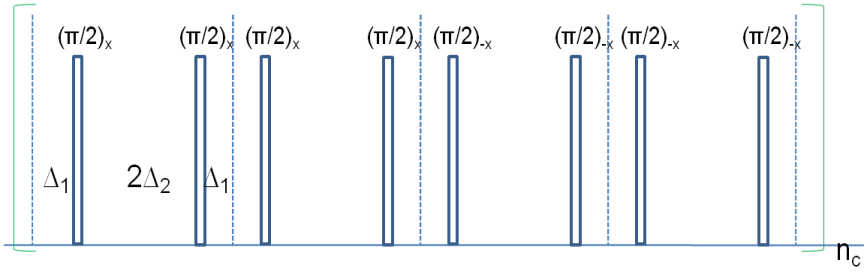

Figure 2.4 *Multiple-quantum pulse sequence with appropriate delays between 90^o pulses and phases.*

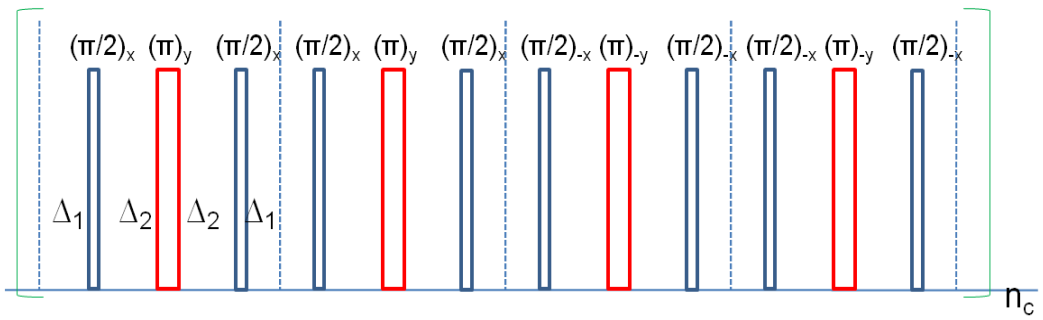

Figure 2.5 *Multiple-quantum pulse sequence with 180^o phase cycling in between 90^o pulses.*

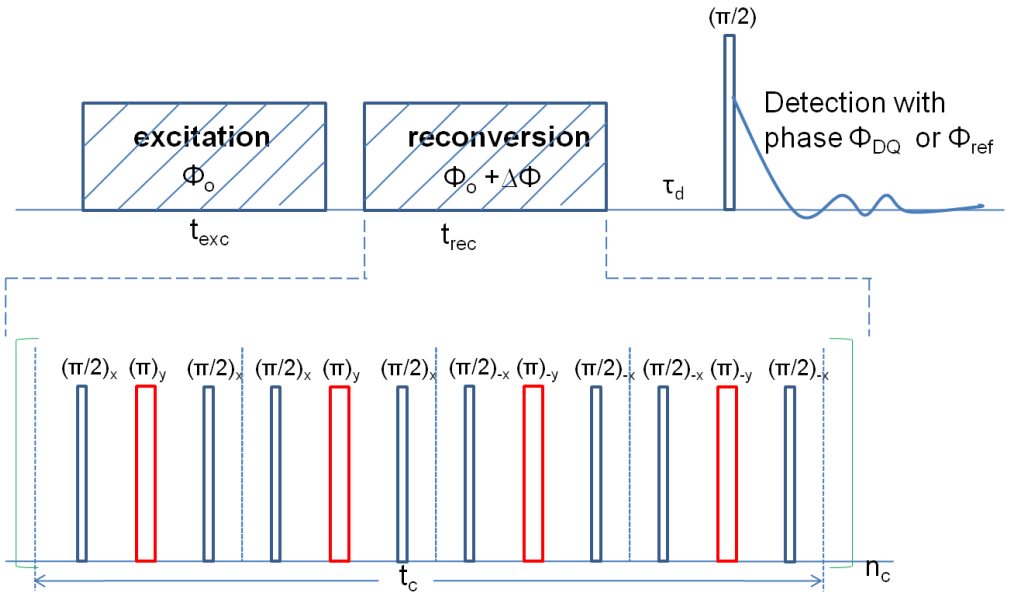

Figure 2.6 *Stages of a typical multiple-quantum experimental scheme*.

2.4 Residual dipolar coupling, order parameter relation with crosslink density

Residual tensorial NMR (^{2}H quadrupolar, ^{1}H dipolar) interactions originate from imperfect motional averaging of chain segments fluctuating rapidly between topological constraints such as crosslinks or chain entanglements, and may reach magnitudes of several percent of the corresponding static interaction. The autocorrelation function ($C(|t_a - t_b|)$ is usually taken as a fundamental object for the description of the polymer chain dynamics and is expressed with Equation (2.13)

$$C(|t_a - t_b|) = \langle P_2(\cos\theta_{t_a}) \cdot P_2(\cos\theta_{t_b}) \rangle \tag{2.13}$$

Where

$$P_2(\cos(\theta)) = \frac{1}{2}(3\cos^2\theta - 1) \tag{2.14}$$

The autocorrelation function clearly is a decreasing function of time, but a characteristic behavior exists for crosslinked polymers. The characteristic of a network consists of two behaviors: Fast segmental motions, which are destroy more or less 99% of the correlation very rapidly (in the time scales of ns-μs), but the residual correlation (due to the crosslinks and to topological constraints) decreases more slowly, only through cooperative motions (in the time scales of ms-s) such a behavior is as shown in the schematic Figure 2.7.

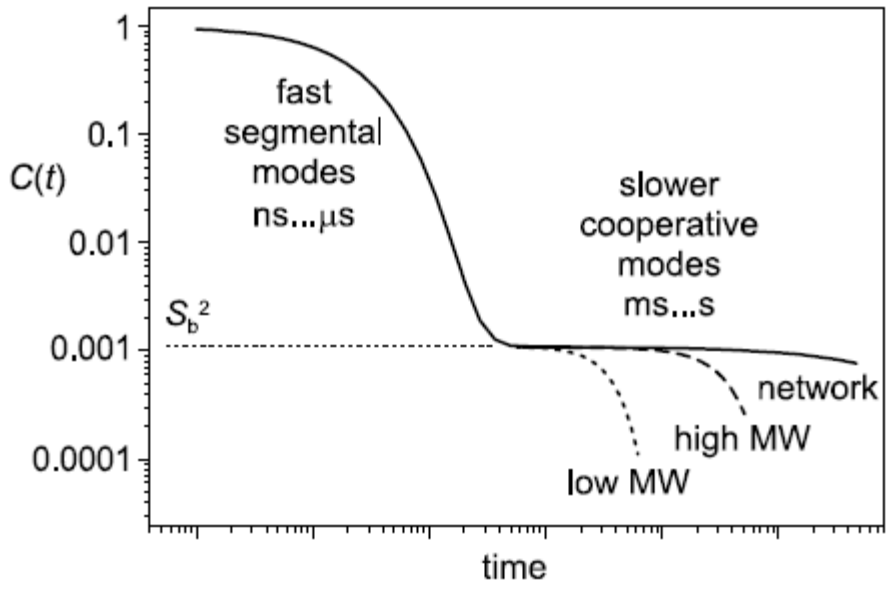

Figure 2.7 *Orientation autocorrelation function for various chain dynamics in polymer melts above the glass transition temperature [2].*

The following couple of assumptions or hypotheses have been the basis for obtaining separation of time scales in autocorrelation functions.

(i) The topological constraints are constant during the time scale of the NMR experiment and (ii) All local segmental motions are fast on the basis of the Figure 2.7.

Under these hypotheses, the autocorrelation function presents a plateau between these two time scales, whose height is by definition the square of the order parameter S_b^2.

The experimentally obtained residual dipolar coupling D_{res} is directly proportional to dynamic chain order parameter S_b and given by Equation (2.15)

$$S_b = k\frac{D_{res}}{D_{stat}} \tag{2.15}$$

Where

- D_{res} "*residual dipolar coupling*" as a result of time averaging of the dipolar tensor over the time in the plateau region
- D_{stat} "*static limit dipolar coupling*" obtained from the simulations by assuming that there would be no motion.
- k accounts for the averaging due to very fast intra-segmental motions (pre-averaging).

Due to lack of exact timescale separation, S_b or equivalently, D_{res} is not easily accessible in polymer melts or poor crosslinked systems.

Orientation dependence of dipolar/quadruple coupling is given by the second Legendre polynomial (P_2) of cosine of angle between the magnetic field direction and vector $\vec{r}$ joining two spinning dipoles as written in Equation (2.16).

$$P_2(\cos(\theta)) = \frac{1}{2}(3\cos^2\theta - 1) \tag{2.16}$$

By pre-averaging the vector $\vec{r}$ becomes the polymer backbone.

The basic formula for $S_b$is given by Equation (2.17).

$$S_b = \frac{D_{res}}{D_{stat}} \cdot \frac{1}{\langle P_2(\cos\alpha)\rangle} \tag{2.17}$$

But assuming a fast-limit pre-averaging of the static-limit coupling by local segmental motions which are cylindrically symmetric with respect to polymer backbone, a simple Legendre addition theorem may be used to show that the average denominator $\langle ... \rangle$ can be omitted in actual calculations.

The order parameter S_b also defined by Equation (2.18), according to Kuhn, the pre-factor $\frac{3}{5}$ is obtained under the assumption of Gaussian statistics for the vector r [53]:

$$S_b = \frac{3}{5}\frac{r^2}{N} \tag{2.18}$$

Where $r^2 = \boldsymbol{r}^2/\boldsymbol{r}_0^2$, $\boldsymbol{r}$ is the end to end vector between constraints (crosslinks), and $\boldsymbol{r}_0$ is the end to end vector for chains in the unperturbed melt state.N is the number of Kuhn segments between constraints.

According to literature [46] chains can take up different conformations, but on average, they are oriented parallel to the direction that connects the two adjacent crosslinks or entanglements and hence the lower limit for the value of the dynamic order parameter S_b of a polymer chain between two spatially fixed points depends only on its number of Kuhn segments, N, between them [54] and hence S_b is defined by Equation (2.19).

$$S_b = \frac{3}{5} \cdot \frac{1}{N} \tag{2.19}$$

Equation (2.19) is derived from Equation (2.18) by substituting$r^2 = 1$.

The order parameter S_b is also linked to the *tube diameter* (according to Rouse tube model of polymer dynamics) [2]. Through the model of semi-flexible chains, it is possible to obtain an equation for the molar mass between crosslinks M_c as presented in Equation (2.20).

$$M_c = \frac{3}{5} \cdot \frac{\frac{D_{stat}}{k}}{D_{res}} \cdot \frac{C_\infty}{4c^2} \cdot M_0 \tag{2.20}$$

Where M_0 is the molar mass of the monomer unit, C_∞ is Flory's characteristic ratio, $c = l/l_p$ is the ratio between the root-mean-square bond length l and the projection length l_p of the bond to the polymer back bone at it maximum extension.

The numerical constants appearing in the Equation (2.20) are summarized in the Table 2.1 for polybutadiene and polyisoprene polymers [55].

Table 2.1 *The static residual dipolar coupling constant, Flory characteristic ratio ($\boldsymbol{C_\infty}$), root mean square bond length (I) and the projection length(I_p) of the bond to the polymer backbone at maximum extension (c) and molar mass of monomer unit (M_o) for natural rubber (or polyisoprene) and polybutadiene polymers.*

Polymer	$\frac{\boldsymbol{D_{stat}}}{k}$ (Hz)	$\boldsymbol{C_\infty}$	$\boldsymbol{c}$	$\boldsymbol{M_0}$ (g/mol)	$\boldsymbol{M_c}$ $(Hz\ Kg/mol)$
Natural rubber	2πx 6300	4.7	0.7	68.1	$\frac{617}{D_{res}/2\pi}$
Polybutadiene	2πx 8100	4.9	0.7	54.1	$\frac{656}{D_{res}/2\pi}$

2.5 Experimental

2.5.1 Solid-state NMR Spectroscopy

Solid-state ^{1}H MQ TD-NMR experiments were carried out on a Bruker minispec mq20 spectrometer operating at a resonance frequency of 19.65 MHz with a 90^o pulse length of 2.2 µs and a dead time of 14 µs and acquisition was done with128 scans in order to be more

precise and obtain high signal to noise ratio. The recycle delay had set according to T_1 relaxation time measurement of each sample. Two 3 mm thick and 7 mm diameter circular disc samples were centered in a standard minispec 8 mm inner diameter glass tube. Sample tube thermalized inside the instrument 10 minutes before starting the experiment and spectrometer (minispec) was also set to the temperature minimum 6 hours prior to starting the experiment, to stabilize the magnetic unit temperature and avoid the temperature gradient in the sample surroundings. All the measurements were performed at 353 K temperature. Only to show the temperature independence of network parameters (D_{res}) well above the glass transition temperature, measurements were performed at variable temperature.

2.6 The network parameters obtained from multiple-quantum data

2.6.1 MQ NMR data analysis

The success of MQ NMR technique is that it not only provides build-up curve that is dominated by spin-pair DQ coherences[45] which contains structural information but also provides the access to fully dipolar-refocused MQ decay function which can be used independently to analyze the effect of dynamics on the measured data. By the simple assumption that, in networks, where larger scale chain dynamics (free dangling chains or sol in a network etc.) is mostly absent, the shape of the MQ decay is almost identical to the relaxation part of the DQ build-up signal, such that a temperature independent normalized build-up function can be obtained that solely depends on the network structure.

In addition to DQ signal intensity I_{DQ} the reference signal intensity I_{ref} is obtained with the very same pulse sequence, but with missing receiver phase inversion for alternating scans. This signal is therefore due of all magnetization which has not evolved into DQ coherence after t_{exc} and is denoted reference signal and hence allowed to separate structural information from the dynamics. The reference (I_{ref}) and DQ (I_{DQ}) intensities of typical MQ experiment are shown in Figure 2.8. The sum of two signal intensities is defined as $I_{\Sigma MQ} = I_{ref} + I_{DQ}$. In networks the relaxation contributions to I_{DQ} and $I_{\Sigma MQ}$ are nearly equal, such that the effect of molecular motions (dynamical information) on I_{DQ} can be removed by point-by-point division to

give I_{nDQ} and is called normalized double-quantum intensity. Note that experimental intensities are functions of DQ evolution times (τ_{DQ}).

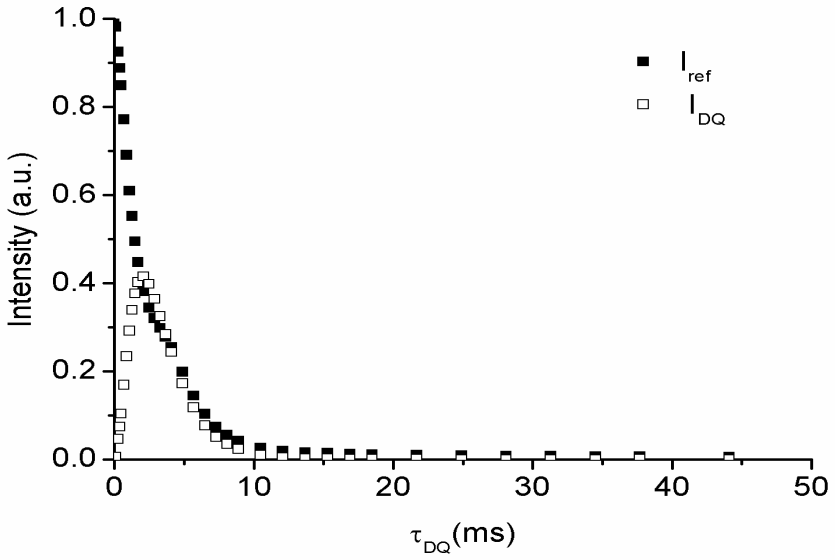

Figure 2.8 *Typical two sets of data obtained from MQ NMR experiment for the sample NR5.*

The normalization of DQ signal intensity with $I_{\Sigma MQ}$as shown in Equation (2.21), I_{nDQ} has to attain a long-time intensity plateau at 50% (because $\mathrm{I_{DQ}}$ only contains half of the excited quantum orders) if the investigated material consist only elastically active network chains. However in real networks, additional components such as short dangling chains, sol or some solvent may be present and causes $I_{\Sigma MQ}$ slowly decayingas represented with dotted lines in Figure 2.9.

The normalized build-up curve intensity (I_{nDQ}) is expressed by Equation (2.21) and is a function of the excitation plus reconversion time τ_{DQ} which is given by Equation (2.22).

$$\mathrm{I_{nDQ}} = \frac{\mathrm{I_{DQ}}}{\mathrm{I_{ref}} + \mathrm{I_{DQ}}} = \frac{\mathrm{I_{DQ}}}{I_{\Sigma MQ}} \tag{2.21}$$

$$\tau_{DQ} = a(\psi) n_c t_c \tag{2.22}$$

Where τ_{DQ}, $a(\psi)$, n_c and t_c are DQ excitation time, scaling factor, number of cycles and cycle time respectively. The normalized DQ intensity I_{nDQ} depends on the duty cycle of the sequence [56]. Here τ_{DQ} can increase by increasing the number of cycles or cycle time. The scaling factor is given by Equation (2.23).

$$a(\psi) = 1 - 12 \cdot \frac{t_p}{t_c} = 1 - \frac{3}{4}\psi \tag{2.23}$$

Where

$$\psi = 16\, t_p / t_c \tag{2.24}$$

Where t_p is 90° pulse length, t_c is the cycle time.

The duty factor ψ governs the performance of a multiple-pulse sequence.

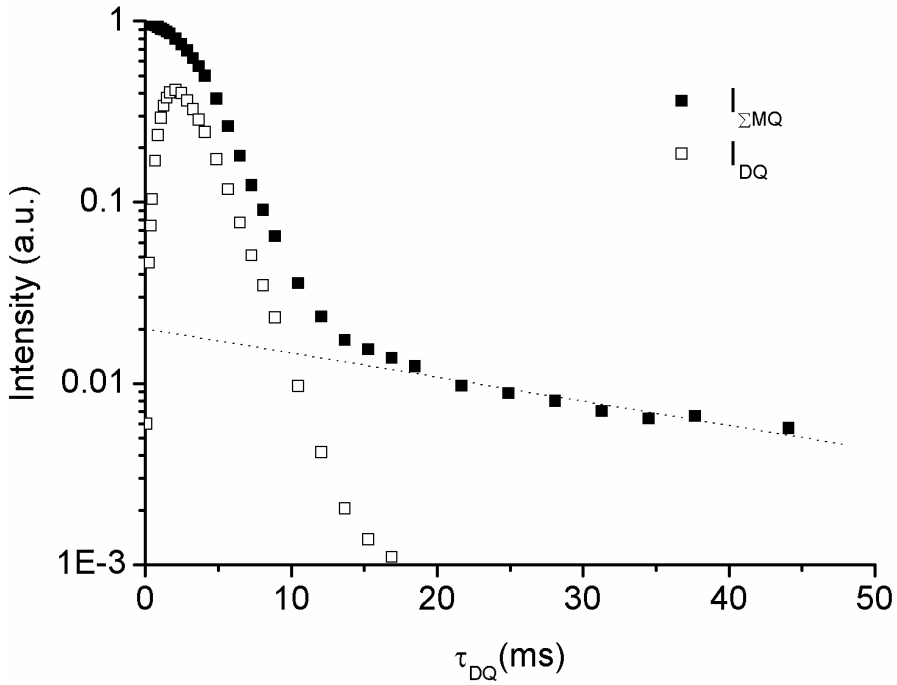

Figure 2.9 *DQ and MQ (sum of I_{ref} and I_{DQ}) intensities versus DQ excitation time of NR5 sample, slowly decaying component in the MQ intensity is arise from network defects(such as dangling ends, sol etc.).*

It is necessary to remove these slowly relaxing contributions by suitable fitting and subtraction of the tails. After subtraction of slowly decaying components, we reach stable plateau in network relevant time scales according to Equation (2.25).

$$I_{nDQ} = \frac{\mathrm{I_{DQ}}}{\mathrm{I_{ref}} + \mathrm{I_{DQ}} - B\exp(-2\tau_{DQ}/T_{2B})} \tag{2.25}$$

Where B component is the long tail exponential in I_{ref} - I_{DQ}

The normalized DQ intensity I_{nDQ} according to Equation (2.21) without subtracting the slow relaxing component is shown in Figure 2.10.

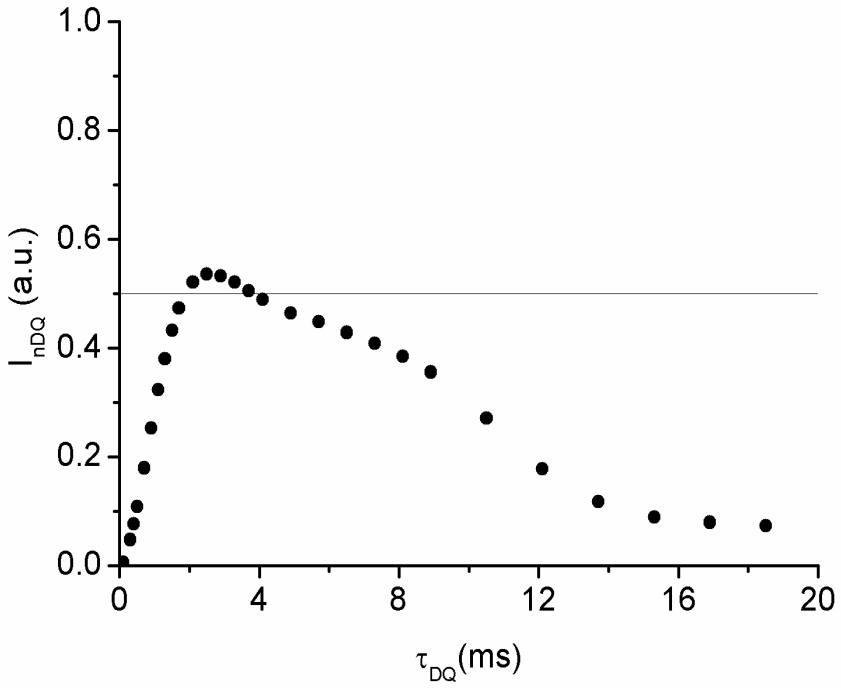

Figure 2.10 *Point-by-point normalized DQ intensity of sample NR5 according to Equation (2.21), the slow decaying is due to the additional components (dangling ends, sol fraction etc.)*

To remove the slow decaying part, plot $I_{ref} - I_{DQ}$ in a y-log scale and (starting from nearly 10 ms) a long exponential tail is seen and subtracts it from I_{nDQ}. Moreover, if with this long tail subtraction I_{nDQ} does not tend to 0.5, then a procedure is necessary in order to adjust this. Second exponential is needs to subtracted. We plot $I_{ref} - I_{DQ}$ (the new I_{ref}) in a y-log scale and subtract it from I_{nDQ} as shown in Figure 2.11.

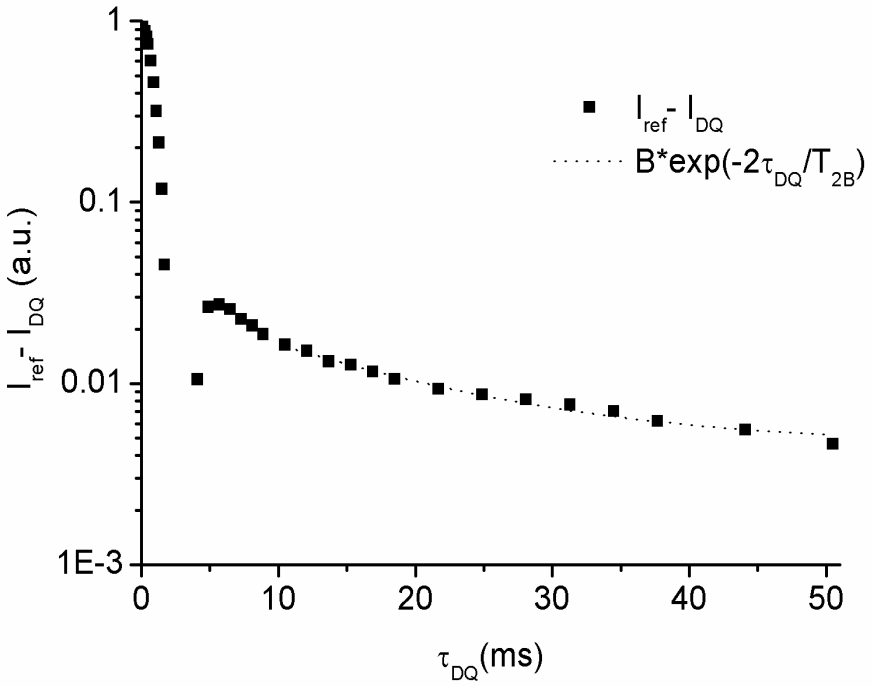

Figure 2.11 *I_{ref}-I_{DQ} of NR5 sample fit with exponential function (dotted line) in order to subtract slowly relaxing components and reach stable plateau of I_{nDQ}*

The subtraction of slowly decaying exponential tail from I_{nDQ} according to Equation (2.25), the normalized intensity reached way better to 0.5 plateau shown in Figure 2.12.

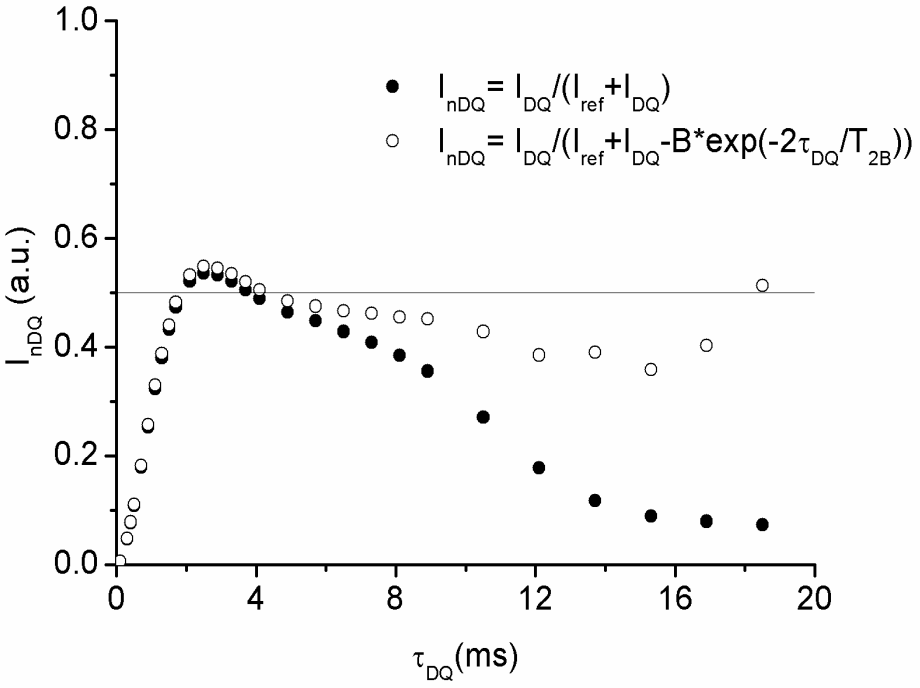

Figure 2.12 *Comparison of NR5 sample normalized intensity after subtraction of single exponential tail. The corrected I_{nDQ} reached close to plateau at 0.5.*

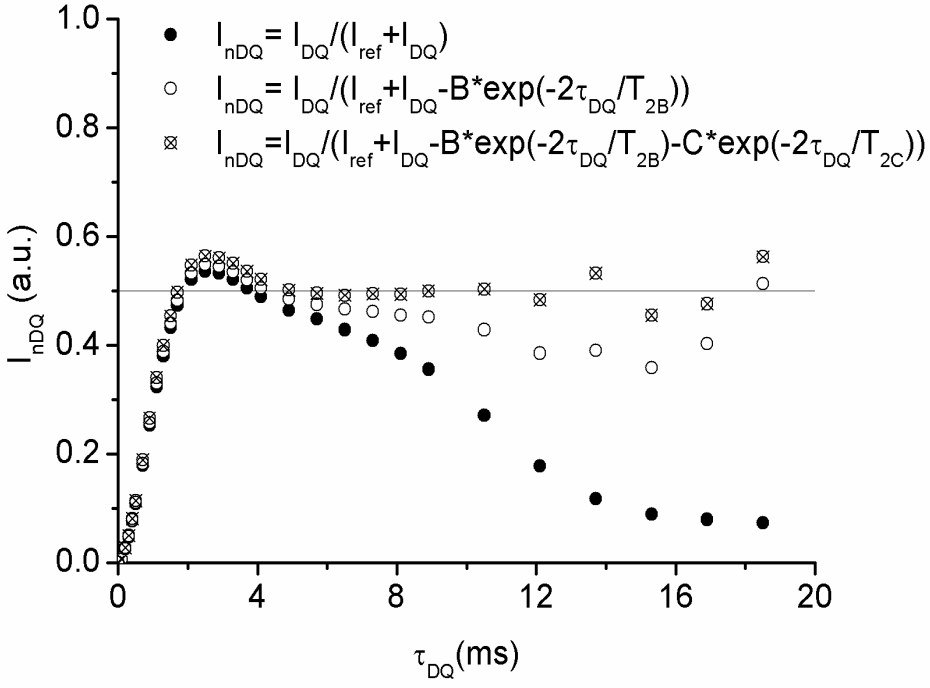

Figure 2.13 *Comparison of NR5 sample normalized intensity after subtraction of single and double exponential decay tail. The corrected I_{nDQ} reached a plateau at 0.5 even for longer times after second exponential tail subtraction.*

The exponential tail (slow relaxation components) corrected I_{nDQ}curves could analyze in quasi-static limit by fitting with Equation (2.26) and obtain single average D_{res}.

$$I_{nDQ}(D_{res}) = \frac{1}{2}\left(1 - \exp\left[-\frac{2}{5}D_{res}^2\tau_{DQ}^2\right]\right) \tag{2.26}$$

The obtained coupling constant (D_{res}) is directly proportional to crosslink density, $1/2M_c$ according to Equation (2.20). The static dipolar coupling constant is known for studied polymers from the literature were given in Table 2.1. The Equation (2.26) approximates the very well I_{nDQ} up to 0.45 and allows to measure average D_{res}.To evaluate not only D_{res}but also possible distribution effects, I_{nDQ} can be fitted under the assumption of Gaussian distribution of dipolar couplings, which yields both an average apparent coupling constant(D_{res}) and its standard deviation(σ) characterizing the distribution width in units of rad/s. A numerical inversion procedure based on Equation (2.27) with σ→0 as kernel function and fast Tikhonov regularization [58, 59] had been used to obtain quantitative picture of residual dipolar coupling constants [56].

$$I_{nDQ}(D_{res},\sigma) = \frac{1}{2}\left(1 - \frac{exp\left\{-\frac{\frac{2}{5}D_{res}^2\tau_{DQ}^2}{1+\frac{4}{5}\sigma^2\tau_{DQ}^2}\right\}}{\sqrt{1+\frac{4}{5}\sigma^2\tau_{DQ}^2}}\right) \tag{2.27}$$

When the samples shows narrow distribution of dipolar couplings both regularization and fitting with Equation (2.27) works well and gives same results and also perfectly define the initial raise in I_{nDQ} as seen for sample NR5 in Figure 2.12 and 2.13.

However, in samples where the distribution is broader or inhomogeneities in the spatial distributions, the initial rise of the experimental build-up cannot be described by the Gaussian fit (Equation (2.27)) as is particularly need for randomly crosslinked inhomogeneous network analyses. In such as cases the regularization procedure is the preferred approach [60].

Due to this reason experimental data were analyzed using fast Tikhonov regularization (*ftikreg*) procedure [61] in the present work to obtain the average residual dipolar coupling constant (D_{res}) and its distribution.

2.6.2 Fast Tikhonov regularization (ftikreg) procedure for MQ data analysis

In inhomogeneous polymer networks with broad or even multimodal distribution of D_{res} such as spatially separated bimodal or multimodal chain length distributions, the Equation (2.26) does not give a proper fit, because it only considers a single D_{res} and is suit well for I_{nDQ} up to 0.45 only and corresponding time limit of DQ excitation $\tau_{DQ=2.4/D_{res}}$ resulting systematic error in the component fraction and distribution shape obtained by *ftikreg*. The response is then generally given by a Fredholm distribution integral Equation (2.28).

$$g(\tau_{DQ}) = \int_0^\infty k[D_{res}, \tau_{DQ}]\, f(D_{res}) dD_{res} \tag{2.28}$$

Where $g(\tau_{DQ})$, $f(D_{res})$ and $k[D_{res,}\, \tau_{DQ}]$ represents function contains experimental obtained information, required distribution function and kernel function respectively.

In addition, the regularization result is sensitively dependent on a user-defined error parameter ε, which should ideally reflect the uncertainty for each data point. This uncertainty, however, is not constant for normalized I_{nDQ} data, as the noise-related error in the two experimental functions is constant, but its relative importance increases at long times due to division of small quantities and more details can be found in the ref [61].
The required distribution functions $f(D_{res})$ in Equation (2.28) is not directly obtained from the experimental data but it is related with experimentally obtained $g(\tau_{DQ})$ and is obtained with an operator Equation (2.29):

$$g = Af \tag{2.29}$$

Therefore the inverse of Equation (2.29) is of interest and can be written as Equation (2.30).

$$A^{\dagger} g = f \tag{2.30}$$

In Equation (2.30), instead of exact g value, noise data g_{ε} with a noise level ε is available and is expressed as Equation (2.31).

$$\|g_{\varepsilon} - g\| \leq \varepsilon \tag{2.31}$$

If the inverse operator $A^{\dagger}$ of A exists but is discontinuous, Equation (2.29) is called ill-posed and the solution has to be calculated numerically. In order to solve this problem, Tikhonov proposed a variation algorithm where the regularization parameter α, which quantifies a smoothing of the fitted distribution and stabilizes the result, is found such that Equation (2.32) is fulfilled.

$$\|Af_{\alpha} - g_{\varepsilon}\| = \varepsilon \tag{2.32}$$

Tikhonov regularization is that it calculates the regularization parameter α and thus the resulting distribution for a given error parameter ε, which in turn is directly related to the known noise of the measured input data g_{ε}. The meaningful ε has to choose, not to overestimate nor underestimate the accuracy of measured input data. The choice of meaningful data is indicated with arrow in the Figure 2.14.

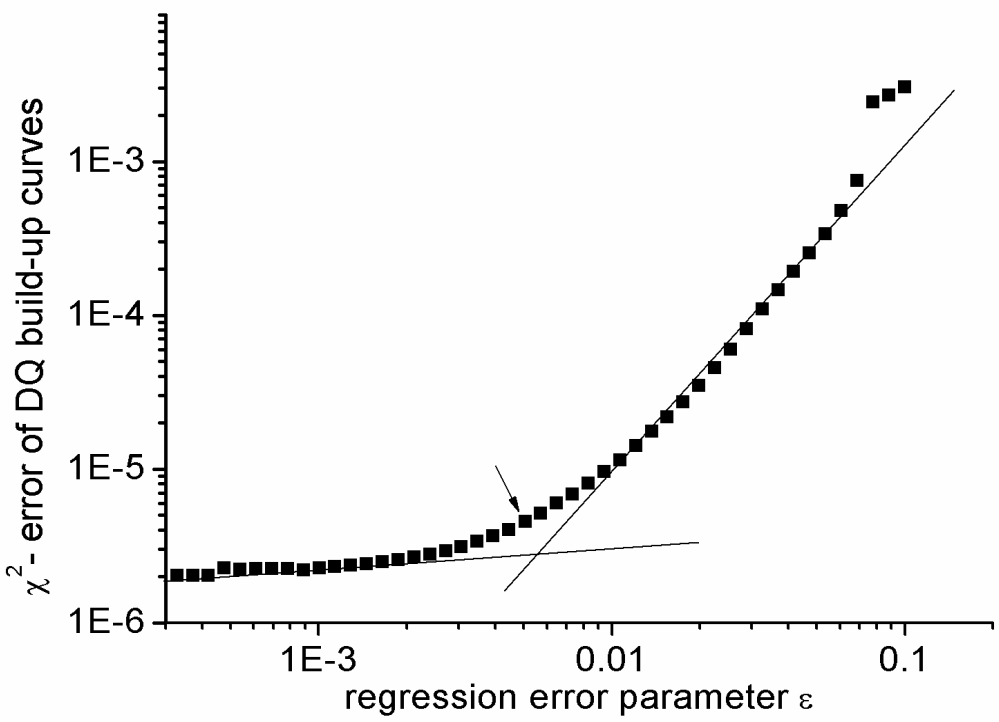

Figure 2.14 *Calculated χ^2 for series of error parameter* ***ε*** *of NR5 sample data. The appropriate* ***ε*** *parameter is indicated with arrow.*

The comparison of experimental data after removing appropriate exponential decay intensity by applying above discussed treatment are overlapped very well with fast Tikhonov regularization (*ftikreg*) procedure simulated build-up curves seen in Figure 2.15.

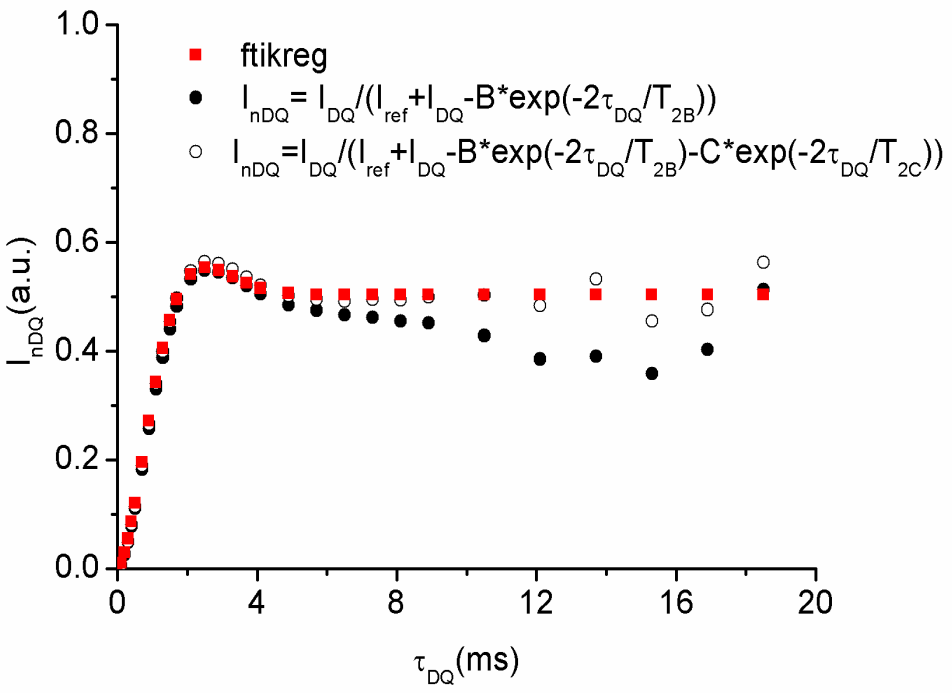

Figure 2.15 *Comparison of normalized DQ intensity (I_{nDQ}) build-up curves of NR5 (3.1 phr sulfur) sample after exponential tail correction and regularization data obtained by applying ftikreg programme.*

2.6.3 Performance of MQ experimental schemes

As explained elsewhere [2] the performance of original Baum-Pines and modified (improved) Baum-Pines sequence is clearly seen from the Figure 2.16. The 180^o compensated pulse improves the performance of the sequence by avoiding pulse imperfections, field inhomogeneities etc. Due to the loss in the signal, estimated D_{res} suffers an error. The D_{res} constant of NR5 sample obtained using two MQ sequence is shown in Table 2.2.

The D_{res} obtained from the original Baum-Pines sequence has underestimated due to considerable signal loss causes error in D_{res} is around 52 %. The error is clearly seen from the drastic change in the initial slope of DQ build-up curve as shown in Figure 2.17. The DQ excitation times could increase by increasing number of cycles (n_c) or increasing cycle times (t_c) or both. We were increased the t_c and kept n_c =2 to compare both the sequences. The variable number of cycles (n_c) also used to check the performance and the corresponding

reference and DQ intensity are plotted in Figure 2.18. Saalwachter et al. reported that n_c =1, version apparently fails to compensate for imperfections at long times and also demonstrated that with n_c increment experiments, DQ build-up is slightly less efficient. To improve long-time performance of time-incremented MQ experiments, it is recommended to use n_c=2 with second cycle inverted phase. The D_{res} values obtained from the variable n_c data is plotted in Figure 2.18 and the corresponding values are reported in Table 2.3. It is clear that, the initial raise of DQ intensity is not much influenced with increasing n_c but there is a considerable decreasing D_{res} trend is observed. Due to the above discussed facts and literature recommendations, throughout the present work, the modified (improved) Baum-Pines pulse sequence with increasing cycle times at constant number of cycles, n_c =2 have been applied.

Table 2.2 *Comparison of D_{res} constant obtained from two different MQ pulse sequence.*

MQ Pulse sequence	***$D_{res}/2\pi$ (Hz)***
Original Baum-Pines[18]	132
Modified Baum-Pines[2]	251

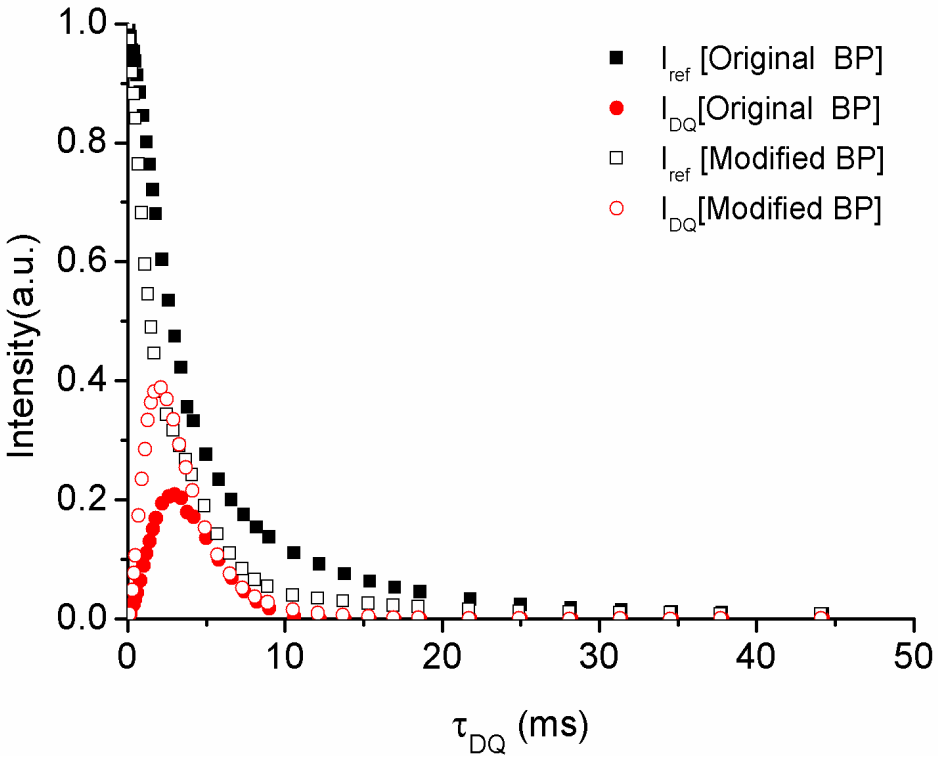

Figure 2.16 *Comparison of Original Baum-Pines (BP) sequence and modified Baum-Pines sequence results of NR5 sample, performed on low field instrument.*

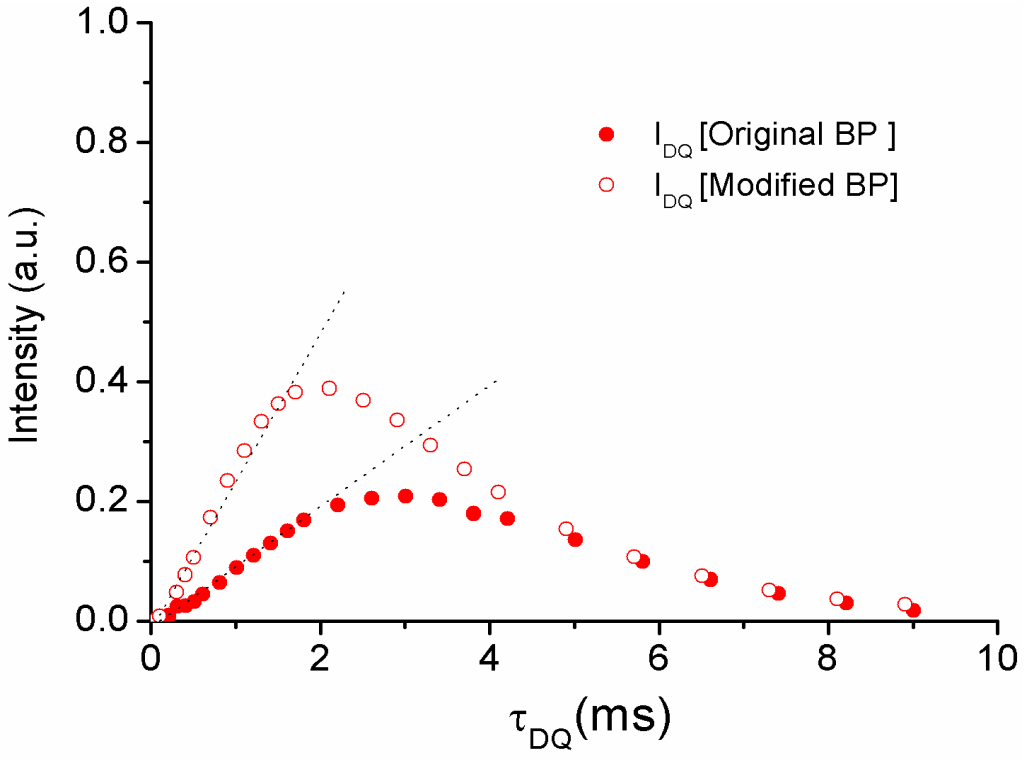

Figure 2.17 *DQ intensities of NR5 sample obtained by original and modified Baum-Pines pulse sequence. The change in slope of initial build-up intensity is clearly seen.*

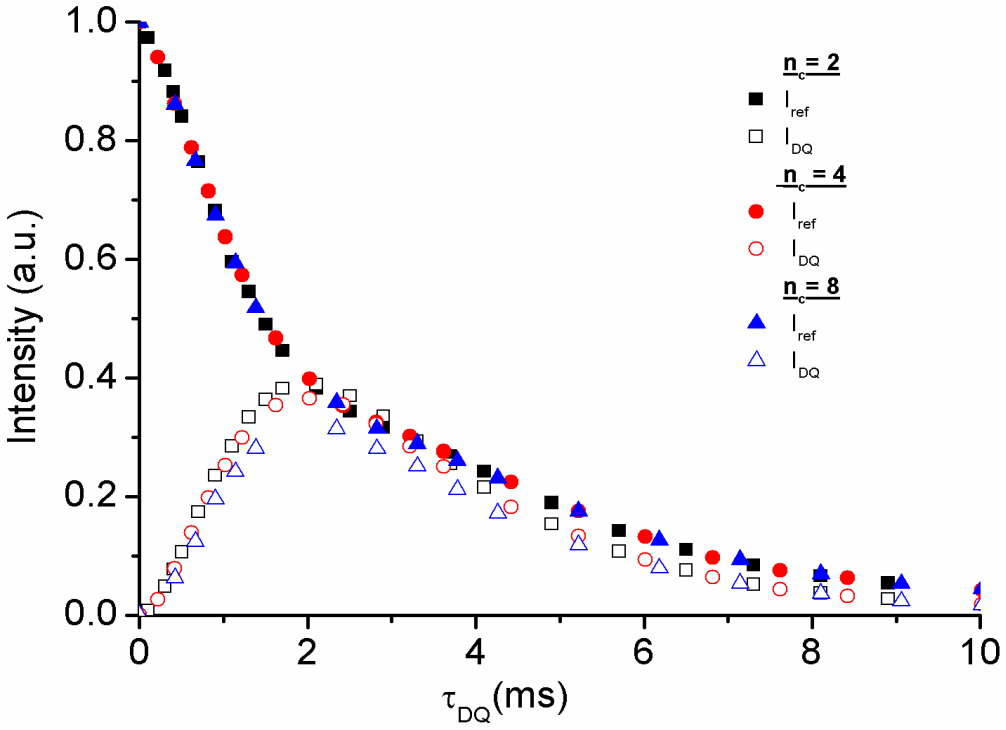

Figure 2.18 *Reference and DQ intensity for NR5 sample obtained at variable n_c using modified Baum-Pines pulse sequence.*

Table 2.3 *D_{res} of NR5 sample measured with variable number of cycles (n_c)*

n_c	$D_{res}/2\pi$ (Hz)
2	251
4	242
8	225

2.7 Results and Discussion

2.7.1 Crosslink density obtained by MQ NMR

In addition to chemical crosslinks, there are other types of physical network junctions may occur in elastomeric materials: (1) temporary and trapped chain entanglements, (2) junctions that are formed due to chain adsorption at the surface of active fillers, (3) junctions that are formed by crystallites, (4) junctions deriving from strong hydrogen and ionic bonds, and (5) junctions that are formed at the interface in polymer blends and in materials that reveal nano-scale phase separation [63]. Knowledge about all types of junctions in the rubbery materials is important because the mechanical properties are influenced not only by the chemical crosslink density but also by the physical network junctions and network heterogeneity. The strength of MQ NMR is that it provides not only crosslink density but also network distribution and heterogeneities. The MQ NMR is probing the network structure in the molecular level scales and is sensitive to the all kinds of constraints imposing restrictions on the network junctions. Some of the above mentioned restrictions are partially removed (disentangled) in swollen state or due to other facts; it is not possible to estimate with equilibrium swelling method.

The MQ experimental obtained reference and DQ intensity of studied natural rubber samples are shown in Figure 2.19 and Figure 2.20 respectively. The point-by-point normalized DQ intensity I_{nDQ} of Natural rubber networks including slowly decaying component and after subtractions of such a slowly decaying component are shown in Figure 2.21 and Figure 2.22 respectively. It is very clear from the increased slope in initial build intensity I_{DQ} with sulfur content and is an indication of crosslink yield proportional to sulfur content seen from the

Figure 2.20. The D_{res} constants of natural rubber networks obtained by analyzing the MQ NMR data with previously discussed procedure are plotted versus sulfur content. The expected linear relation is seen from the Figure 2.24. The good linear relationship between D_{res} and sulfur content is observed, which implies a constant yield in the vulcanization reaction and implies increased topological constraints. The lowest sulfur content sample (NR1) is slightly deviated from the rest of the samples, may be because the network is just above the percolation threshold. The y-intercept value is indicative of the fact that NMR is sensitive not only to the crosslinks but also other topological constrains such as entanglements, which are equally important restrictions to the segmental motions. The residual temperature dependence of normalized DQ data possible lead to an overestimated D_{res} and is the reason that D_{res} has obtained at temperatures well above ($>T_g$+120 K) the glass transition. The glass transition temperature (T_g) of the natural rubber networks varied from 212 to 219 K measured by DSC. To take proper temperature dependence into account all the measurements were performed at 353 K where plateau regime is reached. The variable temperature measured D_{res} has maintained almost constant value from 303 K to 363 K temperature seen from the Figure 2.23, which is safe temperature regime for studied natural rubber samples in order not to overestimate D_{res} due to temperature dependency as well as not to degrade the network. We can clearly see at 383 K the D_{res} has started decreasing due to network degradation. To check any temperature aging degradation of network, the repeated measurements were performed on same sample showed network degradation is not important factor for such a short experimental time around 45-150 min (depends on T_1 and number of scans). The conversion of D_{res} into M_c according to Equation (2.20) and hence crosslink density is plotted in Figure 2.25. In the higher networks (3.1 and 3.7 phr sulfur) even after single exponential correction I_{nDQ} is not maintaining plateau even up to 8 ms seen from Figure 2.22. Since these networks are less mobile than others, second more rapidly decaying component may be due to dangling ends (B), while the longer time tail is attributed to low molecular weight sol components (C). These two higher crosslinked networks exponential have fitted with double exponential and subtracted both exponents from the I_{nDQ} are shown in Figure 2.13.

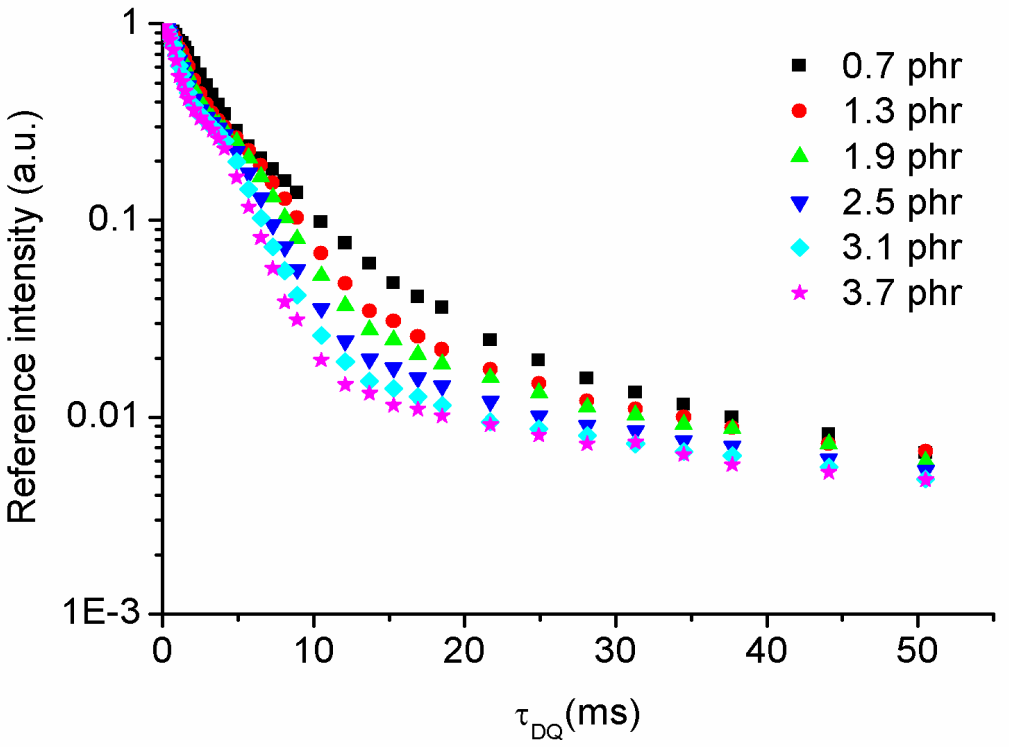

Figure 2.19 *The reference intensity (I_{ref}) of natural rubber networks. The increased sulfur content indicates increased crosslink yield and relatively faster decaying of reference intensity. The numbers in the legend represents sulfur content in phr.*

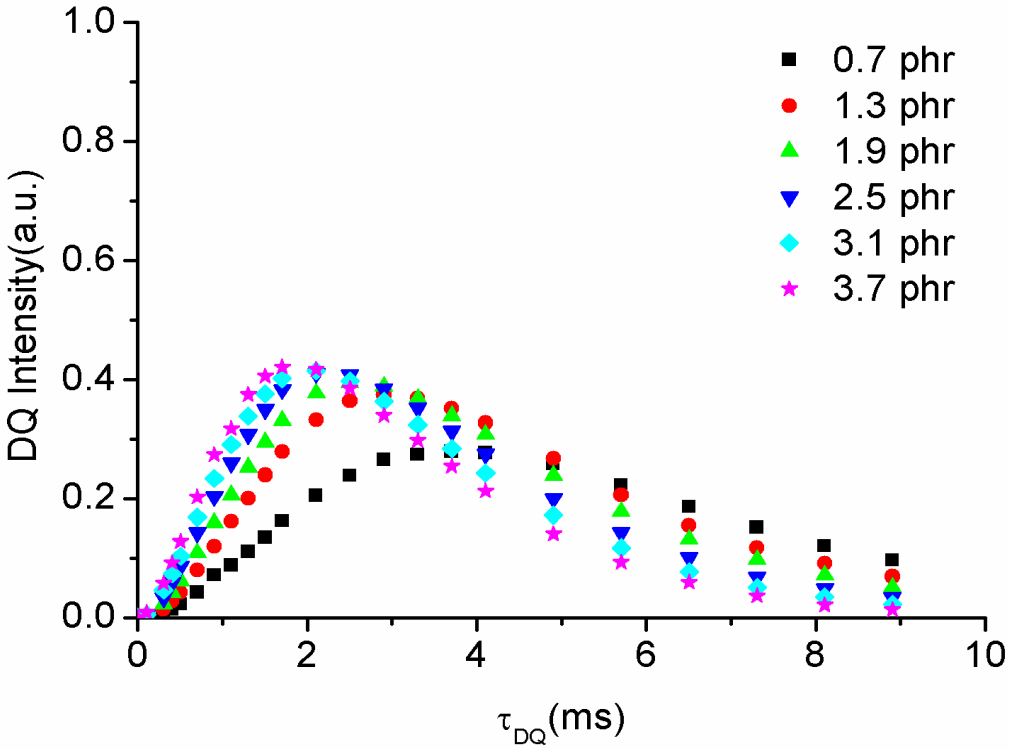

Figure 2.20 *The DQ intensity (I_{DQ}) of natural rubber networks. The increased sulfur content indicates increase crosslink yield and increased initial slope of DQ build-up curve.*

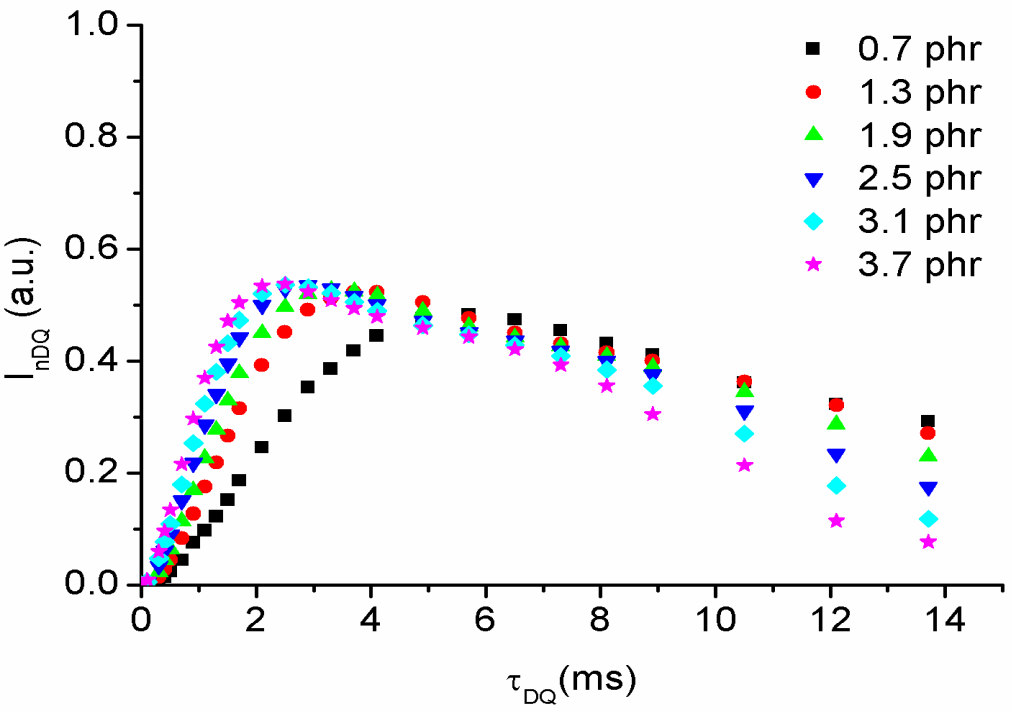

Figure 2.21 *Normalized DQ intensity (I_{nDQ}) without correcting slowly decaying components of natural rubber networks.*

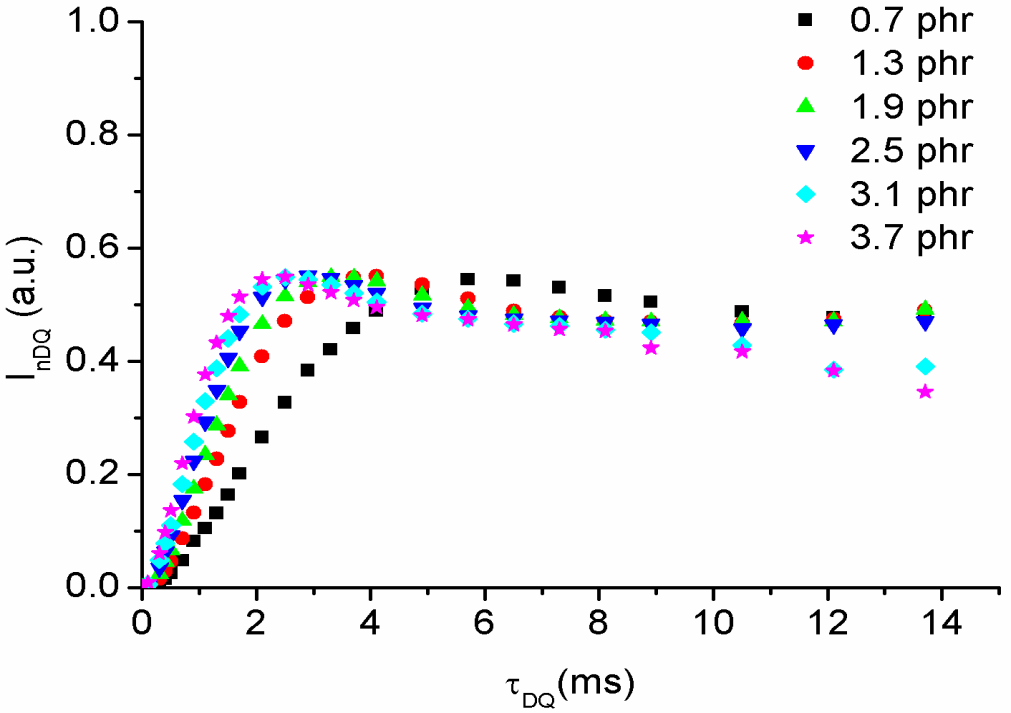

Figure 2.22 *Normalized DQ intensity (I_{nDQ}), after subtraction of slowly decaying exponential components for natural rubber networks.*

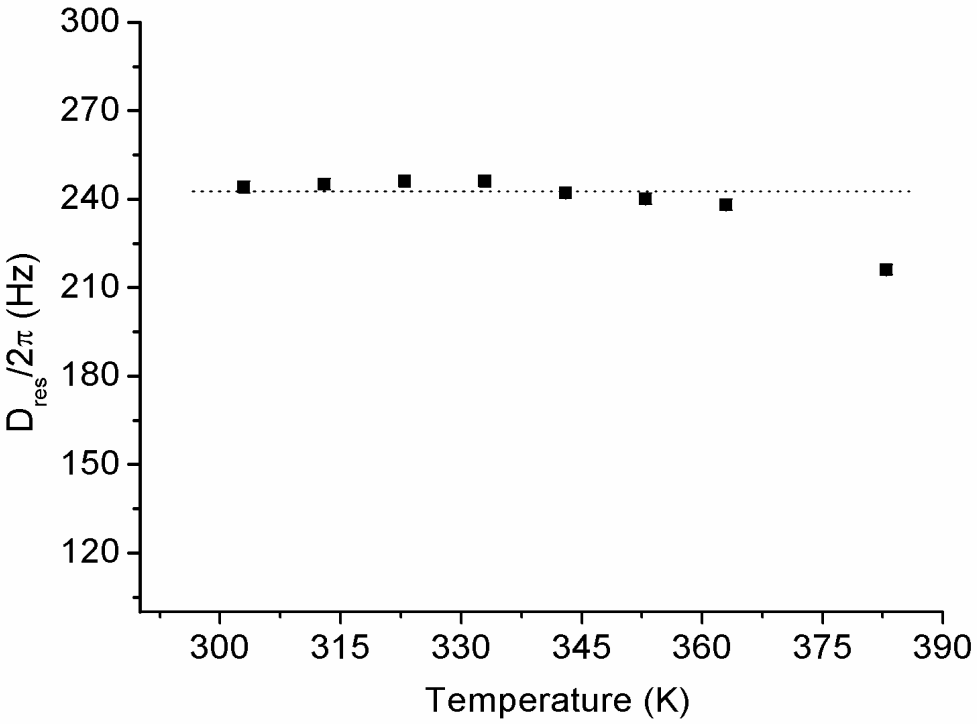

Figure 2.23 *Residual dipolar coupling constant (D_{res}) of sample NR5 measured at variable temperature.*

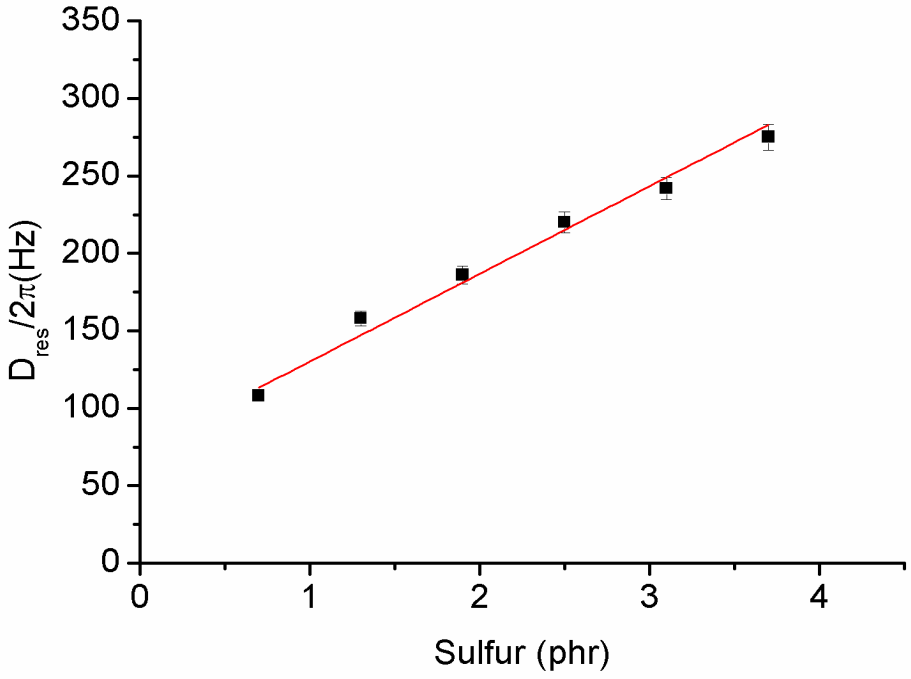

Figure 2.24 *Sulfur content versus MQ NMR obtained D_{res} constant of natural rubber samples. The red line is a linear fitting.*

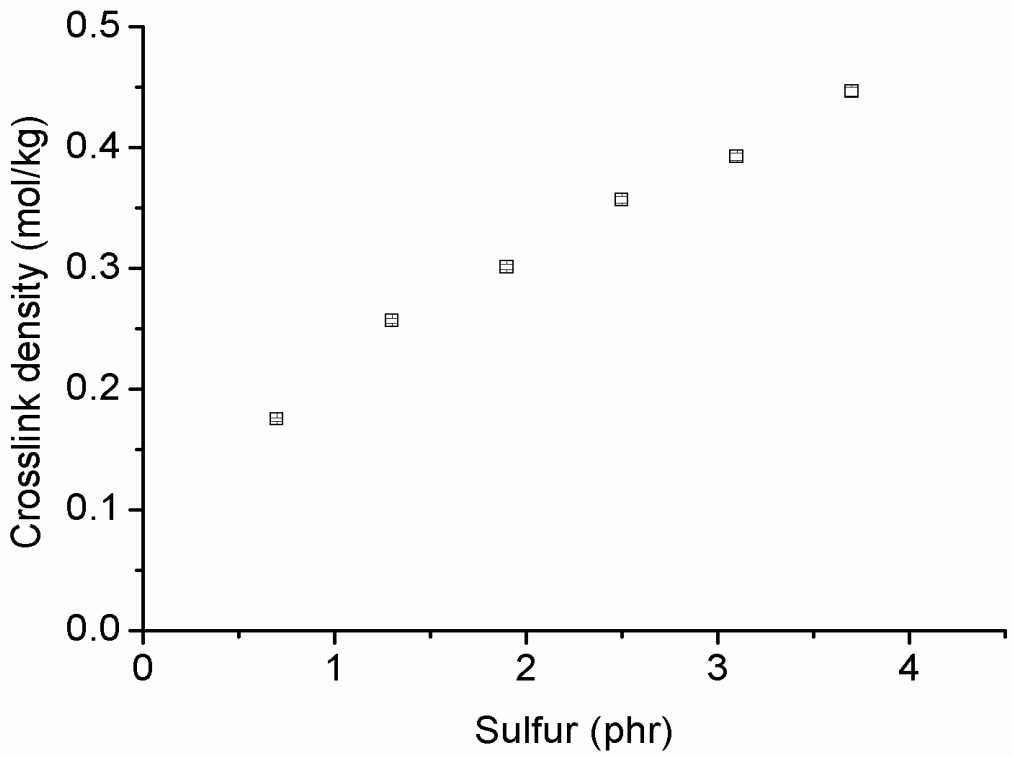

Figure 2.25 *Sulfur content versus MQ NMR measured crosslink density of natural rubber networks.*

2.7.2 Crosslink distribution obtained by MQ NMR

Vulcanization is a complex chemical process; during vulcanization different reactions that take place not only lead to variations in the overall crosslink density but also their spatial distributions. Mechanical properties of crosslinked elastomers are influenced by network distribution and heterogeneity. There are different heterogeneities that occur in rubbery materials as listed as follows.

1) Molecular-scale heterogeneity, which is caused by the chemical heterogeneity of uncured elastomers, network defects and heterogeneous distribution of network junctions on a molecular level.
2) Morphological heterogeneity of rubber compounds and other components due to spatially heterogeneous distribution in the rubber of co-agents and fillers,
3) Spatial heterogeneity due to differences in curing conditions such as temperature and concentration of crosslinking agents throughout the sample volume,

The curatives concentration dependent crosslink distribution is shown in Figure 2.26. The lower sulfur networks exhibited narrow distribution; the distribution becomes relative broadening with sulfur content or with crosslink yield seen in the present work. The distribution maximum also moving towards higher average crosslink density values with strong mono-modality. Polymer back bone structure, the network crosslink pathways also influence the distribution of crosslinks, mean that peroxide vulcanization with radical pathway, and generate more heterogeneous structure in comparison to sulfur vulcanization systems [60]. The change in the network distribution may not relate to the inherent impurities from the source of natural rubber such as proteins and lipids since all the networks made from same rubber at least come from same lot. However these impurities may influence on chain scission reaction. The polybutadiene networks crosslink distribution is seen to be broader than corresponding natural rubber and polyisoprene networks and will be discussed in chapter 4.

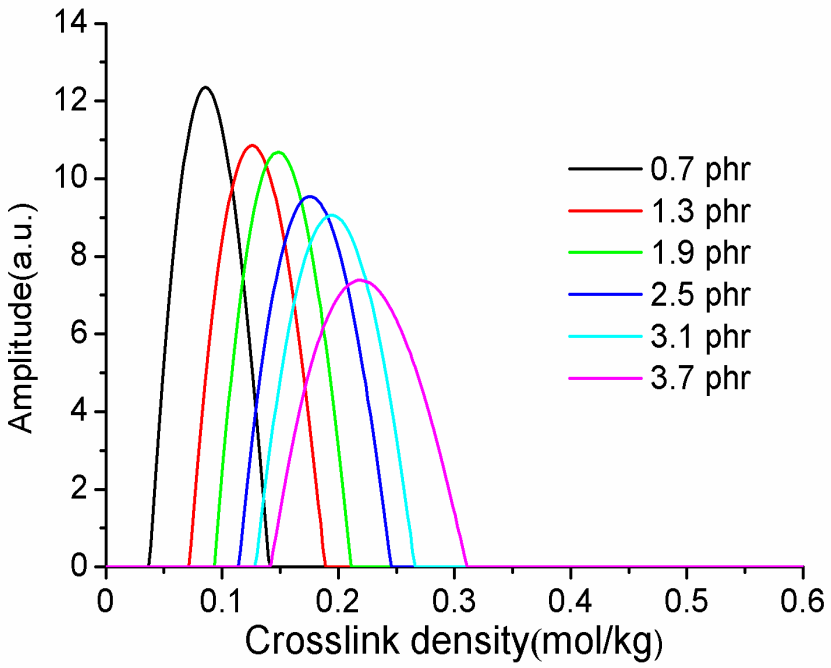

Figure 2.26 *Effect of sulfur content on crosslink distribution in natural rubber networks. The sulfur content is represented in the image legend in phr.*

2.7.3 Estimation of network defects by MQ NMR

In real networks, especially randomly crosslinked networks, it is easy to introduce defects such as sol, dangling ends, loops etc. as shown in Figure 2.27. These are not contributing to elasticity of networks, and it is necessary to estimate and remove from the networks. Since the mechanical properties of crosslinked elastomers are also influenced by the network heterogeneity and defects. The sol fraction may be easily removed in equilibriums swelling experiments, dissolved during swelling, however, the loops, dangling ends cannot be removed. The local methods which probe molecular properties are very suitable for determining degree of heterogeneity [62].The MQ NMR is a method probing the networks in the molecular level, which allows estimating and removing these kinds of defects from the network, due to the slower long time decaying behavior as shown in the Figure 2.12, that the normalized DQ intensity I_{nDQ} does not maintain proper plateau due to the overlapping of defects related slowly decaying components on structural related DQ intensity. By fitting these slowly decaying component with exponential function allows separate network defect related components from the structural information contained I_{nDQ}. The amplitude of exponential fit of slowly decaying component gives the quantity of defects in the network. The estimated network defects of natural rubber networks are plotted versus sulfur content in Figure 2.28. The lowest sulfur content samples (NR1) has highest percentage of network defects, the major contribution of defects in this sample may due to sol fraction and is also clearly evident from the shape of reference decay shown in Figure 2.19. Due to the lower content of sulfur, it is possible to miss more polymer chains without chemically linking to other chains in the crosslink network. From the sample consists of sulfur content 1.3 phr (NR2) to 3.7 phr (NR6) defects fraction is less but still following a trend of decay due to crosslink yield. The highest sulfur content samples has as low as less than 2% of defects, which are majorly due to elastically ineffective dangling ends and loops. In conclusion it is worth to stress that MQ NMR is a technique that allows estimating the network defects.

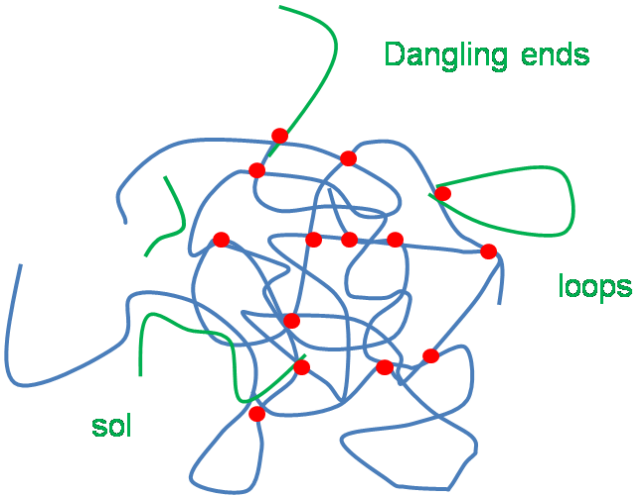

Figure 2.27 *Schematic representation of network consists of various network defects (sol, dangling ends, loops etc.). The defects indicated with green color and chemical crosslink junctions indicated with red dots.*

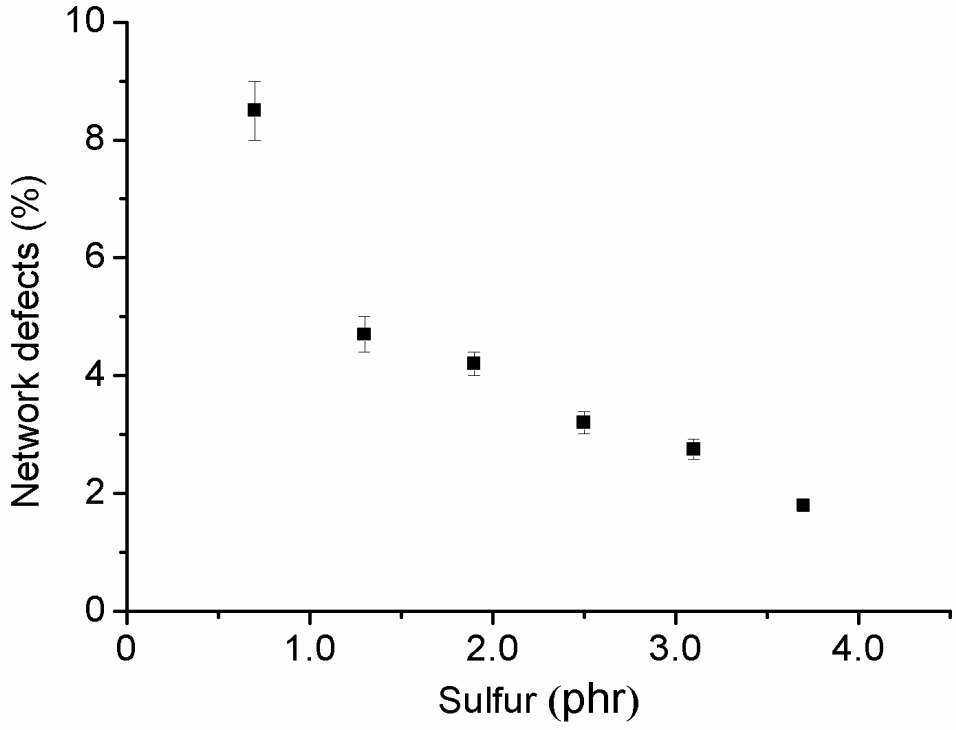

Figure 2.28 *The change in network defects with sulfur content in natural rubber networks.*

2.8 Conclusions

In this chapter, the basic multiple-quantum (MQ) NMR spectroscopy excitation schemes and recent literature has been reviewed. The complete procedure for MQ experimental data acquisition to data analysis has been given. One should easily use this application to characterize unlabeled polymer networks. Variable sulfur content mono-modal crosslinked natural rubber vulcanized networks have been studied by MQ NMR technique applied on low field NMR instrument. The crosslink density, crosslink distribution (or heterogeneity) has been obtained by application of Tikhonov regularization procedure on experimental data. The network defects also quantified from the MQ NMR experimental data. It has been observed that the crosslink yield increased with sulfur content as expected and the network heterogeneity or distribution becomes broader. The defect fraction (slowly relaxing components) decreased with sulfur content.

Chapter 3
Network Analysis by Equilibrium Swelling method and comparison with NMR

3.1 Introduction

A crosslinked polymer when placed in a good solvent, rather than dissolving completely, it will absorb a solvent and subsequently swell. The swollen network gel is characterized as solution. The extent of swelling represents a competition between two forces. (1) The free energy of mixing will causes the solvent to penetrate into the network and try to dilute the polymer-solvent solution. (2) The polymer chains of network begin to stretch under the action of solvent and generate an elastic force in opposition to this deformation. When these two forces balance each other swelling stops and system reaches equilibrium swelling state. The study state of swelling is a direct function of extent of crosslinking in the network.

Equilibrium swelling is a simple and most widely used technique for measuring crosslink density of elastomeric networks. This technique helps to determine the important network parameter called molecular weight between crosslink junctions M_c and hence network density. This method based on the Flory-Rehner theory of network models developed from the ideal network assumptions. The network models are derived for assessing any mechanical deformations occur in the network. We take this advantage and the insoluble characteristic of networked polymers in solvents, we derived an equation and this equation gives the network parameter M_c. In this chapter we will briefly recall the network theories we need at this point without going into the ocean of polymer theory.

The fundamental basis for both the empirical (phenomenological) and molecular models is that first to estimate fundamental nature of the elastomeric network in undiluted (dry network) state. Second is that to consider the specific behaviour of the same network in swollen gel state in a similar treatment. In both the cases the elastic free energy function (Helmholtz function) of the network is to be estimate. In gel state formation of a mixing free

energy as a function of the swelling ratio is also required in addition to the elastic free energy. In this chapter our interest is mostly on swollen gel networks.

Both the models are useful in real time. In phenomenological models, the molecular structure of network can obtain from the macroscopic behaviour of network by analysis of experimental results. Molecular models helps to predicting the future measurements from the known molecular structures and is more important for future development or improvement of subject and synthesis of new materials, to meet our increased demands.

3.2 Network models

There are several models available to derive the molecular parameters of the networks from experimental obtained results. The models are mainly classified as empirical and molecular models (theoretical models). The earlier one is derived based on models and experimental results and later one is purely derived by the assumption of ideal network. The different theoretical models are derived by consideration of different assumptions. The final network structure parameters certainly depend on the choice of the model [1] used for data analysis. Additionally the network structure at supermolecular level is depends on the experimental conditions such as temperature, chemical nature of crosslinker etc. During network formation there is a possibility of formation of defects in the network, but most of the models are derived by excluding these defects. It is always remains as unresolved task to decide which model is appropriate. In addition to all these difficulties the physical state of the network also matters. In case of the dry network we need to consider purely elastic response, where as in swollen gel state of network, in addition to the elastic response (elasticity term), thermodynamical mixing term of polymer-solvent also need to account and it play a role. In case of swollen networks, the entanglements are partially disentangled or released and it will discuss in NMR measurements. The network models will discussed in the subsequent sections.

3.2.1 Statistical models (Molecular models)

The primary goal of any statistical model is to derive the equation of state for elastomeric molecular network, which could explain all kinds of deformation within the network system. This equation of state could hold for swelling deformation also. These equations of state could derive, starting from the certain assumptions on the motion of network junctions upon mechanical force applied on macroscopic system. Our main focus is mainly restricted to affine and phantom models only, however these two models are two limiting cases [64] of real network behaviour. The schematic of ideal network with 9 crosslink junctions and 12 elastically active chains is shown in Figure 3. 1.

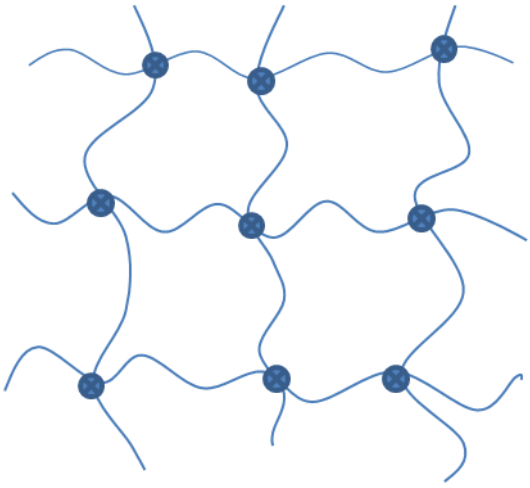

Figure 3. 1 *Schematic of an ideal network with 9 crosslink junctions and 12 elastically active chains, solid dots represents network crosslink junctions.*

However a real network mostly deviates from the ideal network, it is worth to define the ideal network parameters as a reference to compare the experimentally obtained results of real network which are measured in a macroscopic scale. The extent of crosslinking can express in several ways such as

1) The concentration of elastically active chain
2) The molecular weight between crosslink junctions
3) The crosslink density

4) The cycle rank density.

The elastically active chain is one, which is connected between two active junctions, and an active junction is, a point connecting at least three elastically active chains.

The concentration of elastically active chains is defined as a number of elastical active chains exist per unit volume of dry network. The crosslink density is already defined and cycle rank density is defined as number of independent loops exists in unit volume of dry network. Cycle rank is defined as number of cuts need to reduce a network to a tree and network with cycle rank 4 is shown in Figure 3. 2. In the rest of the work we restricted ourselves to only one network parameter called molecular weight between crosslink junctions (M_c) and from that crosslink density will obtain.

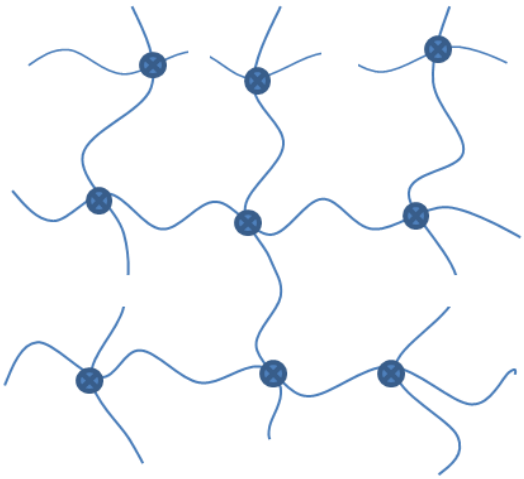

Figure 3. 2 *Schematic of an ideal network with 9 crosslink junctions and 12 elastically active chains, with cycle rank 4. The cycle rank is defined as number of cuts needed to reduce the network to tree.*

The exceptional behaviour of polymer networks is that the reversible deformation of several times to their size. The simplest model that explains the rubber elasticity is the affine network model proposed by Kuhn. The main assumption of affine model is that *Affine deformation*.

3.2.1.1 Affine network model

The relative deformation of each network strand is same as the macroscopic relative deformation imposed on the whole network. Or the displacement of the mean positions of the network junctions and of the end-to-end vectors of the chains are transformed affinely (i.e. linearly in the macroscopic strain). In affine model the crosslink junctions are fixed to an elastic boundary as shown in Figure 3. 3.

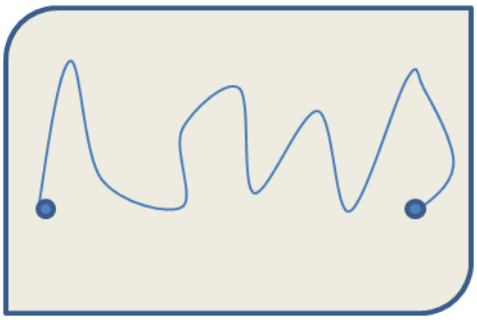

Figure 3. 3 *Affine model, the ends of each network strands are fixed to an elastic background, circular dots are crosslink junctions*

The stress strain relation of affine model is given in Equation (3.1) the derivation will be given in next section.

$$\sigma = G(\lambda^2 - \frac{1}{\lambda}) \tag{3.1}$$

$$G = \frac{\rho RT}{M_c} \tag{3.2}$$

Where σ is stress, G is shear modulus, λ is deformation ratio, ρ density of polymer, R gas constant, T absolute temperature and M_c molecular weight between crosslink junctions or molecular weight of network strands.

3.2.1.2 Phantom network model

The phantom network model assumption is differing from the affine model is that the crosslinks are not fixed in space; they can fluctuate around their mean positions. In real network the ends of the network strands are attached to the other strands at crosslink point as shown in Figure 3.4. The recent literature [53] also suggest that phantom network model is closer to real network modes

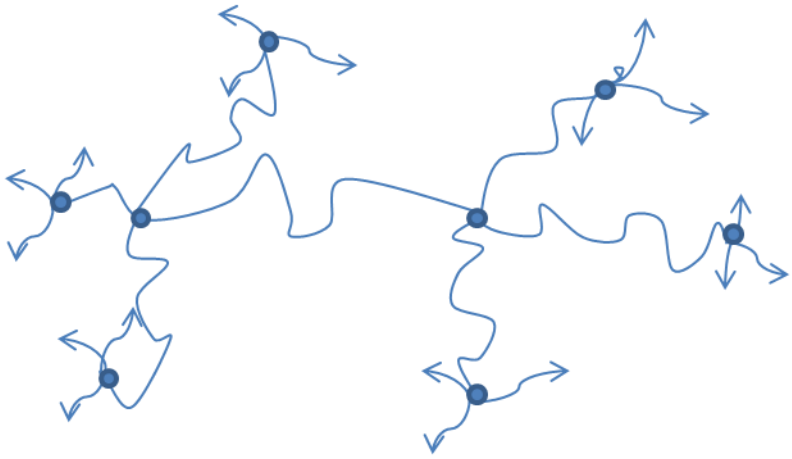

Figure 3.4 *Phantom network model, the ends of each network strands are joined to other network strands at crosslink points and the crosslink junctions are free to fluctuate around mean positions. Circular dots are crosslink junctions and arrows indicate the extension of network.*

As mentioned in the introduction the phantom model network strands are ideal network strands free from all the defects (loops, dangling ends). There is also consideration that the network strands at the surface of the network are attached to the elastic non-fluctuating boundary of the network similar to affine model and is necessary to prevent the collapse of the network. Obviously this kind of simple models undermines the excluded volume effects. By these assumptions we can arrive at the phantom network model shear modulus equivalent to Equation (3.2) is

$$G = \frac{\rho RT}{M_c}(1 - \frac{2}{f}) \tag{3.3}$$

Where σ is stress, G is shear modulus, λ is deformation ratio, ρ density of polymer, R gas constant, T absolute temperature, M_c molecular weight between crosslink junctions or molecular weight of network strands and f is the crosslink functionality.

For any functionality f the Phantom network modulus is lower than the affine network modulus, since fluctuated crosslink points soften the network. For same number density of network strands, the phantom modulus is lower than affine model modulus. The functionality of crosslinks *f* is four or three. For higher functionality, crosslink fluctuation is much reduces and the crosslink points are similar to the one attached to surface and phantom model is equivalent to affine network model. This is the reason why affine and phantom network models are two limiting cases or extremes of real network. The real network is always somewhere in between two limits [53, 65].

3.2.2 Phenomenological models (Semiempirical models)

The phenomenological models for elastomeric networks were developed by Mooney and Rivlin. The bases of these models are also same as molecular models, obtaining the stress strain response of the deformed network and deriving the equation for elastic free energy of network. As already mentioned in the previous section, that first we need to find the stress-strain response of dry network to calculate elastic free energy term, later similar treatment is applied to swollen gel to obtain the polymer-solvent mixing free energy.

3.2.2.1 Crosslink density of dry networks obtained from stress-strain experiments

Deriving strain energy density function for dry network

The stress-strain response of elastic materials is obtained by the Finite Elasticity Theory originally developed by Rivlin and others [66, 67]. Valanis-Landel strain energy density function [68] is most successful in describing the mechanical response of crosslinked rubbers

and is very useful for understand the swollen behaviour of similar (crosslinked networks) kind of materials and is our primary aim of this chapter. Let us start with considering a sample of rubber having initial dimensions of l_1, l_2 and l_3. We deformed it by an amount $\Delta l_1, \Delta l_2$ and Δl_3 and stretch ratio $\lambda_i = (l_i + \Delta l_i)/l_i$, Finite Elasticity Theory will relate the deformation of the material to stress needed to obtain such a deformation. This will achieve through the Strain Energy Density Function (W ($\lambda_1, \lambda_2\, \lambda_3$)) using Valanis-Landel (V-L) formalism and is a mechanical contribution to the Helmholtz Free Energy.

The strain energy function is a separable function of the stretches λ_i according to the assumption of Valanis and Landel [68].

$$W(\lambda_1, \lambda_2, \lambda_3) = w(\lambda_1) + w(\lambda_2) + w(\lambda_3) + a \ln(\lambda_1\lambda_2\lambda_3) \tag{3.4}$$

Because of the incompressibility assumption, logarithmic term $a \ln(\lambda_1\lambda_2\lambda_3)$ is not important in mechanical response and it may important in case of swollen gel.[69] The principle stresses σ_{ii} in any deformation can be related through the strain energy function and deformations as follows:

$$\sigma_{ii} - \sigma_{jj} = \lambda_i w'(\lambda_i) - \lambda_j w'(\lambda_j) \tag{3.5}$$

Where $w'(\lambda)$ is the derivative to V-L function $w(\lambda)$.

As already mentioned that incompressibility assumption mean that generally in dry networks the shape changing is much easier than volume changes. In case of uniaxial deformation λ in one direction,

$$\lambda_1 = \lambda;\ \lambda_1\lambda_2\lambda_3 = 1\ ; \lambda_2 = \lambda_3 = \frac{1}{\sqrt{\lambda}} \tag{3.6}$$

$$\sigma_{11} - \sigma_{22} = \lambda w'(\lambda) - \lambda^{-1/2} w'(\lambda^{-1/2}) \tag{3.7}$$

For uniaxial extension, $\lambda > 1$, while for uniaxial compression $\lambda < 1$.

Equation (3.7) gives the stress-strain relation of a materials if $w(\lambda)$ is known and is obtained in the laboratory by different mechanical measurement techniques such as shear experiments by combining of tension and compression experiments describe in [70,71].

The commonly used phenomenological models, which are derived from V-L functions, are Neo-Hookean form and Mooney-Rivlin.

For Mooney-Rivlin materials the strain energy density function is written as

$$w(\lambda_1, \lambda_2, \lambda_3) = C_1(\lambda_1^2 + \lambda_2^2 + \lambda_3^2 - 3) + C_2(\lambda_1^{-2} + \lambda_2^{-2} + \lambda_3^{-2} - 3) \tag{3.8}$$

Where C_1 and C_2 are called Mooney-Rivlin coefficients.

Differentiating the Equation (3.8) then

$$w'(\lambda_i) = 2C_1\lambda_i - 2C_2\lambda_i^{-3} \tag{3.9}$$

Substuting Equation (3.9) in Equation (3.7)

$$\sigma_{11} - \sigma_{22} = \left(\lambda^2 - \frac{1}{\lambda}\right)(2C_1 + \frac{2C_2}{\lambda}) \tag{3.10}$$

For Mooney-Rivlin materials $C_2 = 0$.

For the assumption of network made from the infinitely long polymer chains and assume that there are no free chain ends and the crosslink functionality is four the density of chains is twice that of crosslinks, so that C_1 can relate with crosslink density [72].

$$C_1 = \frac{\rho RT}{2M_c} \tag{3.11}$$

Where M_c = number–average molecular weight of the network chains.

In real networks, always there is a possibility of presence of network defects such as dangling chain ends, loops etc. The crosslink density obtained from the Equation (3.11) is not always same as experimental obtained values. The crosslink density obtained from Equation (3.11) is exceeds the concentration of chemical crosslinks introduced by vulcanization. The crosslink density obtained from C_1 is apparent value. Because physical crosslinks (entanglements) contribute to elastic constant of the network, especially in dry samples and may partially remove in the swollen state. Mullins [73] by performing mechanical measurements on swollen network, able to calibrate the physical crosslinks and has derived the semiempirical equation for determine chemical crosslinks density and valid for natural rubber and synthetic polyisoprene rubber networks also.

$$C_1 = \left[\frac{\rho RT}{2M_{c(chem)}} + 0.78x10^6\right]\left[1 - 2.3\frac{< M_{c(chem)} >}{< M_n >}\right] \tag{3.12}$$

The units of C_1 is *dyne/cm*^{2}. The constant *0.78x10*^{6} is a correction term which maximum contributes to entanglements. $< M_n >$ is the mean molecular weight of the rubber immediate before vulcanization.

Once we know C_1 value from the mechanical measurements, by substituting into Equation (3.11) or (3.12), one can estimate the crosslink density of networked polymers.

3.3 Real network including defects

The modulus obtained from the Equation (3.3) is truly applicable to defect free network and in fact randomly crosslinked real networks inevitable includes defects as shown in Figure 3. 5 . The network strand connected only one end and other end are freely hanging is called the

dangling end and is not contribute to modulus. The network strands whose two ends are connected at the same junction is called loop and is also not contribute to elasticity and modulus.

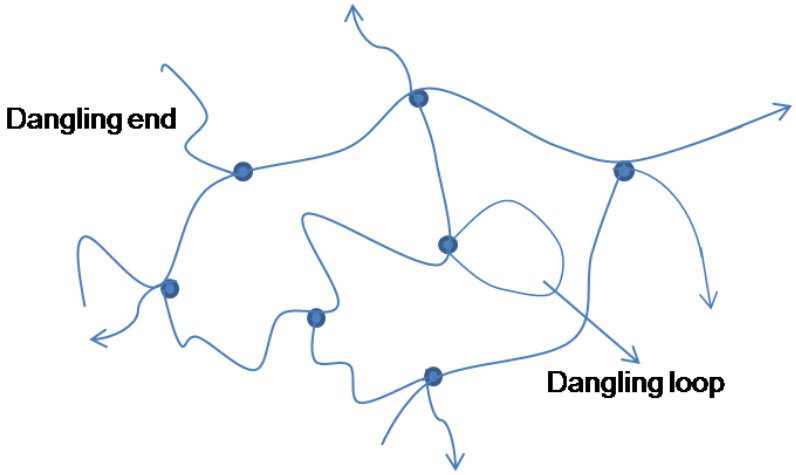

Figure 3. 5 *Randomly crosslinked network with defects (dangling ends and dangling loops). Arrows indicates extension of network.*

3.4 Equilibrium swelling crosslink density from molecular network models

Equilibrium swelling is defined as the point at which mixing free energy (ΔG_{mix}) of polymer-solvent and elastic free energy (ΔG_{ela}) from the networked polymer balancing each other, when networked polymer is immersed in a good solvent. The free energy of polymer-solvent system is:

$$\Delta G_{system} = \Delta G_{mix} + \Delta G_{ela} \tag{3.13}$$

At the beginning of swelling, the $\Delta G_{mix} << 0$, $\Delta G_{ela} > 0$, $\Delta G_{mix} + \Delta G_{ela} < 0$, so the swelling is favoured and the solvent diffuses into the network. During the process of swelling, the ΔG_{mix} and ΔG_{ela} both increased until $\left|\Delta G_{mix}\right| = \left|\Delta G_{ela}\right|$ and $\Delta Gs_{ystem} = \Delta G_{mix} + \Delta G_{ela} = 0$, so that the driving force for swelling is gone: equilibrium swelling is reached and swelling stops.

The Equation (3.13) can be written in terms of change in chemical potential of the solvent, $\Delta\mu_{system}$, by differentiating with respect to the number of moles of solvent

$$\frac{\Delta\mu_{system}}{RT} = \frac{\Delta\mu_{mix}}{RT} + \frac{\Delta\mu_{ela}}{RT} \tag{3.14}$$

Where R and T are gas constant and temperature respectively.

The mixing term can be defined according to Flory-Huggins expression.

$$\frac{\Delta\mu_{mix}}{RT} = \ln(1 - v_r) + \left(1 - \frac{V_s}{V_p}\right) v_r + \chi v_r^2 \tag{3.15}$$

Where v_p is the molar volume of polymer and is infinite for crosslinked polymer and the Equation (3.15) written as

$$\frac{\Delta\mu_{mix}}{RT} = \ln(1 - v_r) + v_r + \chi v_r^2 \tag{3.16}$$

The elastic contribution term to the chemical potential is expressed in term of a molecular theories discussed in earlier text of this section.

By taking Affine deformation model [53], the Flory-Rehner expression the chemical potential of elastic term is written as

$$\Delta\mu_{ela} = \frac{RT}{2M_c}\left(\lambda_x^2 + \lambda_y^2 + \lambda_z^2 - 3\right) - \frac{2}{f}\frac{RT \ln\left(V/V_0\right)}{M_c} \tag{3.17}$$

Where λ_x, λ_y and λ_z are the elongation in x, y and z-directions respective. V and V_o are the volume of gel and pure polymer respectively. f is the functionality of crosslinks.

From equilibrium condition the elastic free energy and mixing free energy balancing each other, so that $\Delta G_{system} = 0$. By combining the Equation (3.14), (3.16) and (3.17), the Flory-Rehner equation is obtained as:

$$\ln(1-v_r)+v_r+\chi v_r^2=-\frac{\rho_r V_s}{M_c}(v_r^{1/3}-\frac{2v_r}{f}) \tag{3.18}$$

Consider the Phantom network model ($G=\frac{\rho RT}{M_c}(1-\frac{2}{f})$) to obtain elastic term, Equation (3.18) written as

$$\ln(1-v_r)+v_r+\chi v_r^2=-\frac{\rho_r V_s}{M_c}(1-\frac{2}{f})v_r^{1/3} \tag{3.19}$$

3.5 Equilibrium swelling crosslink density from phenomenological models

The fundamental quantity obtained from the equilibrium swelling experiments is the volume fraction of polymer network in the swollen gel (v_r) and the important network parameter, molecular weight between crosslink junctions (M_c) relations is given by the Flory-Rehner[74, 75] and Flory-Huggins expression [76-78]. As defined in the Equation (3.18)

$$-[\ln(1-v_r)+v_r+\chi v_r^2]=\frac{\rho_r V_s}{M_c}(v_r^{\frac{1}{3}}-2\frac{v_r}{f}) \tag{3.20}$$

In Equation (3.20), parameters, v_r will obtain from the experiment, ρ_r density of polymer known, V_s molar volume of solvent known, f crosslink functionality known and χ polymer-solvent interaction parameter also called Flory-Huggins interaction parameter known for particular polymer and solvent pairs [79].

From equating the Equation (3.11) and (3.20), we can obtain the relation between equilibrium swelling experimental obtained observable (v_r) and mechanical obtained elastic constant C_1.

$$-[\ln(1-v_r)+v_r+\chi v_r^2]=2C_1\frac{V_s}{RT}(v_r^{\frac{1}{3}}-2\frac{v_r}{f}) \tag{3.21}$$

From the Equation (3.21) and (3.11) one can easily obtain elastic constant from swelling data and vice-versa and hence M_c and crosslink density.

3.6 Experimental

3.6.1 Sample preparation

Natural rubber (Malaysian rubber (SMR 20)) (NR), samples were kindly supplied by Pirelli tyre company. All the recipes were sulfur based cured systems, and the details of the natural rubber compound recipes are given in Table 3. 1. Samples were prepared in an open two-roll mill using standard mixing procedure.

Table 3. 1 *Natural rubber vulcanizates recipes*

Sample	Natural rubber (phr)	Sulfur (phr)	ZnO (phr)	Stearic acid (phr)	CBS* (phr)
NR1	100	0.7	5	2	0.14
NR2	100	1.3	5	2	0.26
NR3	100	1.9	5	2	0.38
NR4	100	2.5	5	2	0.50
NR5	100	3.1	5	2	0.62
NR6	100	3.7	5	2	0.74

* N-cyclohexyl-2-benzothiazole sulfonamide, a curing accelerator

3.6.2 Vulcanization

Vulcanization is the process of introducing chemical bonds between polymer chains and transforms the linear polymer into networked polymer in order to achieve elasticity. A crosslink may be a group of sulfur atoms in a short chain, a single sulfur atom, a carbon to carbon bond, a polyvalent organic radical, an ionic cluster, or a polyvalent metal ion. The vulcanization is usually carried out by heating the rubber, mixed with vulcanizing agents, in a mold under pressure. Vulcanization is also often called curing.

Natural rubber samples were vulcanized in pneumatic double plate press at 150 °C for optimum time (t_{95}) obtained from rheometry.

3.6.3 Rheometric study of vulcanization

Rheometry analysis was performed on Monsanto Rheometer MDR (Moving Die Rheometer) 2000E. 6 g of analyzed samples compound were placed on disc to perform the test. Curing curves of natural rubber compounds were obtained at 150 °C temperature for 50 minutes of time. The optimum cure time (t_{95}) and other vulcanization characteristics deduced from the vulcanization curves (shown in Figure 3. 6) are shown in Table 3. 2.

Table 3. 2 *Vulcanization characteristics of natural rubber networks measured by rheometry.*

Sample	Sulfur (phr)	M_H-M_L (dNm)	t_{s2} (min)	t_{95}(min)	t_{95}-t_{s2} (min)
NR1	0.7	1.95	10.4	23.8	13.4
NR2	1.3	3.92	8.17	15.8	7.6
NR3	1.9	4.57	6.53	13.3	6.7
NR4	2.5	6.57	5.87	13.9	8.0
NR5	3.1	7.7	5.9	13.8	7.9
NR6	3.7	8.55	5.7	13.9	8.2

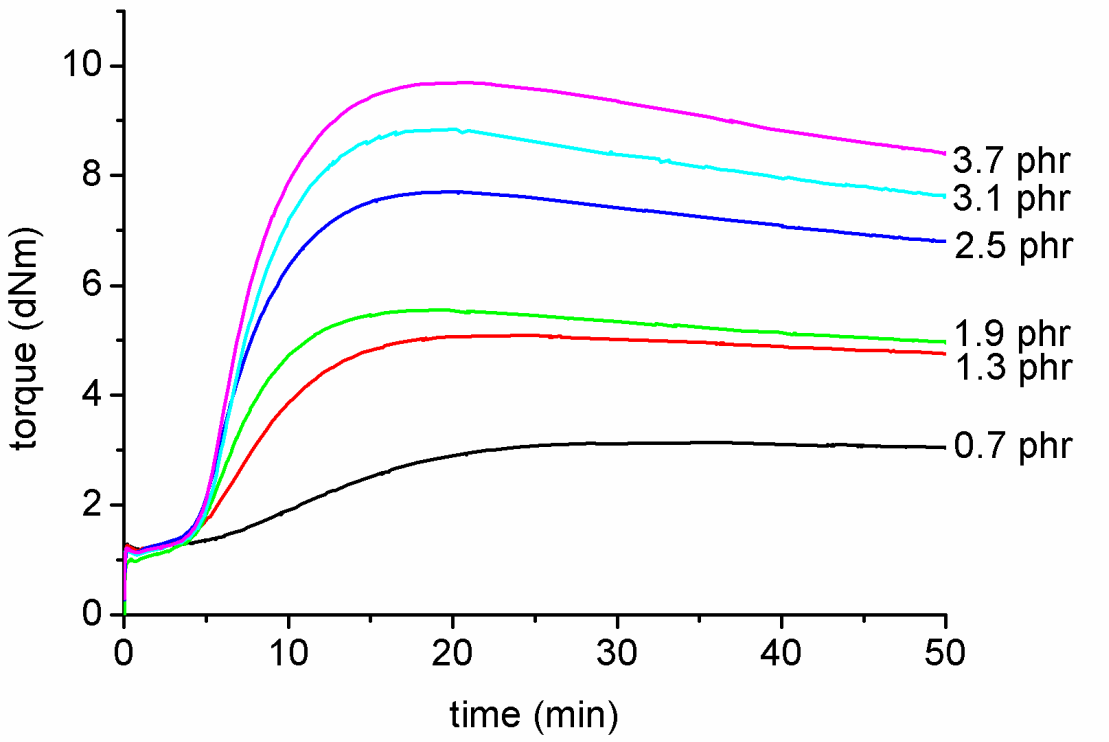

Figure 3. 6 *Vulcanization curves of natural rubber compounds obtained from rheometry. Sulfur content is represented in the image in phr.*

Rheometric data acquired during vulcanization are interpreted with the assumption that torque is proportional to progress in crosslink density. In vulcanization curves, three regions or periods can be observed [8]. The first region is called induction period or scorch time during which accelerator reactions occurs. The second is curing period, during which actual crosslink process takes place and network structure is formed. The third and the last stage is over-cure or post cure period during which torque can increase, decrease or remain constant depending on the particular vulcanization system [80] and nature of the elastomer. In general at increased temperature cure reaction starts faster and reduces the scorch period, increases the cure rate and hence reduces the overall time of cure. Over reduction of scorch period and fast curing also result in adverse effects on mechanical properties and final product quality. There is a necessity of proper optimization of cure temperature and time for determining a safe scorch delay [9] to achieve the desired quality of vulcanized product. The maximum torque value increased with sulfur content indicates the increasing crosslink density. Except the lowest sulfur content samples (NR1and NR2) the optimum cure time (t_{95}) is almost same

for all the samples. The difference in maximum and minimum torque is linearly increased with sulfur content and is direct evidence of progress of crosslink density with sulfur content shown in Table 3. 2.

3.6.4 Network Characterization by Equilibrium swelling

The vulcanized rubber network crosslink density was determined by equilibrium swelling measurements performed in toluene solvent at 20 °C temperature. Specimens were prepared as 1 mm thick and 15 mm x15 mm pieces. For total crosslink measurement, specimens were pre-swollen in n-heptane for two days under nitrogen atmosphere to assist diffusion of reagents, before being taken for the probe and control treatments. For mono and di-sulfidic crosslinks measurement, specimens were pre-swollen in n-heptane for one day and reacted for two hours with 0.4 M piperidine and 0.4 M propane-2-thiol. Then they were thoroughly washed with n-heptane and again soaked in n-heptane for one day. Then, n-heptane was drained from both the total and mono-di sulfidic crosslink samples and were washed with petroleum ether and dried in a vacuum oven overnight at room temperature. The dried samples were soaked in the toluene in specially designed glass tubes with stopper, flushed with nitrogen and left in the dark to swell up to equilibrium swelling state The time required to reach this equilibrium state is commonly considered as three days (72 hours). The samples were removed and blotted with a filter paper to remove the extra solvent, placed in clean closed container and immediately weighed. The samples were dried for 24 hours in a vacuum oven at 70 °C and re-weighed to obtain the weight of the dry network and the amount of the imbibed solvent.

After the swelling experiments performed we measure the volume fraction of rubber in the swollen gel (v_r)

$$Volume\ fraction\ of\ rubber\ in\ swollen\ gel\ (v_r) = \frac{volume\ of\ polymer\ in\ gel}{(volume\ of\ polymer + volume\ of\ solvent)} \quad (3.22)$$

$$Volume\ of\ polymer = \frac{Initial\ weight\ of\ dry\ network}{density\ of\ polymer} \quad (3.23)$$

$$Volume\ of\ solvent\ in\ gel = \frac{Swolleng\ gel\ weight - dry\ network\ weight}{density\ of\ solvent} \quad (3.24)$$

By substituting the v_r in any of the Equations (3.18) or (3.19) or (3.21) we obtained crosslink density. Equations (3.18), (3.19) and (3.21) give the affine, phantom and Mooney-Rivlin crosslink density respectively.

We used the value of $\chi = 0.39$ for toluene-natural rubber and toluene-isoprene rubber pair, $\chi = 0.36$ for toluene-butadiene [79] in the present work. Crosslink functionality f is taken as 4. Polymer density (ρ_r) = 0.92 g/cm^3 and solvent (toluene) molar volume (V_s) = 107 mL/mol and density 0.87 g/cm^3

3.7 Results and Discussion

3.7.1 Crosslink density

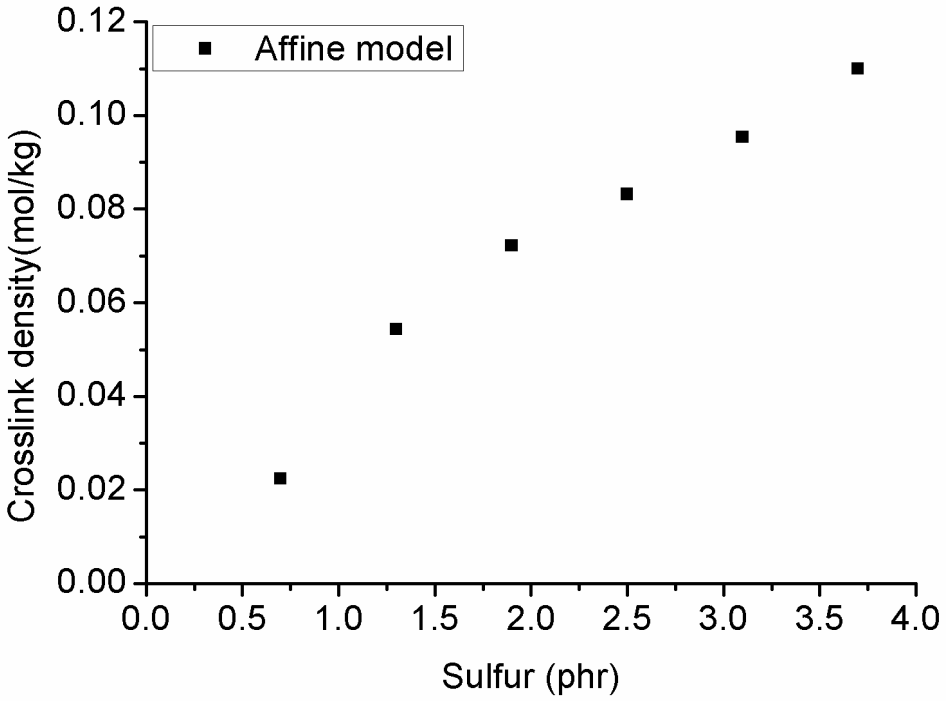

Figure 3. 7 *Sulfur content versus crosslink density of natural rubber networks obtained from affine network model adoption.*

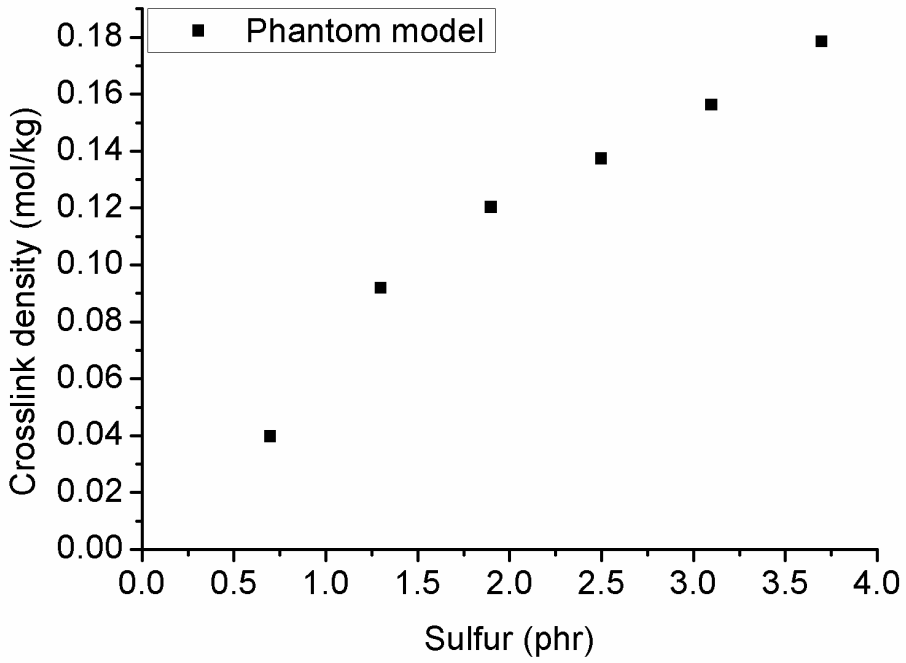

Figure 3. 8 *Sulfur content versus crosslink density of natural rubber networks obtained from phantom network model adoption.*

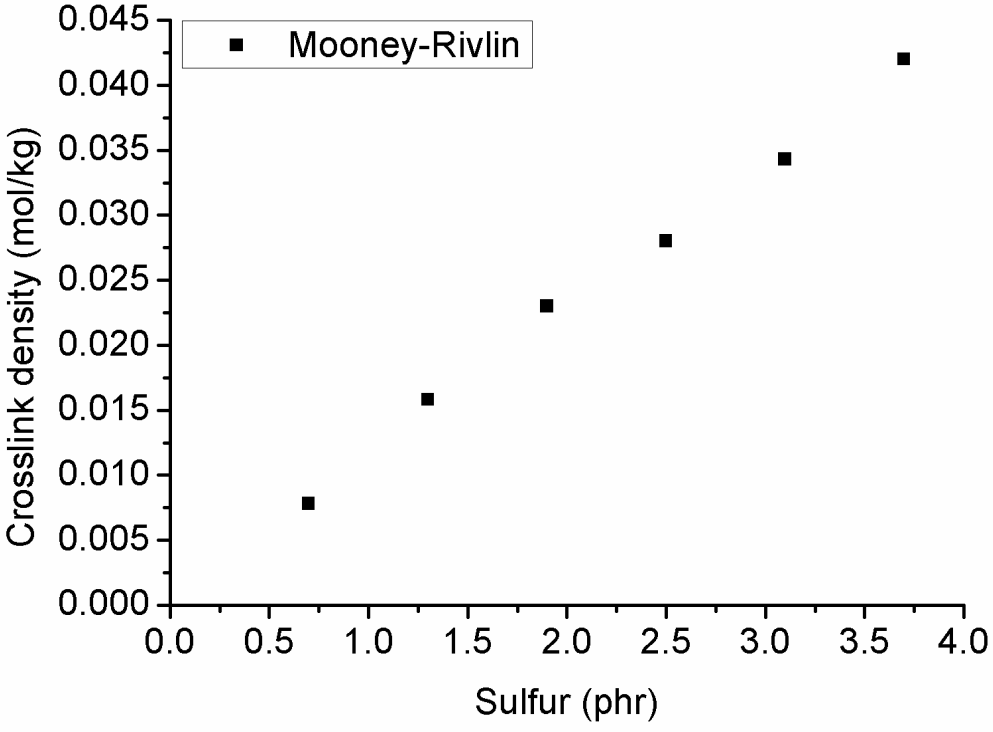

Figure 3. 9 *Sulfur content versus crosslink density of natural rubber networks obtained from phenomenological model adoption.*

The crosslinks are introduced by the creation of chemical bonds between polymer chains. In sulfur based compounds, sulfur is a crosslink agent and is the reason for increasing the crosslink density by increasing of sulfur content and is shown in Figure 3. 7, Figure 3. 8 and Figure 3. 9. It is very clear that the crosslink density obtained from both the molecular network models and phenomenological models are proportional and qualitatively agree with each other's. The crosslink density quantity is depends on the choice of model [1].

The lower crosslinked sample (NR1) is slightly deviates from the line of linearity in affine and phantom model. The reason for deviation of low crosslinked samples is that entanglements are partially removed in swollen samples and is more effective at very low crosslinked samples. In Mooney-Rivlin method all the points are more aligned on the straight line because in semiempirical equation (Equation (3.12) and (3.21)) has accounted the physical crosslinks (entanglement) as a function of chemical crosslinks and appropriate constant obtained from the experimental results are added [72].

3.7.2 Estimation of different sulfur bridges population

In sulfur vulcanized rubber networks, the mechanical properties may vary depends on the rank of sulfur bridges links between two polymer chains. The sulfur bridges population depends on the type of vulcanization system. Conventional vulcanization (CV) system contains maximum polysulfidic bridges and efficient vulcanization system (EV) contains the minimum and semi efficient vulcanization (SEV) system is in between CV and EV [81]. These vulcanization systems were classified according to the sulfur to accelerator ratio in the compound recipe [81]. The present natural rubber samples are conventional vulcanization systems. This is the reason why we observed more than 50% polysulfidic links even in the lowest amount of sulfur networks. The poly-sulfidic links percentage is slightly increasing with sulfur content is shown in Figure 3. 10. The mechanical properties such as fatigue resistance, tear resistance may high in higher polysulfidic bridges rubber network. The disadvantages with the high polysulfidic bridges rubber networks are low reversion resistance; low heat aging resistance and high heat build up [81]. Estimation of sulfur bridges rank in the rubber network is essential for appropriate application of the vulcanized elastomer. With the help of thiol probe and selective cleavage of poly sulfidic bridges and applying the equilibrium swelling methods, we were estimated the mono and di sulfidic

bridges and subtracting those mono-di sulfidic bridges from total sulfidic bridge crosslinks, we estimated the polysulfidic bridge crosslink percentage and plotted verses sulfur content shown in Figure 3. 10.

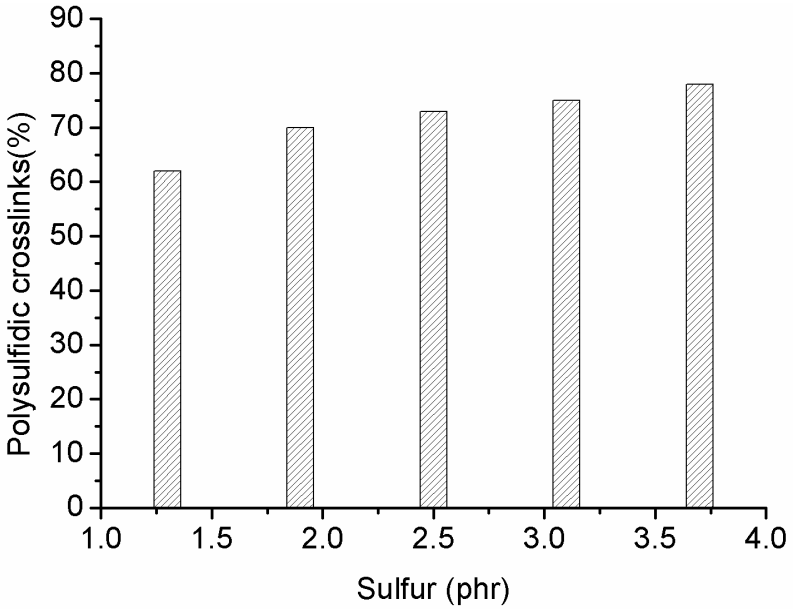

Figure 3. 10 *Poly sulfidic crosslinks percentage variation with sulfur content.*

3.7.3 Comparison of crosslink density obtained from different models

The comparison of crosslink density obtained from both network models and phenomenological models are shown in Figure 3. 11. The error in each measurement also estimated by measuring the crosslink density of five specimens of each sample and the error bars included in the plot shown in Figure 3. 11. It is very clear and expected that phantom network model crosslink density is higher than affine network model crosslink density due to the assumptions of each model developed [1]. The simple difference between affine and phantom models is that fluctuation of crosslink junctions. The affine model assumes that crosslinks are strongly connected to the macroscopic body and the ends of the network strands deform same manner with the macroscopic deformation. The phantom model assumes that the crosslinks are not rigidly fixed and are free to fluctuate around the network junction up to certain distance. So the deformation of the network strand is suppressed by the fluctuating crosslink junction. Due to these simple differences, the affine model modulus is double that of phantom model. Resultant the crosslink density is higher for phantom network model and is clearly evident from the Figure 3. 11. With increase of concentration of crosslinks the model shifts from phantom to affine [8]. In both the network models, the very

less amount crosslinked network (sample NR1) data point is slightly deviated from the linearity of the rest of the networks crosslink density. This is due to the fact that under percolation threshold of crosslink yield, the entanglements play a role and these entanglements are disentangled during the swelling and less trapped entanglements present in the network.

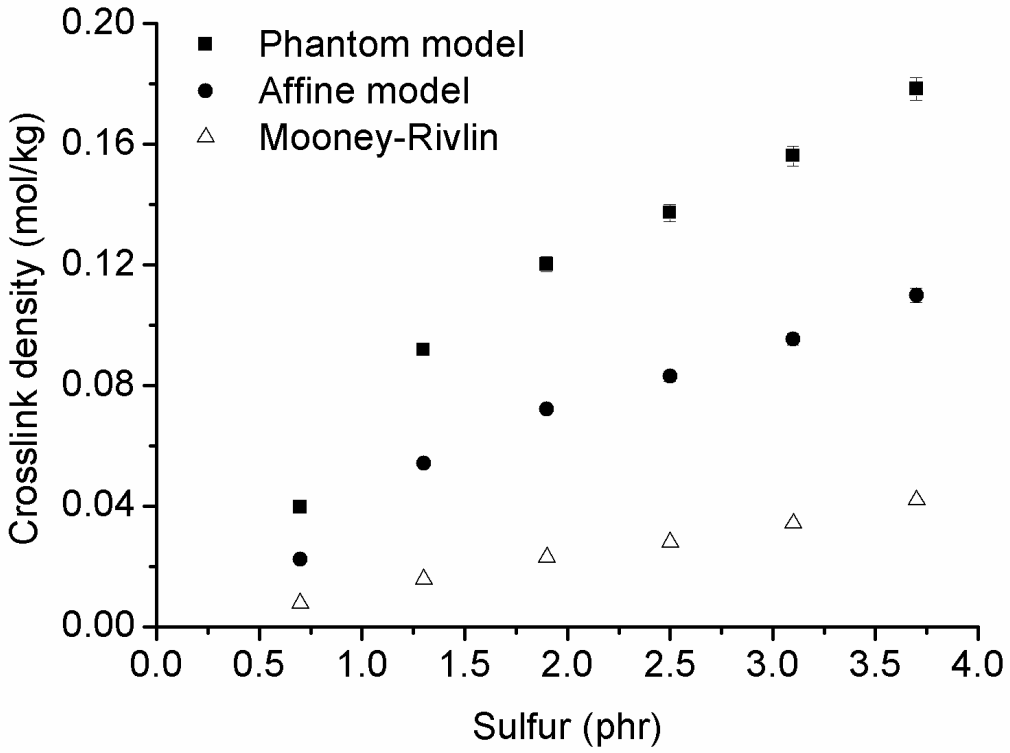

Figure 3. 11 *Comparison of crosslink density of natural rubber networks obtained from different models.*

The quantitative difference between molecular network models and phenomenological model obtained crosslink density numbers is due to the reason that in Mooney-Rivlin, we used the entanglement corrected Equation (3.12). Interestingly after adding entanglement molecular weight or molecular weight between two entanglements [83, 84], the Mooney-Rivlin crosslink density lie between affine and phantom molecular model crosslink densities. It is worth to mention that affine and phantom models are two extremes of real networks [53, 65]. The real networks are in between affine and phantom models and also need to recall that, when crosslink functionality is high the ends of the network strands or network junctions are more restricted to move (more rigid) and phantom model approaches to affine model. Figure

3. 12 is suggests that Mooney-Rivlin crosslink density numbers moving from phantom model to affine model with increase of crosslink concentration (or sulfur concentration) in agreement with mechanical measurements proven in literature [82].

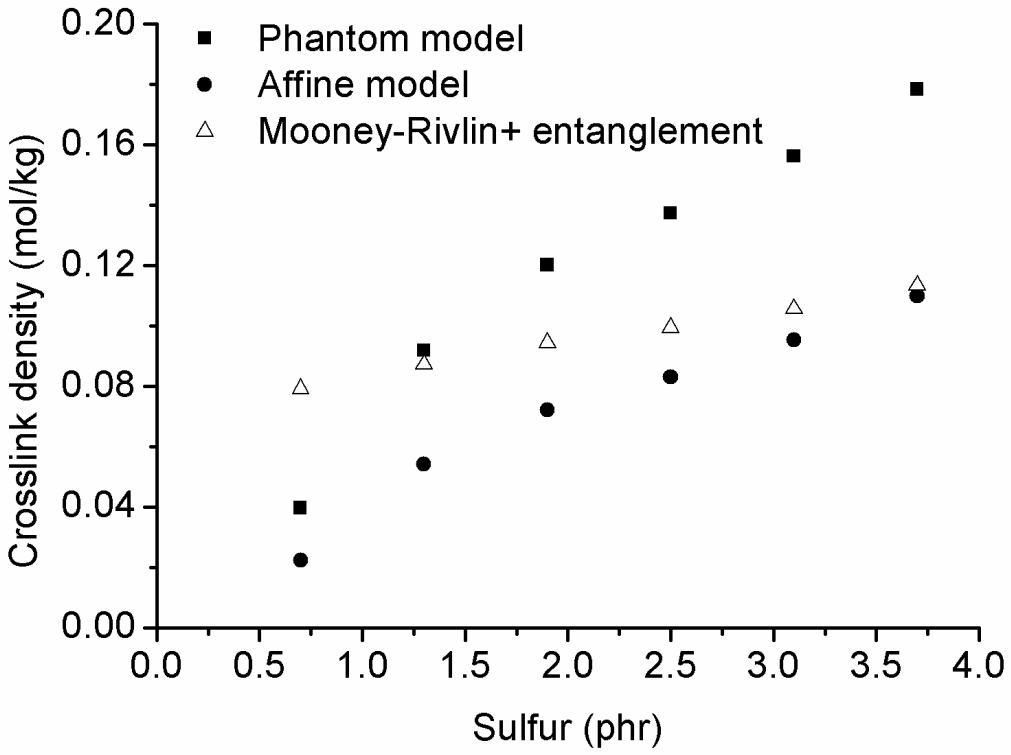

Figure 3. 12 *Crosslink density of natural rubber networks measured by molecular and phenomenological models. In Mooney-Rivlin, entanglement crosslink density also added.*

Irrespective of the model adopted for measuring the molecular parameters such as molecular weight between crosslink junctions, the swelling experimental observable that is volume fraction of rubber (polymer) (v_r) in the swollen gel network should give us the relative quantitative network density. The v_r is a function of all kinds of restrictions given to the motion of network strands or network junctions. The crosslink agent concentration versus volume fraction of rubber is plotted in the Figure 3. 13 .

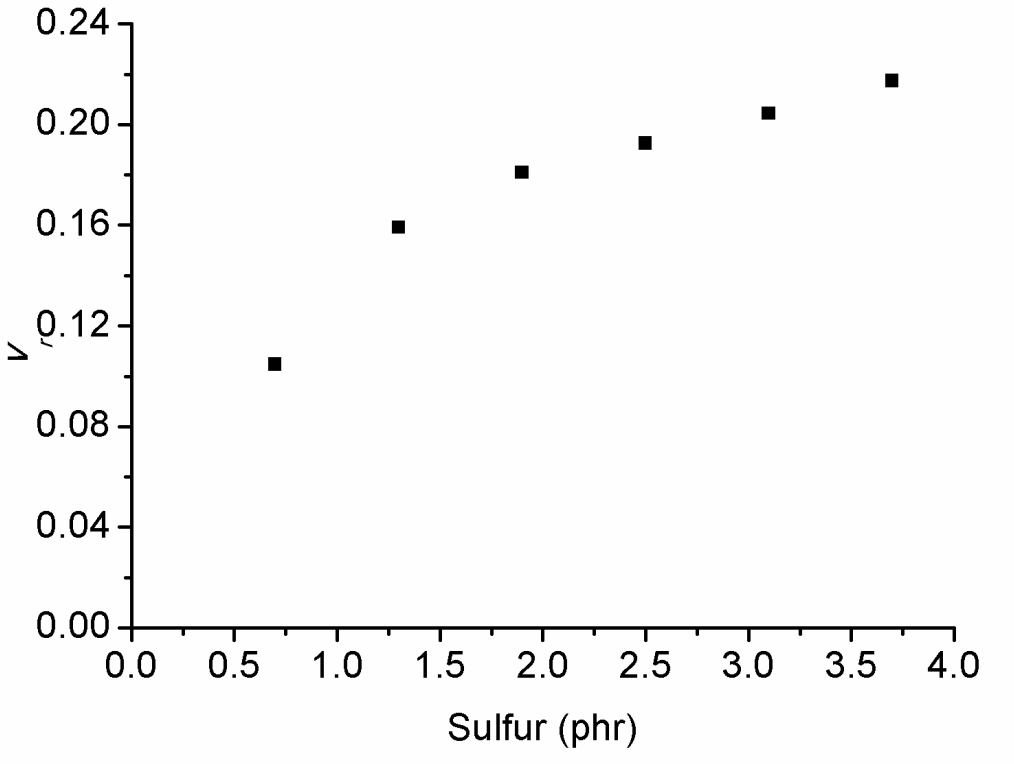

Figure 3. 13 *Sulfur concentration versus volume fraction of rubber (V_r) in natural rubber swollen networks.*

3.7.4 Comparative study of crosslink density obtained by Equilibrium swelling and MQ NMR

In the present section will discuss the crosslink density of natural rubber networks obtained by two independent methods (equilibrium swelling and MQ NMR) and detailing the strengths and weaknesses of two mthods.

For the last three decades the MQ NMR is emerging as an excellent tool for measuring crosslink density in polymer melts and gels but the most traditional method is equilibrium swelling. Here the quantitative results obtained by two methods are compared. As already discussed earlier in this chapter that the equilibrium swelling results are molecular model dependent. The recent literature [53] suggested that phantom statistical model is more appropriate.

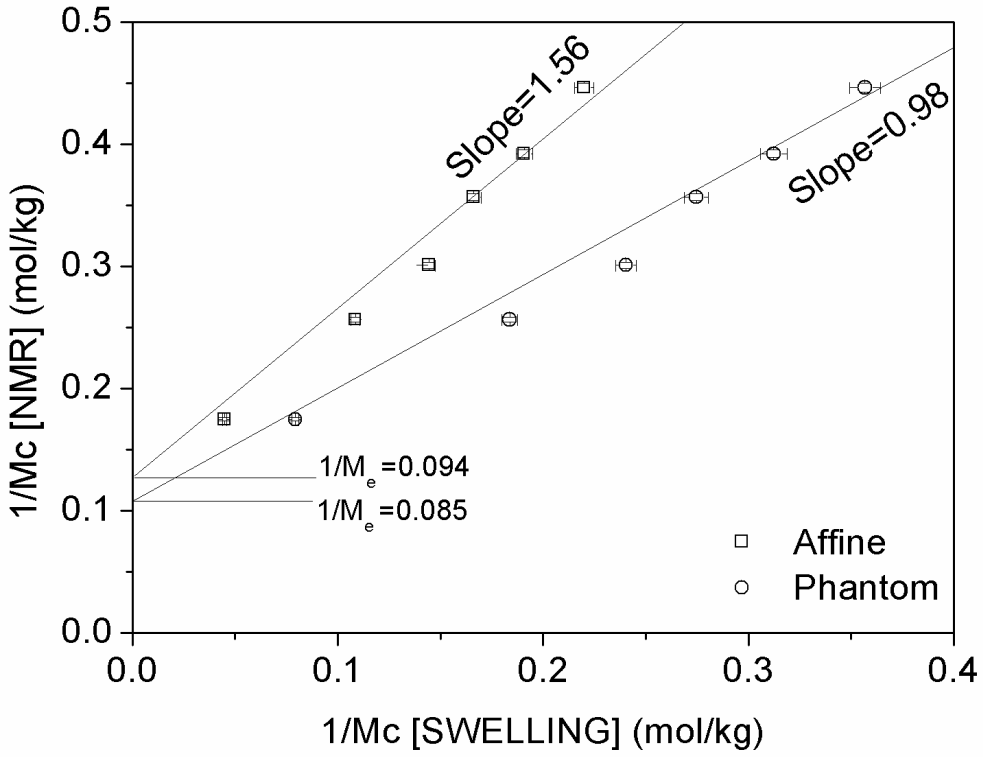

Figure 3.14 *The reciprocal of molecular weight between crosslinks for natural rubber networks obtained by two independent techniques, equilibrium swelling and MQ NMR.*

The linear relationship between M_c obtained from MQ NMR and swelling method by applying affine and phantom models are as shown in Figure 3.14 . If both swelling and NMR gave correct, absolute results, the slope and intercept could be unity and zero respectively in Figure 3.14 . The slope is close to unity (0.98, obtained R^2- value for linear fitting is 0.98) for phantom model where as higher slope (1.56, obtained R^2- value for linear fitting is 0.984) is observed for affine model. The reason is due to the assumptions of each model are different. The reason for existence of y-intercept is explained by the following relation [53]:

$$\frac{1}{M_C(NMR)} + \frac{1}{M_e} \approx \frac{1}{M_c(swelling)} + \frac{1}{M_{te}} \tag{3.25}$$

It arises due to the fact that NMR is not only measuring chemical crosslink restrictions but also additional restrictions, imposed by entanglements in bulk samples and are partially released at equilibrium swelling state, that means M_e (total entanglements) greater than or equal to M_{te} (trapped entanglement)[37,85,86]. In conclusion, NMR results are sensitive to crosslinks, entanglements and trapped entanglements whereas the swelling experiments is determined only crosslinks and trapped entanglements that could not be released under swollen conditions. Therefore, the y-intercept is equal to the difference of total entanglements measured by the NMR and trapped entanglements present in swollen state.

3.8 Conclusions

The equilibrium swelling is more traditional and well popular method for measuring crosslink density in vulcanized and other polymer networks. However the quantitative results obtained are model dependent. Equilibrium swelling method could not only gives overall crosslink density but also mono-di and polysulfidic crosslinks population in the sulfur cured systems by applying thiol probe and selectively cleaving of different sulfur bridges. The swelling crosslink density numbers are quantitatively well agree with independent MQ NMR results, only when phantom model is applied for swelling method. The comparative study of two independent methods revealed the strengths and weaknesses of each method.

Chapter 4
Study of over-cure effects in sulfur-cured rubber compounds by NMR and Swelling methods

4.1 Introduction

The elastic and mechanical properties of rubbers are regulated by crosslinks between highly mobile long polymer chains, formed in a complex chemical process called vulcanization. A full understanding of the resulting three dimensional network structure-property relationship is still the subject of vigorous research [80]. In fact, mechanical and thermal properties of vulcanizates are influenced by the amount and distribution of crosslinks [87] that in turn may depend [60] on the vulcanization system, backbone structure of the polymer, concentration of curing agents, cure temperature etc.

Moreover, addition of fillers and blending between different polymers are commonly used in industry to fine tune the properties of materials, further complicating their analysis. Different grades of carbon black are the most commonly used fillers in tire industries [5, 6] alone or combined with nonblack fillers [3, 4]. Further opportunities are provided by the emerging class of nano-fillers: nanoparticles [8], carbon nanotubes [9] and graphene [10]. The interaction between filler and rubber and the influence of fillers on the vulcanization reaction itself are aspects that still attract attention of researchers from both academia and industry. Blending between different polymers, including natural rubber (NR), polyisoprene (IR), polybutadiene (BR) and various grades of styrene-butadiene rubber (SBR), is also widely employed to combine desired features of different polymers[88]. Properties of the blends often differ from the weighted average of component rubbers, due the formation of different but interconnected phases [89] and to distribution of fillers and additives within them [90]. Diffusion of curatives and reaction rates are also different at different cure temperature in BR and IR. For example, in a given blend, different cure conditions can favor the crosslinking of one polymer rather than other [91]. As a result crosslink distribution also varies, making the characterization of cured blends particularly challenging [92]. Further options are provided

by the use of compatibilizing agents [93] or by the interaction of a filler with a blend, where the partition of the particles between different phases is a factor influencing the macroscopic properties [94].

In presence of so many different parameters, whose control in an industrial context is subject to time and cost constraints, variations in the final properties of the material are easily introduced. Thus, there is increasing need of faster and more precise characterization techniques to assist the production or post-production.

The single most important parameter for structure-property correlation is the molecular weight between crosslink junctions (M_c), which is inversely proportional to crosslink density. The most commonly used methods for the estimation of the crosslink density are equilibrium swelling[65], mechanical measurements [95], high resolution NMR [96] and low resolution TD-NMR at high [97] and low field [2]. Instruments were also developed for measurement in inhomogeneous magnetic field, allowing applications also on finished products [98].

Rheometry can analyze rubber compounds at the macroscopic level, and is thus used to determine cure parameters phenomenologically. For example, rheometric analysis of vulcanization is based on the assumption that measured torque during vulcanization reaction is proportional to the effective crosslinking [9].

Equilibrium swelling is a widely applied technique to determine crosslink density of elastomer networks. This method is based on the Flory-Rehner theory of network models developed from the ideal network assumptions. These models are derived for any deformation in the network including swelling [83] caused by the absorption of solvent. The quantitative results obtained from this method always depend on the choice of model as demonstrated in chapter 3 and of the thermodynamic parameters related to the polymer-solvent interaction. Erman [65] reviewed the molecular foundation of affine and phantom models in detail by comparison of several experimental techniques with theoretical predictions of real networks. Equilibrium swelling method qualitatively agrees well with any other independent method in characterizing unfilled (“gum”) vulcanizates as proven in the chapter 3, but in case of practically important filler-reinforced rubbers such direct agreements could not be established, especially with methods investigating the molecular level.

Even in absence of a comprehensive theoretical model on the issue of filler restrictions on swelling, Lorenz and Parks [99], and later Kraus [100], were able to assess the filler

restriction on swelling. According to their observations on filled vulcanizates, at constant loading of given filler, the apparent number of network chains is approximately a constant multiple of the number of crosslinks in the unfilled vulcanizates. This approximation is independent of network crosslink density in the unfilled vulcanizates. The constant multiple depends on the volume fraction of loaded filler and filler type. This relationship helps in evaluating physical crosslinks or swelling restrictions caused by the filler in the filled vulcanizates.

NMR spectroscopy is a powerful tool for studying the structure and dynamics of a variety of polymer systems such as elastomers [101], filled rubbers [102], polymer melts [103] and block copolymers [104]. The traditional transverse ^{1}H-NMR relaxation [97] was recently complemented by multiple-quantum nuclear magnetic resonance method (MQ NMR), whose application to unfilled and filled rubbers was extensively described by Valentin [53, 85]. The existence of crosslinks or any topological constraints in the rubber matrices causes anisotropic fluctuations in the semi-local segmental level of polymer chains and generates residual dipolar couplings. The magnitude of residual dipolar coupling constant (D_{res}) can be measured by MQ NMR and is related to network microscopic parameters such as crosslink density, entanglement length and the presence of other topological constraints [37], and can be used to follow in detail the evolution of a polymer network, for example when crosslinking is induced by radiation [86].

The primary aim of present chapter work was to precise determination of the crosslink density in sulfur cured polyisoprene and polybutadiene networks and their blends. This was performed by applying TD-NMR to challenging tasks like following minute network evolution during over-cure period. The technique has been previously [53] tested on samples with much larger range of crosslink density, obtained through different amounts of sulfur rather than by modification of the same network. The effects of fillers on same compounds were also studied. Results were compared with swelling measurements, demonstrating MQ NMR can provide equivalent data with higher precision and less experimental time. Moreover, TD-NMR can provide data on crosslink distribution that are inaccessible by swelling [105]. To the best of my knowledge there are no reports available on studying blend crosslink density and distribution at the microscopic level using MQ NMR. Here we took advantage of NMR for studying polyisoprene/polybutadiene blends crosslink densities compared to pure polyisoprene and polybutadiene networks prepared in similar conditions.

4.2 Experimental

4.2.1 Sample preparation

Polyisoprene (IR) and polybutadiene (BR) rubber samples were kindly supplied by Pirelli Tire. The label IR indicates high cis-polyisoprene (cis-1, 4 content 97% min) low viscosity (Mooney viscosity (ML (1+4) 100°C) 70±5 MU) obtained by solution polymerization with Ziegler/Natta catalyst. BR samples were high cis-polybutadiene (cis-1,4 content 97% min) low viscosity (Mooney viscosity (ML (1+4) 100 °C) 43±3MU) polymerized by Neodymium catalysts. Details of the sulfur based cure recipes, including the type of carbon black (N234) used for filled samples are given in Table 4. 1. Compounds were prepared in an open two-roll mill using standard mixing procedure and vulcanized in pneumatic double plate press at a temperature of 170 °C and 150 °C for unfilled and carbon black filled samples respectively. The optimum cure time (t_{95}) was deduced from the rheometric curves shown in Table 4. 2. Samples were prepared with varying cure time, starting from 7 minutes, which was slightly below optimal cure time for carbon black filled compounds, up to 50 minutes.

Table 4. 1 *Unfilled and carbon black filled polyisoprene, polybutadiene and blends vulcanizates recipes.*

Sample	Polyisoprene (phr)	Polybutadiene (phr)	Carbon black N234 (phr)	Sulfur (phr)	ZnO (phr)	Stearic acid (phr)	CBS* (phr)
BR	-	100	-	1.2	2.5	2	2.8
IR+BR	50	50	-	1.2	2.5	2	2.8
IR	100	-	-	1.2	2.5	2	2.8
BR (CB)	-	100	50	1.2	2.5	2	2.8
IR+BR (CB)	50	50	50	1.2	2.5	2	2.8
IR (CB)	100	-	50	1.2	2.5	2	2.8

* N-cyclohexyl-2-benzothiazole sulfonamide, a curing accelerator.

4.2.2 Rheometry

Rheometry analysis was performed on a Monsanto MDR (Moving Die Rheometer) 2000E. Cure curves were recorded for 50 minutes as shown in Figure 4. 1.

4.2.3 Equilibrium swelling

The vulcanized rubber network crosslink density was determined by equilibrium swelling measurements performed in toluene solvent at temperature of 20 °C. Experiments were also performed on samples treated with cleaving agents that break polysulfidic links, following established literature procedures [106].

The modified Flory-Rehner equation was used to calculate the network crosslink density by adopting phantom model according to the equation (3.19).

We used the values of χ = 0.39 for toluene-polyisoprene rubber pair, χ = 0.36 for toluene-polybutadiene [79] rubber pair.

In reporting crosslink density values, we considered both the statistical error of the measurement and the error due to differences in samples from different batches produced with the same nominal parameters. This last aspect is important, since it was verified by forensics studies on rubber gloves of commercial origin that NMR results can vary significantly even within a single batch [13]. Thus, statistical error was evaluated by five measurements on samples prepared at the same time from the same compound, resulting in a standard deviation ±2.2% in the measured crosslink density. By measuring five separately cured samples with the same nominal recipe and cure time, an error of ±7% was instead determined.

In filled vulcanizates, filler particles adsorb elastomer chains and act as physical crosslinks and create swelling restrictions, thus increasing the apparent crosslink density. In order to obtain actual chemical crosslink number, it was necessary to make the following correction [72] according to the type and volume fraction of the loaded filler:

$$Actual\ crosslink = Apparent\ crosslink/(1 + K\emptyset) \quad (4.1)$$

$\emptyset$ is the volume fraction of filler in the compound, and K is the constant for given filler (K= 4.53 for N234 carbon black). K depends on the structure and morphology of filler and is obtained from DBP measurements. Measuring the structure or morphology of carbon black is a more difficult task. The current industry test index is the dibutyl phthalate absorption number (DBPA). Dibutyl phthalate (DBP) absorption measures the relative structure of carbon black by determining the amount of DBP a given mass of carbon black can absorb before reaching a specified viscous paste.

4.2.4 TD-NMR Spectroscopy

Solid-state ^{1}H MQ NMR experiments were carried out on a Bruker Minispec the instrument details and sample preparation were given in chapter 2. All experiments were performed at 353 K temperature, well above the glass transition, to obtain temperature-independent structural information [53]. The instrument pre experimental conditions were given in chapter 2. Data acquisition was done with 128 scans and setting the recycle delay to 1 second. Even though good signal to noise ratio was obtained with 32 scans, due to the analytical nature of the work and probing small network differences, data acquisition done with higher number of scans.

The molecular weight between crosslinks junctions M_c was measured using a recent version [2] of the Baum and Pines MQ experiment [18]. Experimental data were analyzed using fast Tikhonov regularization (*ftikreg*) procedure [61] to obtain the average residual dipolar coupling constant (D_{res}) and its distribution. Statistical error on D_{res} was evaluated at ±0.8% on the basis of five measurements, while the error associated to measuring five separately cured samples with the same nominal recipe and cure time was estimated at ±2%. The residual dipolar coupling constant is related to M_c according to the Equation (2.20). The crosslink density can be obtained from M_c according to the crosslink density expression ($1/2M_c$).

4.2.5 High Resolution Magic-Angle Spinning- ^{13}C NMR

Vulcanized rubber compounds ^{13}C-NMR measurements were performed on Bruker Avance 400 NMR spectrometer at ^{13}C frequency of 100.62 MHz. Measurements were performed at room temperature on a high resolution MAS probe using magic angle spinning at 5 kHz. Data acquisition was done with 30,000 and recycle delay had set to 2 s. To shorten measurement time 0.08 M $Cr(acac)_3$ paramagnetic relaxation agent were used in $CDCl_3$ solvent.

4.3 Results and Discussion

4.3.1 Rheometric study of vulcanization

Cure curves of unfilled and carbon black filled compounds are shown in Figure 4. 1. Addition of carbon black accelerates the cure kinetics, thus different temperatures were chosen for the two groups of samples in order to obtain similar optimum cure times.

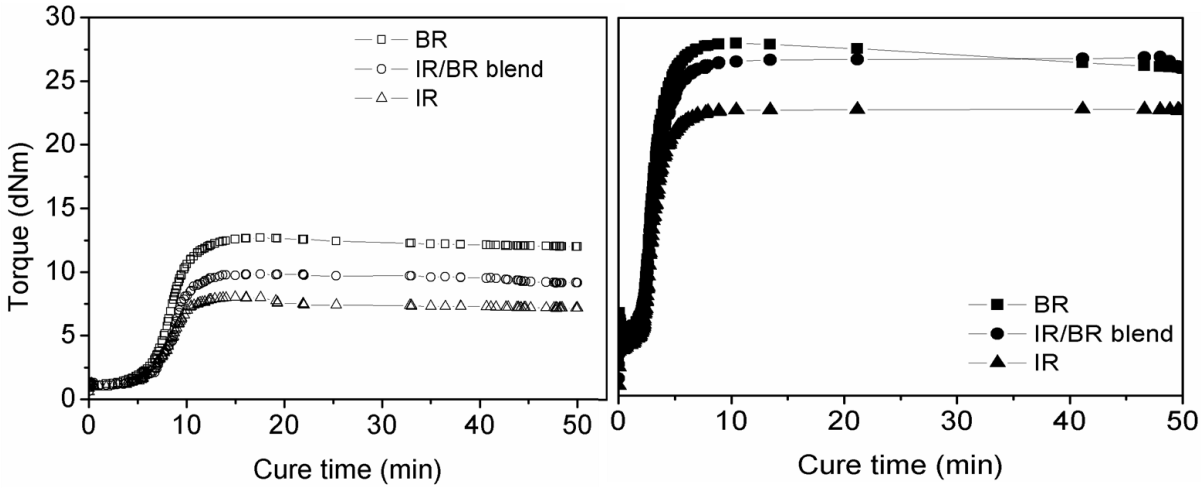

Figure 4. 1 *Vulcanization curves of unfilled (left) and carbon black filled (right) compounds cured at 170 °C and 150 °C temperature respectively. Samples were over cured for several tens of minutes after reaching the optimum values (t_{95}).*

The curves follow the typical behavior where three periods can be observed. The first period, during which torque is relatively constant but accelerator reactions occur, is called induction period or scorch time. It is followed by cure period, during which actual crosslinking process takes place and network structure is formed. The third and last stage is over-cure or post cure

period, during which torque can increase, decrease or remain constant depending on the particular vulcanization system [80] and nature of the elastomer.

It is evident from the rheometry curves that the torque increased substantially where filler was added to the gum rubbers. Polyisoprene compounds exhibit lower torque values than polybutadiene compounds in both unfilled and filled samples, while the unfilled blend displays intermediate values. The filled blend tends towards filled BR values. The negative slope of filled polybutadiene torque during over-cure period indicates network degradation by reversion. Vulcanization characteristics obtained from cure curve analysis, such as the difference between maximum and minimum torque value M_H-M_L, scorch time (t_{s2}) and optimum cure time (t_{95}) are shown in. Table 4. 2.

Table 4. 2 *Vulcanization characteristics of studied compounds measured by rheometry. t_{s2} is the scorch time, t_{95} is the time required to reach 95% of maximum torque, while the time difference of t_{95} and t_{s2} is the actual cure time or second period of cure curve.*

Sample	M_H-M_L (dnm)	t_{s2} (min)	t_{95}(min)	t_{95}- t_{s2}(min)
BR	9.76	7.8	9.8	1.9
IR/BR	7.87	7.5	9.6	2.1
IR	6.88	5.8	8.7	2.9
BR (CB)	27.46	4.4	8.4	3.95
IR/BR (CB)	24.12	5.3	9.8	4.5
IR (CB)	19.91	4.9	9.9	5.0

Details of the kinetics depend on the sample: for example optimum cure time, t_{95} is reduced by adding carbon black to polybutadiene rubber compounds and increased for polyisoprene rubber compounds. Despite minor differences, for all samples t_{95} is around 8-9 minutes, thus for the study of over-cure we characterized samples prepared with a minimum of 7 minutes cure time, and subsequent increments of 10 minutes up to 50 min.

4.3.2 Crosslink density and network structure

Crosslink density was calculated from swelling data by applying the phantom network model (see Equation (3.19)). For all unfilled samples not treated with cleaving agents, crosslink density is plotted against curing time in Figure 4. 2. For ease of comparison, the correction indicated in Equation (4.1) was applied on the filled samples, which are also plotted in Figure 4. 2.

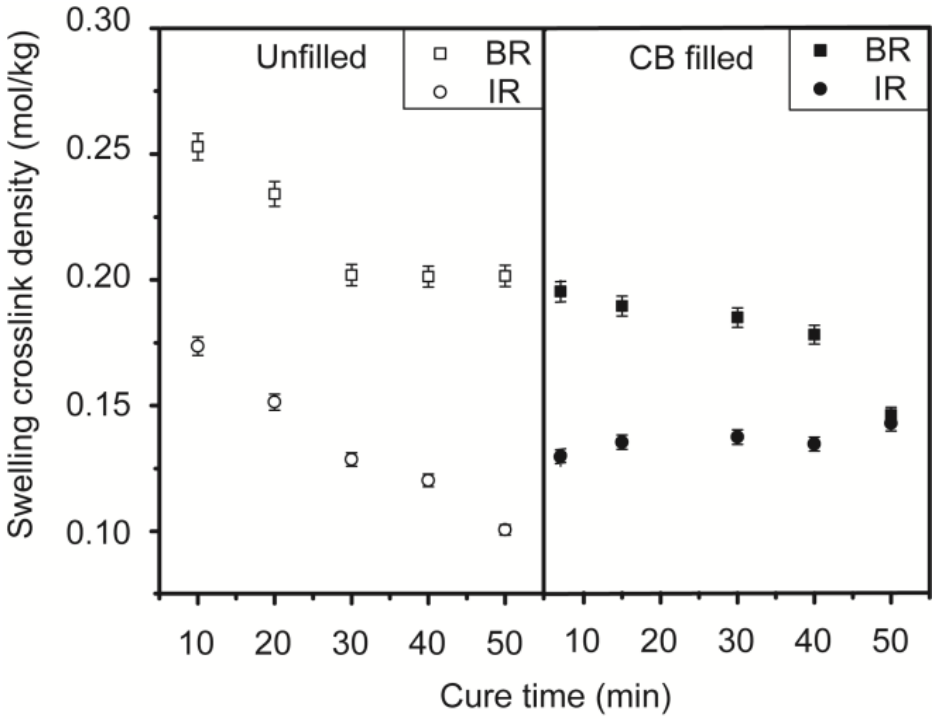

Figure 4. 2 *Crosslink density of unfilled (left) and filled (right) vulcanizates evaluated by equilibrium swelling method, and thus comprehensive of both mono-di and poly sulfidic links. Crosslink densities in filled compounds are plotted after subtracting the filler restrictions on swelling.*

The same calculation was performed on filled and unfilled samples treated with cleaving agents, obtaining lower crosslink values. Since cleaving agents are selective, the reduction of crosslink density corresponds to the quantity of polysulfidic crosslinks in the pristine rubbers, as reported in Figure 4. 3.

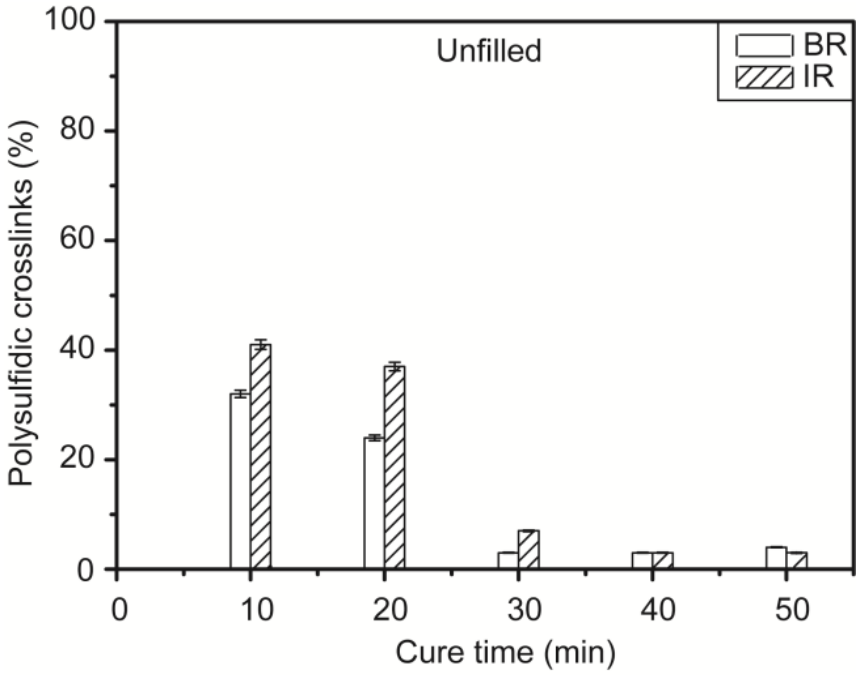

Figure 4. 3 *Percentage of crosslink density attributed to polysulfidic bonds in unfilled polybutadiene (BR) and polyisoprene (IR) vulcanizates as function of cure time. They were evaluated by difference between the swelling data of untreated and thiol/piperidine treated samples.*

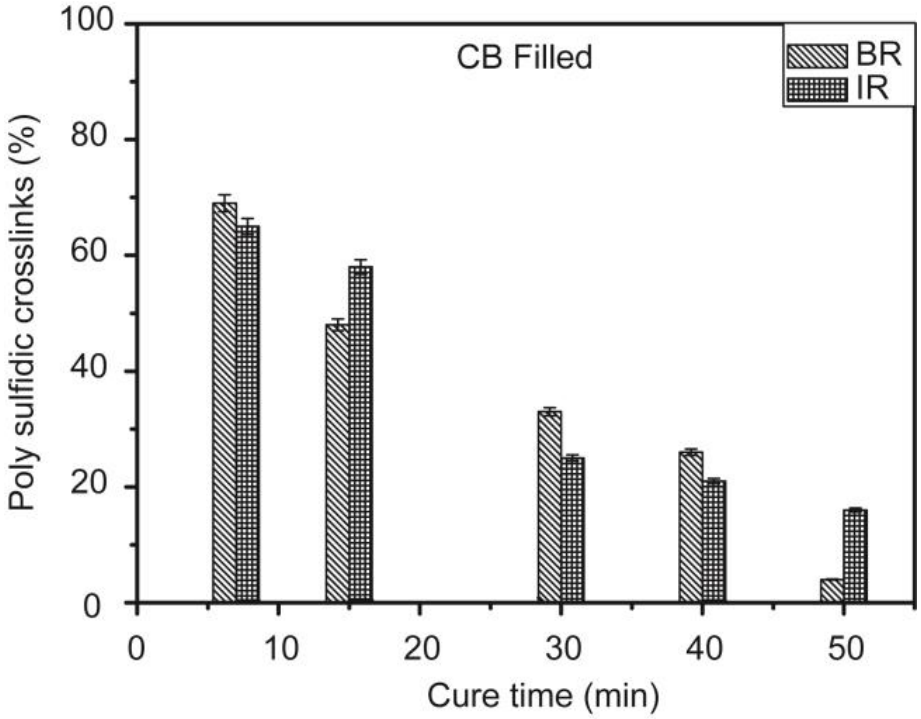

Figure 4. 4 *Percentage of polysulfidic crosslinks in carbon black filled polybutadiene and polyisoprene vulcanizates as a function of cure time. They were evaluated by comparing swelling data of untreated and thiol/piperidine treated samples.*

During cure time both the breaking and reformation of crosslinks are active. Thus, the evolution of the systems can be described as continuous breaking of less stable [80] polysulfidic links, partially or totally compensated by reforming of shorter sulfidic bridges. For example, unfilled polybutadiene network total crosslink density is decreasing with cure time up to 30 min, and is then almost constant up to 50 minutes. Polysulfidic links in the same system also decrease from a starting value of 30% to less than 5% within the first 30 minutes. Unfilled polyisoprene networks contain a higher proportion of polysulfidic crosslinks relative to polybutadiene networks. Those crosslinks decay from the starting value of more than 40% measured at 10 minutes of cure time to values of 7% at 30 minutes and 3% at 40 minutes. The overall crosslink density of polyisoprene networks instead decreases with cure time up to 50 minutes.

Thus, in BR the evolution of crosslink density is dominated by breakdown of the polysulfidic bonds. When they are depleted, at 30 minutes, further reduction of the total crosslink density is difficult. In IR, the evolution of total crosslink density is also initially dominated by polysulfidic degradation like in polybutadiene samples. After they are depleted lower degree polysulfidic link are also breaking.

Filled networks exhibiting higher amount of polysulfidic links at all cure times compared to corresponding unfilled compounds are shown in Figure 4. 4. The amount of total crosslink density variation is minute in polyisoprene network and continuous decay is observed in polybutadiene network shown in Figure 4. 2 (right). The constant overall crosslink density and at the same time decaying of polysulfidic links indicates that both the mechanisms of breaking and reformation of sulfidic links are competing in carbon black filled polyisoprene network.

4.3.3 TD-NMR results and comparison with swelling

MQ TD-NMR measured crosslink density of unfilled and carbon black filled polybutadiene and polyisoprene network are shown in Figure 4. 5.

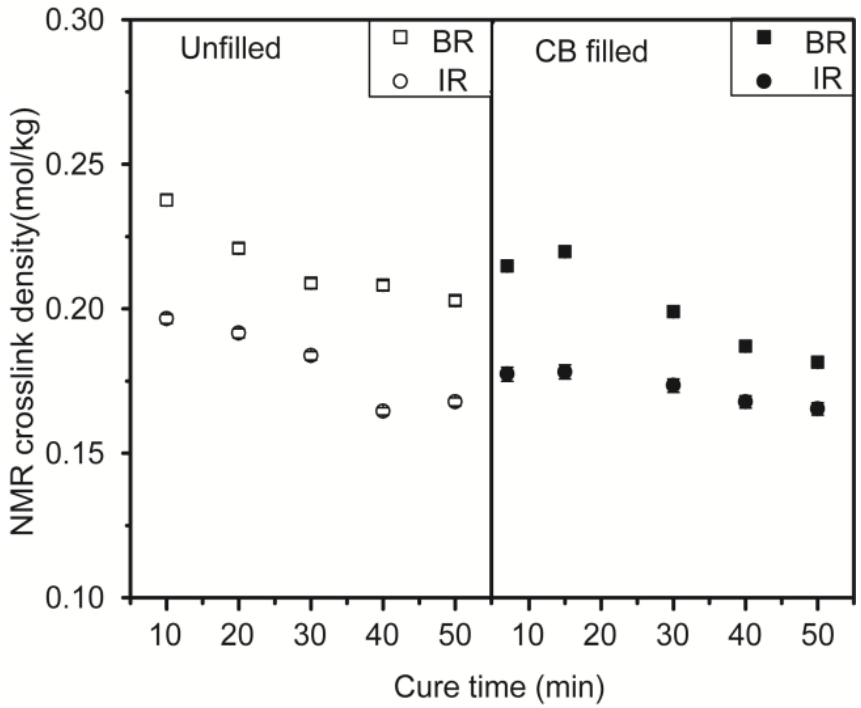

Figure 4. 5 *Crosslink density of unfilled (left) and filled (right) vulcanizates evaluated by multiple-quantum NMR method and plotted versus cure time.*

The values and their evolution with cure time are in agreement with equilibrium swelling method. Unfilled polybutadiene crosslink density is decreasing with cure time up to 30 minutes, and remains constant during further cure due to the presence of more stable mono-di sulfidic bridges, in agreement with Figure 4. 3. Polyisoprene networks crosslink density display a trend of continuous decay. Filled polybutadiene network crosslink density decays throughout the range of cure time due to the predominance of breaking of sulfidic bridges over the re-participation of broken sulfidic chains in cure. In filled polyisoprene compounds, the two mechanisms compete with each other, thus there is no clear tendency of decay or growth, as shown in Figure 4. 2 (right).

A comparison between crosslink density measured with the two methods in unfilled polyisoprene and polybutadiene networks is shown in Figure 4. 6.

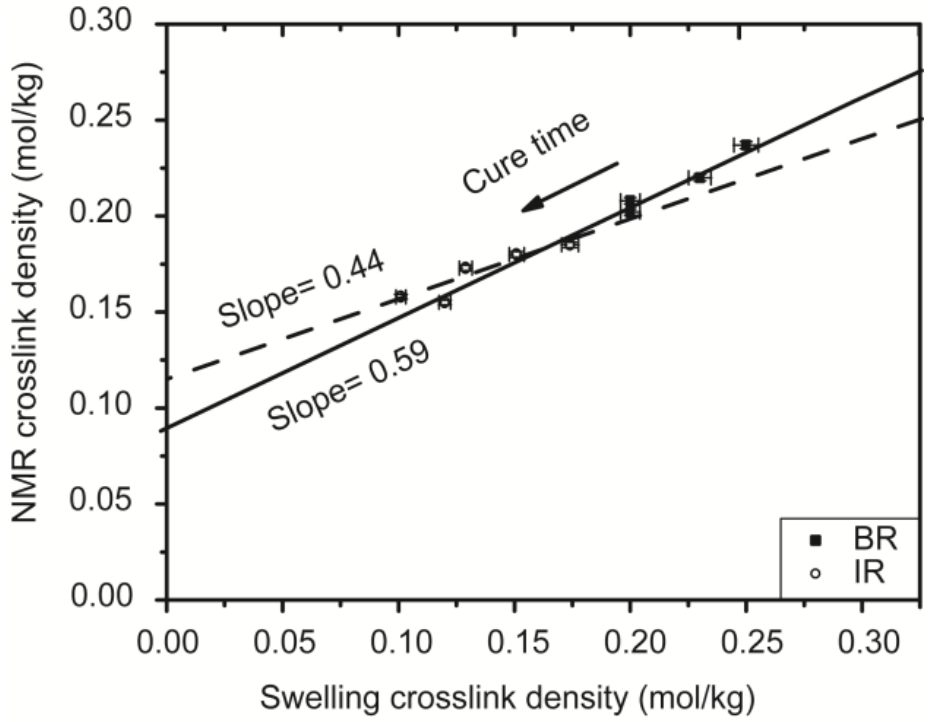

Figure 4. 6 *Polybutadiene and polyisoprene vulcanizates crosslink density measured by equilibrium swelling and MQ TD-NMR (arrow indicates progress of cure time). The good correspondence between the two methods is indicated by the linear fitting.*

Data are interpolated with linear functions, where slopes of polyisoprene and polybutadiene samples are 0.44 (R^2 = 0.93), and 0.59 (R^2 = 0.96) respectively. Intercepts are 0.11 and 0.09, values that differ from zero since NMR is not only measuring chemical crosslink restrictions but also physical restrictions imposed by entanglements that are partially released at equilibrium swelling state. This is understood by the relation given in Equation (3.25).

In Equation (3.25) the mass M_e of polymer chain entanglements is less than or equal to the M_{te} (trapped entanglement) [55-107]. Therefore, the y-intercept indicates a difference between total entanglements measured by the NMR and trapped entanglements present in swollen state. This is point out that mono and di sulfidic links are the same in NMR point of view, despite the fact that mono and poly sulfidic links can have different effects on the macroscopic mechanical properties [81, 109].

For a discussion of the validity of the correction proposed in Equation (4.1), uncorrected equilibrium swelling against NMR crosslink density of carbon black filled networks are shown in Figure 4. 7.

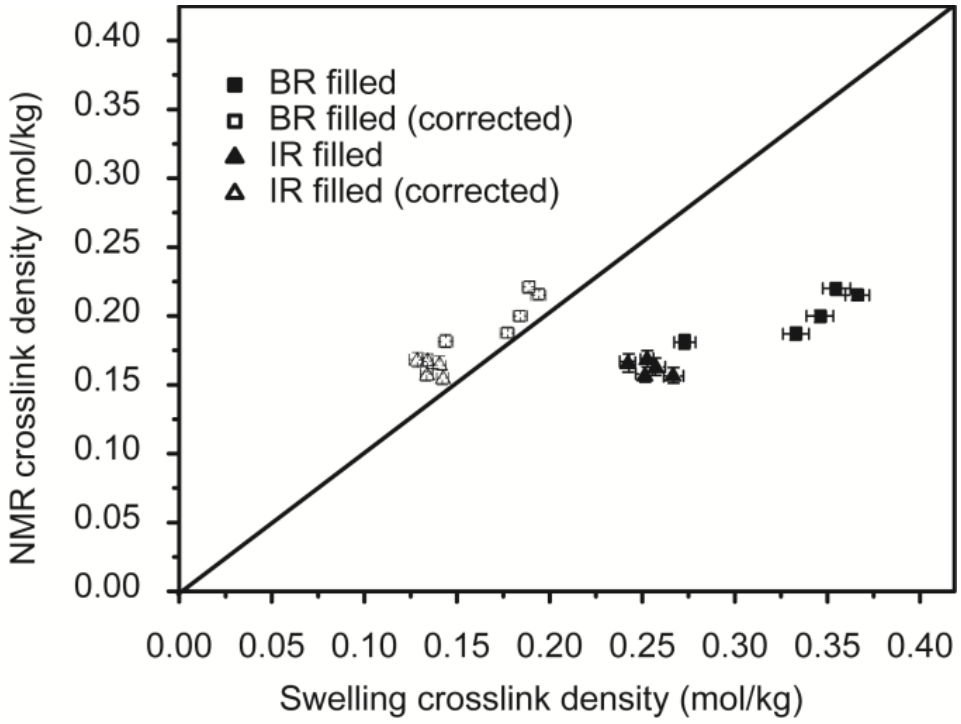

Figure 4. 7 *Carbon black filled polybutadiene and polyisoprene vulcanizates crosslink density measured by equilibrium swelling and MQ TD-NMR. A straight line passing through the origin having unity slope and zero intercept is displayed for indicating how the filler corrected results more closely match NMR results after the correction.*

In filled compounds, a substantial reduction of network swelling was observed compared to corresponding unfilled networks. The reason is the adsorption of polymer chains by the filler or by meshes of filler particles glued together, as described in literature [85]. Filled samples shown in Figure 4. 7 presented higher swelling crosslink density compared to corresponding unfilled sample. After subtraction of filler restrictions according to the Equation (4.1), swelling results are in better agreement with NMR. In filled networks, the linear correlation between successive data points is absent, indicating a limitation in the estimation of very minute network differences in presence of fillers. Note that filled samples in the present work actually span an even smaller range of crosslink density than unfilled samples. Still, corrected values are much closer to MQ TD-NMR results, corroborating the Lorenz, Parks and Kraus relation for filler restrictions on swelling.

In conclusion linearity between swelling and NMR is obtained in unfilled networks whereas in filled networks, filler restrictions has to be subtracted to obtain better matching of the data.

4.3.4 Network crosslink density and distribution by TD-NMR in blends

The calculation of crosslink density from the D_{res} proposed in Equation (2.20) is applicable to the polymers with a known D_{stat} constant and is not available for polymer blends. For a model free discussion of the IR/BR blend network, direct comparison of the MQ TD-NMR D_{res} is presented in Figure 4. 8 for the blend and the component rubbers. The weighted average of the D_{res} values of the two components, calculated considering the proton % associated to each polymer, is also presented. D_{res} values are also presented in Table 4. 3 and Table 4. 4. Polybutadiene displays higher residual dipolar coupling constant than the corresponding polyisoprene network. Unfilled blend D_{res} constants are very close, but always lower than the weighted average of pure components. This difference, while only marginally greater than the experimental error, can indicate preferential solubility of curatives in the polyisoprene, since the final D_{res} is shifted in the direction of the IR value. This was further validated by verifying that the D_{res} value associated to a mechanical mixture of IR and BR chunks with equivalent quantities is undistinguishable from the weighted average of the two components. This tendency is even less pronounced in filled blends since filler influence on cure kinetics and filler adsorption affinity also differs between polymers [105].

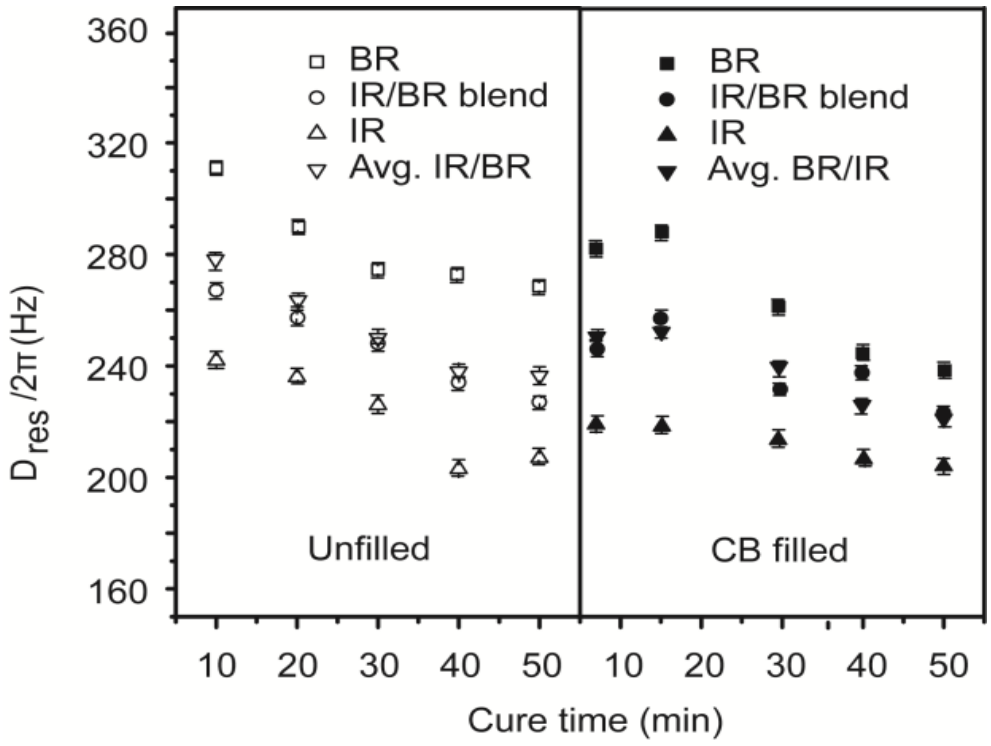

Figure 4. 8 *MQ TD-NMR measured D_{res} constants of polybutadiene (BR), polyisoprene (IR), blend (IR/BR) and weighted average of IR, BR vulcanizates networks at variable cure time. Values for blends are mostly close to the weighted average of the component rubbers.*

Table 4. 3 *D_{res} values of unfilled polybutadiene (BR), polyisoprene (IR), blend of IR and BR (IR/BR) and weighted average of BR and IR networks.*

Cure time (min)	BR $D_{res}/2\pi$ (Hz)	IR/BR blend $D_{res}/2\pi$ (Hz)	IR $D_{res}/2\pi$ (Hz)	Avg. IR&BR $D_{res}/2\pi$ (Hz)
10	311	267	242	276.5
20	290	258	236	263.0
30	274	248	226	250.0
40	273	234	203	238.0
50	266	227	207	236.5

Table 4. 4 *D_{res} values of carbon black (N234) filled polybutadiene (BR), polyisoprene (IR), blend of IR and BR (IR/BR) and weighted average of BR and IR networks.*

Cure time (min)	BR (CB) $D_{res}/2\pi$ (Hz)	IR/BR (CB) blend $D_{res}/2\pi$ (Hz)	IR(CB) $D_{res}/2\pi$ (Hz)	Avg. IR & BR (CB) $D_{res}/2\pi$ (Hz)
7	282	246	219	250.5
15	288	257	220	254.0
30	261	232	214	237.5
40	245	238	207	226.0
50	238	223	204	221.0

Analysis of MQ NMR data also provides a distribution of D_{res} values, and thus an experimental approach to measuring crosslink distribution that can be more informative on the network structure than a simple average, for example by detecting the presence of local inhomogeneities [56]. Sulfur cured polyisoprene networks near the optimal cure time exhibit a narrower distribution than the corresponding polybutadiene networks under same cure conditions as shown in Figure 4. 9.

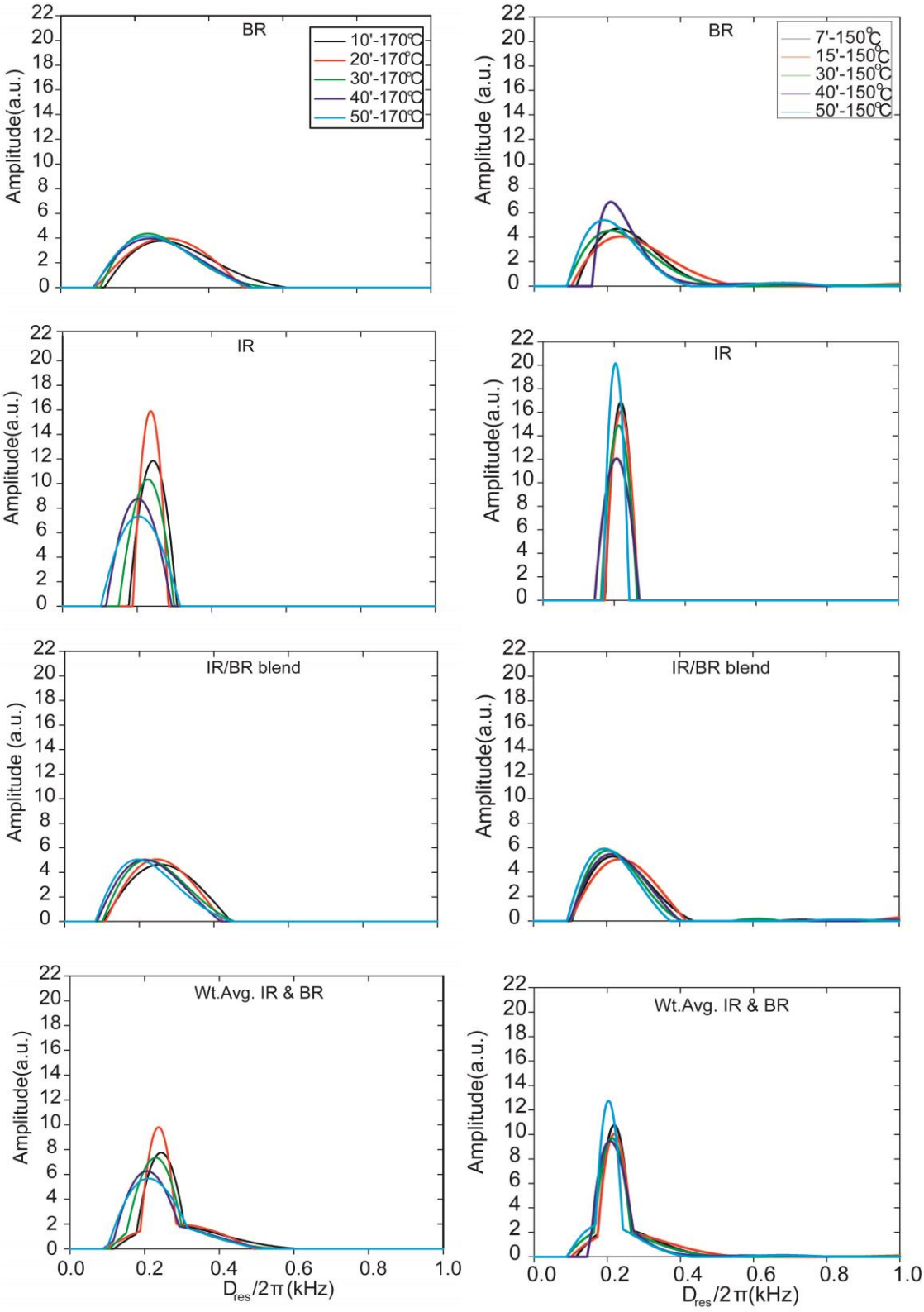

Figure 4. 9 *Over-cure effect on crosslink density distribution in unfilled (left) and carbon black filled polybutadiene (BR), polyisoprene (IR) and blend (IR/BR) networks. Numbers in the image legend indicate cure time and temperature respectively.*

Upon over-curing, unfilled polyisoprene changes drastically, probably due to the extensive restructuring of the greater number of polysulfidic links present. Its network D_{res} distribution becomes broader with cure time progress. The increased amplitude at low D_{res} values is evidence of chain scission, while increased amplitude at higher values is a sign of the formation of additional crosslinks. Since the average is moving towards low D_{res} values, the dominant phenomenon is chain scission in agreement with the decrease of total and polysulfidic crosslinks during over-cure period as shown in Figure 4. 2 and Figure 4. 3 respectively. In polybutadiene rubber networks D_{res} distribution is less affected by cure time, also in agreement with the crosslink density change observed by NMR and swelling methods. Filled compounds display a slightly narrower D_{res} distribution compared to corresponding unfilled vulcanizates shown in Figure 4. 9 (right). Their evolution over time follows the same trends discussed for unfilled vulcanizates.

For unfilled rubbers, a direct comparison between the D_{res} distribution of the blend and the weighted average of the two components is presented in Figure 4. 10. It is apparent that the system cannot be considered a simple juxtaposition of two separate rubbers, even though the IR/BR blend is known to present phase separation in the range of hundreds of nm [110], much greater than the scale probed by MQ NMR.

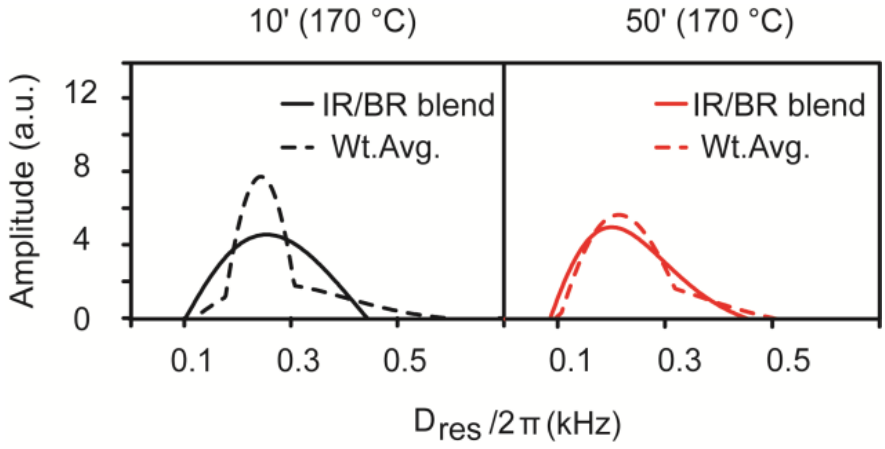

Figure 4. 10 *Over-cure effect on crosslink density distribution in blend (IR/BR) network compared with weighted average of constituting polymer networks. The cure time and temperatures are presented in the image.*

A possible explanation for this observed behavior and for the average D_{res} values observed in Figure 4. 8 involves the effect of different solubility and reactivity of curing agents in the two phases, resulting in much greater inhomogeneities even within the IR phase at low curing time.

4.3.5 ^{13}C HR-MAS NMR studies of vulcanizates

^{13}C HR-MAS NMR spectra of unfilled polybutadiene and polyisoprene compounds are shown in Figure 4. 11. The predominant monomer peaks are labelled in the image along with chemical structure. Detail of the aliphatic region of polybutadiene (BR), polyisoprene (IR), and blend (IR/BR) spectra of uncured and cured compounds are presented in the Figure 4. 12. The assignment of peaks for different crosslink structures [96] are numbered in the images. Structure labelling is presented in Table 4. 5 and Table 4. 6. In polybutadiene spectrum, many of expected crosslink peaks were not present. In polyisoprene cured compounds different crosslink structures [96] resonance peaks and peak broadening is observed. In blend resonance peaks related to two component polymers were observed. Parenthesis followed by peak number indicate polymer. Resonance peaks without literature attribution are represented by letter 'x'.

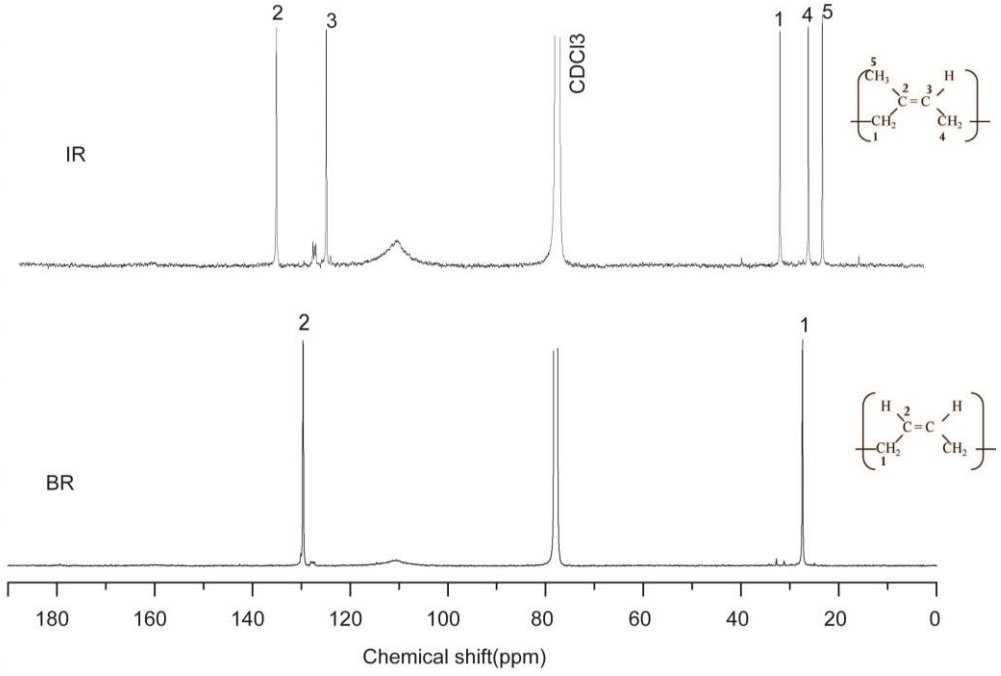

Figure 4. 11 *^{13}C HR-MAS NMR spectra of uncured polybutadiene (BR) and polyisoprene (IR) compounds.*

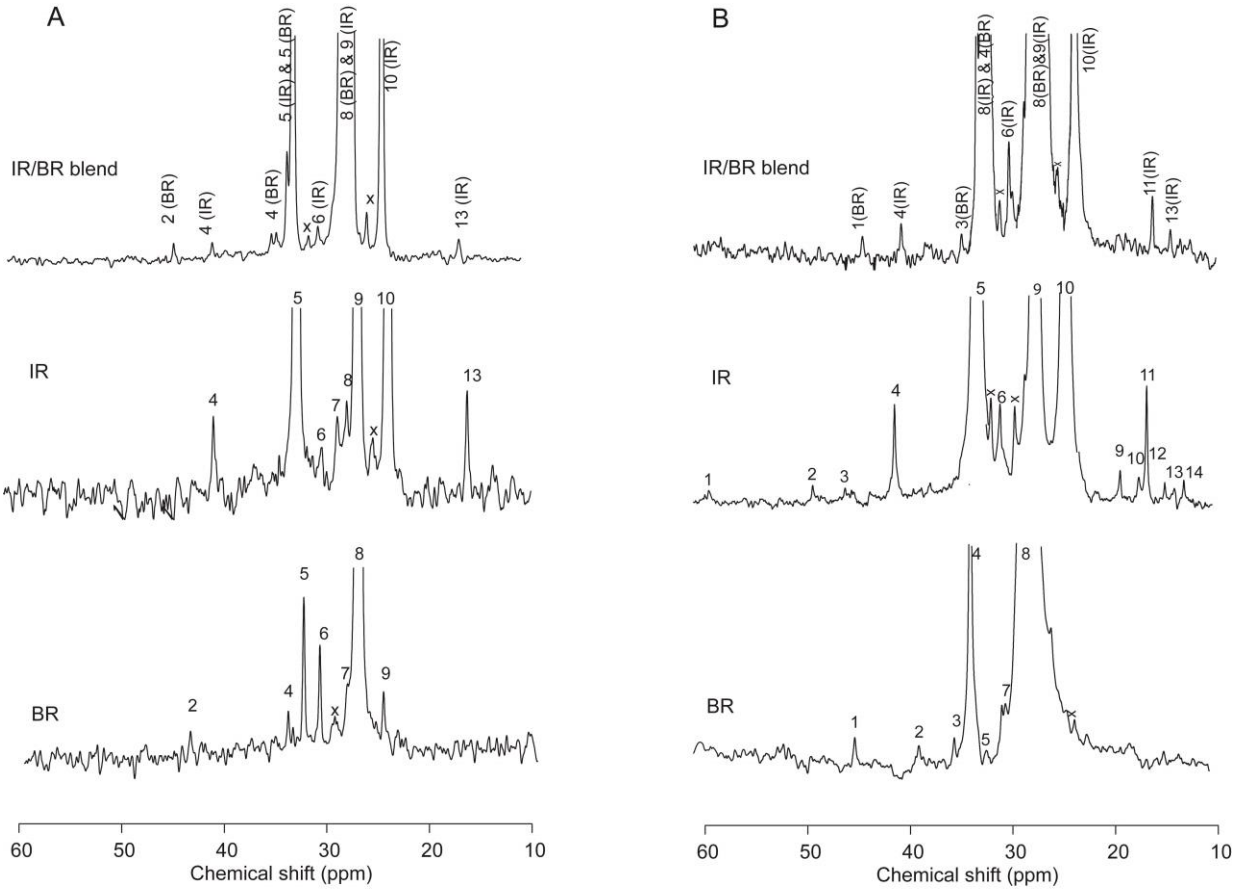

Figure 4. 12 *(A) Details of the aliphatic region of uncured BR, IR and Blend (IR/BR) compounds and (B) corresponding cured compounds for 10 min at 170 °C. In blend spectra peak labeling, in parenthesis IR and BR represents peaks corresponding to polyisoprene and polybutadiene components respectively.*

Table 4. 5 *Chemical shifts and possible structures of both uncured and cured polybutadiene compounds.*

Peak label	Chemical shift(ppm)	Structural unit
1	44.4(cured)	Polysulfidic crosslink
2	43.8(uncured)	1,2-dichloroethane(impurities present in $CDCl_3$)[111]
3	37.5(cured)	Stearic acid
4	34.3(both)	cis-1,4 monosulfidic-CH_2 –[96]
5	32.8(cured)	trans-1,4 C1
6	31.2(uncured)	Unassigned –CH_2-[96]
7	28.6(both)	cis-1,4 C1
8	27.4(both)	cis-1,4 C1
9	25.0(uncured)	cis-1,4 C1

Table 4. 6 *Chemical shifts and possible structures of both uncured and cured polyisoprene compounds.*

Peak label	Chemical shift(ppm)	Structural unit
1	59 (cured)	B1c-p(α)
2	48(cured)	B1c-p(α)
3	44.4(cured)	A1cm(ɤ)[112]
4	40.0 (uncured)& 40.1(cured)	cis -1,4 C1 & trans-1,4 C1
5	32.19(uncured),32.8(cured)	cis-1,4 C1
6	30 (both)	Fatty acid –CH_2-
7	28.3(both)	cis-1,4 C4
8	27.4(both)	Cis-1,4,C1
9	26.4(both)	trans-1,4 C4
10	23.5 (both)	cis-1,4 C5
11	18.0(cured)	B1c-p(ɤ)
12	17.5(cured)	B1t-p(ɤ)
13	16.0(both)	trans-1,4 C5
14	14.0(cured)	B1t-p(ɤ)

Some expected crosslink structure resonance peaks were not detected in butadiene compounds, possibly due to low intensity relative to the solvent ($CDCl_3$) peak shown in Figure 4. 11. It was difficult to quantify the crosslink density of small network differences with high resolution ^{13}C-NMR spectra.

4.4 Conclusions

In this present chapter, we detected minute differences in network structure by TD-NMR with high precision. Errors associated to those measurements are much smaller than the corresponding values measured with swelling experiments. Moreover, the experimental time is significantly reduced, thus demonstrating the feasibility of MQ NMR as a technique for quality control in industrial context and was the primary goal of present thesis work. In line with the analytical nature of this work, we set a relatively high number of accumulations. Even in these conditions, the required experimental time for crosslink measurement is limited to few hours for actual quality control applications; the experimental time could be further reduced by a factor of 2 or 4. Quantitatively good linear relation between two methods were observed in unfilled compounds whereas higher swelling measured crosslink density values were observed in carbon black filled samples, due to filler restrictions on swelling that have no equivalent at the microscopic level probed by NMR. After subtracting the filler related restrictions on swelling results both methods strongly agreed, thus validating the current approaches for filler correction at least in the case of conventional CB fillers. Changes occurring in the sulfur networks beyond the optimum cure time and the distribution of crosslinks are also discussed together with the effect of carbon black filler. Crosslink distribution in IR/BR polymer blends is studied by MQ TD-NMR for the first time. The comparison of residual dipolar coupling constants of blends and their distributions with those of pure components provides qualitative clues about different solubility/reactivity of curatives in the two rubbers composing the blend. High resolution ^{13}C-NMR could allow measuring the crosslink density from the peak intensity but the quantification of crosslink density in small network difference samples is tedious and need expert's hands for analyzing the data.

Chapter 5
Ionic elastomer Networks and Characterization with Low-Field ^{1}H-NMR

5.1 Introduction

Ionic elastomers are thermoplastic polymers with small amount of ionic groups in hydrocarbon polymers and exhibit unique physical and mechanical properties. Ionic elastomers are crosslinked by the association of ionic groups, forming multiplets or clusters and they are thermolabile in nature due to ionic domains. The covalent crosslinks are permanent and irreversible and are good candidates for elasticity. Besides its advantages, irreversibility creates greater recycling problems in rubber objects. Thermoplastic polymers are developed [113-114] to overcome the recycling problems. Ionic elastomers are one among them due to thermolabile nature and also exhibit exceptional mechanical properties. Ionic elastomers are characterized by a strong physically crosslinked network resulting from a phase separation of ionic-rich nano-domains. The ionic groups (e.g. carboxylic, sulfonic, phosphoric acids etc.) are either pendent to or incorporated in the nonpolar main chains. These groups are usually neutralized with metal cations forming ion pairs, which constitute the simplest form of inter or intra chain interaction. They tend to aggregate into more complex structures (multiples of different sizes) according to the ion content, nature and size of the polyion and counterion, dielectric constant of matrix polymer, glass transition temperature of the ion pair relative to the backbone, stearic constraints, amount and nature of added plasticizers, presence of added fillers, etc.

The theoretical basis for clustering of ionic groups in the organic polymers has been studied by A. Eisenberg [115]. Two decades later the same group developed the multi-cluster model [116] by considering much experimental results advancement in the same field. This model explains that an ionic groups form random ionic multiples, which reduce the mobility of the polymer chains in their vicinity. These kinds of isolated multiple acts as multi-functional crosslinks and increasing the glass transition temperature of the material. With increasing of

ionic content the multiples overlap to form larger contiguous regions of restricted mobility. When these regions become sufficiently large, they exhibit phase-separated behaviour and are termed clusters. The model is in good agreement with experimentally observed phenomena based on the dynamical mechanical and X-ray scattering techniques. In this chapter we tried to explain preparation and characterization of both covalent and ionic crosslinks as well as the immobile polymer around the ionic clusters with low resolution NMR.

In the present study we used carboxylated nitrile butyl rubber (XNBR) as rubber matrix, MgO metal oxides to create ionic crosslinks and dicumyl peroxide (DCP) crosslink agent for create covalent crosslinks. Commercial available micro TiO_2 powder and home-made (laboratory synthesize) TiO_2 nanoparticles were also used in this work. The main objective in using TiO_2 nanoparticles is to obtain optical properties in addition to the thermo reversible shape-memory effects.

By synergy between ionic (physical) and covalent (chemical) crosslinks in the polymer matrix, good mechanical and thermo reversibility properties could obtain and these polymers are called the *shape-memory polymers* (SMPs). Shape-memory polymers (SMPs)are polymeric smart materials that have the ability to return from a deformed state (temporary shape) to their original (permanent) shape induced by an external stimulus (trigger), such as temperature changes [117]. We aimed a step ahead and to complement shape memory effect with optical properties in this present work. The schematic of ionic and covalent mixed crosslink network with shape memory effect is shown in Figure 5.1.

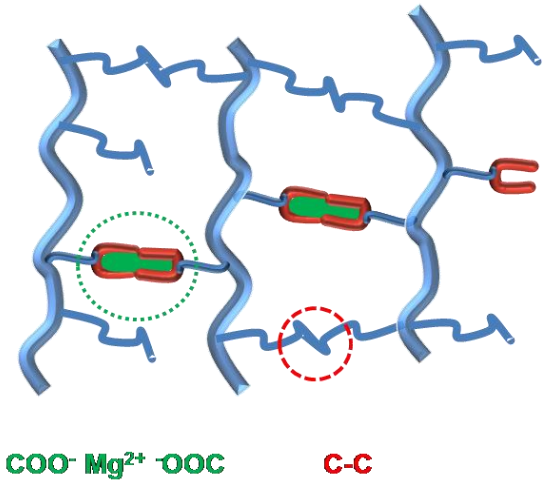

Figure 5.1 *Schematic illustration of ionic and covalent crosslink networks in the XNBR polymer with MgO and DCP.*

5.2 Carboxylated nitrile butyl rubber (XNBR) and ionic crosslinks

Carboxylated nitrile butyl rubbers (XNBR) are terpolymers of acrylonitrile, butadiene, and monomers containing carboxyl groups such as carboxylic acids (R-COOH) R- refers to the rest of the molecule. The pendent carboxyl groups provide ionic crosslinks by utilizing metal oxide curing agents, such as MgO, CaO, ZnO etc. Salts and esters of carboxylic acids are called carboxylates. Each divalent metal oxide neutralizes two pendent carboxylic acid molecules and form ion pair. Group of ion pairs creates multiples and such a multiples creates ionic clusters in nano size [118] and provides self-reinforcement to the XNBR matrix. These ionic domains are thought to act as multifunctional crosslinks and fillers, thereby producing high reinforcement and good mechanical properties. The mechanical properties such as tensile strength again depend on the size of metal ions.

5.3 Experimental

5.3.1 Ionic crosslink compounds preparation

Carboxylated nitrile rubber (XNBR) was supplied by Lanxess Elastomers SAS (Germany) under the trade name of Krynac X740. It contains 26.5 wt % acrylonitrile and 7 wt % carboxylic groups (−COOH) according to the manufacturer. The vulcanization system was based on magnesium oxide (MgO, supplied by Akrochem with the trademark Elastomag170 Special) to create ionic crosslinks. The detailed compound recipes were given in Table 5.1 and Table 5.2. Compounds were prepared on a Gumix laboratory two-roll mill with a cylinder diameter of 15 cm and a length of 30 cm and a friction ratio of 1:1.15. The rolls were kept cold during the mixing procedure by circulating cold water through them. The MgO (ionic) and DCP (covalent) crosslink agent reaction mechanism with XNBR is shown in Figure 5.2.

Table 5.1 *Formulation of ionic, covalent and mixed crosslinked XNBR compounds. Quantities are expressed in parts per hundred rubber (phr).*

S.No.	Sample_ID	XNBR rubber(phr)	MgO (phr)/	DCP (phr)
1	XMD1	100	4	0.5
2	XM1	100	4	0
3	XD1	100	0	0.5

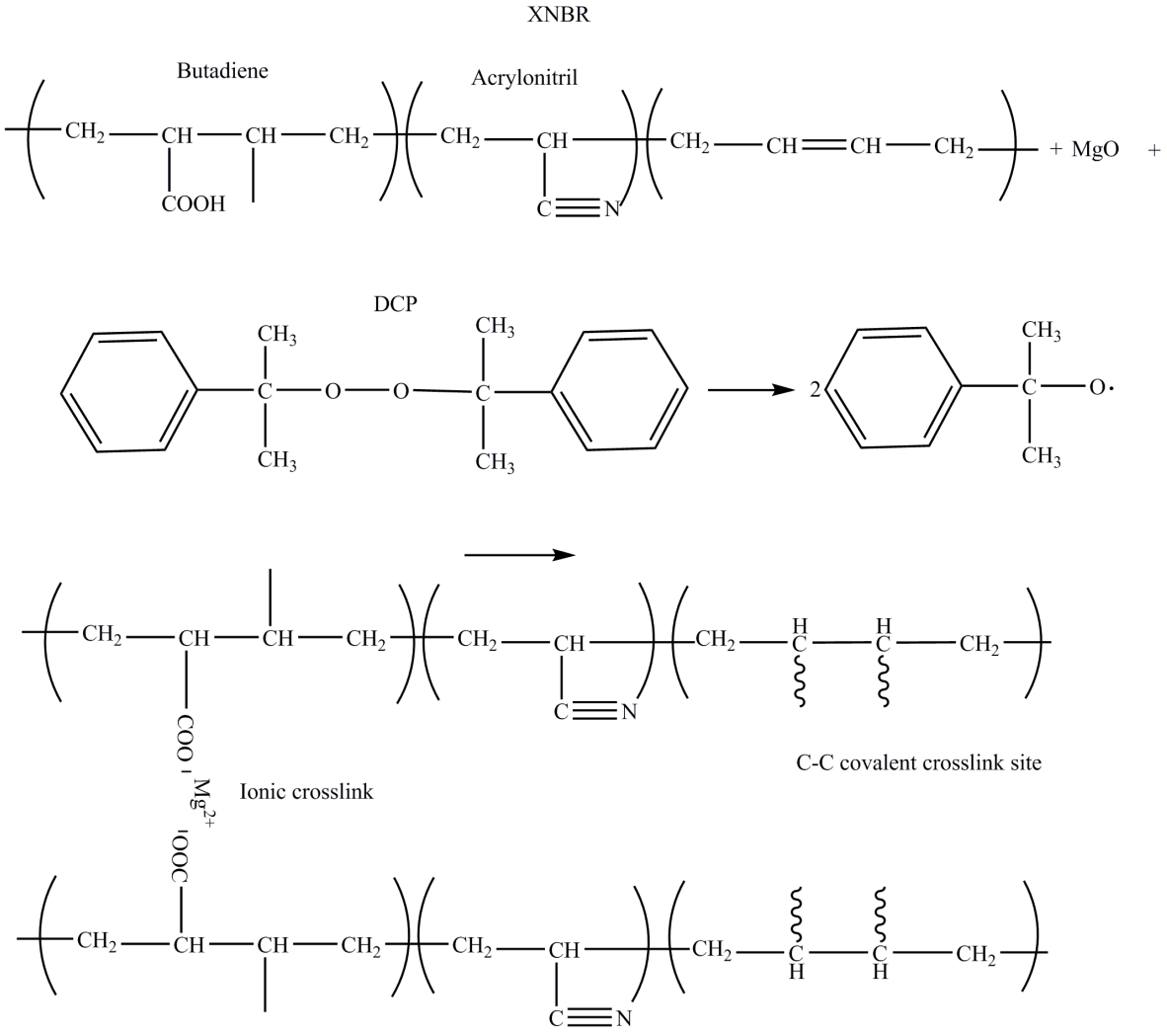

Figure 5.2 *Schematic of ionic and covalent crosslinks formation in XNBR polymer matrix with MgO and DCP respectively.*

5.3.2 Micro size TiO_2 based compounds preparation

These compounds also prepared in two-roll mill as explained in previous section and the recipe details are given in Table 5.2.

Table 5.2 *Formulation of micro TiO_2 and XNBR compounds. Quantities are expressed in parts per hundred rubber (phr).*

S.No.	Sample_ID	XNBR rubber (phr)	Micro TiO_2 (phr)
1	XT1	100	3.1
2	XT2	100	6.2
3	XT3	100	12.4

5.3.3 TiO_2 nano particle based compounds preparation

TiO_2 nano particle based compounds were prepared in a solution mixing of polymer and other ingredients, unlike the two-roll mill mixing. The polymer were cut into tiny pieces and completely dissolved in a DMF solvent and subsequently MgO, DCP and TiO_2 nanoparticles were mixed under continuous stir for 2 days at room temperature. The well dissolved solution was collected into watch glass and completely evaporated solvent in the solution at 80 °C in an oven.

Table 5.3 *Formulation of TiO_2 nanoparticle, XNBR compounds. Quantities are expressed in parts per hundred rubber (phr).*

S.No.	Sample_ID	XNBR rubber (phr)	MgO (phr)	DCP (phr)	TiO2nanopart(phr)
1	XMD	100	4	0.5	0
2	XMDT 2	100	4	0.5	2
3	XMDT 5	100	4	0.5	5
4	XMDT 10	100	4	0.5	10

5.3.4 Vulcanization

Vulcanization curves were obtained in a rubber process analyzer RPA 2000 (Alpha Technologies) with a deformation of 6.98% and an oscillatory frequency of 1.667 Hz. The vulcanization was carried out in a hydraulic press at variable temperatures and times also represented in respective images. Pure covalent samples (DCP) were vulcanized for optimum time (t_{97}). The optimum vulcanization time (t_{97}) deduced from the rheometer curves.

5.3.5 Rheometry

In addition to basic vulcanization curves, Frequency-sweep experiments were carried out after the vulcanization process on rubber process analyzer RPA 2000 (Alpha Technologies). The shear modulus was measured at frequencies from 0.002 to 33.33 Hz at temperatures from 40 to 230 °C. Using the frequency-temperature superposition [124] a combined master curve was plotted to obtain the stress relaxation of the modulus in a wide range of frequencies.

5.3.6 Dynamic Mechanical Analysis (DMA)

The mixed crosslinked network sample was characterized by DMA by using a Perkin Elmer DMA7 with parallel plate geometry and thermal control accessory using liquid nitrogen cooling. The sample was prepared as a disc with 6 mm diameter and 3 mm thickness. During a typical experiment, a disc was inserted between the plates and compressed with a static force of 1.0 N and a dynamic force of 0.3 N, using a frequency of 1 Hz. The temperature scan runs from 173 K to 473 K with heating rate of 5 K min^{-1}. The dynamic force was large enough to obtain significant amplitude even at the low temperature glassy state of the material.

5.3.7 NMR Spectroscopy

Solid-state ^{1}H MQ TD-NMR experiments were carried out on a Bruker minispec mq20 spectrometer operating at a resonance frequency of 19.65 MHz with a 90^{o} pulse length of 2.2 µs and a dead time of 14 µs and acquisition was done with 32 scans. Magic sandwich echo

(MSE) experiments acquisition was done with 128 scans. Depends on the thickness of the sample, enough number (to achieve 5 mm height) of circular discs of 7 mm diameter were centered in a standard minispec 8 mm inner diameter glass tube. Sample tube thermalized inside the instrument 10 minutes before starting the experiment and minispec was also set to the temperature minimum 6 hours prior to start the experiment, to stabilize the magnetic unit temperature and avoid the temperature gradient in the sample surroundings. All the measurements were performed at variable temperatures depends on the purpose and type of network.

5.3.8 Optical characterization

Nanocomposite films transmission spectra were obtained with a *Lambda 950 UV/VIS spectrometer* (Perkin Elmer) with integrated sphere and air as the reference spectrum.

Refractive index of nanocomposite films were measured with *Prism coupler Instrument* (Model 2010) Metricon operated with He-Ne laser wavelength 632.9 nm and 1mW output power. Reported values are average of five measurements.

5.3.9 Thermal characterization (DSC)

Differential scanning calorimetry (DSC) measurements were performed with a METTLER TOLEDO STAR^{e} thermal analysis system equipped with a liquid N_2 low-temperature apparatus, running the experiments under N_2 atmosphere. Sample of the polymer (about 6.5 mg, accuracy of 0.05 mg) were sealed into 40 μL aluminium pans under dry conditions, quenched to 173 K, and then heated to 473 K at 20 K min $^{-1}$. Indium is used as standard for temperature and heat flow calibration. Glass transition temperature (T_g) is obtained as the mid-point of the step transition in the calorimetric curve.

5.4 Results and Discussion

5.4.1 Rheometry

The basic vulcanization curves of three (ionic, covalent and mixed) different crosslinked networks are shown in Figure 5.3. As expected the mixed (ionic and covalent) crosslink network sample showing the higher torque due to summing effect of ionic and covalent crosslinks together. Due to only covalent crosslink, DCP samples showing lower torque. The MgO sample showing the intermediate torque since MgO content is more than stoichiometric (3.26 phr) value and is able to neutralize all the carboxylic groups and also note that ionic crosslinks are candidates for good mechanical strength.

The ionic domains are acts as dynamical crosslinks and are free to break down, reform and redistributes at elevated temperatures. In order to address the effect of ionic rearrangement life times on the terminal chain dynamics, we studied this process by applying the frequency−temperature superposition principle to the data obtained from the rubber process analyzer, in order to obtain a master curve that represents the stress relaxation of the shear modulus (G') in a wide range of frequencies for different crosslinked XNBR samples shown in Figure 5.4. Polymer chains in XNBR ionomers can flow via ionic exchanged between discrete aggregates without breaking all their ionic associations simultaneously, but this slow process requires high temperatures to take place on manageable time and frequency scales. Opposite to this behavior, the XNBR matrix covalently crosslinked by using 0.5 phr of DCP showed a clear elastic plateau over a certain high temperature or low frequencies. The corresponding shift factor (a_T) also plotted in Figure 5.5 and is also indicates that well above the glass transition temperature (>T_g+100) shift factor also maintains plateau.

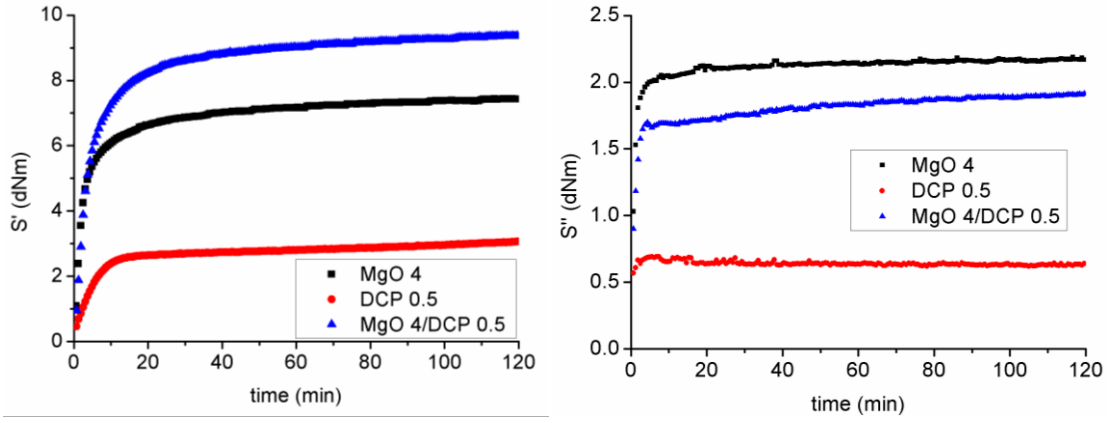

Figure 5.3 *Cure curves of ionic (MgO), covalent (DCP) and mixed (MgO/DCP) crosslink systems obtained at 160 ^oC temperature for 120 min. Legend number indicates respective ingredient in phr.*

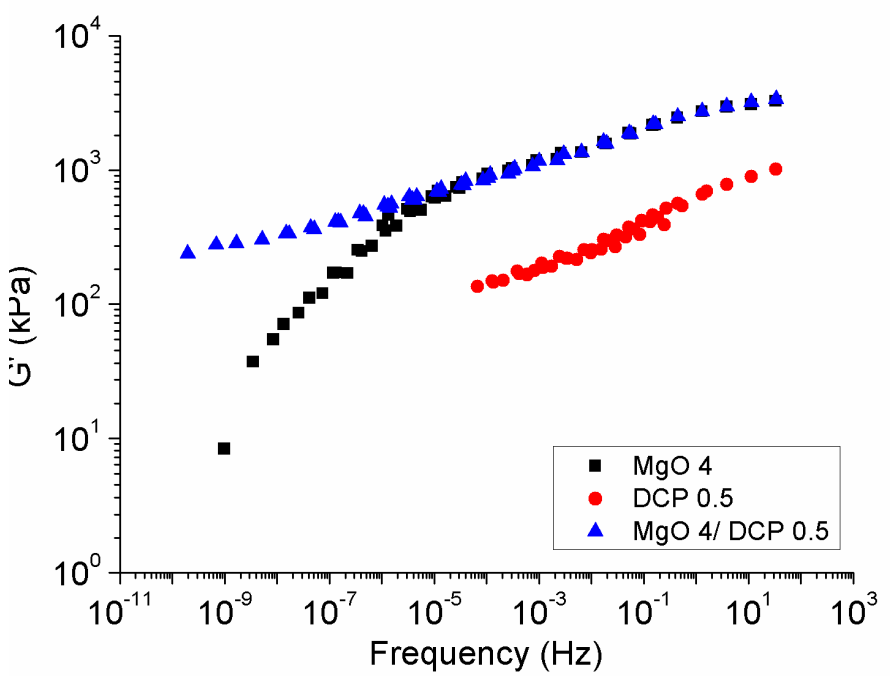

Figure 5.4 *Flow curves of ionic (MgO), covalent (DCP) and mixed (MgO/DCP) crosslink systems obtained by measuring the shear modulus at different frequencies and temperatures, plotted for a reference temperature of 40 °C. The displacement factors used for frequency-temperature superposition were different for each sample. The numbers in the image legend indicates respective ingredients in phr.*

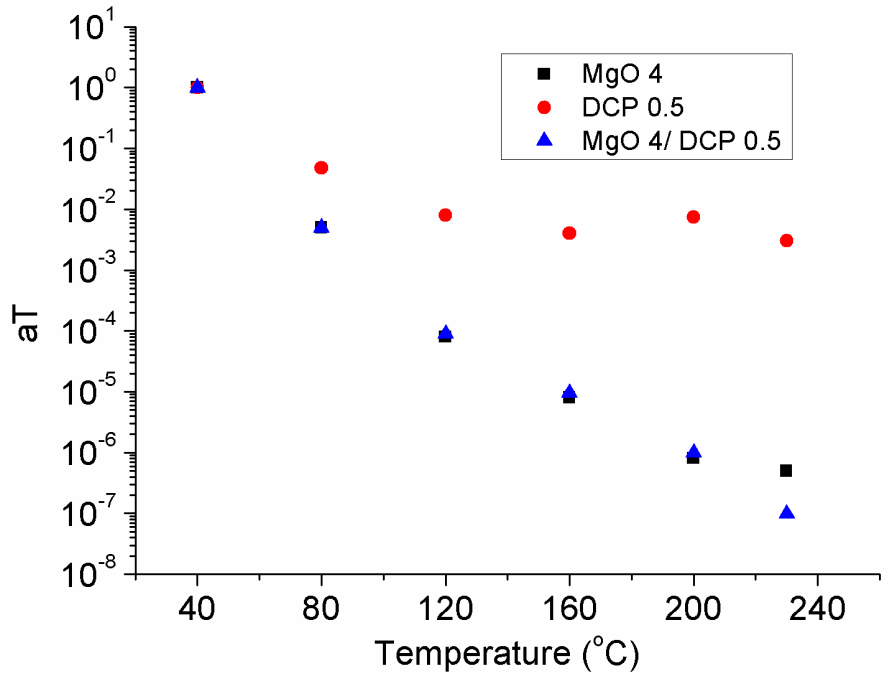

Figure 5.5 *Temperature versus displacement factor of ionic (MgO), covalent (DCP) and mixed (MgO/DCP) crosslink systems obtained from frequency-temperature superposition principle.*

5.4.2 Phase Morphology and confirmation of presence of ionic crosslinks

Existence of ionic crosslinks or ionic clusters has been confirmed by many experimental methods, such as small angle X-ray scattering (SAXS) [119] transmission electron microscopy (TEM) [118], dynamic mechanical analysis [118] etc. FTIR-ATR spectroscopy is the very quick and easy technique for confirmation of presence of ionic crosslinks. It could help us to understand the morphology and phase structure of the system. By simple observation of absorption bands related to appropriate functional groups one infers the chemical transformation or changes.

Metal oxides react with carboxylic groups grafted in the XNBR matrix forming the corresponding carboxylates salts [120,121]. This has been followed by FTIR-ATR spectra shown in Figure 5.6 demonstrating that both the MgO samples the vibrational band at 1591 cm^{-1} has been observed where as in, only DCP system the vibration band at 1698 cm^{-1} present. The absorption band at 1698 cm^{-1} indication of presence of carboxylic acid groups (-COOH) which are grafted to polymer chain and absorption band at 1591 cm^{-1} indication of presence of carboxylates [137]. In MgO (metal oxide) samples, metallic cations created ionic bonds with carboxylic acid groups and form neutralize carboxylate salts (-COOMg) and is the reason for disappearance of 1698 cm^{-1} vibrational band and appearance of 1591 cm^{-1} vibrational band and is true only when metal oxides concentration above the stoichiometric value (3.26 phr for 100 phr rubber, according to the concentration of carboxylic groups in the rubber matrix), while at lower concentration both the carboxylic and carboxylate bands should observe. These carboxylate moieties tend to aggregate into multiplets and clusters in a hierarchical structure that acts as multifunctional crosslink network structure. In DCP sample there is no changes in the carboxylic acid (-COOH) groups, since only covalent crosslinks forms between C-C by the decomposition of dicumyl peroxide (DCP) during vulcanization. The mixed ionic and covalent crosslinks mechanism is shown in Figure 5.2.

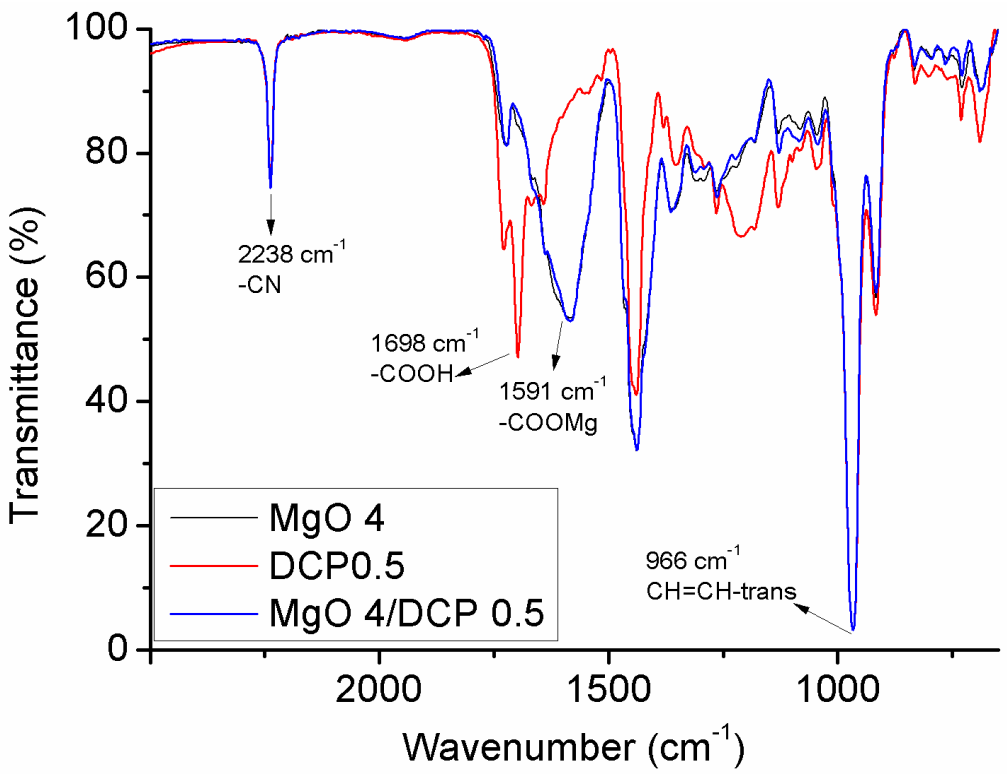

Figure 5.6 *FTIR-ATR spectra of XNBR with different crosslink systems (MgO, DCP and MgO/DCP) cured at 160 ^{o}C for 120 min. Legend number indicates respective ingredient in phr.*

5.5 Micro size TiO_2 based ionic networks

TiO_2 nanoparticles are good candidate for optical properties [123,124] and here we tried to use the TiO_2 for dual purpose to create ionic crosslinks as well as achieve optical properties. Started with micro TiO_2 and TiO_2 nanoparticles; we could not even create ionic crosslinks with the micro TiO_2 since TiO_2 is inactive metal compound [125].

5.5.1 Rheometry

Cure curves of micro size TiO_2 sample shown in Figure 5.7, it evident that there is no increment in the torque values with TiO_2 content. This is an indication of inactiveness of

TiO_2 to create ionic crosslinks. Even increasing of cure temperature, there is no improvement in torque shown in Figure 5.8.

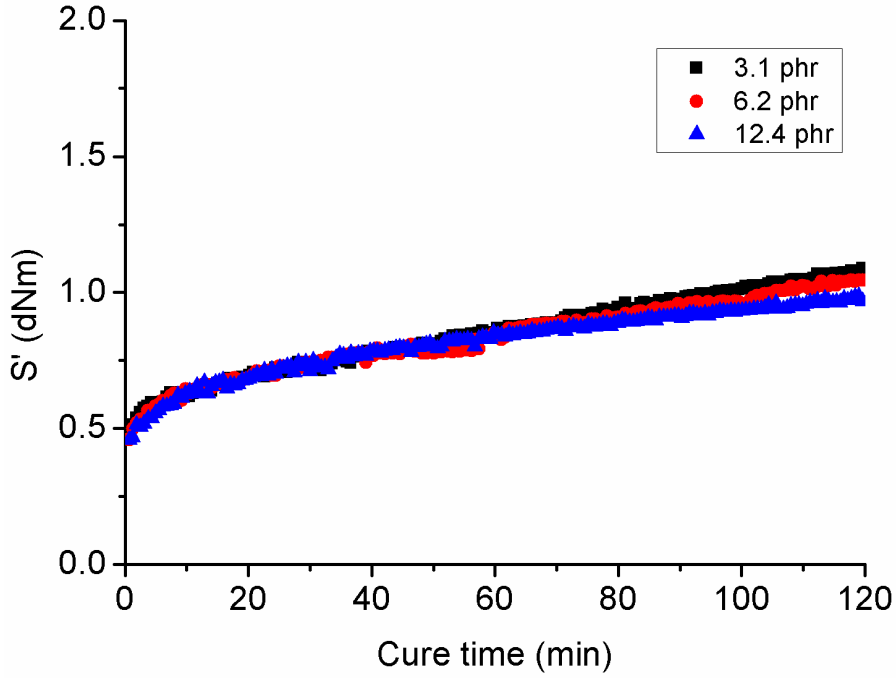

Figure 5.7 *Cure curves of XNBR with variable amounts of TiO_2 cured at 160 ^oC for 120 min. The legend numbers indicates that TiO_2 in phr.*

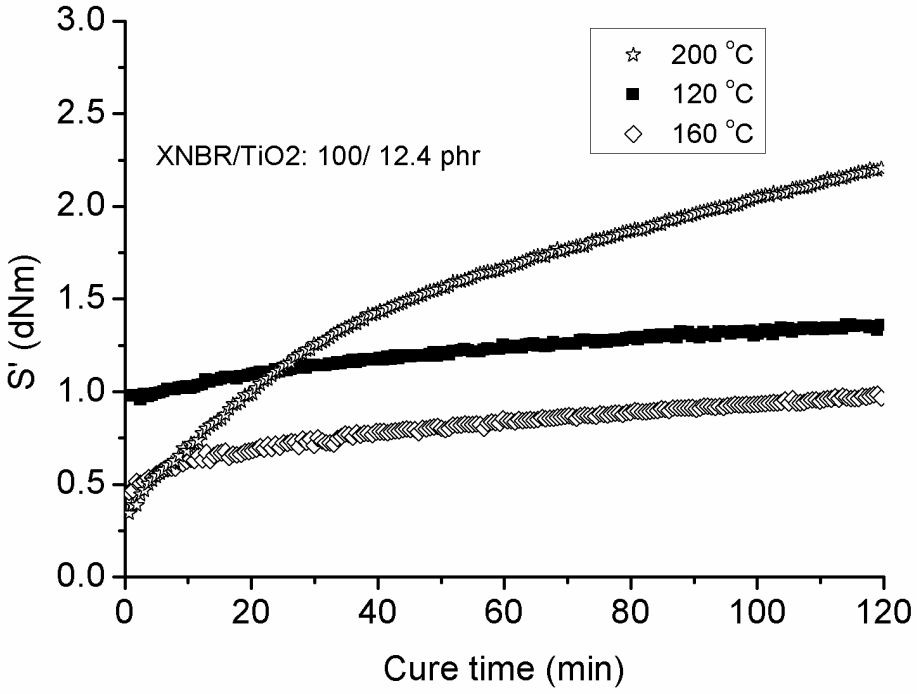

Figure 5.8 *Cure curves of XNBR and TiO_2 (12.4 phr) cured at variable temperature for 120 min.*

5.5.2 Confirmation of ionic crosslinks by FTIR-ATR spectra

The inertness of TiO_2 compounds to create ionic crosslinks is also clearly evident from the presence of carboxylic acid (-COOH) absorption peak at 1698 cm^{-1} in FTIR-ATR spectra at different contents of TiO_2 even above the stoichiometric value shown in Figure 5.9. Even at increasing cure temperature also there are no changes in the carboxylic groups is as shown in Figure 5.10.

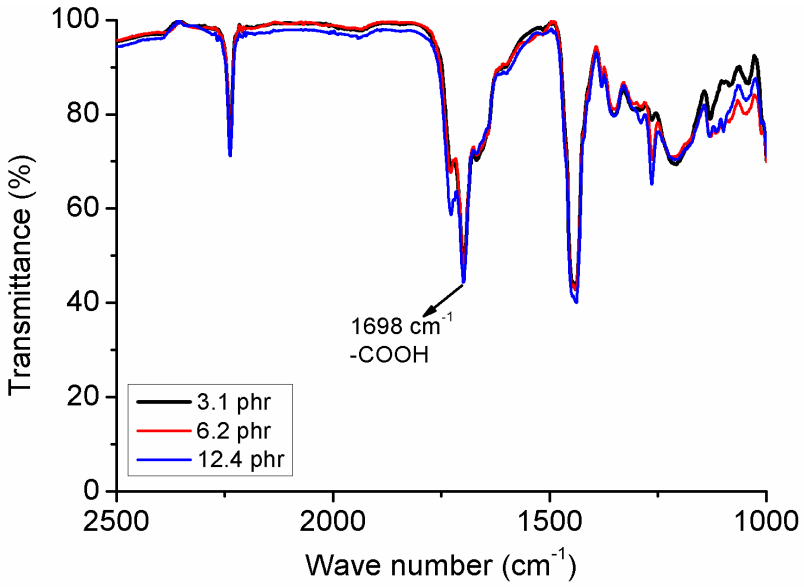

Figure 5.9 *FTIR-ATR spectra of XNBR with variable amounts of TiO_2 cured at 160 ^oC for 120 min. The legend numbers indicates that TiO_2 in phr.*

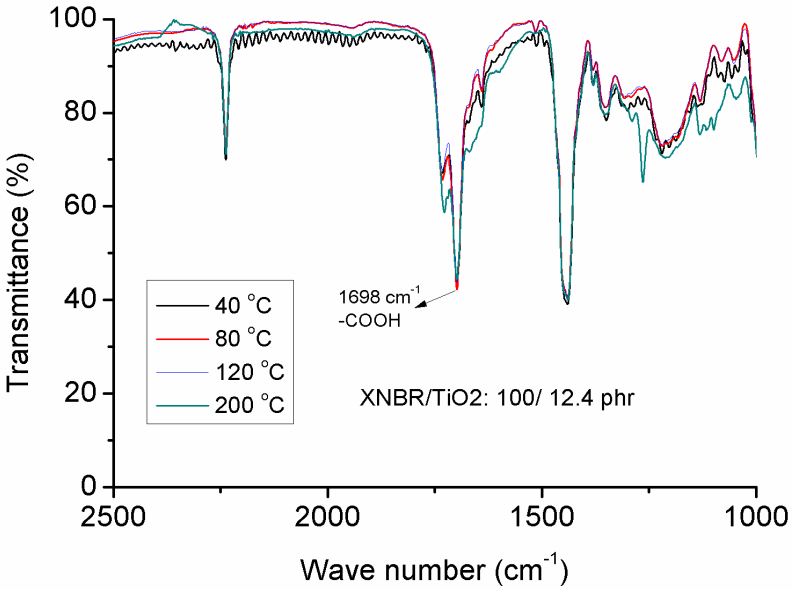

Figure 5.10 *FTIR-ATR spectra of XNBR and TiO_2 (12.4 phr) cured at variable temperature for 120 min.*

5.6 TiO_2 nanoparticle based ionic networks

As already clear from the previous section that TiO_2 is inactive metal compound but the TiO_2 nanoparticles surface activity may not same as micro size, so we used our laboratory synthesized TiO_2 nano particles but there is no improvement in the creation of ionic crosslinks and is clear from the FTIR spectra shown in Figure 5.11.

5.6.1 Phase Morphology and evidence of presence of ionic crosslinks

It is well known that TiO_2 nanoparticles are potential candidates for optical properties, so we keep the TiO_2 nanoparticles for the very same purpose and MgO to create ionic crosslinks and DCP for the creation of covalent crosslinks. In order to evenly and well disperse the nanoparticles all over the polymer matrix, we have chosen the solution mix of compounds rather than mechanical mixing. We have succeeded in creating ionic crosslinks without vulcanization also and is evident from the comparison of FTIR spectra of solution mixed unvulcanized and vulcanized samples shown in Figure 5.12. In both the unvulcanized and vulcanized films (–COOMg) absorption peak been observed at 1591 cm^{-1}.

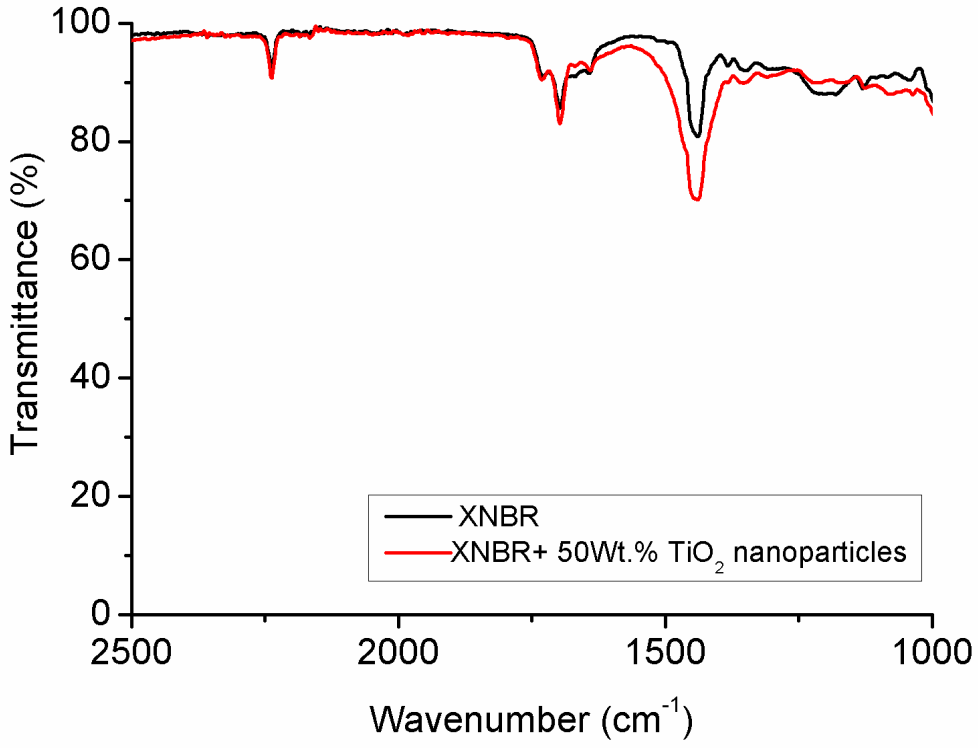

Figure 5.11 *FTIR-ATR spectra of XNBR with 50 Wt. % TiO_2 nano particle samples.*

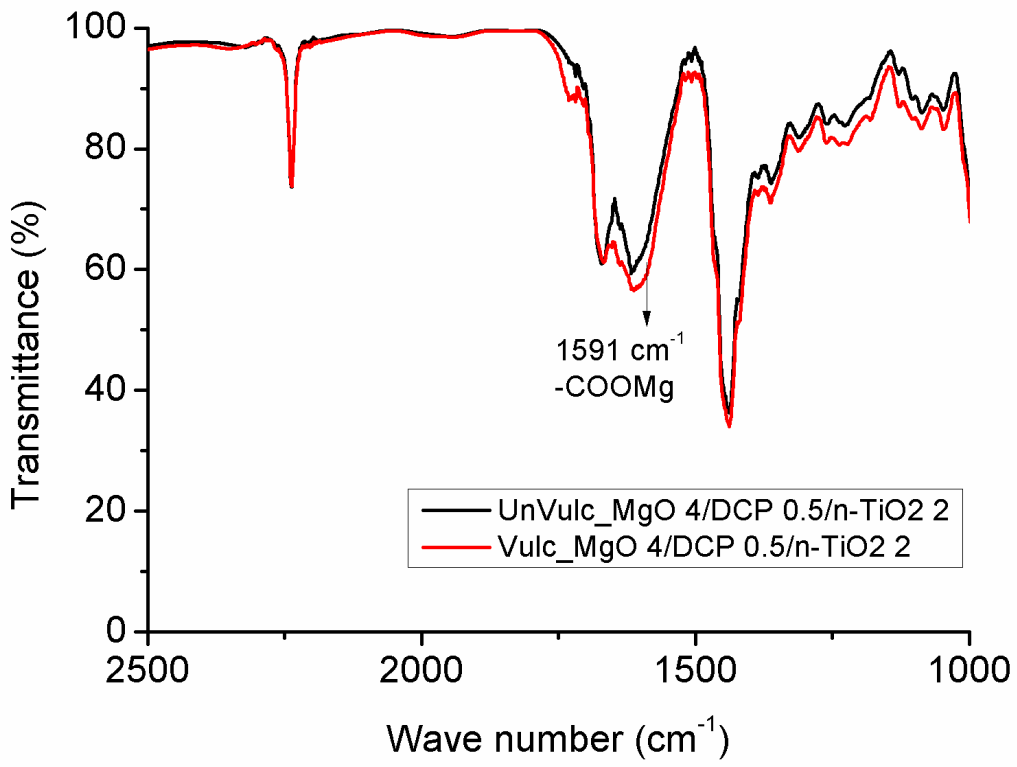

Figure 5.12 *Comparison of FTIR-ATR spectra of unvulcanized and vulcanized TiO_2 nano particle samples prepared in solution mixing. The numbers in the image legend indicates the respective ingredients in phr.*

5.6.2 Crosslink Network Structure Analysis by low field TD-NMR

5.6.2.1 MQ NMR Spectroscopy

Multiple-quantum NMR is the prominent technique for characterization of crosslinked networks as addressed in the chapter 2. The Baum-Pines 8 pulses MQ NMR sequence is robust for evaluate the weak dipolar coupled constant by proper evaluation of higher order dipolar coherence Hamiltonian also. In case of strong dipolar coupled rigid samples, structure information contained DQ intensity build up and also dynamical related reference intensity decays in shorter times, with in the single cycle time of lengthy double-quantum pulse sequence. To overcome this problem, it is necessary to use subcycles [122, 97] of lengthy Baum-Pines sequence for characterization of rigid limit dipolar coupled samples. In our present case of ionic elastomer networks, dipolar coupling constants of bound rubber around the ionic domains are very high and dipolar coupling constants of soft rubber segments

between crosslinks are weak. To characterize both the strong and weak dipolar coupling constant, we used different MQ coherence excitation schemes.

In MQ NMR, two sets of data are recorded as a function of the DQ pulse sequence (evolution) time $\tau_{DQ,}$ the DQ build-up curve, I_{DQ}, and the reference decay curve, I_{ref}. The sum of both (after subtraction of a non-coupled defect contribution), $I_{\Sigma MQ} = I_{DQ} + I_{ref} - defects$, is commonly used to obtain a point-by-point normalized build-up function, $I_{nDQ} = I_{DQ}/I_{\Sigma MQ}$, as it was explained in the literature [2]. This I_{nDQ} contains the residual dipolar interactions related to the network structure. In case of elastomeric ionomers the overall signal decay function in MQ experiments, $I_{\Sigma MQ}$, based upon the usual Baum-Pines sequence exhibits a substantial overall loss of signal due to the limitation imposed by the minimum pulse sequence cycle time (around 90 μs, and is depends on the pulse length and phase switching times). This is not effect on weak dipolar coupled elastomer network intensity but it poses a serious problem to characterize ionic elastomers because the trapped polymer with reduced dynamics is strongly dipolar-dipolar coupling (coupling constants in the order of 10 kHz), and the associated signal decays almost completely during a single cycle of the Baum-Pines sequence.

5.6.2.2 Alternative approach for the analysis of MQ experimental data obtained from different excitation schemes

To overcome the loss of strong dipolar-dipolar coupled intensity in Baum-Pines multiple-quantum NMR experiments, due to the limitation of minimum pulse sequence cycle time, one may use a shorter version of overall five pulses[122] (Two pulses for excitation block and two for reconversion block and final pulse for FID evolution). The excitation and reconversion block contains simple two-pulse segment$(\frac{\pi}{2})_x - \tau_{DQ} - (\frac{\pi}{2})_x$ for excitation and reconversion of multiple-quantum coherences. This short pulse sequences are less efficient as to excitation of higher-order coherences than the Baum-Pines sequence. Nevertheless the theory explained for spin pairs are completely valid apart from the multiplicative factor (3/2). In order to improve the long-time performance of five-pulse sequence, a refocusing π pulse could add in the center of two $\frac{\pi}{2}$ pulses with equal phase $(\frac{\pi}{2})_x - \tau_{DQ}/2 - (\pi)_x - \tau_{DQ}/2 - (\frac{\pi}{2})_x$. Another important point is that the normalized double-quantum intensity I_{nDQ} obtained

by five-pulse excitation schemes does not reach the 50% limit and $I_{ref}+I_{DQ}$ is subject to notable homogeneous dephasing. Due to these reason and nature of our present samples (presence of strong and weak dipolar couplings) a combination of both experimental approaches is required to characterize both the rigid segments from the trapped polymer around ionic interactions and the softer rubber segments between crosslinks. In this way, the signals from both schemes superimpose at times close to the minimum Baum-Pines cycle time shown in the vertical dashed line in Figure 5.13. The combined signal provides the complete information on this heterogeneous material composed by rubber segments in quite different dynamics regimes shown in Figure 5.14. In order to avoid mathematical artifacts caused by the manipulation of weak signal intensities, $I_{\Sigma MQ}$ and I_{DQ} signals have been fitted simultaneously. $I_{\Sigma MQ}$ reflects information about the temperature-dependent segmental dynamics, while I_{DQ} depends on both temperature-independent network structure effects and segmental dynamics [2]. Since two rather well-separated dynamic processes coexist in the elastomeric ionomers, the $I_{\Sigma MQ}$ signal was fitted assuming two stretched exponential decay functions shown in Equation (5.1).

$$I_{\Sigma MQ} = B \cdot \left(A \cdot \exp\left(-2\tau_{DQ} / T_{2,1} \right)^{\beta_1} + (1-A) \exp\left(-2\tau_{DQ} / T_{2,2} \right)^{\beta_2} \right) \tag{5.1}$$

Where B is the y-intercept value related to fraction of dipolar coupled protons and A is the trapped polymer fraction, whereas $T_{2,1}$ and $T_{2,2}$ are the characteristic relaxation times and β_1 and β_2 are the shape factors of the decay functions for the trapped rubber phase and the bulk (mobile) rubber, respectively.

Due to the chemical structure of the XNBR terpolymer and the complex and inhomogeneous network structure, fits to the D_{res} contained DQ build-up intensity a broader distribution needs to consider. Here, we could use a build-up function defined by a gamma distribution of dipolar couplings [126] with a width of distribution defined by the average residual coupling constant D_{avg}.

The coexistence of weakly dipolar-coupled rubber segments between crosslinks, and strongly dipolar-coupled segments that are trapped around ionic contacts, it is relevant to use two

gamma distributions in order to analyze both environments. Taking into consideration both structural and dynamics requirements, I_{DQ} can be fit with Equation (5.2).

$$I_{DQ} = B \cdot \left(A \cdot g_1(\tau_{DQ}, D_{avg1}) \cdot \exp\left(-2\tau_{DQ} / T_{2,1}\right)^{\beta_1} + (1-A) \cdot g_2(\tau_{DQ}, D_{avg2}) \exp\left(-2\tau_{DQ} / T_{2,2}\right)^{\beta_2} \right) \tag{5.2}$$

Where B is the y-intercept value related to fraction of dipolar coupled protons and A is the trapped polymer fraction, g_1 and g_2 are Gaussian functions whereas $T_{2,1}$ and $T_{2,2}$ are the characteristic relaxation times and β_1 and β_2 are the shape factors of the decay functions for the trapped rubber phase and the bulk (mobile) rubber respectively. D_{avg1}, D_{avg2} are residual dipolar coupling constants of rigid rubber fraction (trapped polymer),mobile rubber fraction (rubbery polymer between constrains) respectively.

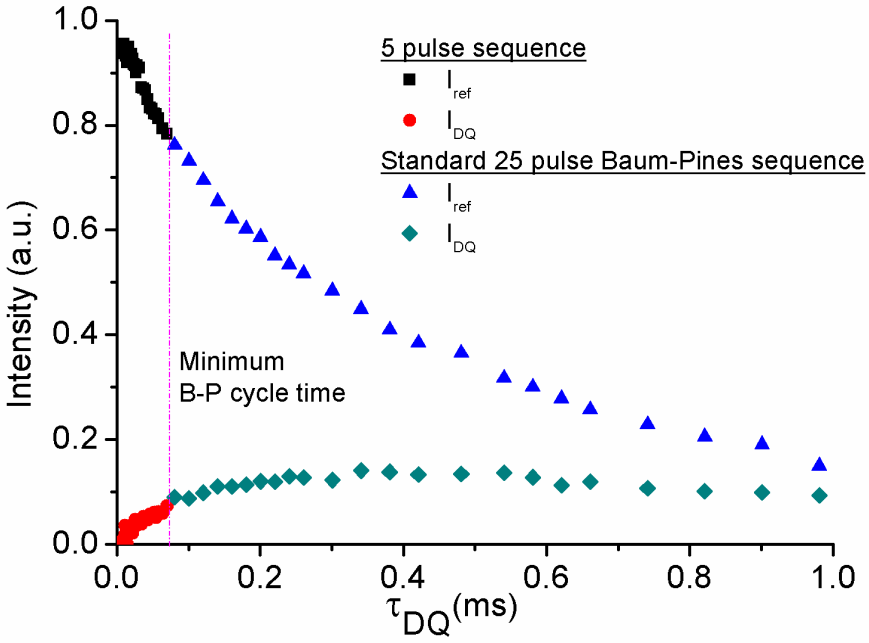

Figure 5.13 *Proton MQ data for sample XMDT10 at 80 °C obtained using standard 25 pulse Baum-Pines sequence and improved five-pulse sequences. For the five pulse sequence time axis was scaled with scaling factor (3/2) to combine with standard sequence. The vertical dashed line identifies the minimum pulse sequence cycle time of Baum-Pines sequence.*

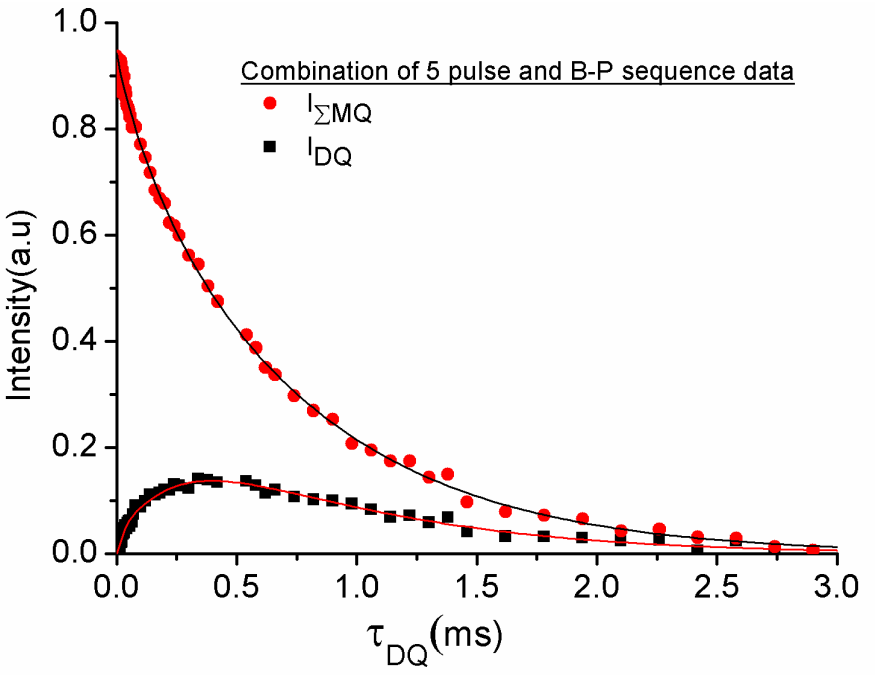

Figure 5.14 *Proton MQ data for sample XMDT10 at 80 °C obtained using standard 25 pulse Baum-Pines sequence and improved five-pulse sequences. For the five pulse sequence time axis was scaled with scaling factor (3/2) to combine with standard sequence.* $I_{\Sigma MQ}$ *and* I_{DQ} *signals were fitted with Equation (5.1) and Equation (5.2) respectively.*

5.6.4 TiO_2 nanoparticle effect on ionic elastomers networks

The decisive advantage of ionic elastomers over conventional elastomers is their thermo reversible behavior. It is necessary to understand the behavior of ionic elastomers at variable temperatures. At higher temperatures ionic elastomers behave as a melt-flow due to the increased mobility of ionic pairs and their ability to rearrange between aggregates. From Figure 5.15, it is clear that the trapped rubber fraction residual dipolar coupling constants are higher and decreasing the same quantity with temperature. This behavior of D_{res} decreasing with temperature is expected, due to the relatively decreasing of trapped polymer around the ionic multiplets. Temperature also causes redistribution of ionic multiplets within the ionic cluster and also between clusters. This phenomenon also supported by the fraction of higher dipolar coupled rubber fraction in the polymer matrix shown in Figure 5.17. It is evident from FTIR spectra that TiO_2 does not creating any ionic or other kinds of crosslinks in the polymer composite and just physically adsorbed in the polymer matrix. TiO_2 nanoparticles may act as

filler and polymer molecules trapped around the nanoparticles. If this phenomenon is true, it is expected that increasing of trapped rubber residual dipolar coupling constant with TiO_2 content until below the temperature range where polymer molecules are freed from the nanoparticle as shown in the Figure 5.15. Once cross the certain temperature limit, the nano particles quantity will not be influence any restrictions to the polymer chains and may be the reason, the trapped rubber D_{avg1} constant not influence by TiO_2 content at 120 ^{o}C.

In order to obtain the shape memory effect in our samples, we introduced two kinds of crosslinks, i.e. ionic and covalent. The ionic crosslinks structure and dynamics depends on the temperature where as covalent crosslink structure is independent of temperature well above the glass transition [53]. Due to the very same reason, weak dipolar coupling (D_{avg2}) constant related to rubber fraction between covalent crosslinks or unbound rubber is almost constant irrespective of temperature shown in Figure 5.16. The temperature at which transitions occur in ionic crosslink networks is called the ionic transition temperature, which is varies depends on the quantity of ionic fraction in the network [138]. The ionic transition in our present studied samples took place at above the 60 ^{o}C temperature, understood from the changes in loss factor (tan delta) with temperature shown in Figure 5.21.

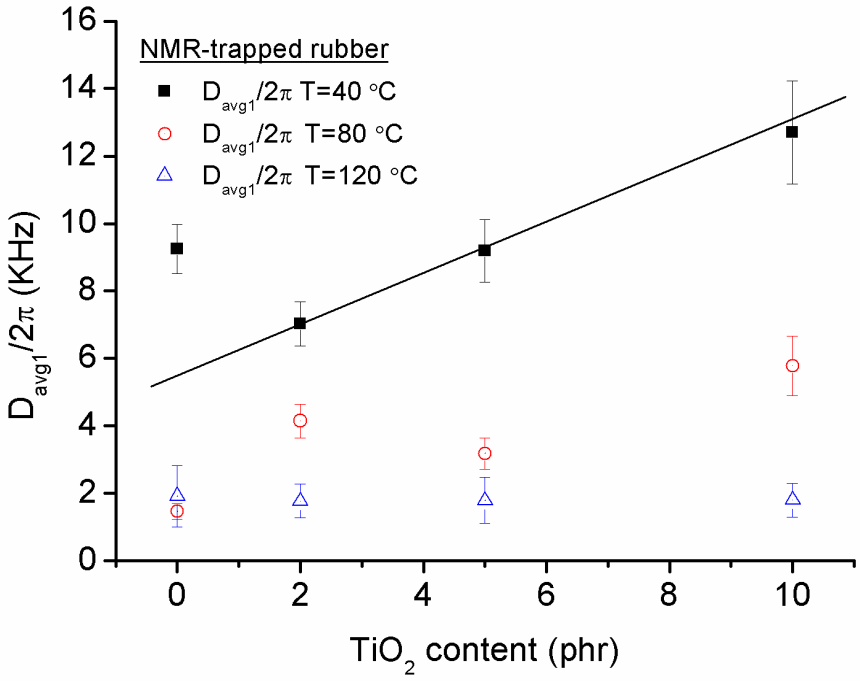

Figure 5.15 *Variable TiO_2 nanoparticles content ionic elastomer trapped (rigid) rubber fraction dipolar coupling constants measured at variable temperatures and obtained by combined fitting of $I_{\Sigma MQ}$ and I_{DQ} signals with Equation (5.1) and Equation (5.2) respectively.*

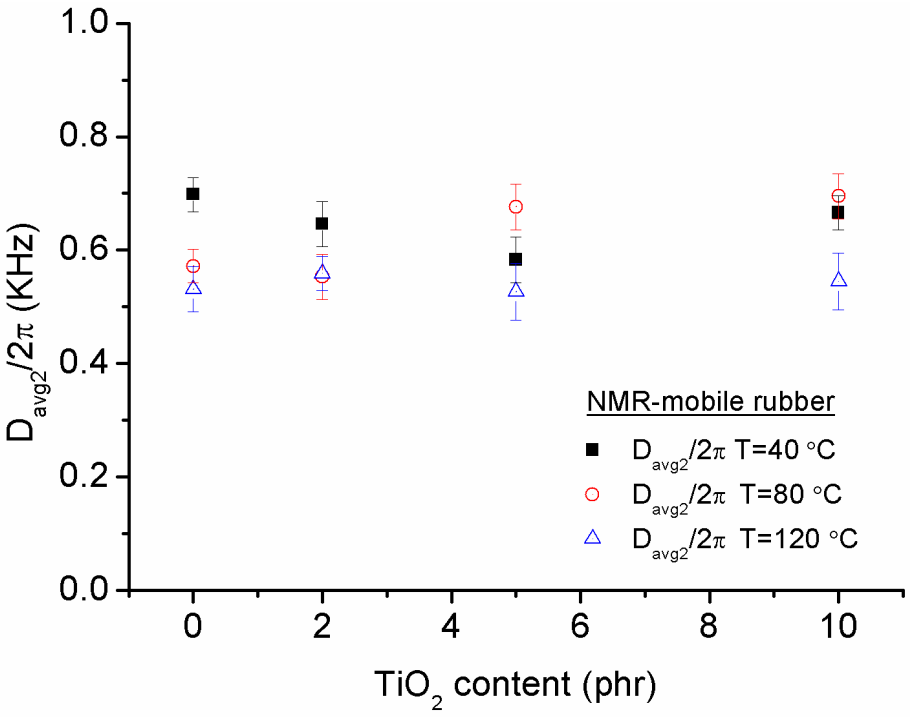

Figure 5.16 *Variable TiO_2 nanoparticles content ionic elastomer soft rubber fraction dipolar coupling constants measured at variable temperatures and obtained by combined fitting of $I_{\Sigma MQ}$ and I_{DQ} signals with Equation (5.1) and Equation (5.2) respectively.*

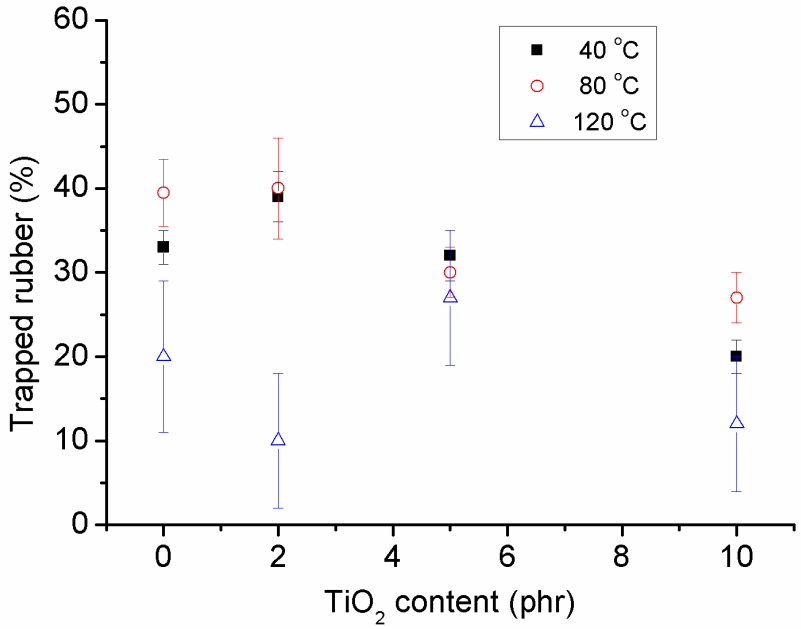

Figure 5.17 *Variable TiO_2 nanoparticles content ionic elastomer trapped rubber fraction measured at variable temperatures and obtained by combined fitting of $I_{\Sigma MQ}$ and I_{DQ} signals with Equation (5.1) and Equation (5.2) respectively.*

5.6.4.1 Bound (trapped) rubber fraction determination (MSE-FID Measurements)

Due to the strong dipole-dipole couplings in a solids and or semicrystelline polymers, spectral information of such a systems directly linked to molecular mobility, rigid and mobile fraction in a polymer materials. Solid-state NMR allows measuring the direct crystallinity or hard/soft composition information, which is also applicable to measure the degree of phase separation in block copolymers where one component is above the glass transition and the other one below the glass transition temperature by simple free induction decay (FID) signal by fitting with appropriate function, however this simple procedure has potential disadvantage especially on low-field instruments due to the long receiver dead time. In case of crystalline and rigid polymers, significant amount of rigid part signal, which usually decays within the 20 μs, and is a potential loss in a longer dead time (>10 μs) of low-field instruments. Magic-sandwich echo (MSE) experiments [134] allow direct measurement of rigid/soft phase by solving the receiver dead time problem. In our present ionic elastomer samples contains signal from rigid trapped rubber around ionic moieties and soft mobile rubber fraction between crosslinks. Thus, by analysis of initial 0.300 ms of refocused MSE-FID was possible by using a weighted superposition of stretched exponential functions [134-136] and the fitting of MSE experimental data is shown in Figure 5.18. Trapped rubber fraction obtained from MSE experiments at 40 ^{o}C temperature also infers that TiO_2 nanoparticle does not created much restriction to mobility of polymer chains shown in Figure 5.16.

$$\frac{I(t)}{I_0} = R\ exp(-\frac{t}{T_2^{rigid}})^{n_1} + (1-\mathrm{R})\exp(-\frac{\mathrm{t}}{\mathrm{T}_2^{\mathrm{mobile}}})^{n_2} \tag{5.3}$$

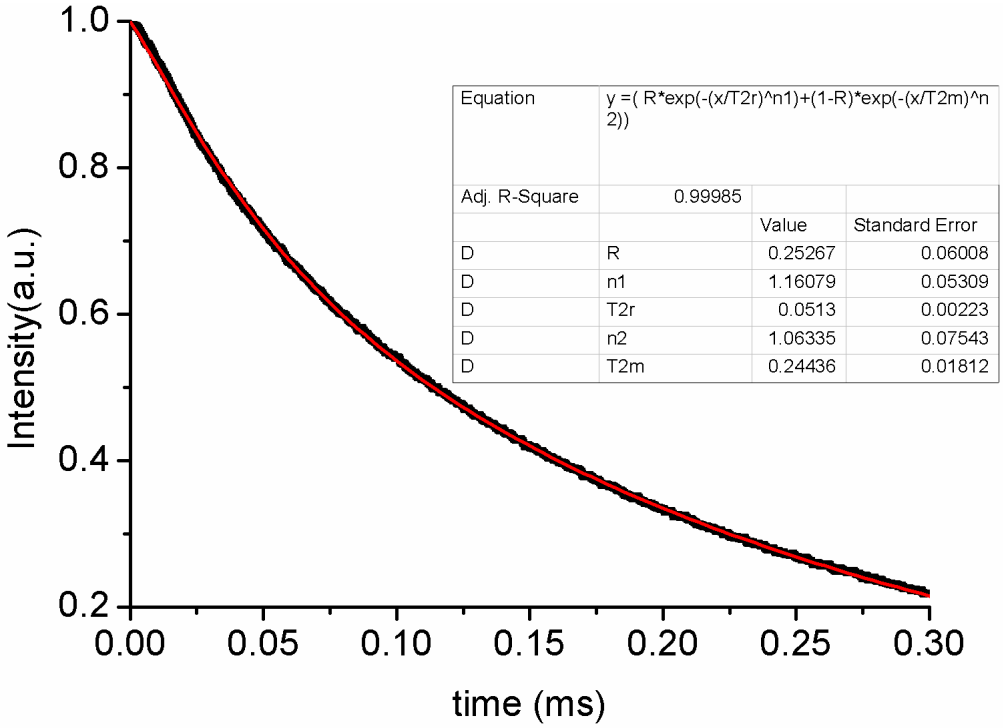

Figure 5.18 *MSE experimental data of XMDT10 sample measured at 40 ^{o}C and fitted with Equation (5.3).*

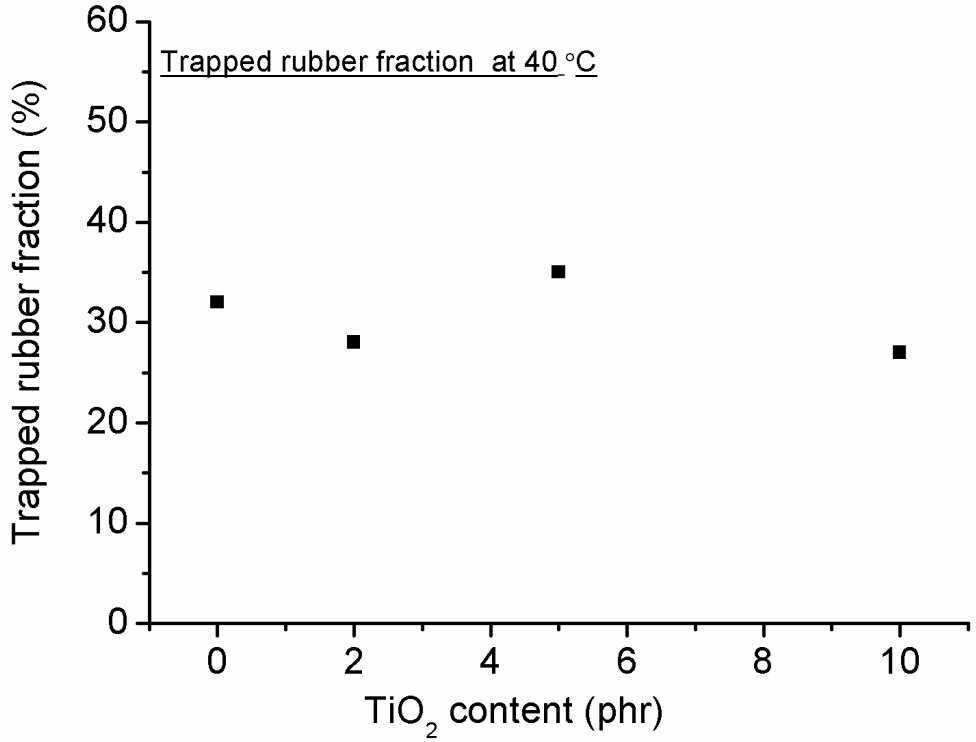

Figure 5.19 *Variable TiO_2 nanoparticles content ionic elastomer trapped rubber fraction measured at 40 ^{o}C obtained from MSE experiments.*

5.6.4.2 Comparison of trapped rubber fraction obtained from MQ NMR and MSE experiments

The trapped rubber fraction quantified based on the FID intensity decay shape fitted with appropriate shape function (Equation (5.3)) and also dipole-dipole coupled Hamiltonian evaluation intensity by the appropriate pulse sequence and fitted with reduced fitting parameters by taking the advantage of simultaneous fitting (Equation (5.2) and Equation (5.1)) of structural (I_{DQ}) and dynamical ($I_{\Sigma MQ}$) related information with Equation (5.2) and (5.1) respectively. Both the methods are agreed within the error limit. The error in the MQ NMR measured rigid rubber fraction is higher even though reduced the fitting parameters. Since MQ NMR measured structural information contains both strongly and weakly coupled dipole-dipole coupling constant and is very difficult to accurate differentiation of both the time scales. However MSE experimental data completely suppresses the weakly coupled dipolar related information by analyzing of first 0.300 ms intensity. However both the techniques are agreed within the error limits shown in Figure 5.20.

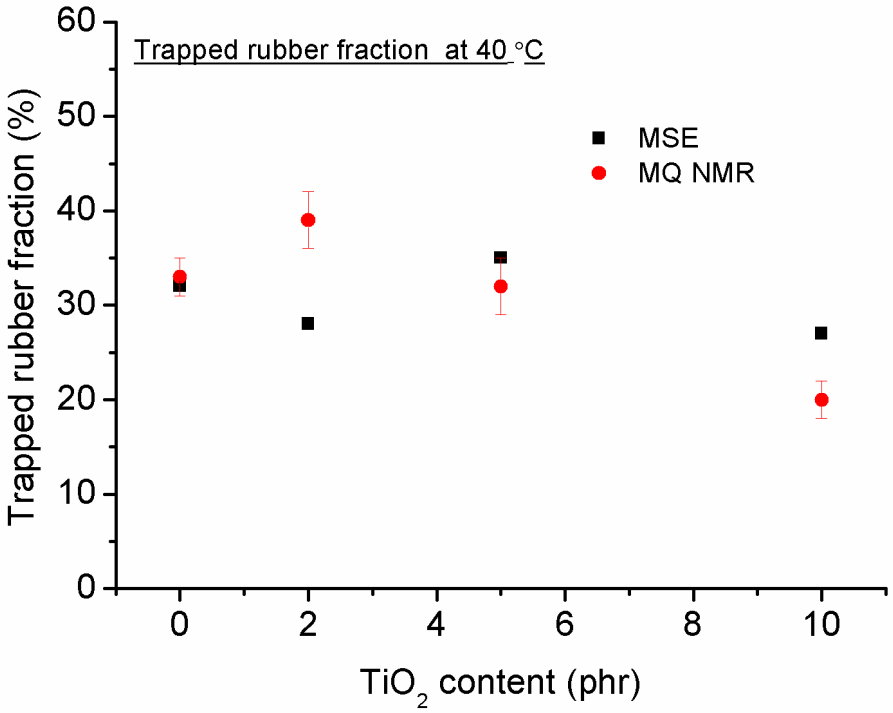

Figure 5.20 *Comparison of trapped rubber fraction obtained from MQ NMR and MSE experiments.*

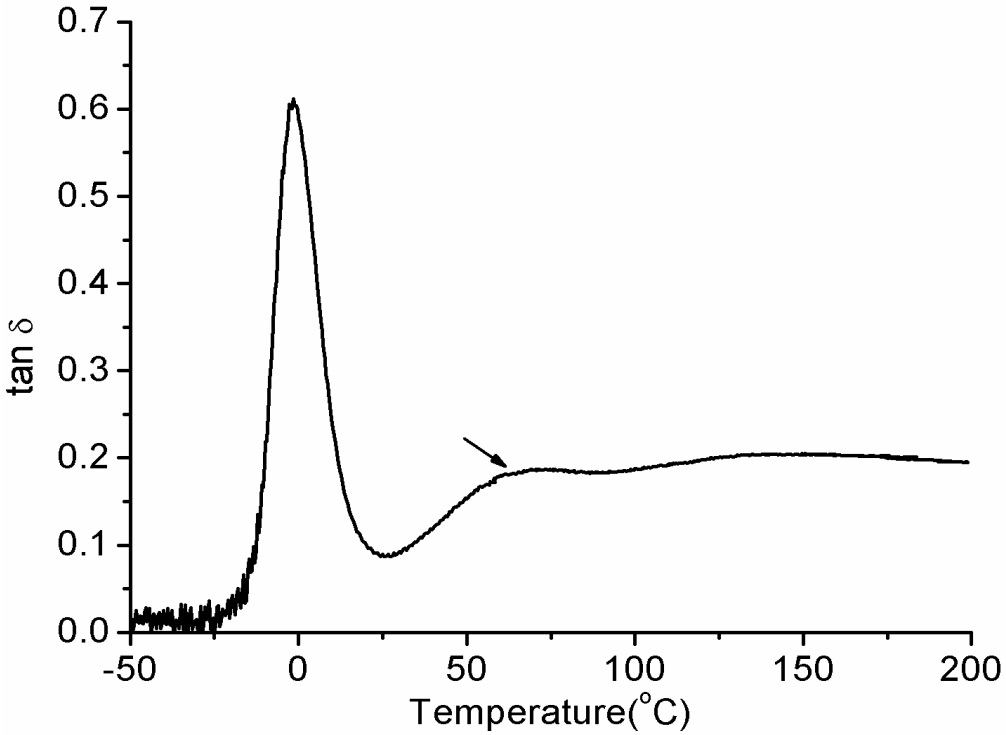

Figure 5.21 *Variation of loss factor (tan δ) with temperature of XMD1 sample (contains both ionic and covalent crosslinks). At constant frequency 1 Hz, obtained from DMA measurement.*

5.7 TiO_2 nanoparticles effect on optical properties of ionic elastomers

Nano particles have potential applications in polymer field due to their improved properties compared to conventional polymers [127, 128]. Even for traditional industrial applications such as rubber industries also paying attention on nano size fillers due to enhancement of mechanical properties [129, 130], thermal stability [131] and gas barrier properties [132] etc. Particularly TiO_2 nanoparticles has been using for optical properties such as UV-radiation absorbers, highly transparent polymer composite preparation [123, 124] and also for highly efficient energy converting electrodes of dye-sensitized solar cells [133] etc.

XNBR and nanocomposite films prepared with increasing concentrations of nanoparticles are optically transparent for the UV-Visible range. Below 400 nm it is possible to observe the pronounced nanocomposite absorption edge, linked to the nanoparticle band gap. It is clear from those transmission spectra shown in Figure 5.23 that nanocomposite films provide the

complete filtering of UV at appropriate concentration. With increasing of nanoparticles concentration in the polymer matrix, the refractive index of the nanocomposite expected to larger than the pure polymer. Even at very lower concentration 2 Wt.% of TiO_2 nanoparticles, the influence is very clear. The effective nanocomposite refractive index was calculated by the following equation:

$$n_{comp} = \Phi_p n_p + \Phi_m n_m \tag{5.4}$$

Where n_{comp}, n_p, n_m are the refractive index of nanocomposite, nanoparticle and polymer matrix respectively and Φ_p, Φ_m, are volume fraction of nanoparticles and polymer matrix respectively and $\Phi_p = 1 - \Phi_m$

The earlier studies [124] confirmed that TiO_2 nanoparticles are well dispersed in the polymer matrix as aggregates of the primary crystallites of about few nano meters. The SEM image showed in the Figure 5. 22 confirm that TiO_2 nano particles are in nano meter size aggregates and presence of MgO particles in the micro meter size. Comparison of experimental and predicted (calculated according to the Equation (5.4)) refractive indices of nanocomposite films shows that the increasing of nanoparticles raising the refractive index. The reason for lower measured refractive index values compared to prediction may be due to the nanoparticles settled down in the bottom and the solution taken from the top to cast nanocomposite film. Nevertheless the trend is clear that increased refractive index with nanoparticle concentration in the nanocomposite matrix shown in Figure 5. 24.

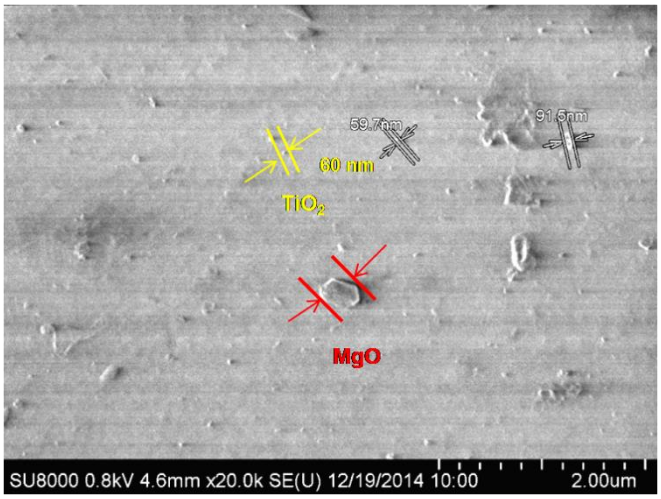

Figure 5. 22 *SEM image of XMDT 2 sample nanocomposite film, confirmation of TiO_2 nanoparticles and MgO micro size particles are present in the film.*

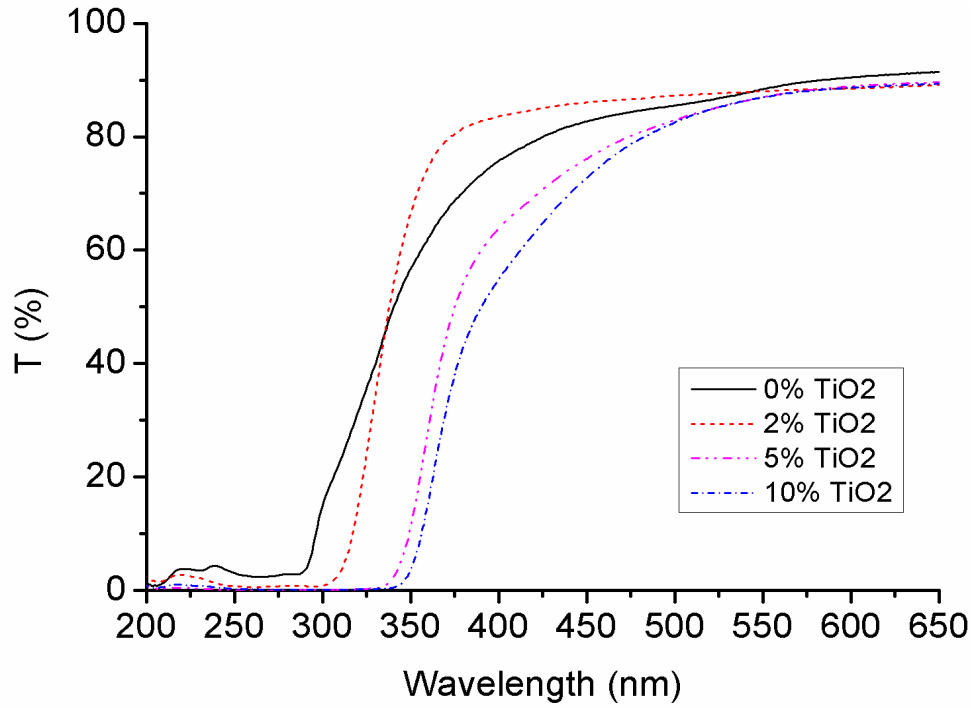

Figure 5.23 *UV-Visible Transmission spectra of ionic elastomers with variable TiO_2 nanoparticle content.*

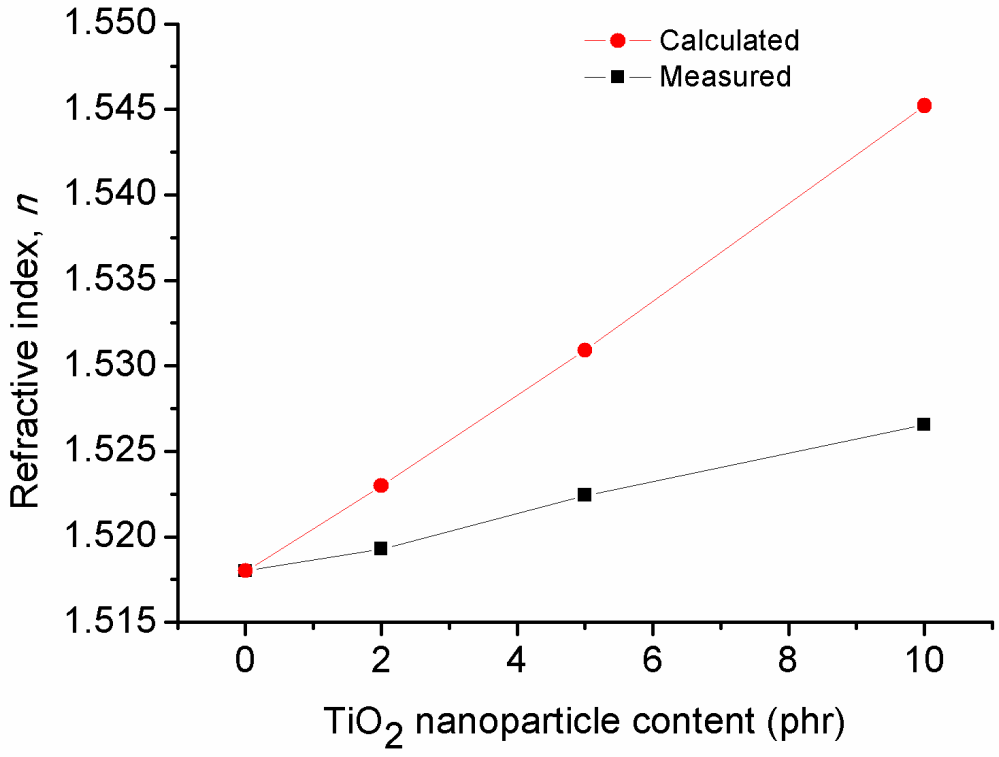

Figure 5. 24 *Change in the refractive index of XNBR polymer nanocomposite with TiO_2 nanoparticle content, the measured values compared with predicted values.*

5.8 Shape Memory Effect

The shape memory materials are stimuli-responsive materials. They have the capability of changing their shape upon application of an external stimulus. A change in shape caused by a change in temperature is called the thermally induced shape-memory effect. Thermal induced shape memory effect of TiO_2 nanocomposite is shown in Figure 5.25. Beyond the transition temperature, the shape of material will changes from temporary shape to original shape and vice versa. The shape memory effect at 110 ^{o}C temperature is demonstrated in Figure 5.25

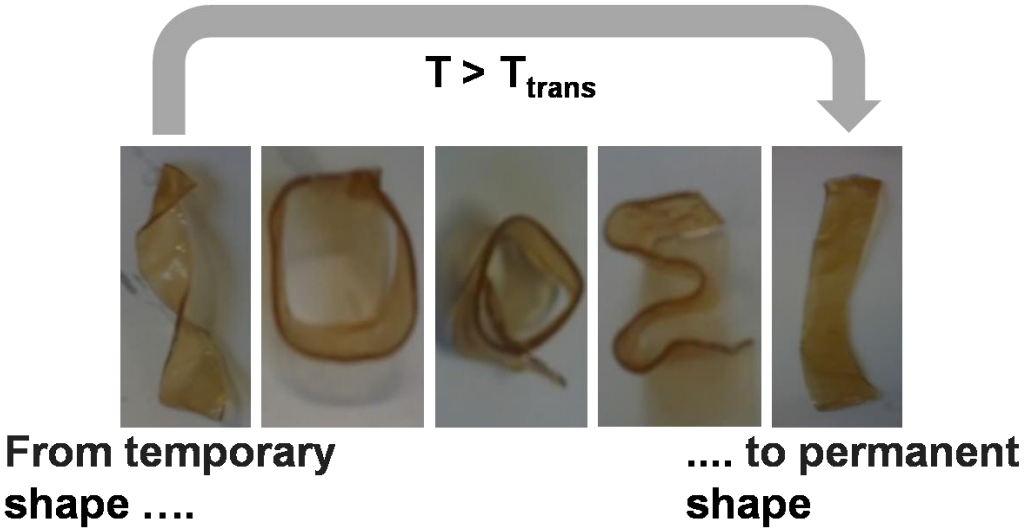

Figure 5.25 *Shape-Memory Effect of sample XMDT 5. By thermal stimulus above the ionic transition temperature (T_{trans}), the shape of polymer changed from temporary to permanent shape and vice versa.*

5.9 Conclusions

The shape memory effect has achieved by incorporation of both ionic and covalent crosslinks in the XNBR polymer matrix. By neutralize carboxylic pendant groups in the XNBR polymer with magnesium metal ion forms ionic physical crosslinks and by radical initiation by decomposing of DCP created chemical bond between the carbon-carbon. These ionic multiplets in the ionic networks acts as a reinforcing fillers and or multifunctional crosslinks as a results improved mechanical properties and thermo reversible properties achieved. The mixed network parameters and bound rubber fraction around the ionic domains has quantified by applying various NMR methods and strategies. TiO_2 both micro and nano size not acts as an active agent for create ionic crosslinks. TiO_2 nanoparticle acted as a good candidate for tuning of optical properties in the nanocomposite ionic elastomer. With TiO_2 nanoparticle content in the polymer matrix, the refractive index increased and nanocomposite act as a UV-absorber and visible light transmitter. By thermal stimuli the shape memory effect has tested.

Chapter 6
Poly (*n*-butyl acrylate) Crosslink Networks Analysis by TD-NMR

6.1 Introduction

Another important class of polymer with elastomeric properties is constituted by polyacrylates. Polyacrylates polymers are not only widely available commercially, but also have potential applications in advanced applications like controlled-released systems or photon managing [139]. Controlled-release systems, where polymer particles are engineered for carrying a load of active molecules to be released within a specified time frame or as response to specific stimuli, have received much attention in different applications such as pharmaceuticals, pesticides, fertilizers, catalysts, cosmetics, etc. [140–143]. Polybutylacrylate polymers are also good candidates for photo managing applications, since they form soft solids with sufficient shape persistence to be used as devices coupled with high local chain mobility that allows photoactive molecules to be in the fast diffusion regime necessary for triplet-triplet annihilation up-conversion (TTA-UC) [144]. All advanced applications require high level of control on both crosslink density and network homogeneity. Thus, it is essential to develop a technique to identify and estimate network structure and homogeneities. The different chemical reactions that occur at different stages of polymerization (conversion of monomer into polymer) are potential sources of inhomogeneities and defects in the network, especially considering that many polyacrylates can self-crosslink even in absence of specific crosslinking agents. The crosslink density, defects and inhomogeneities are influential factors on the mechanical properties of outcome networks.

The network inhomogeneities can be investigated by differential scanning calorimetry, extraction-high pressure liquid chromatography (HPCL), dynamical mechanical analysis, ^{1}H NMR relaxation, ^{13}C NMR spectroscopy [145] etc. The commonly used techniques for network crosslink density measurement are equilibrium swelling [53], mechanical measurement [95], low field [2] and high field NMR [97]. Low resolution MQ NMR is emerging as robust technique for estimating crosslink density and distribution quantitatively with improved pulse sequences and data analysis approaches. This technique could estimate

precisely the residual dipolar coupling (D_{res}) constant induced by semi-local anisotropic motion of polymer chains due to topological constraints such as mainly crosslinks, entanglements or other type of physical restrictions. Baum-Pines sequence as explained in chapter 2 is suitable for weak dipolar coupled network characterization, where as for strongly dipolar coupled networks the pulse sequence has a decisive disadvantage due to limitations on experimental time scales, details are given in chapter 5. This technique could give the model free D_{res} value and is able to convert into M_c and hence crosslink density for samples, whose polymers static dipolar coupling constant is known. The model crosslinked poly (*n*-butyl acrylate) networks with variable content of crosslinker (ethylene glycol dimethacrylate (EGDMA)) were prepared and characterized with MQ NMR and T_2 relaxation measurements. The temperature dependent segmental dynamics were also studied by measuring T_1 relaxation.

6.2 Experimental

6.2.1 Polymer synthesis

n-butyl acrylate with M_n=128 g/mol, ethylene glycol dimethacrylate (EGDMA) with M_n =198 g/mol and radical initiator azobisisobutyronitrile (AIBN, Aldrich 98%) have been purchased from Sigma-Aldrich and used as it is. The radical initiator azobisisobutyronitrile (AIBN, Aldrich 98%) is kept constant 10^{-3} M, *n* -butyl acrylate and amount of EGDMA were varied. Free radical bulk polymerization was carried out in a water bath at 55 °C for 1 day and at 95 °C in an oven for one night until the liquid converted to self standing rubber. Samples were polymerized in 5 mm NMR tubes and their composition details were given in Table 6. 1.

Table 6. 1 *Sample composition details*

Sample	BA (in mass %)	EGDMA (in mass %)
BA1	100	0
BA2	99	1
BA3	95	5
BA4	92.5	7.5
BA5	90	10
BA6	87.5	12.5
BA7	85	15
BA8	80	20
BA9	70	30
BA10	50	50

6.2.2 Differential Scanning Calorimetry (DSC)

DSC measurements were performed on METTLER TOLEDO STAR^{e} thermal analysis system details were given in chapter 5.

6.2.3 Dynamic Mechanical Analysis (DMA)

Dynamic mechanical analysis measures the damping of an oscillatory signal in a material. The technique allows the detection of very weak transitions as well as fast determinations of modulus, damping, viscosity, and compliance as a function of temperature and frequency. It is commonly used to study polymer melts as well as solid polymers. It has the advantage of allowing testing on a wide variety of materials, and both liquids and solids can be handled in the same instrument, making it extremely useful for the study of curing systems. The solid were characterized by DMA, instrument details were given in chapter 5. The sample was prepared in as discs with 6 mm diameter and 3 mm thickness. During a typical experiment, a

disc was inserted between the plates and compressed with a static force of 2 N and a dynamic force of 1 N using a frequency of 1 Hz. The dynamic force was large enough to obtain a significant (5–10 μm) amplitude even at the low temperature glassy state of the material.

6.2.4 Solid-state NMR

Solid-state ^{1}H TD-NMR experiments were carried out on a Bruker minispec, instrument details were given in chapter 2. MQ experiments acquisition was done with 32 scans. T_1 measurements were performed using saturation recovery pulse and acquisition done with 32 scans. Sample preparation and pre experimental conditions were given in chapter 2. MQ experiments were performed at temperature (T>T_g+120 K) well above the glass transition temperature. T_2 relaxation measurements were performed with Hahn echo pulse sequence and experiments data were acquired with 32 scans.

6.2.5 Gel Permeation Chromatography (GPC)

The molecular weight of synthesize poly (*n*-butyl acrylate) polymer was measured by GPC model WATERS 1515 isocratic equipped with a HPLC Pump, WATERS 2414 refractive index detector, four Styragel columns (HR2, HR3, HR4 and HR5). GPC system was calibrated with polystyrene Sigma-Aldrich standards. Samples were dissolved in THF (tetrahydrofuran) and recorded with a flow of 1.0 ml/min.

6.2.6 High resolution ^{1}H NMR

High resolution ^{1}H solution NMR experiment was performed on Bruker Avance AMX-500 at resonance frequency of 500 MHz on 5 mm standard probe. The samples were dissolved in deuterated chloroform ($CDCl_3$).

6.3 Results and Discussion

6.3.1 Network structure of poly (*n*-butyl acrylate) crosslinked with EGDMA

The bulk polymerization with initial monomers of *n*-butyl acrylate, EGDMA with radical initiator AIBN creates tetra functional randomly crosslinked network structure. The expected crosslinking structure is shown in Figure 6. 1.

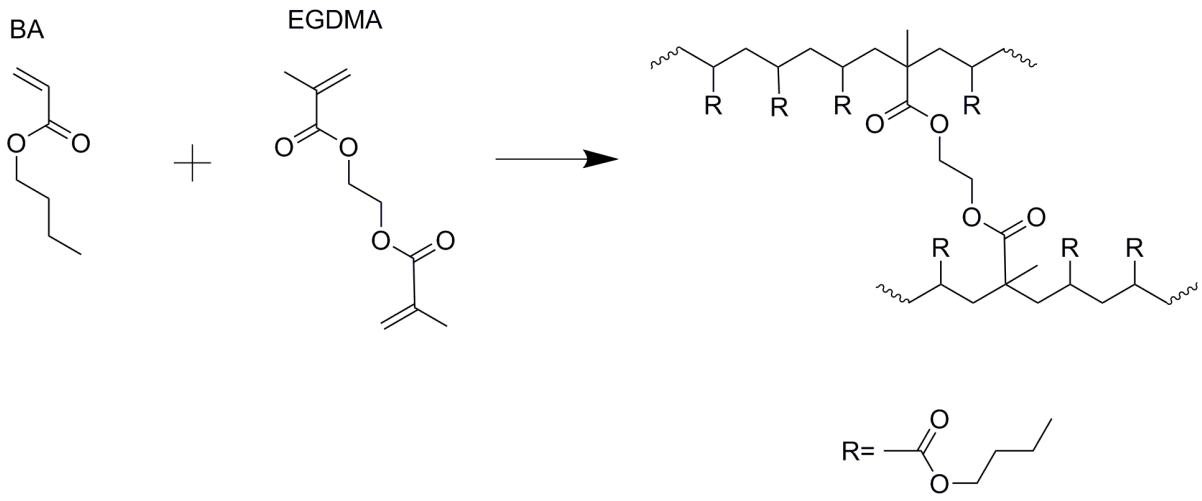

Figure 6. 1 *Schematic structure of EGDMA crosslinks with poly (n-butyl acrylate).*

6.3.2 Glass transition temperature

The well known factor is that the glass transition temperature of polymeric materials depends on the molecular weight, degree of crosslinking and hence structure of the material. Introducing crosslinks into a polymer raises the glass transition temperature. In addition, there is a decrease in the specific volume, since introducing crosslinks involves the exchange of van der Waals bonds for shorter, more compact primary bonds. Thus, the process of crosslinking should affect the segmental mobility and the related properties in a manner similar to the effect of an increase in molecular weight of the primary chains. The Flory-Fox equation [146] gives the relation between T_g and molecular weight of primary polymer chains according to the Equation (6.1).

$$T_g = T_g^{\infty} - \frac{K}{M_n} \tag{6.1}$$

Where T_g^{∞} is the maximum glass transition temperature that can achieve at a theoretical infinite molecular weight and *K* is an empirical parameter that is related to the free volume present in the polymer sample. M_n is molecular weight of macromolecule (polymer).

The T_g dependency on crosslink density of network polymer is given in Equation (6.2) by neglecting certain effects (copolymer effect of network junctions, high functionality of networks junctions, non-Gaussian chain statistics, network defects (dangling ends) etc.)

$$T_g = T_g^{\infty} + \frac{K}{M_c} \tag{6.2}$$

Where T_g^{∞} is the maximum glass transition temperature of theoretical infinite molecular weight, *K* is material constant and M_c is the molecular weight between crosslink junctions, and is inversely proportional to the crosslink intensity (density).

The T_g of synthesized polymer networks was obtained from DSC. It is clear from the DSC curves that, the polymerization is completed confirmed by not observing any monomer traces on DSC thermograms of prepared samples. The samples BA9 and BA10 T_g were not possible to obtain with DSC due to higher crosslinking in the network and hence broader glass transition. The glass transition temperature of the crosslinked networks are increases linearly upon an increase in the crosslink agent (EGDMA) content as shown in Figure 6. 2 according to Equation (6.2). The T_g versus EGDMA weight % is fits linearly with intercept of -43.20 ± 0.38 °C and slope 1.12 ± 0.035. The R^2 of the fit is 0.993. The intercept value is exactly equal to the glass transition temperature of pure poly (n-butyl acrylate) polymer (sample BA1).

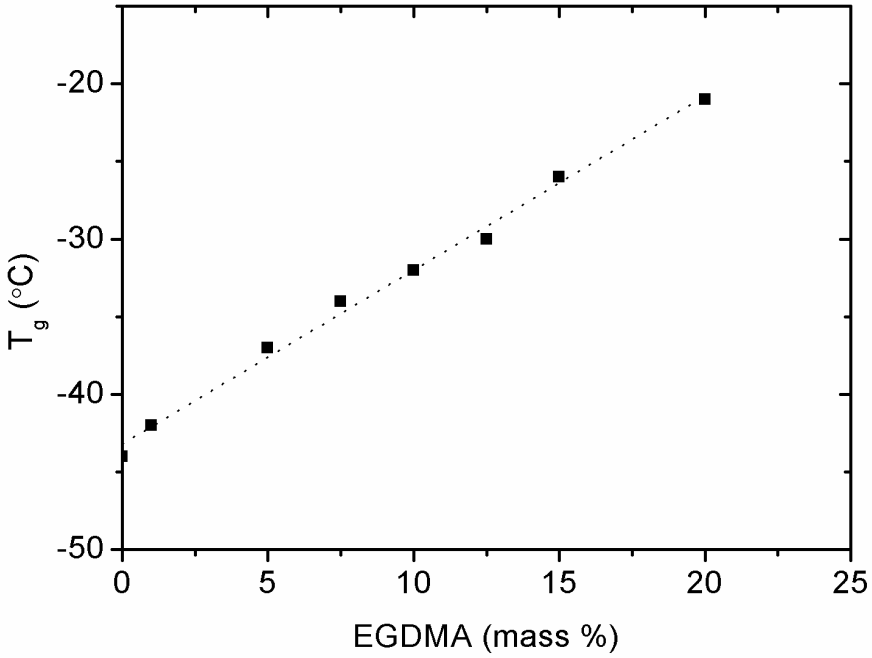

Figure 6. 2 *The glass transition temperature dependency on crosslink agent (EGDMA) content. With increase of crosslinker, the crosslink yield increases and glass transition rising linearly. The linear fit is indicated with dotted line.*

6.3.4 Molecular weight of polymer

The molecular weight of synthesize poly (*n*-butyl acrylate) polymer was measured by GPC on solution polymerized sample by dissolving the polymer in THF solvent. Since the bulk polymerized sample was not possible to dissolve in the solvent due to presence of self crosslinking. The number and weight average molecular weights respectively are M_n= 89224 g/mol, M_w =127376 g/mol and the polydispersity index 1.42. The molecular weight distribution peak maximum (M_p) =133076 g/mol.

6.3.5 Crosslink network analysis by NMR

The physical properties of crosslinked polymer materials depend on the volume-average network density. To understand the structure-property relationship of crosslinked networks, the precise knowledge on crosslink density is prerequisite. The most common methods for measuring crosslink density are equilibrium swelling and mechanical measurements. In addition to the network structure, these methods can provide information that is desirable for practical applications, such as modulus, stress-strain behavior, and glass transition temperature. The statistical and phenomenological theories are used to relate experimental measured quantity to the density of chemical and physical crosslinks. These molecular models have been developed for ideal networks assumed in which no defects are present. Due to these differences between theories and experimental leads several discrepancies in the experimental results. In real networks, chain entanglements, network defects, and network heterogeneity etc. presents and these causes deviation of results from theoretical models. The traditional macroscopic techniques such as mechanical measurements are not capable of providing complete information about network topology.

The well known fact is that when linear polymer is transformed into a crosslinked network, resulting restrictions on the motion of polymer chains induced by topological constraints. The NMR is sensitive enough to detect any local anisotropy caused by such a topological restrictions (crosslinks, entanglements etc.) on the molecular level.

6.3.5.1 NMR Relaxation

Detailed information on the dynamics of the polymer chains is provided by NMR relaxation measurements. The relation of T_1 and T_2 with correlation times depends on the sample nature, field dependency, obtained from the simplified theory is shown in Figure 6. 3. There are several mechanisms by which molecular motions can influence nuclear relaxation: direct interactions with nearby magnetic nuclei (dipole-dipole), chemical shift effects, quadrupole-electric field gradient interaction and rapid modulation of *J*-coupling as explained these interactions in chapter 1. In addition to molecular motion, rotational transitions can also be the source of fluctuating magnetic fields. A local magnetic field is generated by the circular motion of electrons in a rapidly rotating molecule or part of a molecule, such as a methyl

group. Among these interactions, the dipole-dipole interaction is more significant especially in our present case of variable crosslinked samples. The direct dipole-dipole interaction as detailed in the chapter 2 is much pronounced by the local anisotropic motions, which is induced by the crosslinking of polymers.

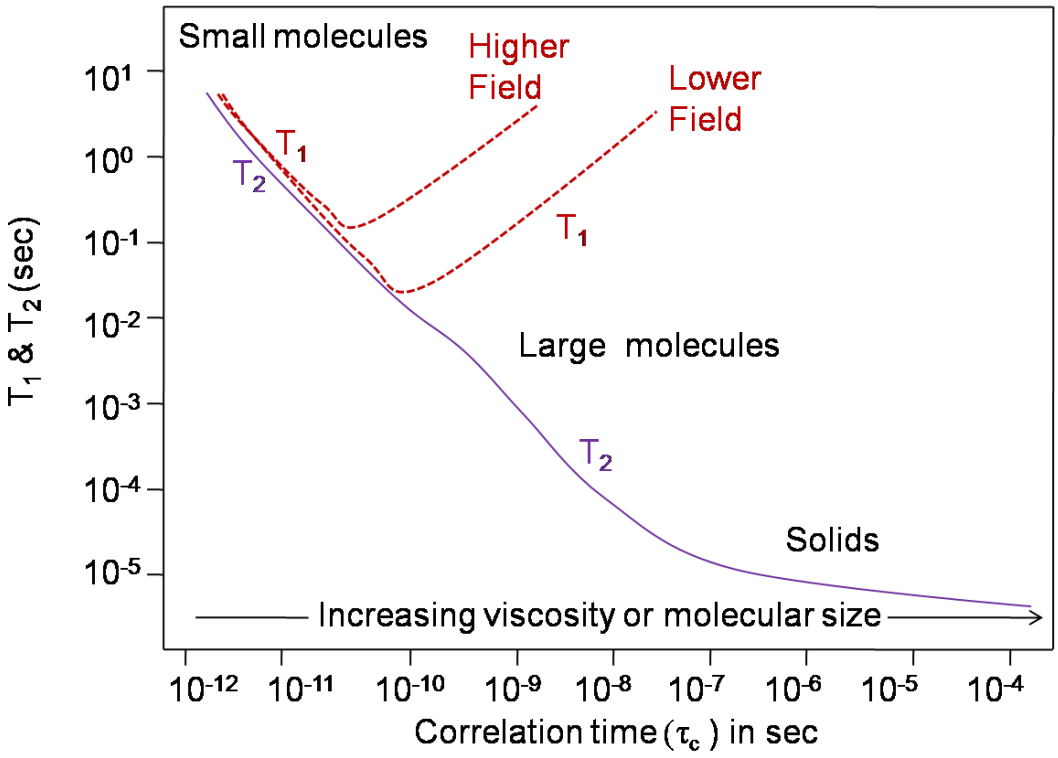

Figure 6. 3 *Dependence of T_1 and T_2 upon τ_c according to the simplified theory in which all interactions are assumed to have the same correlation time (adopted from ref [147])*

In small molecules and liquids, both T_1 and T_2 relaxations are nearly equal and are vary with increasing of molecular weight or viscosity according to the simplified theory as shown in Figure 6. 3. The experimental measured relaxation times are plotted against the EGDMA is shown in Figure 6. 4. Starting from at 0% EGDMA, the T_1 and T_2 are not very close because the molecular weight is higher, around M_W =127400 g/mol with poly dispersity index 1.42 obtained from GPC measurement. It is note that the molecular weight obtained from the sample prepared in solution polymerization. With increasing of crosslink density T_1 is basically constant at low crosslink density, probably due to being dominated by fast relaxation in the highly mobile side chains. Only at very high (>10%) crosslinker fraction, the polymer dynamics undergo relevant modifications that result in increasing T_1, whereas T_2

relaxation time continuously decreases. This first finding confirms that a direct relation between T_2 and crosslink density also exists in polyacrylates.

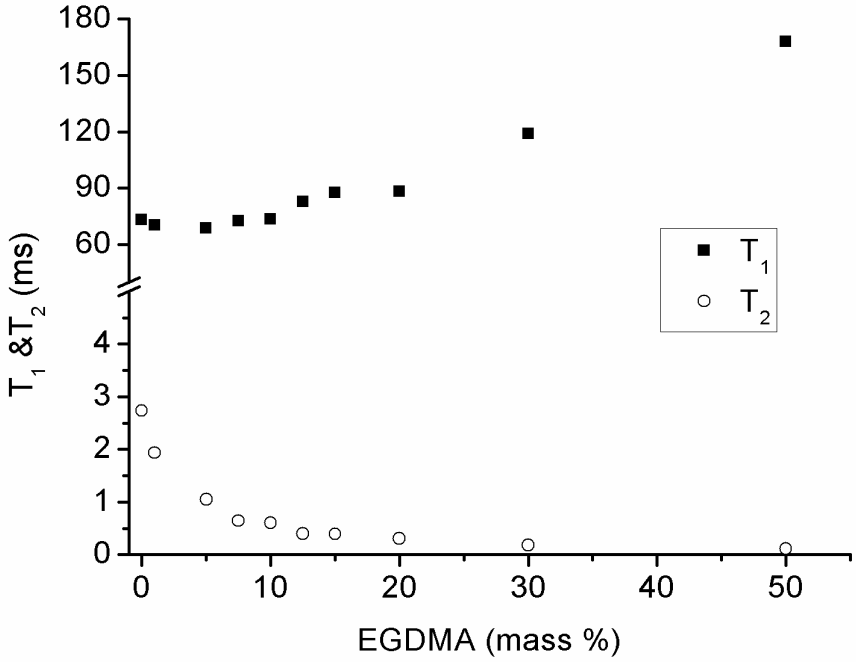

Figure 6. 4 *T_1 and T_2 relaxation times versus EGDMA content.*

6.3.5. 1.1 T_1 relaxation

Different parts of molecules can have different correlation times, and consequently T_1 values. T_1 measurements performed at range of temperatures could allow systematic understanding of internal and segmental motions of high polymers. The temperature dependence of T_1 for two different amounts of crosslinking agent is represented in Figure 6. 5. Below the glass transition temperature T_1 values are nearly over-lapping irrespective of crosslink density since main chains are frozen and side chains are not much influenced by main chain motions. The decaying of T_1 below the 255 and 293 K temperature for 1% and 20% EGDMA samples correspond to the motions of side chain ester alkyl groups [17]. It appears that at the lowest temperatures, the only possible motion (side chains) has specific frequency close to the Larmor frequency in the defined experimental conditions, resulting in very low relaxation value. In fact, due to the presence of spin diffusion phenomena, we basically see the relaxation time of the fastest relaxing nuclei that then act as magnetization sinks for the rest of the material. At higher temperature, differences in network structure produce differences in T_1: the relaxation time of each sample continues to grow until several degrees after the

sample T_g, and then declines. Basically, as temperature increases, the side chains move with higher frequencies and reduce the spin-lattice relaxation rate. On the other side, after T_g the main chains of each polymer gain are less constrained and become the new magnetization sink. Of course, as temperature is increased again, the main chains also move more freely, initially bringing the detected T_1 to a new minimum. Finally, further increase of temperature results in a second increase of T_1 that was only detected in the low crosslink sample due to the impossibility of raising the experimental temperature without degrading the sample itself. As a result, the low crosslinked sample displays two maxima one at low temperature and one at higher temperature while for the higher crosslinked sample only one maximum is observed within measurement temperature range and is shifted to higher temperature (see in Figure 6. 5). The V-shape curve and minimum of T_1 value for 1% and 20% EGDMA samples respectively at higher temperature corresponds to segmental motions and may be influenced by topological constraints in the polymer. To further explore this effect, we measured their values in two differently crosslinked samples of poly (*n*-butyl acrylate) sample without crosslink agent prepared in a solution and bulk polymerization are showing exactly the same trend of temperature dependence shown in Figure 6. 6. However the bulk polymerized sample showing lower T_1 values in the entire range of temperature and may be due to influence of very less amount of self crosslinks present in the bulk polymerization sample.

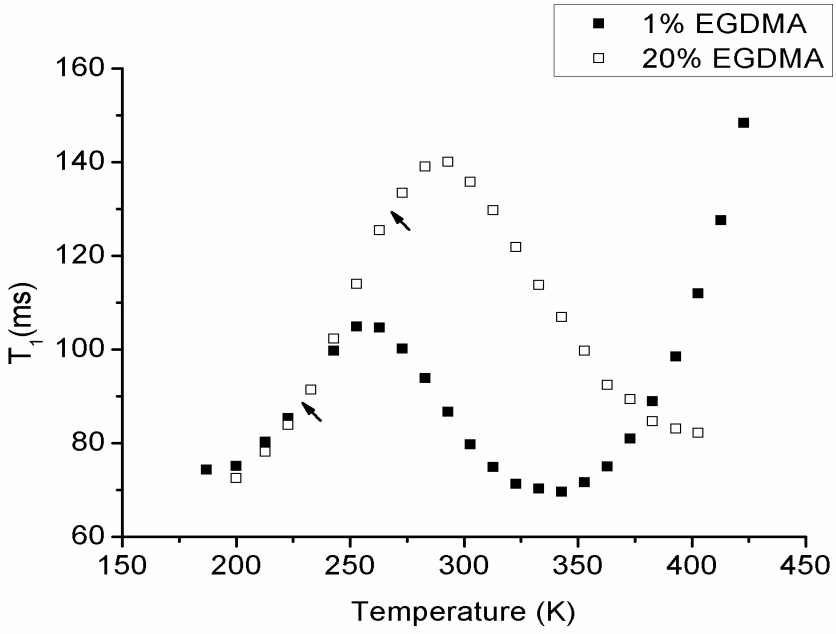

Figure 6. 5 *Temperature dependent T_1 relaxation times of two different amounts of crosslinked samples. The EGDMA % is given in the legend and arrow indicates the T_g of corresponding sample.*

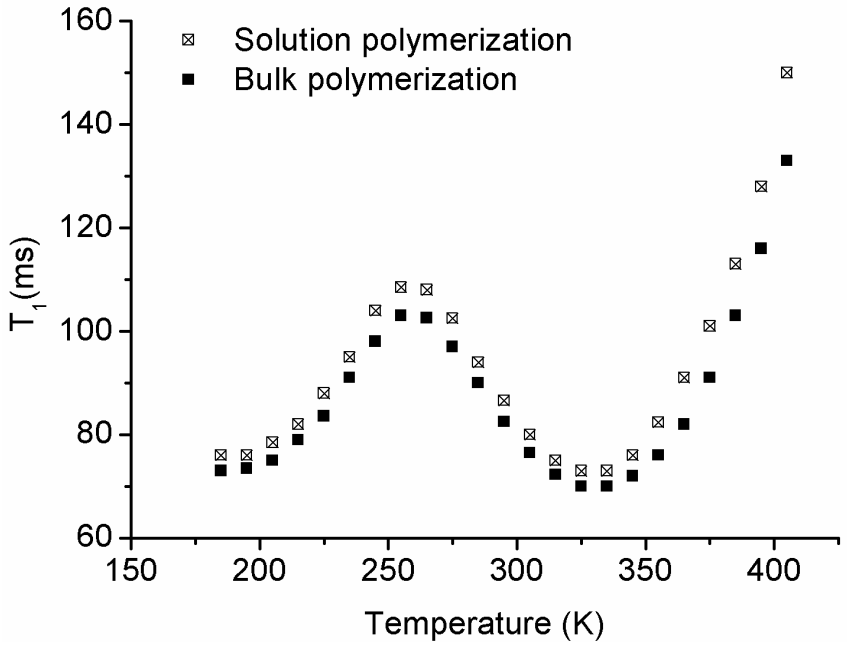

Figure 6. 6 *Temperature dependent T_1 relaxation times of poly (n-butyl acrylate) sample synthesize as bulk and solution polymerization.*

6.3.5.1.1 T_2 relaxation

The relaxation rate ($1/T_2$) at T_g+120 K for samples as a whole reveals also a linear dependence against the content of crosslinker as shown in Figure 6. 7. The relaxation rate at temperatures well above T_g (T>T_g+120K) is proportional to the network density it can be concluded from results plotted in Figure 6. 7. The crosslink densities in cured poly acrylate are proportional to the content of crosslink agent which could create tetrafunctional crosslink networks.

The T_2 relaxation time curves of variable EGDMA content networks consists of fast and slowly decaying components which are represents with characteristic decay time T^s_2 and T^l_2, respectively shown in Figure 6. 8. The superscripts "s" and "l" relate to short (T^s_2) and long (T^l_2) relaxation time, respectively. Two components are observed only after 5% EGDMA content samples. The shorter component reveals T_2 relaxation time, which is typical for crosslinked rubbers, i.e., in the range of milliseconds or shorter. A longer component shows high molecular mobility. This fraction presumably originates from residual uncured material and low molecular weight polymer chains long dangling chain ends, chain loops, and loosely crosslinked chains.

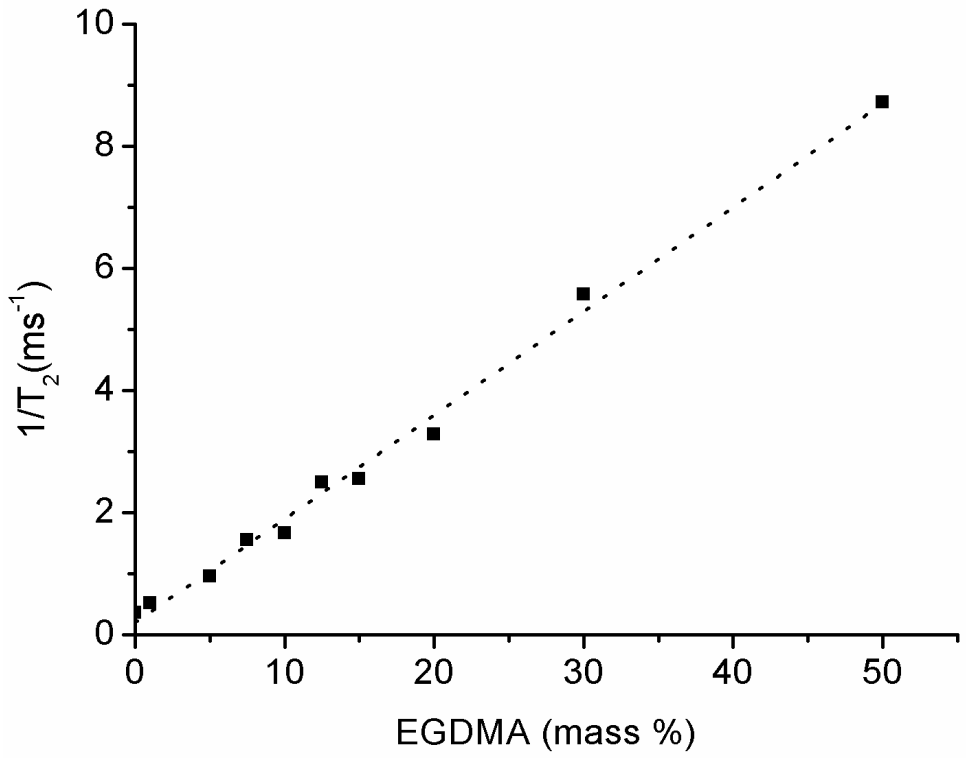

Figure 6. 7 *T_2 relaxation rate at $T>T_g+120$ K versus EGDMA content. The dotted line represents the linear fit of results.*

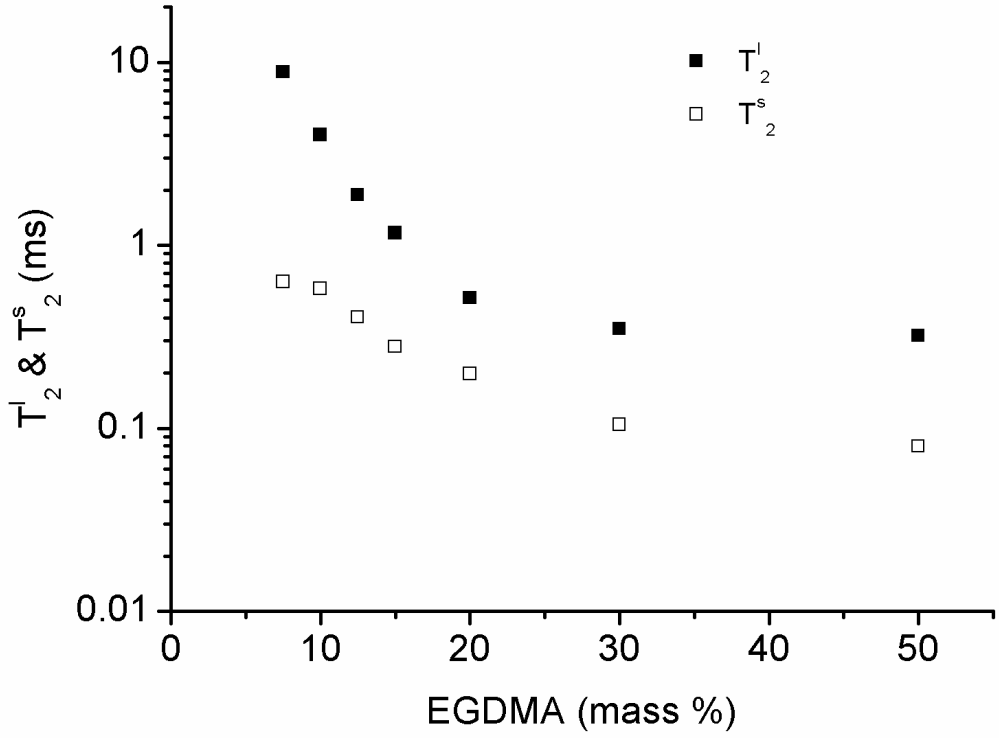

Figure 6. 8 *Shorter and longer components of T_2 relaxation times at variable EGDMA content.*

The mobility of system depends on the nature of the polymer chain as well as on the presence of chemical and physical crosslinking. Even low field instruments can provide sufficient information on the molecular mobility and structure by neglecting the chemical shift resolution and simply analyzing the FID of appropriate experimental data. The simple Hahn echo experiment [101] could also give the crosslink density but recent literature [2] suggesting that, such experimental results are potentially influenced by mathematical fitting artifacts due to fitting of data with multi-variable equation and also suggesting that MQ NMR is more robust for crosslink measurements.

Hahn echo measured relaxation curves of poly (*n*-butyl acrylate) with 0, 10 and 50 Wt.% of crosslinker (EGDMA) are as shown in Figure 6. 9 . The faster decay of intensity with EGDMA content reveals the increasing crosslink yield in the polymer. The longer component is account for network defects and residuals of initial components or lower molecular weight chain molecules may present due to the nature of bulk polymerization. The higher polydispersity index of our sample is evident for presence of shorter molecular weight chains.

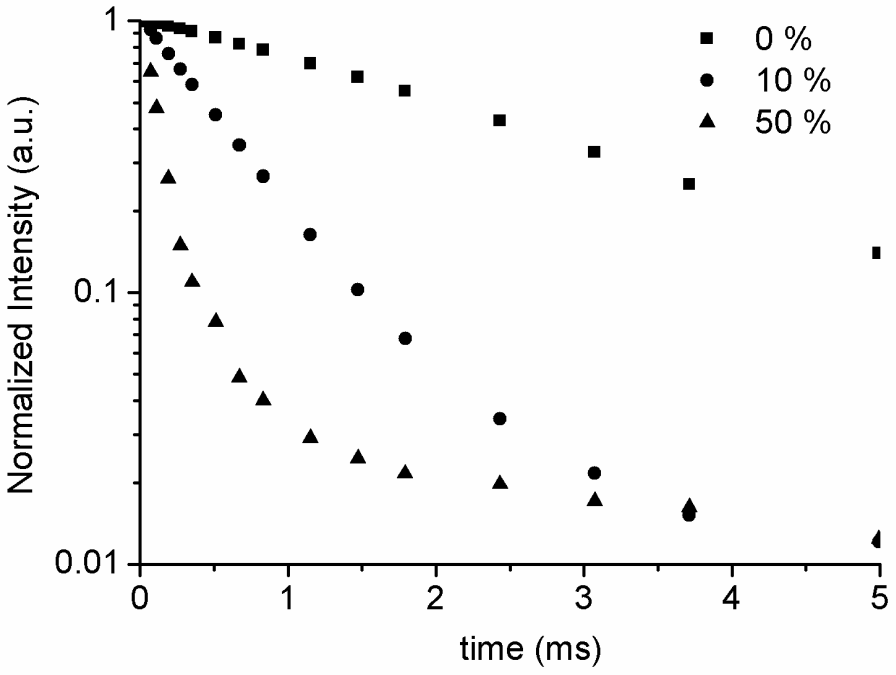

Figure 6. 9 *T_2 Relaxation curves of poly (n-butyl acrylate) samples with variable EGDMA percentage obtained from Hahn echo pulse sequence. The EGDMA percentage is given in the image legend.*

6.3.5.2 Network analysis by MQ NMR

The importance and basic theory behind the multiple-quantum NMR has been discussed in the chapter 2 and is directly applicable to all crosslinked networks. But the lengthy Baum-Pines pulse sequence is directly applied to less crosslinked networks which are consist of weak dipolar coupling constants. In the present poly (*n*-butyl acrylate) networks, at higher concentrations of EGDMA, the system transforming from rubber to self-standing rod like structure due to higher crosslinking. For characterize such a higher crosslinked networks, the lengthy Baum-Pines pulse sequence as it is not suitable due to limitation of experimental time scales. The significant amount of signal will lose within the first single cycle time. To overcome this problem, five-pulse sequence has been used to characterize the strong dipolar coupled networks. The Baum-Pines pulse sequence has been used for characterizing lower crosslink density samples, below 10% of EGDMA, beyond 10%, networks crosslink density is high, due to that reason, the maximum of build-up intensity reaching within the first experimental cycle time as shown in Figure 6. 12 for 12.5% EGDMA sample and corresponding samples reference intensity is shown in Figure 6. 11. The faster decay of reference intensity with increasing EGDMA is also a clear indication of increasing crosslink density. The schematic of different crosslink density network structure is as shown in Figure 6. 10.

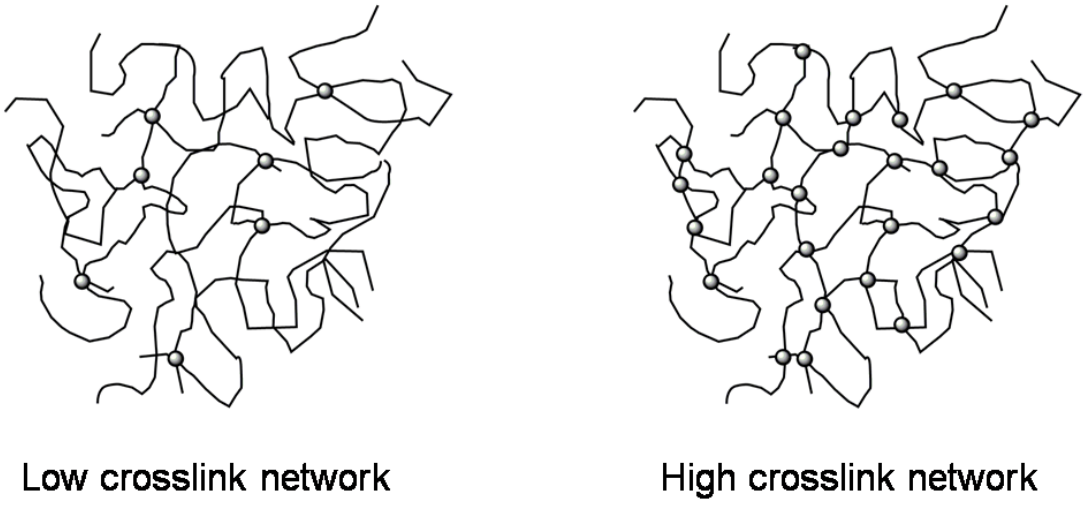

Figure 6. 10 *Low and high crosslink network structures, spherical symbols in the image refer to chemical crosslink junctions.*

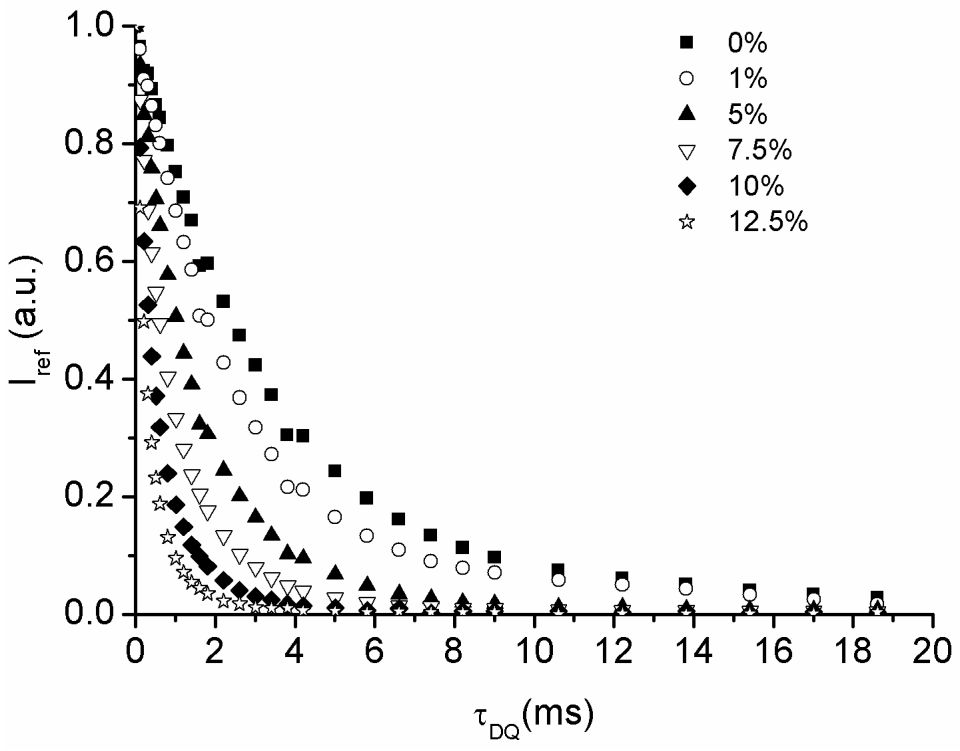

Figure 6. 11 *Variable crosslink density samples normalized reference intensity obtained from MQ NMR experimental results. Legend number indicates EGDMA percentage.*

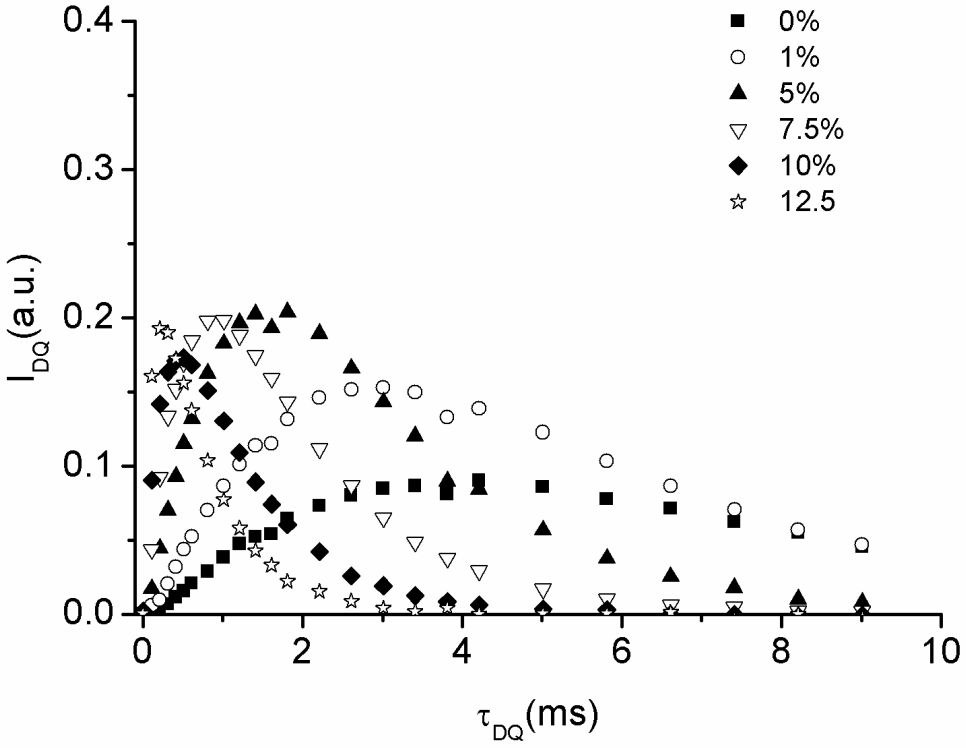

Figure 6. 12 *Variable crosslink density samples normalized DQ intensity obtained from MQ NMR experimental results. Legend number indicates EGDMA percentage.*

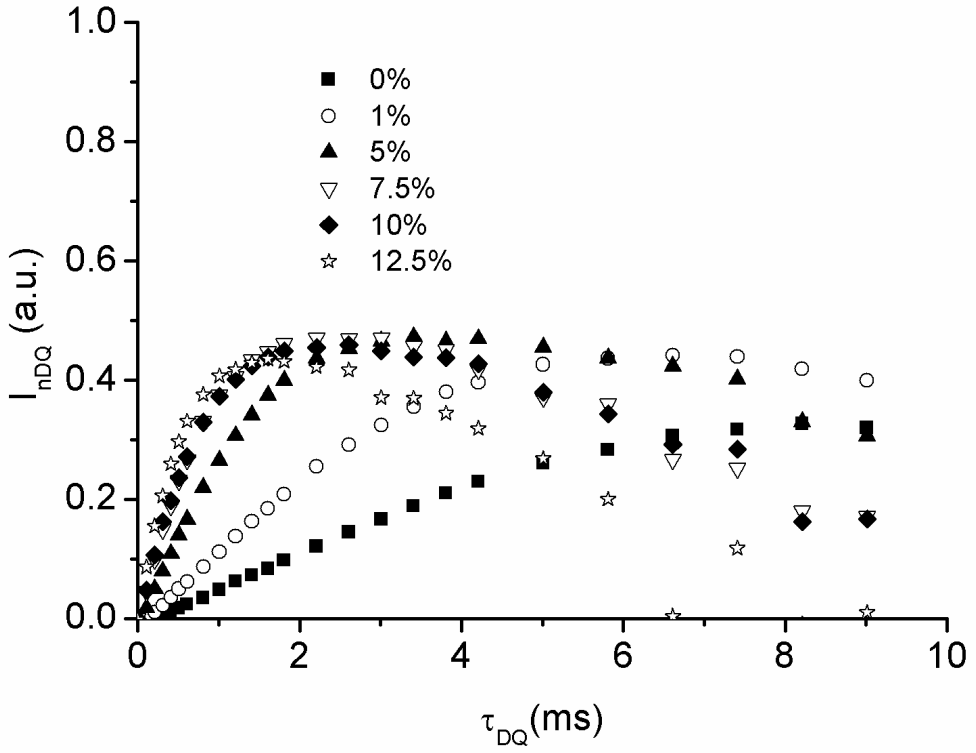

Figure 6. 13 *The normalized DQ intensity (I_{nDQ}) obtained by dividing I_{DQ} with (I_{ref} +I_{DQ}) intensity. Legend number indicates EGDMA percentage.*

The typical DQ build-up intensity and reference intensity are reaching zero very rapid with increasing EGDMA, means increasing of crosslink density. The DQ intensity reaches nearly to zero at 6, 3.2, 1(not shown here) and 0.4 ms time for 15, 20, 30 and 50% EGDMA content. The reference and DQ intensity curves for 50% EGDMA sample is shown in Figure 6. 14. It is note that the five-pulse sequence is less efficient as to the excitation of higher-order coherences than the Baum-Pines sequence. In five-pulse sequence the DQ excitation time (τ_{DQ}) axis is features the common prefactor of 3/2, rendering the build-up quicker. I_{DQ} excited by a five-pulse sequence, normalized DQ intensity (I_{nDQ}) does not reach the 50% limit, and $I_{\sum MQ}$ is subjected to notable homogeneous dephasing [2]. Due to all these reasons, for higher crosslinked samples data treatment, I_{nDQ} limit consider only up to 0.45 (Gauss-kernel).

MQ NMR obtained residual dipolar coupling constant (D_{res}) is directly related to crosslinks and is model free quantity. The obtained D_{res} versus EGDMA content is plotted as shown in Figure 6. 15 . MQ NMR is sensitive enough to detect the minute crosslink variations and also able to measure physical crosslinks and is clearly seen from Figure 6. 16. In bulk polymerization a slight self-crosslinking may exist without any extra crosslink agent and may

be reason that bulk polymerization samples does not dissolved in the solvent, however solution polymerization sample dissolves. Due to such small amount of crosslinks in the bulk polymerized samples, the reference intensity decays relatively faster and DQ build-up intensity is raising faster with increased slope compared to corresponding solution polymerization sample as shown in Figure 6. 16. The D_{res} value of solution polymerization sample is less than corresponding bulk polymerization sample and is indicated with arrow in Figure 6. 15

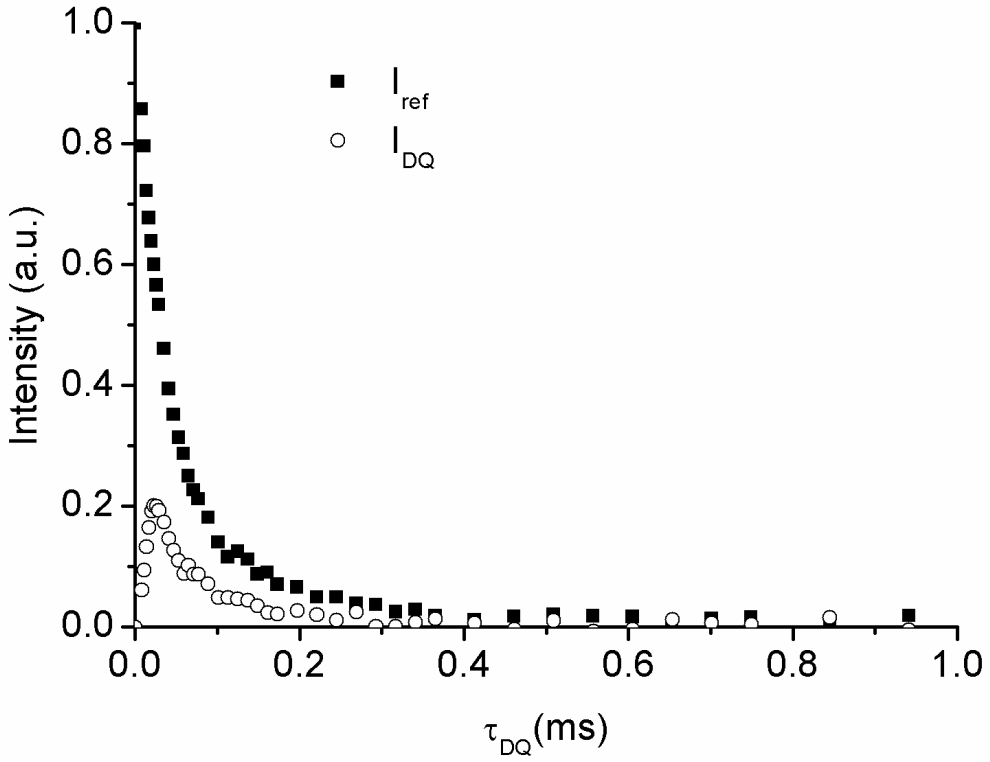

Figure 6. 14 *The reference and double-quantum intensity of MQ NMR experimental data for sample 50% EGDMA obtained from five-pulse MQ NMR sequence.*

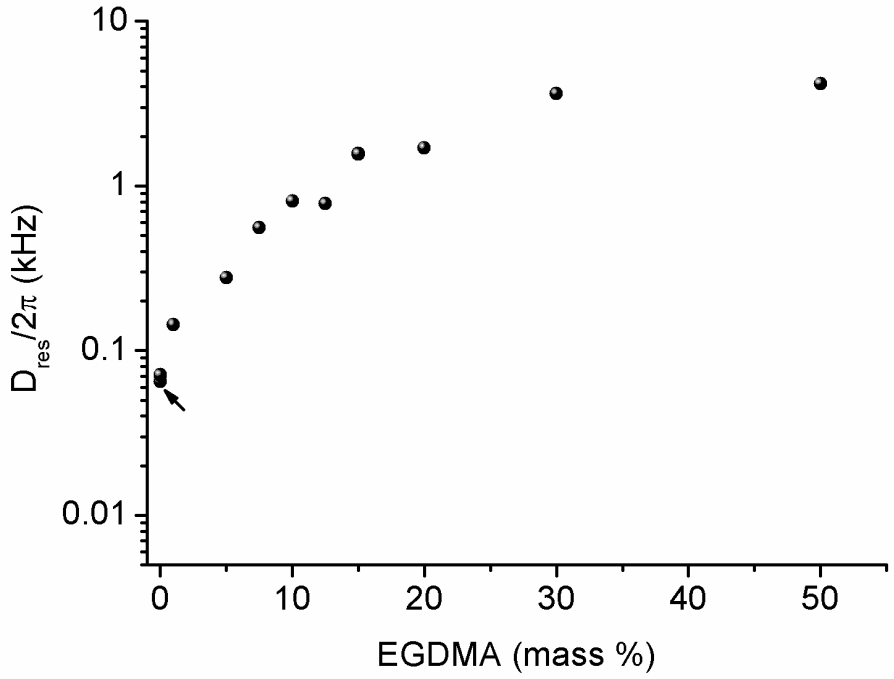

Figure 6. 15 *MQ NMR measured D_{res} constant of poly (n-butyl acrylate) samples versus EGDMA content. Arrow indicates solution polymerized sample (without EGDMA).*

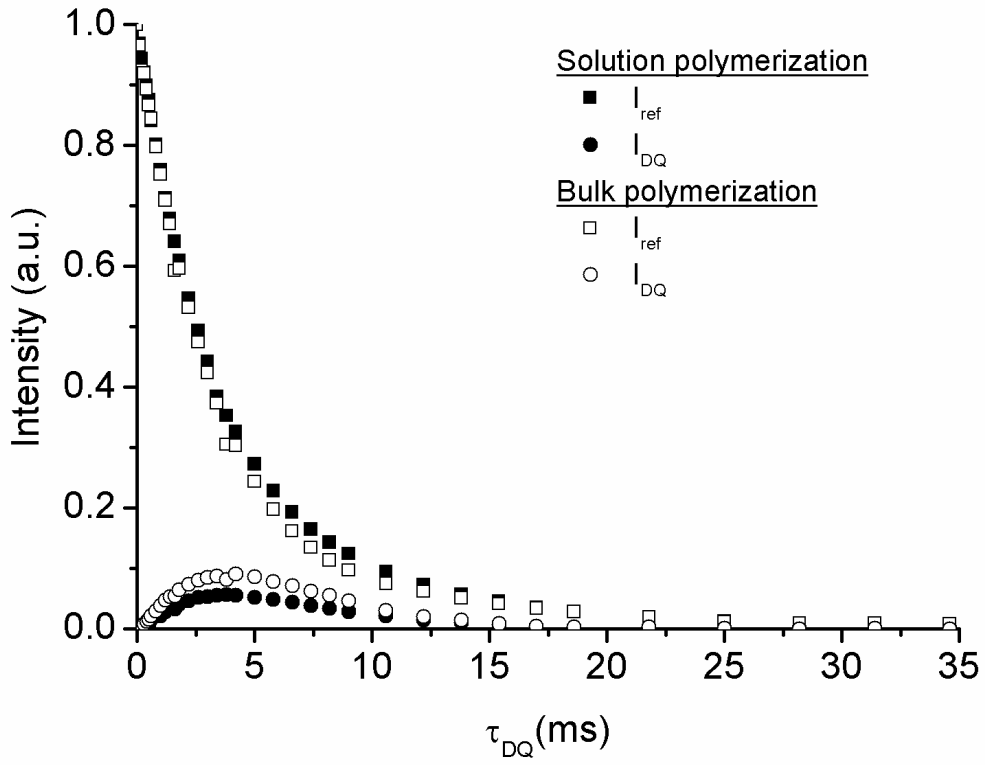

Figure 6. 16 *MQ experimental data of poly (n-butyl acrylate) prepared in solution and bulk polymerization.*

6.3.6 High resolution ^{1}H NMR study

The ^{1}H NMR spectrum of the synthesized polybutylacrylate is shown in Figure 6. 17. The chemical shift at 0.91, 0.93 and 0.94 ppm were attributed to the CH_3 protons. Chemical shift at 1.61 ppm was assigned to -CH_2- protons. 1.9 ppm corresponds to back bone protons of -CH_2-. Peak at 2.27 ppm corresponds to backbone proton represented with letter 'd' in Figure 6. 17. Chemical shift at 4.02 ppm corresponds to -CH_2- proton represented with letter 'a' in Figure 6. 17. It was not possible to dissolve the bulk polymerized sample due to self-crosslinking that rendered the material insoluble.

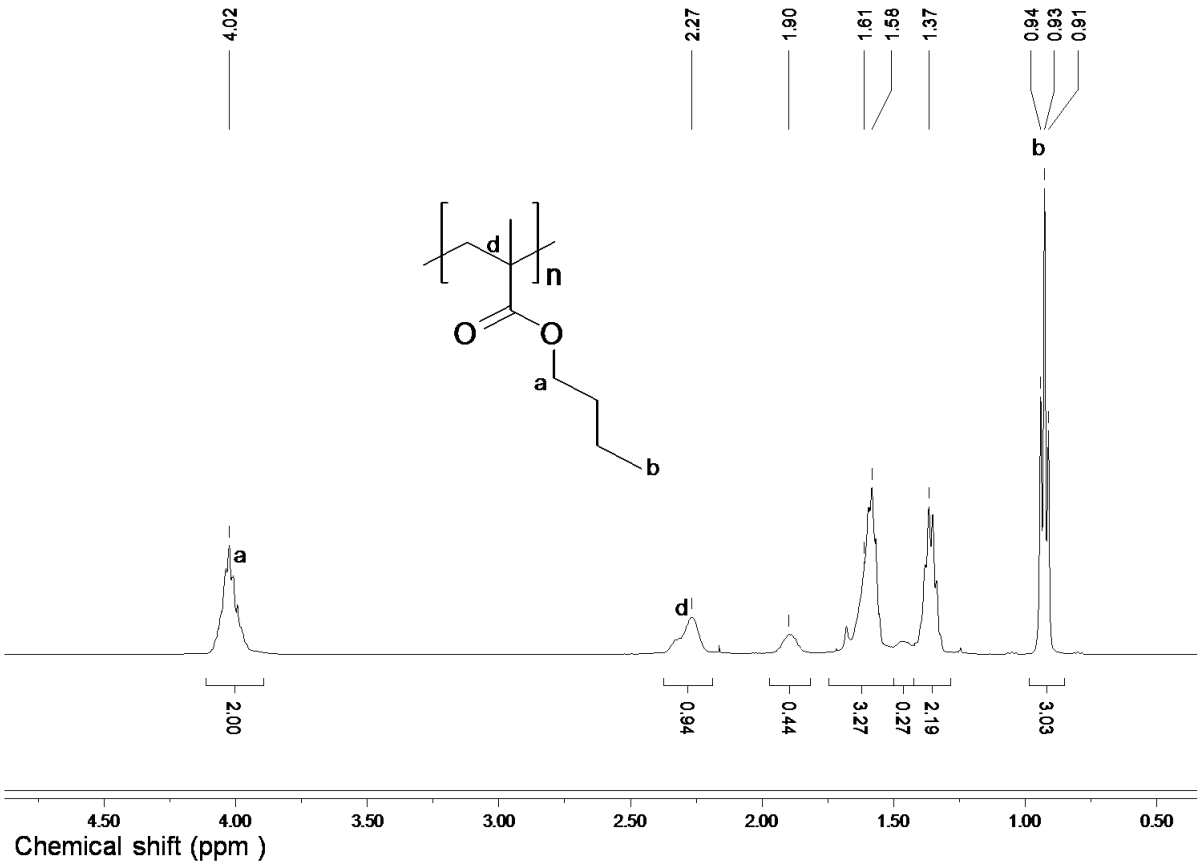

Figure 6. 17 *^{1}H-NMR spectrum ($CDCl_3$, 500 MHz) of the solution polymerized poly (n-butyl acrylate).*

6.3.7 Mechanical measurements

The temperature dependence of modulus was obtained from temperature sweep experiments performed in a broader range of temperature and obtained storage modulus on rubber plateau region at 50 °C is shown in Figure 6. 18. Both T_g and E' increased upon increasing EGDMA content that corresponds to an increase in the crosslink density. Mechanical measurements well agree with molecular level measured NMR results.

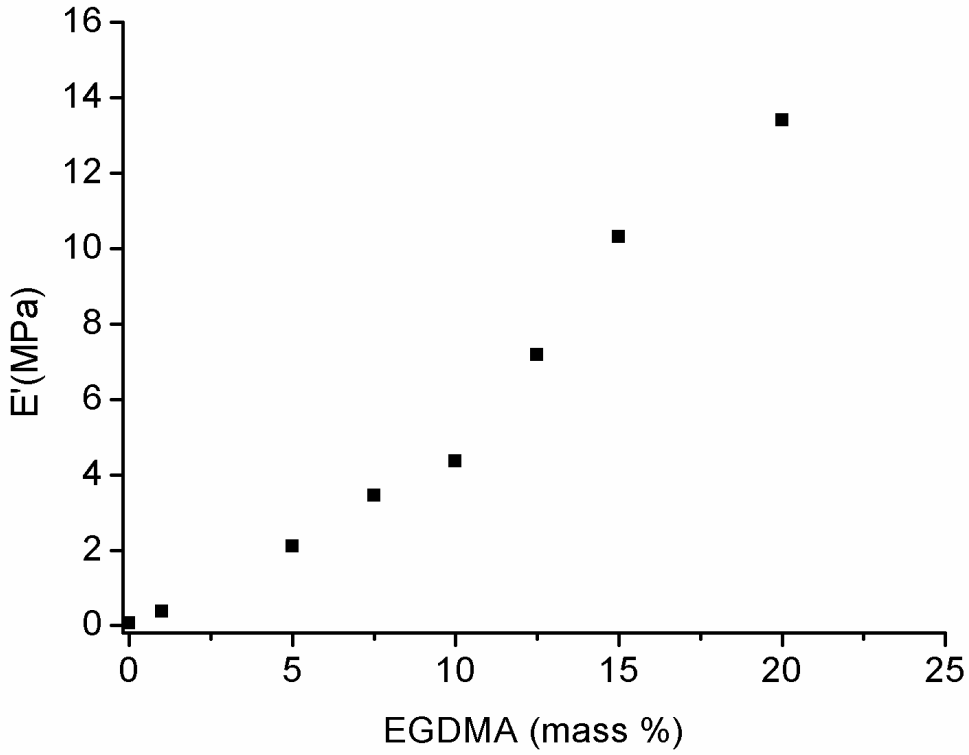

Figure 6. 18 *Storage modulus of crosslinked poly (n-butylacrylate) in the rubber plateau region versus EGDMA content.*

6.4 Conclusions

The network structures in thermal-cured polyacrylates were studied with ^{1}H NMR relaxation, MQ NMR spectroscopy and mechanical experiments. The following conclusions are made from this study: (1) the NMR T_2 relaxation, MQ NMR method shows good correlation with mechanical tests. This suggests that a similar correspondence should be verified with swelling methods (2) T_1 measurements over a range of temperature allow understanding the internal motions of high polymer chains. (3) The bulk polymerization polybutyl acrylate creates a significant amount of self crosslinking whereas solution polymerization does not, and they are detectable by MQ NMR. (4) An increase in the content of EGDMA monomer causes a significant increase in the crosslink density because the EGDMA monomer acts as a tetrafunctional crosslinker. (5) Various NMR techniques could allow understand the various aspects of polymer dynamics, structure in the molecular level scale.

Chapter 7
Conclusions

Time domain NMR was used to characterize crosslink network structure of sulfur cured natural rubber, unfilled and carbon black filled polyisoprene, polybutadiene and polyisoprene/polybutadiene blends. Ionic and covalent mixed crosslink shape memory elastomers and polybutylacrylate model networks were also investigated. Multiple-quantum NMR (MQ NMR) technique has been elected for this purpose due to the robustness in probing network structure of polymer materials and advantages over the traditional equilibrium swelling method.

Present thesis briefs MQ NMR basic theory along with the recent advances in literature. The complete procedure for MQ experimental data acquisition and corresponding data analysis has been discussed that can be easily applied to characterize unlabeled polymer networks. The precision, advantages and limitations of MQ NMR method was compared with that of equilibrium swelling method, a widely used method to measure crosslink density of elastomers.

The natural rubber network crosslink density increases and crosslink density distribution becomes broader with sulfur content as revealed from MQ NMR measurements. Network defect fraction or slowly relaxing component decreases with sulfur content. Above the network percolation threshold, slowly relaxing component and crosslink density slightly deviates from the linearity.

Equilibrium swelling method not only gives overall crosslink density but also mono-di and polysulfidic crosslinks population in the sulfur cured systems by applying thiol probe and selective cleaving of different sulfur bridges. The sulfur bridge ranking has a slight influence on the mechanical properties of crosslinked network. The swelling results are model dependent. The swelling crosslink density numbers are quantitatively in good agreement with independent MQ NMR results, only when phantom model is applied for swelling method. Statistical errors associated with MQ NMR measurements were much smaller than the corresponding values measured with swelling experiments. Moreover, the experimental time

is significantly reduced, thus demonstrating the feasibility of MQ NMR as a technique for quality control in industrial context and was the primary objective of present thesis work.

Quantitatively good linear relation between MQ NMR and swelling methods are observed in unfilled compounds whereas higher swelling measured crosslink density values were observed in carbon black filled samples, due to filler restrictions on swelling that have no equivalent at the microscopic level probed by NMR. After eliminating the filler related restrictions on swelling results by empirical correction proposed by Lorenz, Parks and Kraus both methods were in good agreement, thus validating the current approaches for filler correction at least in the case of conventional CB fillers. This was a significant finding since most of the commercial products contain various fillers; in such a case MQ NMR measurements provide the actual crosslink density of filled compounds without artifact caused by the filler-rubber interface and also avoiding the influence of other effects on swelling method, such as osmotic expansion effects and vacuoles etc. arise in the filled rubber matrix during equilibrium swelling.

Changes occurring in the sulfur networks beyond the optimum cure time and the distribution of crosslinks were also discussed together with the effect of carbon black filler. Crosslink distribution in IR/BR polymer blends were studied by MQ TD-NMR for the first time, detecting differences between samples with higher precision than the swelling experiments. The comparison of residual dipolar coupling constants of blends and their distributions with those of pure components provided qualitative clues about different solubility/reactivity of curatives in the two rubbers composing the blend. High resolution ^{13}C-NMR was used to study the crosslink structure. The precise quantification of crosslink density with high resolution ^{13}C-NMR is tedious especially for quantification of small network differences and need expert's hands for analyzing the data. This technique is time consuming and expensive measurements as compared to MQ TD-NMR measurements are performed on low resolution spectrometers.

The prepared smart polymer material (with shape memory, UV-absorption and visible light transmission properties) network structures were characterized by MQ NMR. Shape memory polymers contain chemical and physical (ionic) crosslinks together to retain both fixation and recovery required for shape memory effect. The mixed network parameters and bound rubber fraction around the ionic domains have been quantified by applying various NMR methods. The redistribution of ionic domains in the ionomer matrix by breaking and reforming of ionic

crosslinks at higher temperature were also understood by the NMR measurements performed at variable temperatures. The incorporation of TiO_2 nanoparticles into shape memory polymer matrix, we were achieved requisite optical properties. With TiO_2 nanoparticles content in the polymer matrix, the refractive index was increased and nanocomposite acts as a UV-absorber and visible light transmitter. By thermal stimuli the shape memory effect was tested by transforming original shape into temporary shape and recovered to its permanent shape by heated up at above the transition temperature.

The network structures, internal and segmental motions in thermal-cured polybutylacrylates were studied with MQ NMR, ^{1}H NMR relaxation spectroscopy and mechanical experiments. The NMR T_2 relaxation, MQ NMR method shows good correlation with measured mechanical storage modulus in rubber plateau region. T_1 measurements over a temperature range allow understanding the internal motions of high polymer chains. The bulk polymerization of polybutyl acrylate creates self-crosslinks (branching) whereas solution polymerization was not. An increase in the content of ethylene glycol dimethacrylate (EGDMA) leads to significant increase in the crosslink density because the EGDMA acts as a tetrafunctional crosslinker. The capability of measuring small variations in polymer properties due to different synthesis could be used to characterize advanced materials such as polyacrylates polymerized in mini-emulsion or embedded in matrices.

In conclusion TD-NMR has been used for probing various polymer network properties. It is a remarkable spectroscopic technique in the perspective of extending the application of inexpensive, fast and solvent-free (green) technique to characterize various polymer networks for quality control and day to day R&D purposes.

Abbreviations and Acronyms

BR	*polybutadiene*
DCP	*dicumyl peroxide*
DMA	*dynamical mechanical analysis*
DQ	*double-quantum*
D_{res}	*residual dipolar coupling constant*
DSC	*differential scanning calorimetry*
D_{stat}	*static dipolar coupling constant*
EGDMA	*ethylene glycol dimethacrylate*
FID	*free induction decay*
GPC	*gel permeation chromatography*
HR-MAS	*high resolution magic-angle spinning*
I_{DQ}	*double-quantum intensity*
I_{nDQ}	*normalized double-quantum intensity*
I_{ref}	*reference intensity*
IR	*polyisoprene*
MQ	*multiple-quantum*
MSE	*magic-sandwich echo*
NR	*natural rubber*
SMPs	*shape-memory polymers*
T_1	*longitudinal relaxation time*
T_2	*transversive relaxation time*
τ_{DQ}	*double-quantum excitation time*
T_g	*glass transition temperature*
XNBR	*carboxylated nitrile butyl rubber*

Bibliography

[1] M. Rubinstein, R. H. Colby, Polymer physics, Oxford University press (2003).

[2] K. Saalwachter, *Prog. Nucl. Magn. Reson. Spectrosc*., **51**, 1-35 (2007).

[3] N. Rattanasom, T. Saowapark, C. Deeprasertkul, *Polym. Test*., **26**, 369-377 (2007).

[4] I. Mora-Barrantes, L. Ibarra, A. Rodriguez, L. Gonzalez,J. L. Valentin,J. *Mater.Chem*., **21**, 17526-17533 (2011)

[5] W. H. Waddell; L. R. Evans. *Rubber Chem. Technol*., **69**, 377-423 (1996).

[6] M-J. Wang. *Rubber Chem. Technol*., **71**, 520-589 (1998).

[7] J.Frohlich, W.Niedermeier, H.-D.Luginsland, *Composites: Part A*, **36**, 449-460 (2005).

[8] M. A. López-Manchado, M. Arroyo, B. Herrero,J. Biagiotti, *J. Appl. Polym. Sci*., **89**, 1-15 (2003).

[9] G. Sui,W. H. Zhong, X. P. Yang, Y. H. Yu, *J. Mater. Sci. Eng. A*, **485**, 524-531 (2008).

[10] J. Wu, W. Xing, G. Huang, H. Li, M. Tang, S. Wu, Y. Liu, *Polymer*, **54**, 3314-3323 (2013)

[11] E.L.Hahn, *Phys.Rev*., **80**(4), 580-594 (1950).

[12] A. Abragam, Principles of Nuclear Magnetism, Oxford University Press, Oxford (1983).

[13] M. Mauri, L. Mauri, V. Causin, R. Simonutti, *Anal.Methods*, **3**, 1802-1809 (2011).

[14] M Mauri, M.K Dibbanti, M Calzavara, L Mauri, R Simonutti, V Causin, *Anal.Methods*., **5** (17), 4336-4344 (2013).

[15]. K. Schmidt-Rohr and H. W. Spiess, Multidimensional Solid- State NMR and Polymers, Academic Press, San Diego, CA, (1999).

[16] H. Y. Carr and E. M. Purcell, *Phys. Rev*., **94**, 630–638 (1954).

[17] T. Kawai, *J. Phys. Soc. Jpn*., **16**, 6 (1961).

[18] J. Baum, A. Pines, *J. Am. Chem. Soc*., **108**, 7447-7454 (1986).

[19] T. C. Farrar, *Concepts Magn. Reson*., **2**, 1-12 (1990).

[20] T.C. Farrar, *Concepts Magn. Reson*, **2**, 55-61 (1990).

[21] S. A. Smith, W E. Palke, J.T. Gerig, *Concepts Magn. Reson.*, **4**,107-144 (1992).

[22] S. A. Smith, W.E. Palke, J.T. Gerig, *Concepts Magn. Reson.*, **4**, 181-204 (1992).

[23] S. A. Smith, W.E. Palke, J.T. Gerig, *Concepts Magn. Reson.*, **5**, 151-177 (1993).

[24] S. A. Smith, W.E. Palke, J.T. Gerig, *Concepts Magn. Reson.*, **6**, 137-162 (1994).

[25] G.Bodenhausen, *Prog. Nucl.Magn.Reson.Spectrosc*., **14**, 137-173 (1981).
[26] D.P. Weitekamp. *Advan.Magn.Reson. (*Vol. **11**, p. 111-274*), Time-Domain Multiple-Quantum NMR.*Academic Press. Inc., New York (1983).
[27] M. Munowitz, A. Pines. *Advan.Chem. Phys. (*Vol. **66**, p. 1-152*), Principles and Applications of Multiple-Quantum NMR*. Wiley-Interscience, New York (1987).
[28] G.E.Pake, *J. Chem. Phys*., **16**, 327 (1948).
[29] F.Creuzet, A.McDermott, R.Gebhard, K.VanderHoef, M.B.Spijker-Assiak, J.Herzfeld,J.Lugtenberg, M.H.Levitt, R.G.Griffin:*Science*,*251*,783 (1991).
[30] J.H.Ok, R.G.S. Spencer, A.E. Bennet, R.G.Griffin:*Chem.Phys.Lett*., **197**, 389 (1992).
[31] J.Baum, M.munowitz, A.N.Garrroway, A.Pines, *J.Chem.Phys*., **83**, 5 (1985).
[32] W.G. Breiland, C.B. Harris, A.Pines, *Phys.Rev.Lett*.,**30**, 158 (1973).
[33] W.S.Warren, D.P.Weitekamp, A.Pines, J.Chem. Phys., 73(5), 2084 (1980)
[34] R.R. Ernest, G. Bodenhausen, A.Wokaun, Principles of Nuclear Magnetic Resonance in One and Two Dimensions,Oxford University Press (1989).
[35] J.P.Cohen-Addad, *J.Chem.Phys*. **60**, 2440 (1974).
[36] J. P. Cohen-Addad, M. Domard, G. Lorentz, and J. Herz, *J. Phys. (*Paris) 45, 575 (1984).
[37] J. P. Cohen-Addad, *Macromolecules*, **22**, 147 (1989).
[38] P. Sotta and B. Deloche, *Macromolecules* **23**, 1999 (1990).
[39] P. Sotta, C. Fulber, D. E. Demco, B. Blumich, and H. W.Spiess, *Macromolecules*, **29**, 6222 (1996).
[40] J. P. Cohen-Addad, *Prog. Nucl.Magn.Reson.Spectrosc*., **25**, 1 (1993).
[41] J. Collignon, H. Sillescu, and H. W. Spiess, *Colloid Polym. Sci*. **259**, 220 (1981).
[42] R. C. Ball, P. T. Callaghan, and E. T. Samulski, *J. Chem. Phys*. **106**, 7352 (1997).
[43] P. T. Callaghan and E. T. Samulski, *Macromolecules*, **30**, 113 (1997)
[44] E. Fischer, F. Grinberg, R. Kimmich, and S. Hafner, *J. Chem. Phys*. **109**, 846 (1998).
[45] R. Graf, A. Heuer, and H. W. Spiess, *Phys. Rev. Lett*. **80**, 5738 (1998).
[46] T. Dollase, R. Graf, A. Heuer, and H. W. Spiess, *Macromolecules*, **34**, 298 (2001).
[47] K. Saalwachter, *Macromol. Rapid Commun*., **23**, 286 (2002)
[48] K. Saalwachter, *Chem. Phys. Lett*. **362**, 331 (2002)
[49] R. Fechete, D. E. Demco, and B. Blumich, *Macromolecules*, **35**, 6083 (2002).
[50] R. Fechete, D. E. Demco, and B. Blumich, *J. Chem. Phys*. **118**, 2411 (2003).
[51] M. Schneider, L. Gasper, D. E. Demco, and B. Blumich, *J. Chem. Phys*., **111**, 402 (1999).
[52] O.N.Antzutkin and R.Tycko, J.Chem. Phys. **110**, 2749 (1999).

[53] J. L. Valentín, J. Carretero-González, I. Mora-Barrantes, W. Chassé, K. Saalwächter, *Macromolecules*, ***41***, 4717-4729 (2008).

[54] J.D. Ferry, Viscoelastic Properties of Polymers, 3rd ed.; Wiley: New York (1980).

[55] K. Saalwachter, B.Herrero, M.A. Lopez-Manchado, *Macromolecules*, **38**, 9650-9660 (2005).

[56] K.Saalwachter, P.Ziegler, O.Spyckerelle, B.Haidar, A.Vidal, J-U.Sommer, *J. Chem. Phys*.,**119**(6), 3468 (2003).

[57] K.Saalwachter, *Rubber Chem. Technol.*,**85** (3), 350-386 (2012).

[58] Weese,J. *Comput.Phys.Commun*., **69**, 99-111 (1992).

[59] Weese,J.*Comput.Phys.Commun*., **77**, 429-440 (1993).

[60] J.L.Valentin, P.Posadas, A.Fernandez-Torres, M.A.Malmierca, L.Gonzalez,W.Chasse, K.Saalwachter, *Macromolecules*, **43**, 4210-4222 (2010).

[61] W. Chasse, J. L. Valentin, G. D. Genesky, C. Cohen, K. Saalwachter,*J. Chem. Phys.*, **134**, 044907 (2011).

[62] T.A.Vilgis, G.Heinrich, *Coll. Pol. Sci.*, **269**, 1003 (1991).

[63] V.M. Litvinov, P.De. Prajna, *Spectroscopy of Rubbers and Rubbery Materials*, Rapra Technologies Ltd., **360** (2002).

[64] M. Rubinstein, S. Panyukov, *Macromolecules*, **35**, 6670-6686 (2002).

[65] O.Guven, In Crosslinking and Scission in Polymers, B.Erman Eds;. Springer: Netherlands, Vol.**292**, p 153-169 (1990).

[66] R.S. Rivlin, *Philos. Trans. R. Soc., A*, **241**, 379 (1948).

[67] L.R.G. Treloar, The Physics of Rubber Elasticity, Clarendon, Oxford (1975).

[68] K.C.Valanis, R.F. Landel, *J. Appl. Phys*., **38**, 2997 (1967).

[69] G.B.McKenna, J.A. Hinkley, *Polymer*, **27**, 1368 (1986).

[70] E.A. Kearsley,L.J.Zapas, J. *Rheol*., **24**, 483 (1980).

[71] D.F. Jones, L.R.G.Treloar, *J. Phys. D. (Appl. Phys.)*, **8**, 1285 (1975).

[72] B. Saville, A. A. Watson, *Rubber Chem. Technol*., **40**, 100-148 (1967).

[73] L.Mullins, *J.Appl.Polym. Sci*., 2, 1-7 (1959).

[74] P.J.Flory, J.Rehner. Jr, *J.Chem.Phys*., **11**,512 (1943).

[75] P.J.Flory, J.Rehner. Jr, *J.Chem. Phys*., **11**,521 (1943).

[76] P.J. Flory, *J. Chem. Phys.*, **9**, 660–661 (1941).

[77] M.L.Huggins, *J. Chem. Phys.*, **9**, 440–440 (1941).

[78] P.J. Flory, *J. Chem. Phys.*, **18**, 108 (1950).

[79] J.Brandrup, E.H.Immergut, E.A.Grulke, Ass.Ed., A. Abe, D.R.Bloch Polymer handbook, 4th Ed., (1998).

[80] P.Ghosh, S. Katare, P.Patkar, J.M.Caruthers, V.Venkatasubramanian , K.A. Walker,. *Rubber Chem Technol.*, **76** (3):592-693 (2003).

[81] R. N. Datta, In Rapra Review Reports, Rapra Technology Limited:2001; Vol.**12**, No.12 pp 1-137.

[82] Y. Akagi, J.P. Gong, U. Chung, Takamasa Sakai, *Macromolecules*, **46** (3), 1035–1040 (2013).

[83] J. E. Mark, In Physical properties of polymers handbook; Frenc Horkay, Gregory B.Mckenna, 2nd Eds.; Springer; Chapter 29, pp 497-522 (2007).

[84] J-M.Chenal, L. Chazeau, L. Guy, Y. Bomal, C. Gauthier, *Polymer*, **48**, 1042-1046 (2007).

[85] J. L. Valentín, I. Mora-Barrantes, J. Carretero-González, M. A. López-Manchado, P. Sotta, D. R. Long, K. Saalwächter,*Macromolecules*, **43**, 334-346 (2010).

[86] R. S. Maxwell, S. C. Chinn, D. Solyom, R. Cohenour,*Macromolecules*, **38**, 7026-7032 (2005).

[87] A. Bandyopadhyay, G. M. Odegard,*Modell. Simul. Mater. Sci. Eng.*, **20**, 045018 (2012).

[88] A. J. Tinker, *Rubber Chem. Technol.*, **68,** 461-480 (1995).

[89] T. Crisenza, H.-J. Butt, K. Koynov, R. Simonutti,*Macromol.Rapid Commun.*, **33**, 114-119 (2012).

[90] D. Mangaraj, *Rubber Chem. Technol.*, **75**, 365-427 (2002).

[91] S. A. Groves,*Rubber Chem.Technol.*, **71**, 958-965 (1998).

[92] P. Boochathum, W. Prajudtake,*Eur. Polym.J.* , **37**, 417-427 (1993).

[93] D. J.Zanzig, F. L. Magnus, W. L. Hsu, A. F. Halasa, M. E. Testa,*RubberChem. Technol.*, **66**, 538-549 (1993).

[94] C. Sirisinha, N. Prayoonchatphan, .*J. Appl.Polym. Sci.*, **81**, 3198-3203 (2001).

[95] P. J. Flory, Principles of Polymer Chemistry: Cornell University (1953).

[96] M.Mori, J.L.Koenig, *Annu. Rep. NMR Spectrosc.*, **34**, 231-299 (1997).

[97] M. A. Voda, D. E.Demco, J. Perlo, R. A. Orza, B. Blümich, *J.Magn.Reson.*, **172**, 98-109 (2005).

[98] G. Zimmer, A. Guthausen, B. Blumich,*Solid State Nucl.Magn.Reson.*, **12**, 183-190 (1998).

[99] O. Lorenz, C. R. Parks,*J.Polym.Sci.*, **50,** 299-312 (1961).

[100] G. Kraus, *J. Appl.Polym. Sci.*, **7**, 861-871 (1963).

[101] U. Heuert, M. Knorgen, H. Menge, G. Scheler, H. Schneider, *Polym. Bull.*, **37**, 489-496 (1996).

[102] V. M. Litvinov, P. A. M. Steeman, *Macromolecules*, **32**, 8476-8490 (1999).

[103] F. Vaca Chávez, K. Saalwächter, *Phys. Rev. Lett.*, **104**, 198305 (2010).

[104] M. Mauri, Y. Thomann, H. Schneider, K. Saalwächter, *Solid State Nucl.Magn.Reson,*. **34**, 125-141 (2008).

[105] E. Gjersing, S. Chinn, J. R. Giuliani, J. Herberg, R. S. Maxwell, E. Eastwood, D. Bowen, T. Stephens, *Macromolecules*, **40**, 4953-4962 (2007).

[106] A. J. Marzocca, M. A. Mansilla, *J. Appl. Polym. Sci.*, **103**, 1105-1112 (2007).

[107] M. Abdel-Goad, W. Pyckhout-Hintzen, S. Kahle, J. Allgaier, D. Richter, L. J. Fetters, *Macromolecules*, **37**, 8135-8144 (2004).

[108] S. Krushev, W. Paul, G. D. Smith, *Macromolecules*, **35**, 4198-4203 (2002).

[109] K. A. J. Dijkhuis, J. W. M. Noordermeer, W. K. Dierkes, *Eur.Polym. J.*, *45*, 3300-3310 (2009).

[110] J. Portal; C. Carrot, J-C. Majeste, S. Cocard, V. Pelissier, I. Anselme-Bertrand,*Polymer Engineering & Science*, **49**, 1544-1552 (2009).

[111] H. E.Gottlieb,V.Kotlyar, A.Nudelman, *J. Org. Chem*., **62**, 7512-7515 (1997).

[112] M. Mori, J. L. Koenig, *J. Appl. Polym. Sci*, **70**, 1391-1399 (1998).

[113] N.R. Legge, G.Holden, H.E.Schroeder, *Thermoplastic Elastomers*. A Comprehensive Review; Carl Hanser Verlag: Munich, Germany, 1004 (1987).

[114] G.Holden, H.R. Kricheldorf, R.P.Quirk, *Thermoplastic Elastomers,* Carl HanserVerlag: Munich, Germany (2004).

[115] A. Eisenberg, *Macromolecule*, **3**, 2, 147-154 (1970).

[116] A. Eisenberg, B. Hird, R. B. Moore, *Macromolecule*, **23**, 18, 4098-4107 (1990).

[117] A. Lendlein, S. Kelch, *Angew.Chem. Int. Ed*., **41**, 2034- 2057 (2002).

[118] K. Sato, "Ionic Crosslinking of Carboxylated SBR", *Rubber Chemistry and Technology*, **56**, 942 (1983).

[119] F. C. Wilson, R. Longworth, and D. J. Vaughan, "The Physical Structure of Ionomers

III. X-Ray Diffraction Studies", *Polymer Preprint*, **9**, 505 (1968).

[120] Ibarra. L, Alzorriz. M. *J. Appl. Polym. Sci*., **87**, 805-813 (2002).

[121] L.Ibarra, A.Marcos; M. Alzorriz, *Polymer*, **43**, 1649-1655 (2002).

[122] R. Fechete, D.E. Demco, and B. Blumich, Journal of Magnetic Resonance, 169, 19–26,

(2004).

[123] A. Colombo, F. Tassone, F. Santolini, N. Contiello, A. Gambirasio and R. Simonutti, *J. Mater. Chem. C*, **1**, 2927-2934 (2013).

[124] A.Colombo,F.Tassone, M. Mauri, D. Salerno, J.K. Delaney, M. R. Palmer, R. D L. Rie R. Simonutti, *RSC Adv*., **2**, 6628-6636, (2012).

[125] P. H. Starmer,*Plastics and Rubber Processing and Applications*, **9**, 209, (1988).

[126] J.L. Valentín., D. Lopez, R. Hernandez, C. Mijangos, K. Saalwachter, *Macromolecules*, **42** (1), 263−272 (2009).

[127] M. Alexandre, P. Dubois, *Mater. Sci. Eng*., R, **28**, 1–63 (2000)

[128] A. C. Balazs, T. Emrick and T. P. Russell, *Science*, **314**, 1107–1110(2006).

[129]A. Usuki, Y. Kojima, M. Kawasumi, A. Okada, Y. Fukushima, T. Kurauchi and O. Kamigaito, *J. Mater. Res*., **8**, 1179–1184 (1993).

[130]Y. Kojima, A. Usuki, M. Kawasumi, A. Okada, Y. Fukushima, T. Kurauchi and O. Kamigaito, *J. Mater. Res*., **8**, 1185–1189 (1993).

[131] P. Kiliaris, C. D. Papaspyrides, *Prog. Polym.Sci*., **35**, 902–958 (2010).

[132] M. A. Osman, V. Mittal, M. Morbidelli, U. W. Suter, *Macromolecules*, **37**, 7250–7257 (2004).

[133] H. S Jung, Jung-Kun Lee, M. Nastasi, *Langmuir*, **21** 10332-10335 (2005).

[134] A. Maus, C. Hertlein, K. Saalwachter, *Macromol. Chem. Phys*., **207**, 1150−1158, (2006).

[135] A. Papon, K. Saalwachter; K. Schaler; L. Guy, F. Lequeux, H.Montes. , *Macromolecules*, **44**(4), 913−922,(2011).

[136] K. Schaler, E. Ostas., K. Schroter, T. Thurn-Albrecht, W.H. Binder, K. Saalwachter, *Macromolecules*, **44** (8), 2743−2754, (2011).

[137] M. Ibrahim ,A. Nada, DiaaEldinkamal, *Indian J pure &Appl phys*, **43**, 911-917 (2005).

[138] Malmierca M. A.,Gonzalez-Jimenez.A,Mora-Barrantes. I,Posadas.P, Rodriguez.A ,Ibarra. L, Nogales.A,Saalwachter.K, and J. L. Valentin, *Macromolecules*, 47, 5655−5667, (2014).

[139] J.Huang, Wen-Jun Wang, Bo-Geng Li, S. Zhu, *Macromol. Mater. Eng.*, **298** (4), 391-399 (2012).

[140] K. E. Uhrich, S. M. Cannizzaro, R. S. Langer, K. M. Shakesheff, *Chem. Rev*., **99**, 3181 (1999).

[141] M. Belting, S. Sandgren, A. Wittrup, *Adv. Drug Deliv. Rev*., **57**, 505 (2005).

[142] A. Nori, J. Kopecek, *Adv. Drug Deliv. Rev*., **57**, 609 (2005).

[143] N. A. Peppas, J. Z. Hilt, A. Khademhosseini, R. Langer, *Adv.Mater.*, **18**, 1345 (2006).

[144] A. Monguzzi, F.Bianchi, A. Bianchi, M. Mauri, R. Simonutti, R. Ruffo, R. Tubino, F. Meinardi, *Adv. Energy Mater.*, **3**, 680–686 (2013).

[145] V. M. Litvinov, A. A. Dias, *Macromolecules*, ***34***, 4051-4060 (2001).

[146] T. G Fox, S. Loshaek, *J. Polym. Sci*. **25**, 371-390 (1955).

[147] N. Bloembergen, E. M. Purcell, R. V. Pound, *Phys. Rev*., **73**(7),679-712 (1948).

Acknowledgements

First and foremost I would like to express my deep sense of gratitude and high regards to my supervisor *Prof. Dr. Roberto Simonutti*, for the opportunity to pursue research in this broad area that allowed me to push back the frontiers of knowledge in ways that neither us could have envisioned when I began this new trek. I, deeply appreciate his invaluable guidance, inspiring suggestions and unconditional support throughout this study. Without his auspices, sound counsel and sympathetic attitude towards all my shortcomings, this work would not have been possible.

- I sincerely thanks to my co-supervisor *Dr. Gabriele Medaglia* from Pirelli Tyre for his support and providing all the available facilities in the Pirelli Research and Development Centre, Milan and fruitful discussions.

- I am immensely pleased in recording my sincere gratitude to the Doctorate School Dean *Prof. Gian Paolo Brivio* for giving me opportunity to carry out my Ph.D.

- I am extending my sincere thanks to *Dr. Juan Lopez Valentin* (CSIC, Madrid, Spain) for providing all the facility and fruitful discussion and transfer of knowledge during my stay in Spain.

- I am also thanking *Dr.Ulrich Scheler* (IPF, Dresden, Germany) for providing NMR facility and discussion during my stay in Germany.

- My heartfelt thank to *Michele Mauri* and *Lucio Mauri* for their support and sharing of knowledge, fruitful discussion and also being close friends.

- I wish to express my cordial appreciation to my senior colleagues and gracious friends *Annalisa Colombo* and *Alberto Bianchi* for their valuable support.

- I am delighted to express my deep feelings to my close friends, *Simone, Matteo, Anna, Daniela* and *Teffa*.

- My very special thank go to *Gian Bonetti* and *Tullia Piantoni* for their love and affection towards me.

- My loving thanks to my parents, brothers, sisters and *Haritha* for providing endless moral support to successfully finish my work without which my work was not fulfilled successfully.

- I also acknowledge the University of Milano-Bicocca for giving me an opportunity for undertaking my dissertation work.

- Last but not least I am extending my gratitude to *PIRELLI TYRE* for providing me scholarship through CORIMAV and PCAM European Doctoral programme.

Murali Krishna Dibbanti